On the role of molecular mechanisms and unequal cleavage during neurogenesis in the *C. elegans* C lineage

Thomas William Mullan

Submitted for the degree of
Doctor of Philosophy

March 2021

Department of Cell and Developmental Biology
Division of Biosciences
University College London

Supervisor: Dr. Richard Poole

Declaration

I, Thomas William Mullan, declare that this thesis was composed in its entirety my myself and that the work described herein is my own unless otherwise stated. In such cases those persons who conducted or assisted in said work are acknowledged in the text either by name or citation.

Thomas William Mullan

Abstract

Required for neurogenesis is a family of evolutionarily conserved bHLH transcription factors known as proneural genes. However, regulation of their initial expression remains a poorly understood aspect of neurodevelopment in any model, particularly *Caenorhabditis elegans*. A key mechanism by which cells acquire different fates is asymmetric division and in neuronal lineages these often generate unequally sized daughters. Whether this unequal size directly affects cell fate regulation is often unknown. Indeed, the question of how control of cell size intersects with fate decisions is poorly understood in biology more generally.

Taking advantage of the single-cell resolution provided by the invariant cell lineage of *C. elegans,* I interrogate these two fundamental biological questions in the C lineage. Expression of the proneural gene *hlh-14/Ascl1* in a single branch of the lineage is required for neurogenesis of the DVC and PVR neurons and is immediately preceded by unequal cleavages. Addressing both molecular and cellular regulators I perform a 4D-lineage based genetic screen for upstream regulators of *hlh-14/Ascl1* and address the effect of unequal cleavage and daughter cell size.

I find that a regulator of other neuronal lineage cleavages, PIG-1/MELK, is also required in the C lineage, yet equalisation does not affect the initiation of *hlh-14/Ascl1* expression. Conversely, I demonstrate that unequal cleavage and acquisition of neuronal fate in separate successive divisions are controlled by the same key regulators. The first by an upstream regulator of *hlh-14*, the Mediator complex kinase module *let-19/Mdt-13* and the second by *hlh-14* itself.

Taken together the results described in this thesis suggest that rather than acting to correctly segregate initial proneural gene expression, unequal cleavages are instead co-regulated by the same factors regulating neuronal fate acquisition. This co-regulation at successive divisions thus coordinates two separable aspects of fate; acquisition of neuronal identity and correct post-mitotic embryonic cell size.

Statement of Impact

In this thesis I describe results that indicate that terminal embryonic neuronal cell size of the *C. elegans* DVC neuron and the acquisition of its neuronal fate are controlled by the same regulators including the proneural gene *hlh-14/Ascl1*. The results indicate that these aspects are regulated in parallel by separate mechanisms downstream of the molecular regulators resulting in the coordination of the correct final cell size and cell fate.

The impact of these findings within the field is multifaceted. In a narrow sense the finding that one of the regulators, *pig-1/MELK,* acts in unequal cleavages in the C lineage is novel. Classically, *pig-1* regulates terminal neuroblast divisions in which one daughter cell dies, neither of the divisions I describe generate an apoptotic daughter cell, which adds to a growing body of evidence suggesting that *pig-1* has a broader role in unequal cleavages. Specifically, that I find *pig-1* is required in successive divisions is a novel finding. This will impact on the field in terms of prompting the investigation of cleavage plane positioning earlier in neuronal lineages rather than solely at the division at which one previously assumed the phenotype was brought about, often the terminal neuroblast division. As such these results could impact both on experimental design and phenotype interpretation.

More broadly, the control and regulation of cell size is a particularly poorly understood aspect of biology, especially with how it relates to the acquisition of cell fate The interpretation of the results described in this thesis as indicating that the same regulators of fate decisions regulate daughter cell size in a parallel yet separable manner increases wider understanding of the coordination of these aspects during development. In a specifically *C. elegans* context, because there is no growth in the embryo cells at hatching must be of appropriate size to function in their terminal fates. The finding that these aspects are controlled separately yet by the same regulators will both aid understanding and inform future experimental design in order to elucidate how terminal cell size is coordinated with fate acquisition.

Outside of a strictly academic setting, as my results add to understanding of the intersection of cell size and the misregulation of proneural genes there is a potential impact on health. The misregulation of proneural genes including *Ascl1*, the human homologue of *hlh-14,* the proneural gene in this study*,* has been implicated in neurodevelopmental and neurological diseases and in

cancers (reviewed in Huang et al., 2014). By characterising additional novel phenotypes of *hlh-14* mutants, the results of this study will inform future investigations that will provide insight into the consequences of proneural gene misregulation in disease. Furthermore, given that aberrant cell size has also been implicated in cell fitness, metabolic diseases and ageing (reviewed in Miettinen et al., 2017), further studies in *C. elegans* informed by my findings may also provide insight into the regulation of cell size that is broadly applicable in a human disease context.

Acknowledgements

I would firstly like to thank my supervisor Dr. Richard Poole for his mentorship and particularly for his encouragement throughout my time in the lab. My introduction to *C. elegans* as a model system and the concepts that went onto form part of my PhD project came from my rotation project in the lab, so I would like thank Rich for providing the setting for that inspiration.

I would also like to thank my colleagues past and present in the Poole and Barrios labs. Their support and friendship have been an invaluable both scientifically and personally. In the same vein I wish to thank members of the Rockefeller 5th floor office from all labs for providing both an enjoyable space to work and a fun group to socialise as part of.

Most importantly I would like to thank my family for their support during my PhD research and particularly during the writing of this thesis. Specifically, I am extremely grateful to my Mum and to Garry for providing me with a place to be able to work and write this thesis, without it this would have been a far harder task.

Additionally, this work was made possible by a studentship from the Wellcome Trust and I am grateful for the opportunity that the funding provided.

Contents

Index of Figures and Tables

"...we should not be childishly disgusted at the examination of the less valuable animals. For in all natural things there is something marvellous"

Aristotle,

On the Parts of Animals

Introduction

Chapter 1

1. General Introduction

Proneural genes are a deeply evolutionarily conserved family of bHLH transcription factors that are both necessary and sufficient to drive neurogenesis across a diverse range of taxa (Bertrand et al., 2002). However, despite being known to be downstream of neural induction very few positive regulators of their initial expression have been described in any model system. This is especially true in the nematode *Caenorhabditis elegans* in which neurons arise non-clonally during development from multiple cell lineages and where the majority of fate decisions are made cell autonomously (Sulston et al., 1983).

Another poorly understood aspect of biology is how cell size relates to cell fate. This stems partially from the fact that the mechanisms by which cells sense and control their size even in a homeostatic sense remains an area of much investigation and debate (Conlon and Raff, 2003; Ginzberg et al., 2018; Rishal and Fainzilber, 2019). How this then relates to fitness, function and ultimately fate remains even more elusive and is complicated by cellular growth (Björklund, 2019; Miettinen et al., 2017; Schmoller, 2017). Asymmetric cell divisions are those that produce daughter cells of two different fates. These divisions also often display unequal cleavage generating daughters of different sizes (Horvitz and Herskowitz, 1992; Knoblich, 2008), yet how these two aspects are linked is often unknown.

In the *C. elegans* embryo a lack of cell growth means that control of cell size can only achieved through unequal cleavage. Taken together with the cell-autonomous nature of many fate decisions in the embryo, the *C. elegans* embryo therefore provides a powerful model for the interrogation of the intersection of fate choice and cell size. Does cell size lead to particular fate choices and if so, is cell size regulated in order to achieve such a fate choice? Is unequal cleavage required for the asymmetric segregation of fate determinants? If regulated in parallel, how is the control of cell size and fate coordinated in the embryo?

In this thesis I sought to combine these concepts by addressing whether unequal cleavage and the resultant asymmetry in daughter cell size bring about fate choices in *C. elegans* neuronal lineages. Specifically, I interrogated the role of unequal cleavage during neurogenesis in the *C. elegans* C lineage. This was with the aim of investigating whether unequal cleavage and resultant cell size led to segregation of upstream regulators of the proneural gene *hlh-14* in order to initiate its expression in the lineage's single neurogenic branch.

Part I

1.1.1. C. elegans as a Neurodevelopmental Model System

The use of nematode species in the study of developmental biology has a long history reaching back to the 19th century. The inspirational nature of much of this early work is exemplified by the studies, and indeed beautiful drawings, by Theodor Boveri of *Ascaris* blastomeres and the identification of their cell lineages in the very earliest stages of development (Boveri, 1899; Boveri, 1910). Concurrent with the study of other nematodes such as *Ascaris* came the description of the species that we now call *Caenorhabditis elegans* by Emile Maupas (Maupas, 1899; Maupas, 1900).

The elevation of *C. elegans* to its present-day position as a mainstream developmental biology system began with Sydney Brenner's search for a new model system during the 1960s. Brenner's original vision in choosing the system stated the desire for a model system in which a complete genetic description of neurodevelopment in addition to the elucidation of the connectome and how these all interconnect to produce behaviour (Brenner, 1974; Sulston and Brenner, 1974). Whilst found worldwide with a preference for rotting fruit (reviewed in Schulenburg and Félix, 2017) the current laboratory reference strain was isolated from a compost heap in Bristol, United Kingdom and is known by its strain designation of 'N2' (Brenner, 1974).

Several features of the species are advantageous to its use as model system. Firstly, the small size of the adult and embryos, at around 1mm and 40-50µm respectively, make them both easily stored in large numbers and easily observed and manipulated in using a dissection microscope. Simple maintenance on bacterial lawns of *Escherichia coli* in petri dishes combines feeding and housing. The life cycle of the animal is also rapid at around three and a half days from egg to laying adult at the standard maintenance temperature of 20°C (Figure 1.1). This rapid life cycle is coupled with a preference for a self-fertilising hermaphroditic reproduction system (X0 males occur at a frequency of ~0.2%) in which XX hermaphrodites lay around 200-300 eggs (Brenner, 1974). These features allow both the maintenance of near isogenic lines, relatively simple

construction of desired strains and swift high-throughput study of developmental processes and consequences of manipulations.

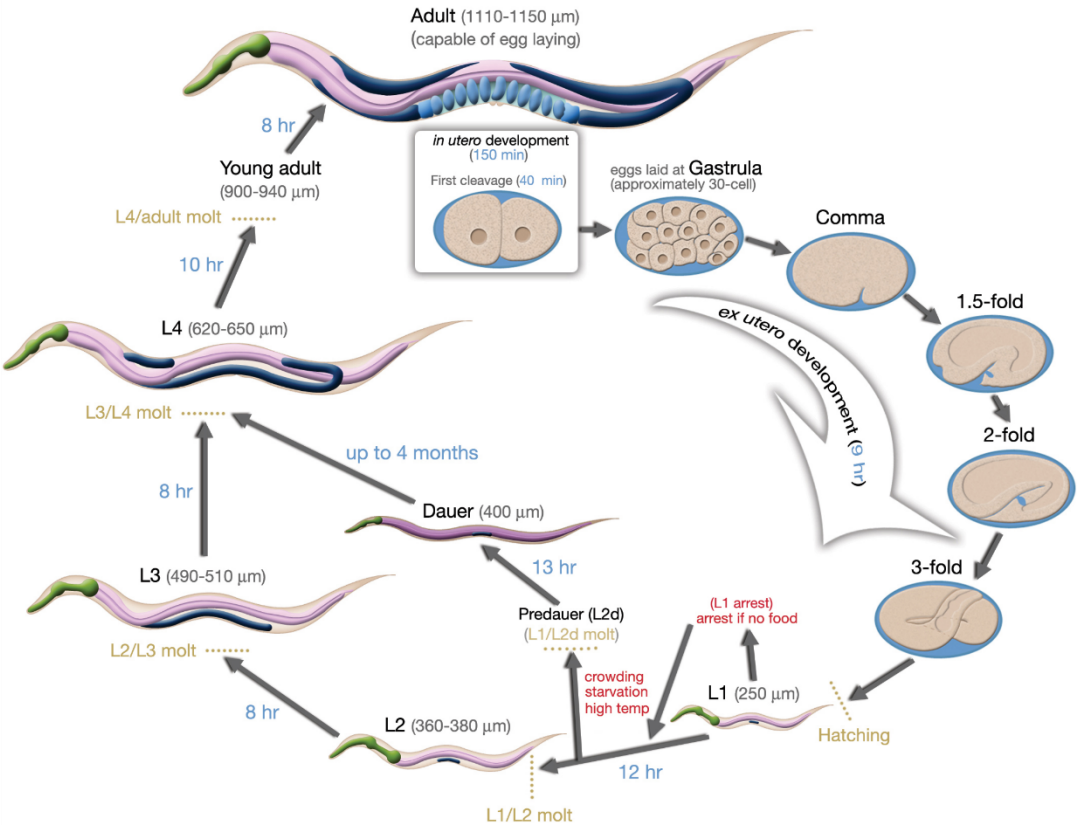

Figure 1.1 *C. elegans* life cycle. *Schematic representing the life cycle of C. elegans from after the first cleavage until gravid adult. The dauer stage is also included, which is an alternative developmental stage entered into as a kind of stasis in response to harsh conditions such as starvation. Timings of stages are representative of development at 22°C. (Adapted from WormAtlas.com).*

From an imaging perspective the transparent nature of both embryos and adults allows for observation in detail of smaller structures at 100X magnification with the use of Nomarski optics (DIC) (Figure 1.2). Furthermore, genetic amenability allows the use of both extrachromosomal and integrated transgenes (Mello et al., 1991; Praitis et al., 2001) and importantly the construction of fluorescent reporter transgenes (Chalfie et al., 1994) allowing simple visualisation of individual cell types and gene expression patterns.

A particular strength of *C. elegans* lies in that an entire reference genome has been available to the community for over twenty years. Indeed, it was the first model system and metazoan in general to have its genome fully sequenced (*C. elegans* Sequencing Consortium., 1998). The genome and genetic amenability allows for rapid mutant discovery. Forward and reverse genetic screens are easily employed using mutagens such as EMS used by Brenner to generate the first behaviour mutants (Brenner, 1974). In addition to the still much used classical technique of RNAi knockdown (Fire et al., 1998), more recent techniques such as targeted genome editing using the CRISPR Cas9 system (Dickinson et al., 2015; Friedland et al., 2013) is readily applicable to worms. Furthermore, the emergence of additional methods for temporally controlled gene knockdown including optogenetic (Johnson and Toettcher, 2018) and the degron-tagged (Beer et al., 2019; Zhang et al., 2015) systems means that a multitude of techniques to investigate gene function through transgene construction and/or gene disruption are available to the *C. elegans* field.

Perhaps the most powerful advantage of *C. elegans* as a developmental model organism is the fact that is has a fully elucidated and invariant cell lineage of 959 and 1031 cells in males and hermaphrodites respectively (Kimble and Hirsh, 1979; Sulston and Horvitz, 1977; Sulston et al., 1983; White et al., 1986) (Figure 1.3). This allows the unrivalled ability to study fate decisions and so assess the lineage consequences of mutation and other manipulations in terms of division pattern and timing at the single cell resolution. All cells in the lineage have a name corresponding to their founder lineage and whether they are an anterior or posterior daughter of a division. For example, Cap is the posterior daughter of the anterior daughter of the C blastomere (Sulston et al., 1983).

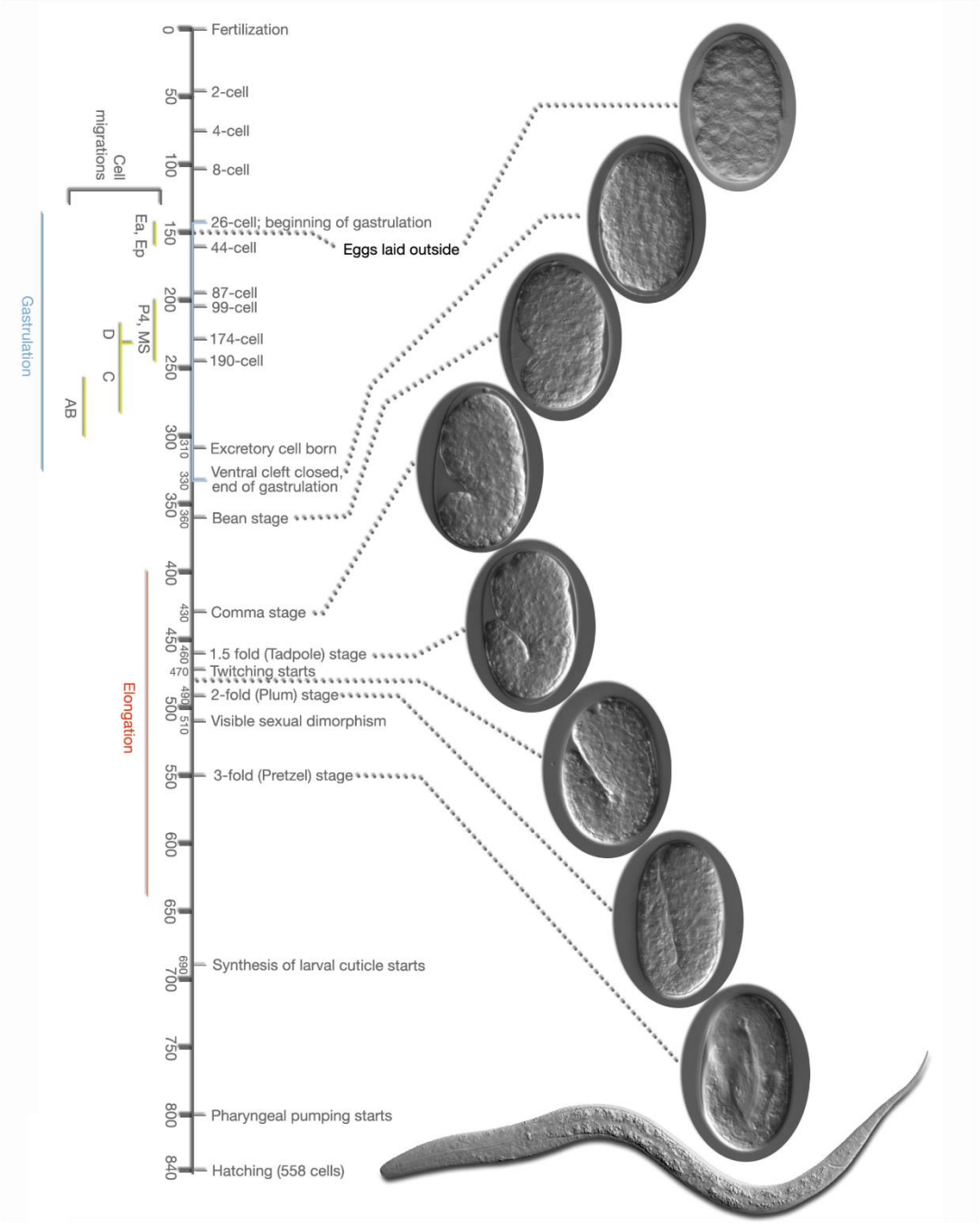

Figure 1.2. Schematic of *C. elegans* embryogenesis. *Developmental time-course of embryogenesis indicating different stages and their respective durations. DIC images of embryos at the individual stages are indicated as being of said stage. Timings are in minutes and represent development at 22°C. (Adapted from WormAtlas.com)*

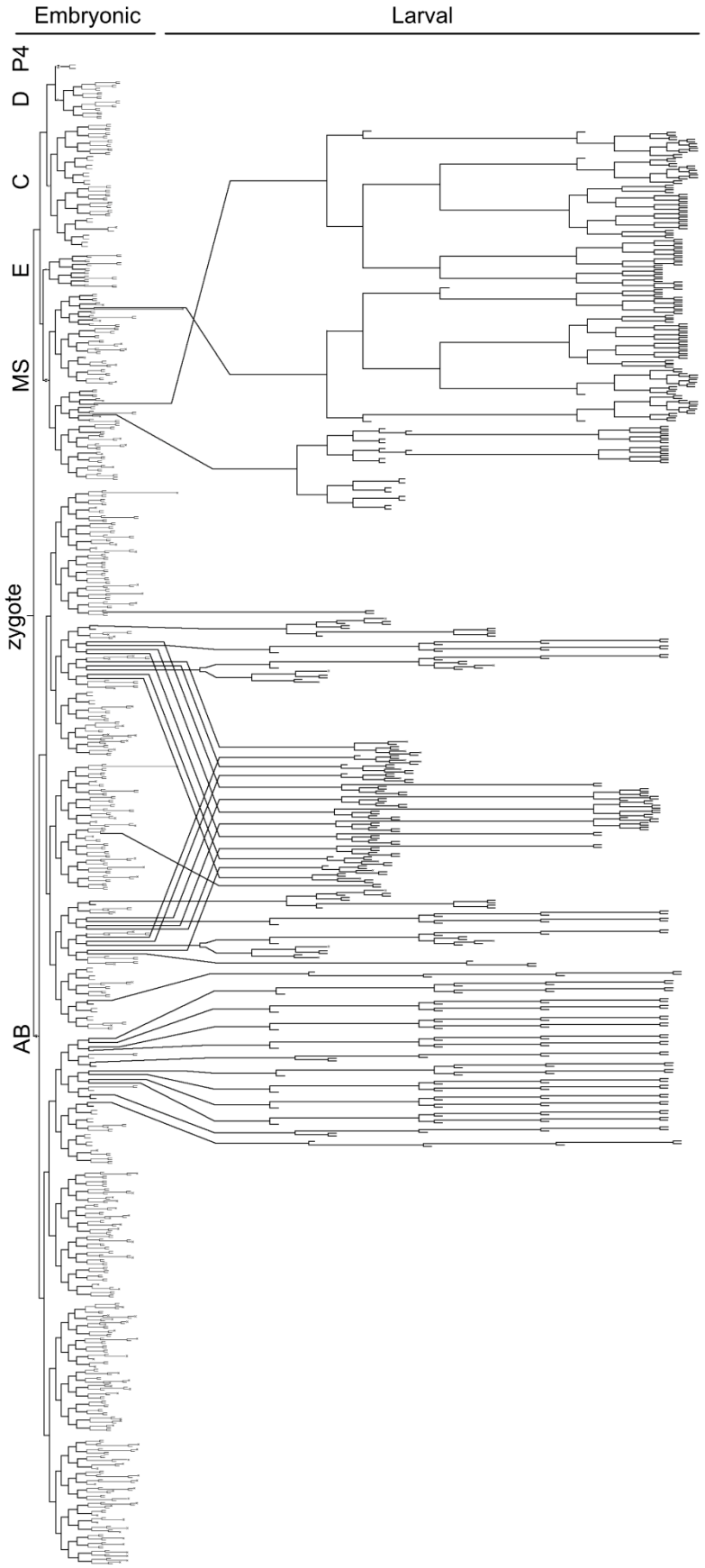

Figure 1.3. Invariant cell lineage of *C. elegans*. *Lineage diagram illustrating the entire invariant cell lineage. Branch lengths are representative of relative division timings Founder blastomere names appear above their respective nodes. (Adapted from WormAtlas.com).*

Highlighting another strength, the physical map of the adult hermaphrodite nervous system was reconstructed from serial electron-micrograph sections early in the development of the *C. elegans* field beginning with the pharynx (Albertson and Thomson, 1976), ventral nerve cord (White et al., 1976) and the entire animal (Hall and Russell, 1991; White et al., 1986). Given the sexual dimorphism of the nervous system in *C. elegans* the physical map of male specific aspects of the nervous system has also been reconstructed in much the same manner (Cook et al., 2019; Jarrell et al., 2012). Importantly. Upon completion it was, and remains, the only complete nervous system map of its kind for any organism (Cook et al., 2019; Varshney et al., 2011; White et al., 1986).

This completed adult connectome evidently allows the probing of putative circuits to reveal functions and behaviours, as demonstrated by early identification of the touch sensitivity circuit based on ablation experiments guided by the connectome (Chalfie et al., 1985). Developmentally the connectome is dynamic. The order in which cells are born in the embryo impacts on the connections made between terminally differentiated neurons during embryogenesis which is altered during the transition to the larval stage at hatching based on a trade-off between connection distance and network topology (Alicea, 2018; Nicosia et al., 2013).

This nervous system of 300 neurons in hermaphrodites and 387 in males (Sammut et al., 2015) is classified into 118 distinct anatomical classes of which over 90% are identifiable by transcription factor profile (Hobert et al., 2016; White et al., 1986). From a neurodevelopmental perspective a great deal of work has gone into understanding the terminal differentiation of these neurons. A number of large studies over the last decade have greatly furthered our understanding of pan-neuronal genes (Stefanakis et al., 2015) and the classification of neurons into both types and subtypes in terms of terminal selector regulatory logic and neurotransmitter identity (Gendrel et al., 2016; Hobert, 2016; Kratsios et al., 2017; Pereira et al., 2015; Serrano-Saiz et al., 2013).

Part II

1.2.1. Proneural Genes

The earliest stages of neurogenesis involve the initiation of neuronal lineages and so the establishment of neuronal progenitor and neuroblast identities downstream of neural induction. Key regulators of these initial steps of neuronal specification are a number of widely evolutionarily conserved transcription factors of the basic helix-loop-helix (bHLH) class now termed 'proneural genes' (Bertrand et al., 2002). The discovery of proneural genes originates from *Drosophila* with the requirement for segregation of members of the *achaete-scute* complex into a subset of neuroblasts (Cabrera et al., 1987), their requirement in neuroblast commitment (Jiménez and Campos-Ortega, 1990) and that proneural genes are necessary and sufficient to drive neurogenesis. The discovery of the proneural activity of *atonal*, a gene from a distinct family of bHLH transcription factors revealed the first proneural gene outside the *achaete-scute* family (Jarman et al., 1993). These early characterisations also revealed key molecular features of proneural genes; the bHLH domain is required for the DNA binding capacity of proneural genes to E-boxes and their capacity for heterodimerisation with other *achaete-scute* complex members (Bertrand et al., 2002; Murre et al., 1989a; Murre et al., 1989b). This domain is also required for heterodimerisation with *daughterless/E*, another bHLH transcription factor involved in neurogenesis, which is now known to be the ubiquitous binding partner for bHLH transcription factors (Bertrand et al., 2002; Caudy et al., 1988; Murre et al., 1989b).

Proneural genes are characterised as belonging to either the Atonal, Achaete-Scute, Neurogenin and Olig gene families and are often found to be required in distinct regional and neuronal subtype contexts across evolution (Bertrand et al., 2002). For example whilst the *achaete-scute* genes are required in the neuroblasts of the *Drosophila* CNS and for development of external sensory organs (Villares and Cabrera, 1987), they are not required in the photoreceptors or chordotonal organ, where *atonal* is the proneural gene (Jarman et al., 1993; Jarman et al., 1994). Increasing evidence suggests this deployment of different proneural transcription factors to specify different neuronal subtypes and regions is a deeply conserved strategy. For example the *achaete-scute* and *neurogenin* homologues in the sea urchin *Lytechinus variegatus* are expressed in distinct embryonic domains and specify the serotonergic neurons of the apical organ and cholinergic

neurons of the ciliary band respectively (McClay et al., 2018; Slota and McClay, 2018). Similarly, this is also true in vertebrates (reviewed extensively in Huang et al., 2014), where for example the *achaete-scute* homologue *Ascl1* (Johnson et al., 1990) and the Atonal family members *Neurog1* and *Neurog2*, (Gradwohl et al., 1996; Ma et al., 1996), are mainly expressed in distinct domains of already patterned neuroectoderm in both the CNS and PNS and confer different neuronal subtypes (Chien et al., 1996; Fode et al., 2000; Lo et al., 2002; Ma et al., 1996; Parras et al., 2002). In contrast to *Drosophila* where proneural genes are explicitly required for the initiation of neuron development, proneural genes are often regulated in cells that are already specified as part of a neuroectoderm. However, in a neuroblast context more akin to the function of proneural genes in *Drosophila, Neurog2* is required cranial placode neuroblast specification (Lassiter et al., 2014). These divergent functions are likely caused by their preferential binding to particular E-box sequences (Bertrand et al., 2002; Chien et al., 1996). A study of *Ascl1* and *Neurog2* targets has recently demonstrated transcription factor specific chromatin remodelling (Aydin et al., 2019) and explains the variability in the ability of one proneural factor to substitute for another other in different nervous system regions (Parras et al., 2002).

1.2.2. Proneural Gene Regulation in *Drosophila* and Vertebrates

Acquisition of neuroblast identities within the *Drosophila* neuroepithelium is controlled in a spatiotemporal manner. The integration of Hox, segmental, columnar and temporal transcription factor patterning confers distinct neuroblast identities to specific regions of neuroectoderm (Doe, 2017; Holguera and Desplan, 2018; Karlsson et al., 2010; Urbach et al., 2003). However, the direct upstream regulators of proneural remain mostly elusive.

A major mechanism by which the restriction of proneural gene expression is controlled is through a Notch signalling mediated system of lateral inhibition. In this system proneural genes become expressed within equivalence groups in the epidermis called proneural clusters (Simpson and Carteret, 1990). Cells which express proneural genes directly activate expression of Notch ligand *delta* with a single cell eventually outcompeting its neighbours for a stronger signal (Kunisch et al., 1994). This signal leads to the transactivation of bHLH repressors of the *enhancer of split* family in the receiving cells (Jennings et al., 1994) and the so the downregulation of both proneural

genes and ligand expression amplifying the notch response in a feedback loop (Heitzler et al., 1996; Schrons et al., 1992).

The initiation of proneural gene expression in vertebrates also begins in neuroectoderm that has already been patterned. In the developing neural tube positional information conferred by dorsal-ventral patterning leads to the distinct neuronal populations arising from these regions, with distinct transcriptional profiles (Briscoe and Novitch, 2008; Briscoe et al., 2000; Cohen et al., 2013; Parras et al., 2002). The best known example of regulation of proneural genes in these regions employs Notch mediated expression by homologues of *enhancer of split,* the Hes genes (Imayoshi et al., 2010). The negative feedback oscillatory expression of the proneural repressor *Hes1* is required to maintain low *Ascl1* expression (Imayoshi et al., 2013; Shimojo et al., 2008). High levels of oscillating Hes1 leads to the stem-like quiescence of the neural precursor (Sueda et al., 2019). With the downregulation of the *Hes1* comes the upregulation of proneural gene expression, which allows proliferation (Castro et al., 2011), and sustained expression drives differentiation of neuroblasts (Imayoshi et al., 2013).

1.2.3. Proneural Genes in *C. elegans*

Despite the first *C. elegans* proneural bHLH gene, an *atonal* homologue *lin-32*, being described not long after that of proneural genes in *Drosophila* (Zhao and Emmons, 1995) the early stages of neurogenesis and in particular the regulation of proneural genes remains a poorly understood area of *C. elegans* neurobiology. Below I will introduce what is known about the spatiotemporal expression and effect of neuroblast identity for a number of *C. elegans* proneural genes in order to draw attention to two key points; firstly that very little is known about the initiation of proneural gene expression and secondly; that an emerging feature of proneural gene action is to act in distinct ways at multiple steps of the neurogenesis pathway.

At the genomic level the *C. elegans* genome contains 39-42 bHLH transcription factors (Reece-Hoyes et al., 2005; Simionato et al., 2007) which despite a higher sequence evolution rate in nematodes generally demonstrate a high degree of sequence homology and function to their *Drosophila* and vertebrate orthologues (Ledent and Vervoort, 2001). Of the proneural genes already introduced above, between five and seven of these *C. elegans* genes are identifiable

homologues of the *achaete-scute* family (*hlh-3, hlh-4, hlh-6, hlh-12, hlh-14, hlh-16 and hlh-19)*, with one *atonal (lin-32)* and one *daughterless/E (hlh-2)* homologue (Simionato et al., 2007).

Yeast two hybrid binding analysis confirmed that in *C. elegans* as in other organisms (Bertrand et al., 2002), the *daughterless* homologue and bHLH proneural factor HLH-2 (Krause et al., 1997) is a promiscuous and near-ubiquitous heterodimerisation partner of other *C. elegans* bHLH proteins, amongst them, homologues of known proneural genes (Grove et al., 2009). In addition to ability to form homodimers, HLH-2 is able to form heterodimers with HLH-3, HLH-4, HLH-6, HLH-8, HLH-10, HLH-12, HLH-13, HLH-14, HLH-15, HLH-19, LIN-32, CND-1, HND-1 and NGN-1. The formation of these heterodimers with HLH-2 enhances the ability of the transcription factors to bind to their target E-box sequences (Grove et al., 2009). In agreement with such a clearly broad role in comparison to its binding partners, the expression pattern of *hlh-2* is broad in the embryo and begins in the comma stage at much the same time as the majority of its binding partners, which in agreement with their more restricted roles, have a much less widespread expression (Grove et al., 2009; Krause et al., 1997). Interestingly, at the 350 cell stage the majority of neuronal precursors and neuroblasts express *hlh-2* (Krause et al., 1997), illustrating its key role for the function of proneural genes.

1.2.4. Expression of Proneural Genes

Despite such molecular characterisation of *C. elegans* proneural gene homologues and the confirmation of HLH-2 as a ubiquitous heterodimerisation partner most proneural genes remain grossly understudied. In fact, a large number of *C. elegans* bHLH transcription factors mentioned above, including proneural genes, remain to have a role characterised in the literature (Table 1.1). Indeed, only a handful of proneural genes have been the subject of study in any detail, namely *lin-32, hlh-3* and *hlh-14*, and of these *hlh-3* has been argued as not being a true proneural gene (to be outlined below). Furthermore, a recent study has described a C2H2 zinc singer TF factor as working with *lin-32* in the postdeirid lineage in a manner reminiscent of a proneural gene, clouding the picture within the field further (Doitsidou et al., 2018).

Gene	Homologue	Neural Role	Classical Proneural Role	Neurons	References
hlh-2	Daughterless	Yes, ubiquitous binding partner	Yes	Many	(Krause et al., 1997)
hlh-3	achaete-scute	Yes, terminal differentiation	Debated	NSM, HSN, I4, (AIY non proneural)	(Doonan et al., 2008; Frank et al., 2003; Lloret-Fernández et al., 2018; Luo and Horvitz, 2017; Murgan et al., 2015)
hlh-4	achaete-scute	Yes, terminal differentiation	No	ADL	(Gruner et al., 2016; Masoudi et al., 2018)
hlh-6	achaete-scute	Yes, terminal differentiation	No	ADL	(Gruner et al., 2016)
hlh-10	?	Yes, terminal differentiation	No	ADL	(Gruner et al., 2016)
hlh-12	achaete-scute	No	No	n/a	n/a
hlh-14	achaete-scute	Yes	Yes	ADL, OLL, ADF, AWB, ASE, ASJ, AVA, PVQ/HSN/PHB	(Frank et al., 2003; Poole et al., 2011)
hlh-16	Oligo	Yes, axon projection	No	AIY	(Bertrand et al., 2011)
hlh-19	achaete-scute	?	?	"head neurons"	(Grove et al., 2009)
lin-32	atonal	Yes	Yes	Rn.A, Q	(Portman and Emmons, 2000; Zhao and Emmons, 2995)
cnd-1	NeuroD	Yes, differentiation	no	"motor neurons", I3	(Hallam et al., 2000; Luo and Horvitz, 2017)
ngn-1	Neurogenin	Yes	Yes	MI	(Nakano et al., 2010)

Table 1.1. Summary of the roles of *C. elegans* proneural genes. *Known roles of identified proneural genes and proneural gene homologues. Whether a gene has an identified role in neurogenesis and/or an identified proneural role in C. elegans is indicated.*

Highlighting this understudied nature is the example of CND-1, of which very few studies exist. *cnd-1* is one of the earlier described proneural genes in *C. elegans* and is a homologue of the NeuroD family of proneural genes known of be required for neuronal differentiation. Expression of *cnd-1* begins in the four descendants of the AB blastomere (Hallam et al., 2000) from which many embryonically ventral cord neurons are derived (Sulston et al., 1983). Postembryonically expression is maintained in ventral cord neurons until hatching. Loss of *cnd-1* leads to a small reduction in the number of ventral cord neurons. These neurons are lost because *cnd-1* is required for the expression of *unc-30, unc-4* and *unc-3* in these neurons (Hallam et al., 2000) which are required respectively for the cholinergic and GABAergic identity of the various ventral chord (Jin et al., 1994; Kratsios et al., 2011; Kratsios et al., 2017). The non-total loss of these markers however suggests *cnd-1* is a non-essential upstream regulator of these genes (Hallam et al., 2000).

Comparatively more is known about the first described *C. elegans* proneural gene, the *atonal* homologue, *lin-32* (Zhao and Emmons, 1995). LIN-32 is required for correct neurogenesis in a number of embryonic and postembryonic lineages and ectopic expression is able to confer neuroblast fate (Zhao and Emmons, 1995). For example, embryonically, *lin-32* has been shown as required for neurogenesis of the ALM and PLM touch neurons (Chalfie and Au, 1989; Zhao and Emmons, 1995), the dopaminergic specification of the CEPD and PDE neurons (Doitsidou et al., 2008; Doitsidou et al., 2018; Romanos et al., 2017) and upstream of terminal differentiation genes such as the homeodomain POU transcription factor *unc-86* in the URX oxygen sensation neurons (Romanos et al., 2017).

More detail is known about its expression and role in patterning the postembryonic neurogenesis of the sexually dimorphic male specific ray neurons. Expression of *lin-32* begins in the ray neuroblast Rn.a and is detected in both its daughters post-division and subsequently lost in the posterior daughter, the lineage leading to the RnB neuron (Portman and Emmons, 2000). *lin-32* is subsequently restricted to anterior daughters in two successive rounds of division, expressed first in Rn.aa and then Rn.aaa (Miller and Portman, 2011) which is maintained in Rn.aaa until it undergoes terminal differentiation as the RnA ray neuron (Portman and Emmons, 2000). The same restriction into anterior lineages is seen for *hlh-2* and heterodimerisation is require for LIN-32 function in the lineage and thus correct ray neurogenesis. Null mutants of *lin-32* display a loss of nearly all ray neurons whereas weaker loss of function alleles display a variable preferential

loss of either RnA or RnB neurons (Miller and Portman, 2011; Portman and Emmons, 2000) suggestive of a role for *lin-32* at multiple lineage levels and thus stages of neurogenesis. One mechanism controlling the segregation of *lin-32* expression to the anterior lineage is the POP-1 asymmetry pathway (to be described in more detail in a following section). Briefly, the system allows for binary fate decisions by allowing or repressing expression of particular genes in daughter cells in the cellular and lineage context inherited from the mother. In the Rn lineage low POP-1 levels in all anterior daughters maintains *lin-32* expression in these branches. *pop-1* mutants display severe defects in the lineage with a conversion to RnA fates due to symmetric *lin-32* expression (Miller and Portman, 2011). Whilst the POP-1 system explains the segregation of the proneural gene into particular branches and is likely to be involved in many analogous cases, it is not responsible for initiation of *lin-32* expression in the lineage in that it does not itself provide the aforementioned lineage context.

lin-32 is also the proneural gene required in the sex-shared Q lineage (Zhao and Emmons, 1995). The Q cell first undergoes an asymmetric division, the anterior daughter of which, Q.a, divides asymmetrically itself to produce an anterior daughter which dies and the neuron A/PQR. Q.p divides asymmetrically to produce a posterior daughter which dies and an anterior daughter which divides asymmetrically to produces the A/PVM and SDL/R neurons (Sulston and Horvitz, 1977). Demonstrating again an emerging concept in that proneural genes can act in multiple steps of the neurogenesis process the absence of *lin-32* leads to the loss of Q neuroblast fate and the conversation to that of its sister, the seam cell V5. Contrastingly weak loss of function alleles lead to the an ectopic A/PQR generated in place of a cell death indicating the symmetrisation of the Q.a division (Zhu et al., 2014).

Another *C. elegans* proneural gene of the *achaete-scute* family is *hlh-14* (Frank et al., 2003). *hlh-14* is the proneural gene with the best characterisation of its expression pattern in terms of all identification of affected embryonically born neurons. These affected lineages predominantly descend from the posterior lineages of the ABalpppp/ABpraaap cell in which *hlh-14* is maintained giving rise to ADL, OLL, ADF, AWB, ASE, ASJ and AVA neurons (Poole et al., 2011). Additional AB lineages requiring *hlh-14* are those of PVQ/HSN/PHB neuroblast (Frank et al., 2003), the AUM/BDU and I1L/R neuroblasts (Poole et al., 2011). The other non AB descended neuroblasts requiring *hlh-14* are that of DVC and PVR which come from a single branch of the C lineage (Frank et al., 2003; Poole et al., 2011).

The loss of *hlh-14* has two distinct neuroblast lineage effects which are dependent on the lineage from which the neuroblast itself descends. The more straightforward effects are exemplified by the DVC and I1L/R neuroblasts in that the loss of neuroblast identity leads to precocious division of the would-be neuroblast and the conversion to the respectively hypodermal or muscle fate of their sister lineages with no change in the number of rounds of division (Poole et al., 2011). Conversely, a greater effect on the loss of neuroblast identity is demonstrated by the PVQ/HSN/PHB neuroblasts and the ABalpppp/ABpraaap lineage. In both cases the conversion to a hypodermal fate is accompanied by the loss of multiple rounds of division such that ABalpppp/ABpraaap produces seven fewer cells (Poole et al., 2011) and the PVQ/HSN/PHB neuroblast adopts the fate of its sister to divide only once and produce a hyp7 and T cell, and so three fewer cells (Frank et al., 2003).

1.2.5. Regulation of Proneural Genes in *C. elegans*

As previously mentioned above very little is known about the regulation of proneural gene expression in *C. elegans* with surprisingly very few closely upstream regulators discovered in genome wide screens and reported in the literature to date.

In vertebrates SoxB1 members Sox1-3 play a key role in vertebrate embryonic neural induction (Nicosia et al., 2013) with Sox2 regulating neural progenitor state (Graham et al., 2003) through regulation of, and feedback from, proneural and neural differentiation genes (Amador-Arjona et al., 2015; Cimadamore et al., 2011; Evsen et al., 2013). The *C.* elegans SoxB1 *sox-2*, whilst transiently expressed in 52 embryonic neuroblasts, has no role in neurogenesis or neuronal commitment in the embryo (Vidal et al., 2015). Instead *sox-2* is necessary for correct cholinergic specification of anterior ganglia neurons URA, URB and IL2 and the glutamatergic specification of the OLL and IL1 sensory neurons (Vidal et al., 2015). This indicates a possible divergent role of SoxB1 family members in aspect of neuronal development.

Despite not being a segmented animal *C. elegans* Hox genes still fulfil the role of anterior-posterior patterning; *ceh-13/Lab* specifies the anterior most fates with *lin-39/Scr*, *mab-5/Antp* and *egl-5/php-3/nob-1/Abd-B* specifying respectively more posterior fates (Clark et al., 1993; Hunter and Kenyon, 1995; Van Auken et al., 2000; Wittmann et al., 1997). Intriguingly however, this expression is not achieved through position but through cell lineage origin (Cowing and Kenyon,

1996; Wittmann et al., 1997). In a neuronal context however, unlike patterning in flies and vertebrates, Hox genes do not appear to be upstream of proneural gene expression and instead lead to neuronal subtype specification in parallel with proneural factors (Kratsios et al., 2017; Zheng et al., 2015).

The inhibition of proneural gene expression through a Notch mediated mechanism was outlined above in both vertebrate and *Drosophila* contexts. The existence of a similar Notch mechanism exists in *C. elegans*, also involving *Hairy/enhancer of split* homologues of the REF-1 family (Alper and Kenyon, 2001). *Enhancer of split* homologue *lin-22* is required in the V1-4 seam lineages to repress expression of *lin-32* and so the formation of ectopic PDE neurons of the postdeirid sublineage (Wrischnik and Kenyon, 1997) (Figure 1.4.) Furthermore, *ref-1* mutants display ectopic AWB and ADF neurons arising from the posterior daughter of either ABpraaa/ABalppp. In *wild types* they arise from a shared neuroblast descended from the anterior daughter of said cells, suggesting that *ref-1* controls neuronal lineage decisions at the ABpraaa and ABalppp divisions (Lanjuin et al., 2006). However, in contrast to its homologues, *lin-22* expression is not activated by Notch signalling, and whilst expression of the REF-1 transcription factor itself is predicted to be able to respond to Notch (Neves and Priess, 2005), constructs of “unresponsive” sequences are able to rescue neuronal lineage defects in ABpraaa/ABalppp (Lanjuin et al., 2006).

One of the only reported mechanisms for direct transcriptional control of a proneural gene is in MI neuron. The transcription factor Otx *ceh-36* is required in the grandmother of MI to activate transcription of both *hlh*-2 and *ngn-1* (Nakano et al., 2010), the *C. elegans neurogenin* homologue. Following division, their action in the MI mother cell is to activate proneural targets as a conventional heterodimer with these targets thought to be then asymmetrically inherited in the anterior daughter, MI (Nakano et al., 2010).

Another *C. elegans* homologues of *achaete-scute* complex is *hlh-3* which has been variously described as non-proneural due to a lack of gross loss of neurons in mutants despite being expressed widely in neuroblasts (Doonan et al., 2008; Luo and Horvitz, 2017) and proneural due its requirement in the specification of the HSN lineage (Lloret-Fernández et al., 2018). In truth it may be that it performs different roles in different cells and indeed that its expression and function are similarly regulated by different mechanisms. In HSN *hlh-3* has very recently been shown to act downstream of the master regulator of HSN specification the transcription factor *unc-86*, being completely lost in mutants, and is required for the acquisition of aspects of serotoninergic fate

(Lloret-Fernández et al., 2018). Conversely, the requirement of HLH-3 in the pharyngeal I4 neuron is not as clear as its loss here leads to only a modest loss of neurogenesis. Further, this is not enhanced by the loss of HLH-2, which itself has no neurogenesis phenotype. Instead the parallel actions of HLH-2 and members of the Mediator complex CDK8 kinase module are required to allow the proneural actions of HLH-3 (Luo and Horvitz, 2017). As the Mediator complex is an evolutionarily conserved protein complex that mediates transcription factor association with RNA polymerase II to regulate gene expression (Grants et al., 2015) it is also possible that HLH-2 directly associates with the Mediator in this context. In the absence of HLH-3, HLH-2 homodimers are presumably sufficient to drive proneural target gene expression. This leads to the interpretation that either *hlh-3* and *hlh-2* are neither strictly proneural in the lineage or that both can be classed as proneural yet only in combination, and not in the ubiquitous heterodimer context discussed (Bertrand et al., 2002; Grove et al., 2009).

As stated above this highlights the lack of current understanding in the field with regards to the regulation of proneural genes. Whilst some understanding has been gained in the regulation of expression after initiation it still remains very unclear how initiation of proneural gene expression is achieved.

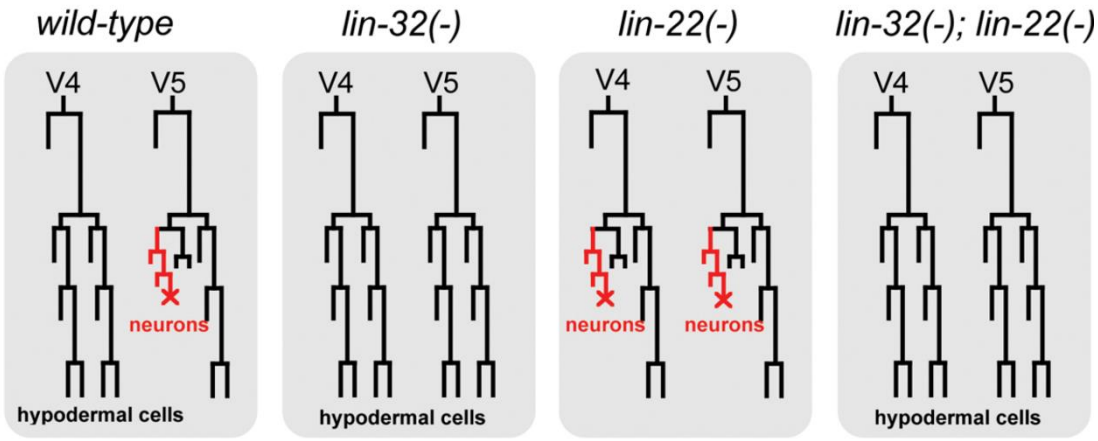

Figure 1.4. Repression of neuronal fate in V1-4 by *lin-22.* *Lineage diagrams illustrating that hypodermal cells derived from V1-4 in postembryonic seam lineages adopt neuronal fate of the postdeirid sublineage in lin-22 mutants due to derepression of the proneural gene lin-32, and that the V cells are unable to generate neurons in lin-32 mutants.(Adapted from Wormbook).*

Part III

1.3.1. Asymmetric and Unequal Divisions

1.3.2. Control of Binary Fate Decisions by the Wnt/β-catenin Asymmetry Pathway

Given that *C. elegans* displays an invariant cell lineage, many fate decisions are made at the single cell level rather than through the patterning of tissues in a field of cells. These thus necessitate the use of asymmetric divisions, divisions that generate daughters of two distinct fates, in order to make fate decisions. Furthermore, the rapid nature of embryonic development means the diversification of cell fates requires a robust system by which to reproducibly couple differentiation patterns to lineages divisions in such an invariant manner. The majority of these divisions are made along the anterior-posterior axis (Sulston et al., 1983) where they employ a noncanonical Wnt pathway known as the Wnt/β-catenin asymmetry pathway in a reiterative fashion (reviewed in Bertrand, 2016). This pathway establishes an anterior-posterior asymmetry in daughter identities across successive divisions through a shared mechanism (Kaletta et al., 1997; Lin et al., 1998). The system is defined by a reciprocal asymmetry (Phillips et al., 2007) in which cells with high nuclear levels of the transcription factor POP-1/TCF and low SYS-1/β-catenin are specified as adopting the anterior fate whilst conversely those with higher nuclear SYS-1 and lower POP-1 are specified as posterior (Kidd et al., 2005; Lin et al., 1998).

Briefly, the establishment of this opposing POP-1 and SYS-1 asymmetry is achieved as follows. During the division of a mother cell, WRM-1, another *C. elegans* β-catenin homologue involved in POP-1 asymmetry (Nakamura et al., 2005), is localised to the anterior cortex in association with a member of the destruction complex, APR-1. In a feedforward loop this leads to WRM-1's cortical localisation and nuclear export (Lin et al., 1998; Mizumoto and Sawa, 2007; Takeshita and Sawa, 2005). SYS-1 is also targeted for degradation by APC resulting in low nuclear levels of both β-catenins in the anterior daughter (Baldwin and Phillips, 2014; Huang et al., 2007; Mizumoto and Sawa, 2007). Conversely in the posterior daughter, free undegraded WRM-1 leads to the phosphorylation of a Nemo kinase homologue, LIT-1, which phosphorylates POP-1 targeting it for nuclear export (Kaletta et al., 1997; Lo et al., 2004; Rocheleau et al., 1999; Yang et al., 2015). In the early embryo this posterior identity is induced in cell pairs through contact

dependant signalling by MOM-2/Wnt and the Frizzled receptor MOM-5 on the soon-to-be posterior cell (Park et al., 2004; Thorpe et al., 1997). However, after the AB^{16} stage in the embryo neither Wnt signalling nor inductive contact is required to maintain the POP-1 SYS-1 asymmetry in successive rounds of division This is despite the continued posterior localisation of MOM-5/Frizzled (Goldstein et al., 2006; Park et al., 2004). How the reiterative anterior-posterior pattern is maintained after this stage is unclear although recently it has demonstrated that cells that are for example the posterior daughters of posterior daughters have significantly higher levels of WRM-1 than the anterior daughter of a posterior daughter and is thus suggestive of a feedforward reinforcement of successive identity (Zacharias et al., 2015). However, lineages frequently demonstrated a reversal of the trend following a division and so it is clear that the mechanism cannot fully describe the maintenance.

This asymmetry system allows for context dependent binary decisions to be enacted given that in association with appropriate lineage specific transcription factors (Figure 1.5). The traditional view of this mechanism has been that POP-1 acts as a transcriptional activator of target genes in association with its coactivator SYS-1 in posterior cells, and in SYS-1's absence in the anterior, mostly as a transcriptional repressor (Bertrand and Hobert, 2010; Kidd et al., 2005). An example of this mode of regulation occurs in the early embryo and the division of the EMS blastomere into the mesoderm founder MS and endoderm found E. The EMS blastomere expresses *skn-1* and downstream effectors *med-1, 2* which in the posterior E cells activate the endoderm specification genes *end-1, 3* in conjunction with POP-1/SYS-1. Conversely, symmetric inheritance of SKN-1 and MED-1,2 in MS occurs in the context of low SYS-1 and high POP-1 and results in the repression of *end-1,3* expression by POP-1 and thus MS fates (Maduro et al., 2001). However, the case of the SMDD/AIY neuroblast demonstrated that there is not only one way by which POP-1 can bring about binary fate decisions. Neuroblast divisions often employ the Wnt/β-catenin asymmetry pathway and the SMDD/AIY neuroblast provides an example of both POP-1 activation and repression of target genes in the presence of low SYS-1 in successive divisions. In the SMDD/AIY neuroblast high POP-1 and low SYS-1 results in the transcription of *hlh-2* and *ttx-3* by a complex of the Zic transcription factor with POP-1(Murgan et al., 2015). In the subsequent SMDD/AIY neuroblast division POP-1 acts as an activator with its classical coactivator SYS-1 in the posterior daughter to activate *ceh-10* only in the AIY precursor. This in turn specifies AIY fate whilst the non-expressing daughter becomes that SMDD neuron (Bertrand and Hobert, 2009).

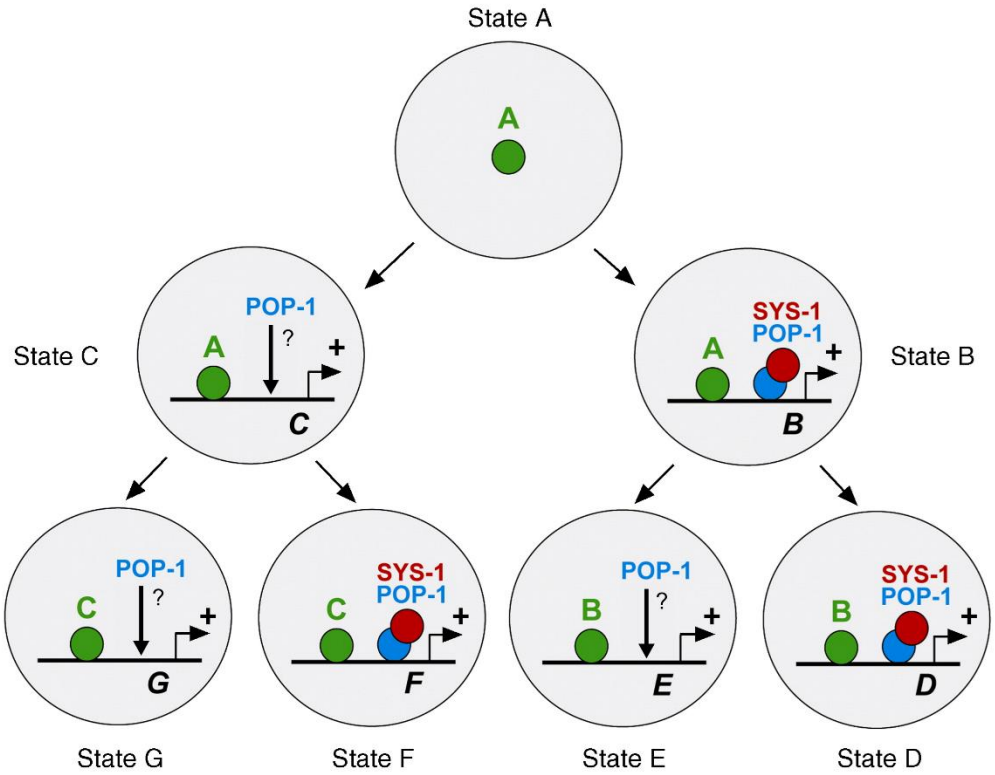

Figure 1.5. Binary fate decisions using the POP-1/SYS-1 Wnt/β-catenin asymmetry pathway. *Schematic representing how the Wnt/β-catenin asymmetry pathway can integrate with lineage context dependent transcription factors to specify a variety of binary fate choices. SYS-1/POP-1 complex shown as a positive regulator of transcription in posterior cells. POP-1 action in anterior cells is indicated with a question mark as it may be either a positive or negative regulator in the absence of SYS-1. Green circles = lineage context dependent transcription factors. (Adapted from Bertrand and Hobert, 2010)*

1.3.3. Unequal Cleavage in Asymmetric Division

The concept of unequal cleavage in asymmetric division has been considered since the late 19th century with the concept and observation of asymmetric inheritance of different developmental potentials and so cell lineages recorded for example in Ascidians (Conklin, 1905), *Ascaris* nematodes (Boveri, 1899) and leeches (Whitman, 1878).

Although the subject of many studies, including in the worm, the term 'asymmetric division' remains poorly defined in the literature. Indeed, it is very often unclear when an author is referring to asymmetry whether this includes unequal daughter sizes or whether they are purely referring to cell fate asymmetry. This confusion has also been evident since the early *C. elegans* literature where Sulston et al., defined "symmetric" as daughters of equal size and symmetrically localised across the midline, "equal" to refer only to size and "equational" to daughters of the same fate (Sulston et al., 1983). Conversely, Schierenberg defined "unequal" as referring to purely size and "non-equational" to be with regards to fate, for example (Schierenberg, 1988). The author of this thesis prefers the term "asymmetric" over "non-equational" and will use the term throughout this work in reference to purely fate or potential. For clarity, reference by this author to "unequal" cleavage during this thesis is purely with respect to relative daughter cell size, which may be otherwise explicitly referred to as "size asymmetry". The continued lack of clarity in the literature is most likely due to the fact that size asymmetries and how they may or may not pertain to fate decisions remains a very under considered aspect of asymmetric divisions. Some of this may stem from the fact that in light of the Wnt/β-catenin asymmetry pathway and its cellular and lineage context control of transcription described above it is conceivable that such biochemical asymmetry may be sufficient to drive the majority of fate choices.

An obvious potential interaction between unequal cleavage and cell fate decisions is through the asymmetric segregation of fate determinants to daughter cells. Conceptually, in such a situation segregation of an already localised determinant to a single daughter cell would require positioning of the cleavage plane such that the determinant was inherited entirely by the appropriate daughter. Additionally, unequal cleavage could also result in asymmetric fate choice through the segregation of a cell fate determinant that is not specifically localised in the mother. In this scenario the difference in daughter cell size would result in different ratios of the fate determinant to other factors such as the genome in each daughter. Therefore, in only one daughter would the interaction kinetics be appropriate to impart the fate (Figure 1.6).

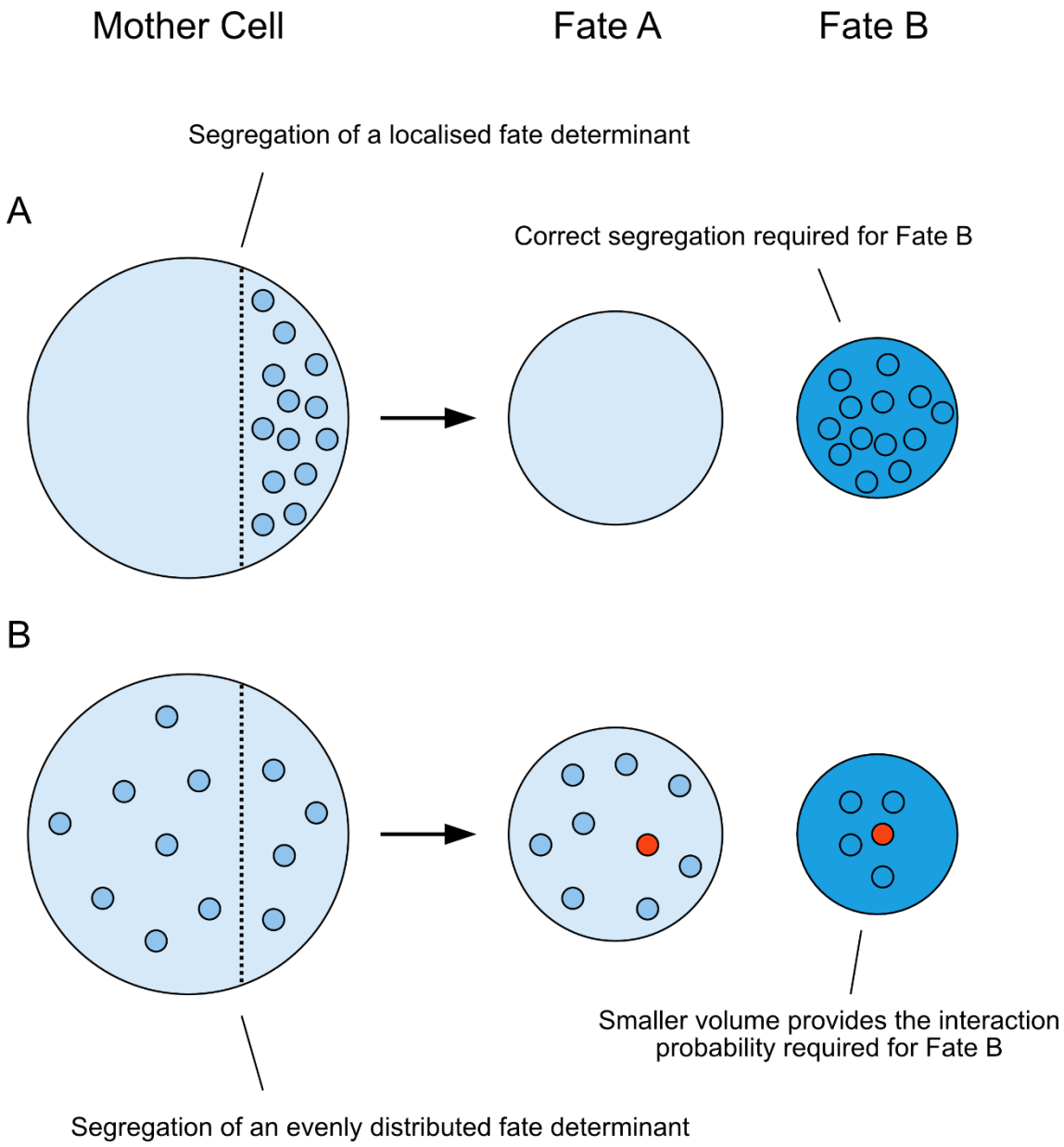

Figure 1.6. Unequal cleavage can result in asymmetric division via two mechanisms. *Schematic representing how unequal cleavage can impact on fate choice. Small blue circles = fate determinant. Dotted line = cleavage plane. Small orange circle = factor that fate determinant must interact with (i.e. another protein or the genome). A) A factor localised in the mother cells requires the positioning of the cleavage plane to correctly partition it. B) A uniformly distributed factor requires a smaller size in order for the cellular dynamics to allow correct probability of an interaction occurring that is required to specify a certain fate.*

In fact the second of these two scenarios is important to consider given that non-localised determinants are nonetheless not uniformly distributed, with the potential for stochastic inheritance (Huh and Paulsson, 2011). Controlling cell size could account for the uncertainly of such heterogeneity, increase potential interaction frequency appropriately. Interestingly the question of how cell size intersects with differentiation is a particularly poorly understood area of biology in general. Certain cell types are known to only differentiate at particular sizes, for example human keratinocytes only begin to do so at diameters in excess of 12µm and are fully committed to differentiation, as opposed to growth, at about 20µm (Barrandon and Green, 1985). Furthermore, it has been demonstrated that controlling cell size in human and mouse mesenchymal stem cells can direct differentiation programs based on volume, irrespective of external fate cues. Smaller cells are biased to adopt osteogenic fates whereas larger cells become adipocytes (Bao et al., 2017; Guo et al., 2017), this is thought to be due to lower mRNA concentration for appropriate osteogenic factors in larger cells (Bao et al., 2017; Padovan-Merhar et al., 2015). As there is no cell growth in the *C. elegans* embryo all divisions are therefore blastomeric cleavage divisions (Deppe et al., 1978; Krieg et al., 1978), this leads to the inevitable successively reduction of cell volumes. Most importantly this means that the acquisition of cell fate with respect to size/volume would only be achieved through the appropriate control of daughter sizes through unequal cleavage. For example, that a neuron cell body is far smaller than that of a hypodermal cell.

1.3.4. Unequal Cleavage of the One-Cell *C. elegans* embryo

The first divisions of the *C. elegans* embryo generating the founder blastomeres AB, MS, E, C, D and P4 are both asymmetric and unequal (Nigon et al., 1960; Sulston et al., 1983). Subsequently most divisions in the AB lineages are generally equal (Arata et al., 2015; Fickentscher and Weiss, 2017; Sulston et al., 1983). Whilst those in all P lineages demonstrate greater degrees of size asymmetry than those of AB (Arata et al., 2015; Fickentscher and Weiss, 2017; Sulston et al., 1983), the divisions of C, MS and E themselves are almost entirely equal (Arata et al., 2015; Fickentscher and Weiss, 2017). Across the entire embryo there is a general but small bias in cell size to the anterior daughter (Arata et al., 2015).

Of these divisions the best understood at a mechanistic level is that of the one-cell embryo. Cortical asymmetry of the one-cell embryo is established by mutual repression by two complexes of PAR proteins, the anterior composed of PAR-3, PAR-6 and the atypical protein kinase C PKC-3 and the posterior of PAR-1 and PAR-2 (Beatty et al., 2010; Kemphues et al., 1988; Tabuse et al., 1998). Downstream of this polarity is the localisation of the cleavage plane and asymmetric pulling forces on spindle poles (Grill et al., 2001). This is achieved through complementary mechanisms at the either anterior or posterior end of the cell. Force generation requires a cortically localised dynein anchoring ternary complex of GOA-1/Gα, GPR-1/2/GoLoco and LIN-5/NuMa (Lorson et al., 2000; Nguyen-Ngoc et al., 2007; Park and Rose, 2008; Srinivasan et al., 2003). The localisation of LIN-5 is biased to the posterior half of the cell with this, and its association with GPR-1/2, controlled by phosphorylation by PKC-3 (Galli et al., 2011; Park and Rose, 2008; Portegijs et al., 2016). Also downstream of PAR polarity is the establishment of a cortical band of LET-99 in the posterior (Wu and Rose, 2007; Wu et al., 2016). Although the precise mechanism is unknown, this LET-99 band is associated with the exclusion of the GOA-1-GPR-1/2-LIN-5 complex (Tsou et al., 2003), leading to the generation of posterior biased pulling force (Krueger et al., 2010) (Figure 1.7). Of the members of the ternary complex, LIN-5 appears to be most critical component for the generation of force and the GOA-1-GPR-1/2 complex for cortical anchoring (Fielmich et al., 2018). Recently it has also been demonstrated that the tumour suppressor APC homologue APR-1 is localised to the anterior cortex by PKC-3 and acts to attenuate force generation by the anterior mitotic spindle by stabilised microtubules (Sugioka et al., 2018). The unequal nature of the division is required for the appropriate segregation of fate determinants. For example disruption of PAR proteins or LET-99 leads to the appropriate localisation but not segregation of the P granules, the determinant of the germline, to the posterior daughter (Kemphues et al., 1988; Rose and Kemphues, 1998; Strome and Wood, 1982).

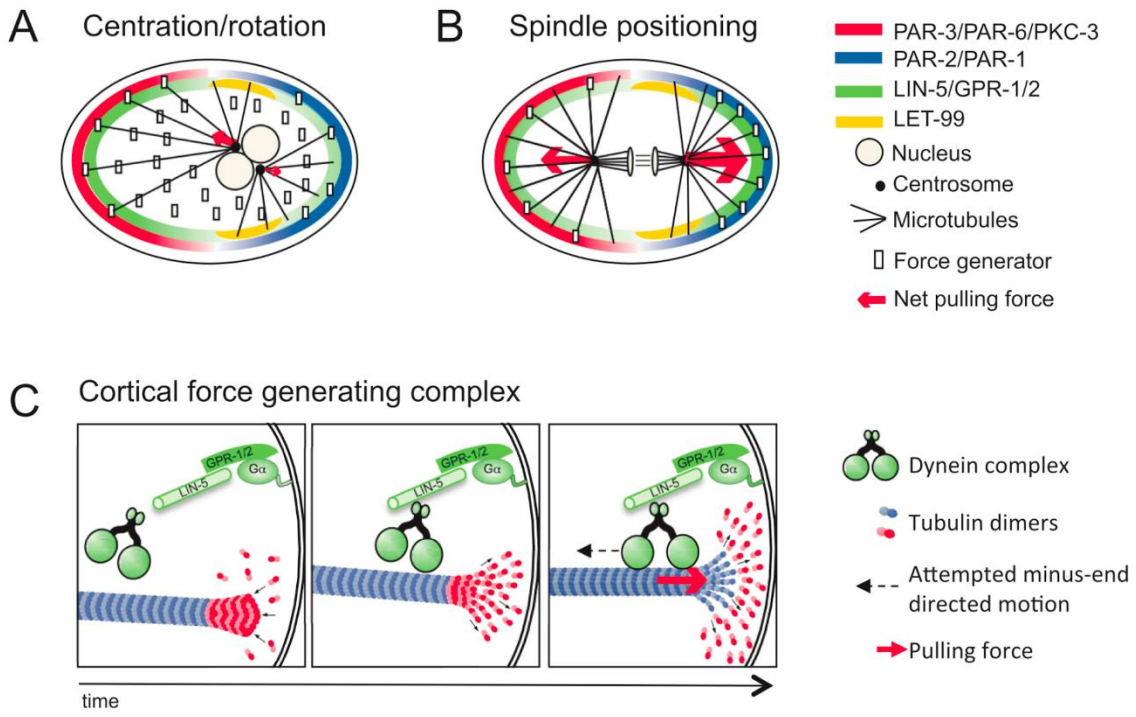

Figure 1.7. Force generation in the unequal cleavage of the C. elegans one-cell embryo. *Stages of unequal cleavage of the one-cell embryo. A) Centration B) Spindle positioning. The cortical band of LET-99 which excludes the ternary complex from the cortex is indicated in yellow. The size of the red arrow indicates the magnitude of the pulling force. C) Representation of how the ternary complex is generally thought to interact with dynein in order to exert force on microtubes. (Adapted from Rose and Gönczy, 2014).*

1.3.5. Asymmetric Division and Unequal Cleavage of *Drosophila* Neuroblasts

In most common embryonic *Drosophila* neuroblasts are called Type I neuroblasts which divide asymmetrically to produce another neuroblast through self-renewal, and a ganglion mother cell which itself divides to produce two neurons. This asymmetric division in *Drosophila* neuroblasts requires the establishment of cortical polarity for correct segregation of fate determinants and the orientation of the mitotic spindle. Two protein complexes are apically located in neuroblasts. The first of these is the apical Par complex comprised of Bazooka-Par-6-aPKC (PAR-3-PAR-6-PKC-3) which is inherited from the neuroepithelium (Rolls et al., 2003), and the second is Gαi-Pins-Mud (GOA-1/2-GPR-1/2-LIN-5) described above in the *C. elegans* one-cell embryo division. Inscuteable acts as adaptor protein linking the two complexes through interactions with Pins (Schaefer et al., 2000; Yu et al., 2000) and Bazooka (Schober et al., 1999). An opposing basal domain is defined by Numb, Prospero and Miranda, whose asymmetric inheritance is required for the segregation of neuronal fate into the GMC. Exclusion from the apical domain and localisation to the basal domain requires, in part, phosphorylation by aPKC and the resultant change in membrane binding affinity (Atwood and Prehoda, 2010; Bailey and Prehoda, 2015; Smith et al., 2007). One of these proteins, Numb, is then localised to the basal domain partly by an adaptor protein Pon (Partner of Numb) (Lu et al., 1998; Rhyu et al., 1994; Uemura et al., 1989). The coiled-coiled protein Miranda localises Prospero and Brat by tethering them to basal cortex through the adaptor protein Staufen (Matsuzaki et al., 1998; Shen et al., 1997; Shen et al., 1998), which acts to prevent Prospero activating its transcriptional targets. Following division, it is inherited only by the GMC (Hirata et al., 1995; Ikeshima-Kataoka et al., 1997). In the GMC, Numb acts as a Notch antagonist (Frise et al., 1996; Guo et al., 1996) by supressing endosomal recycling of Notch receptors (Johnson et al., 2016). Prospero and Brat promote neuronal differentiation and repress cell cycle and self-renewal related gene expression (Betschinger et al., 2006; Choksi et al., 2006; Doe et al., 1991; Southall et al., 2009).

Mechanistically the unequal division of the *Drosophila* neuroblasts is achieved through two parallel mechanisms: one spindle-dependent and one spindle-independent. Both appear to be required for correct cleavage plane placement and are spatiotemporally regulated such that the spindle-dependent mechanism acts after the spindle-independent mechanism (Roth et al., 2015). The spindle-dependent mechanism is reliant on parallel actions of the two apical complexes specifically Baz and aPKC and, Gαi-Pins-Mud. Correct apical localisation of these components is

required for the preferential elongation of apical spindle dependent on G protein signalling which as a result positions the cleavage plane towards the basal pole (Bowman et al., 2006; Cai et al., 2003; Fuse et al., 2003). Whilst apical complex components are required for cleavage plane positioning, loss of components leads to loss of polarity and abnormal segregation of fate components, partially due to additional loss of spindle orientation (Bowman et al., 2006; Cai et al., 2003; Fuse et al., 2003). Embryos mutant for G proteins *Gβ13F* and *Gγ1* however, segregate determinants in a near *wild type* proportion in equalised first neuroblast divisions (Fuse et al., 2003; Izumi et al., 2004; Kitajima et al., 2010). This decreased volume results in neuroblasts entering a quiescent fate after generating fewer GMCs from fewer rounds of division than *wild type* neuroblasts (Fuse et al., 2003; Kitajima et al., 2010). These abnormally large GMCs appear to differentiate normally (Kitajima et al., 2010), suggesting cell size is not a primary driver of neuronal differentiation and instead controls the proliferation rate of the neuroblast.

Whilst not completely understood the spindle-independent mechanism requires contraction of the basal cortex and is dependent on non-muscle myosin II (Cabernard et al., 2010). Prior to nuclear envelope breakdown Rok kinase causes the enrichment of myosin at the cortex (Tsankova et al., 2017), Another kinase, Pkn is recruited to the apical domain by Pins and is required for clearing of cortical myosin in the region, which flows basally towards the cleavage furrow (Connell et al., 2011; Roubinet et al., 2017; Tsankova et al., 2017). This clearing of myosin and a build-up of hydrostatic pressure causes the expansion of the apical cortex (Pham et al., 2019; Roubinet et al., 2017). After a delay of around a minute, basal myosin is also cleared from the cortex and flows apically contributing to cleavage furrow formation (Roubinet et al., 2017). This delay compared to the clearing of myosin in the apical pole, contributes to size differences in cortical expansion (Connell et al., 2011; Roubinet et al., 2017). This also contributes to the basal localisation of Miranda as the formation of the cleavage furrow and clearing of myosin from the basal cortex helps force Miranda into the future GMC (Barros et al., 2003). The regulation of myosin ultimately contributes to daughter cell size asymmetry as part of an unequal cleavage mechanism that works together with the asymmetric position of the spindle described above.

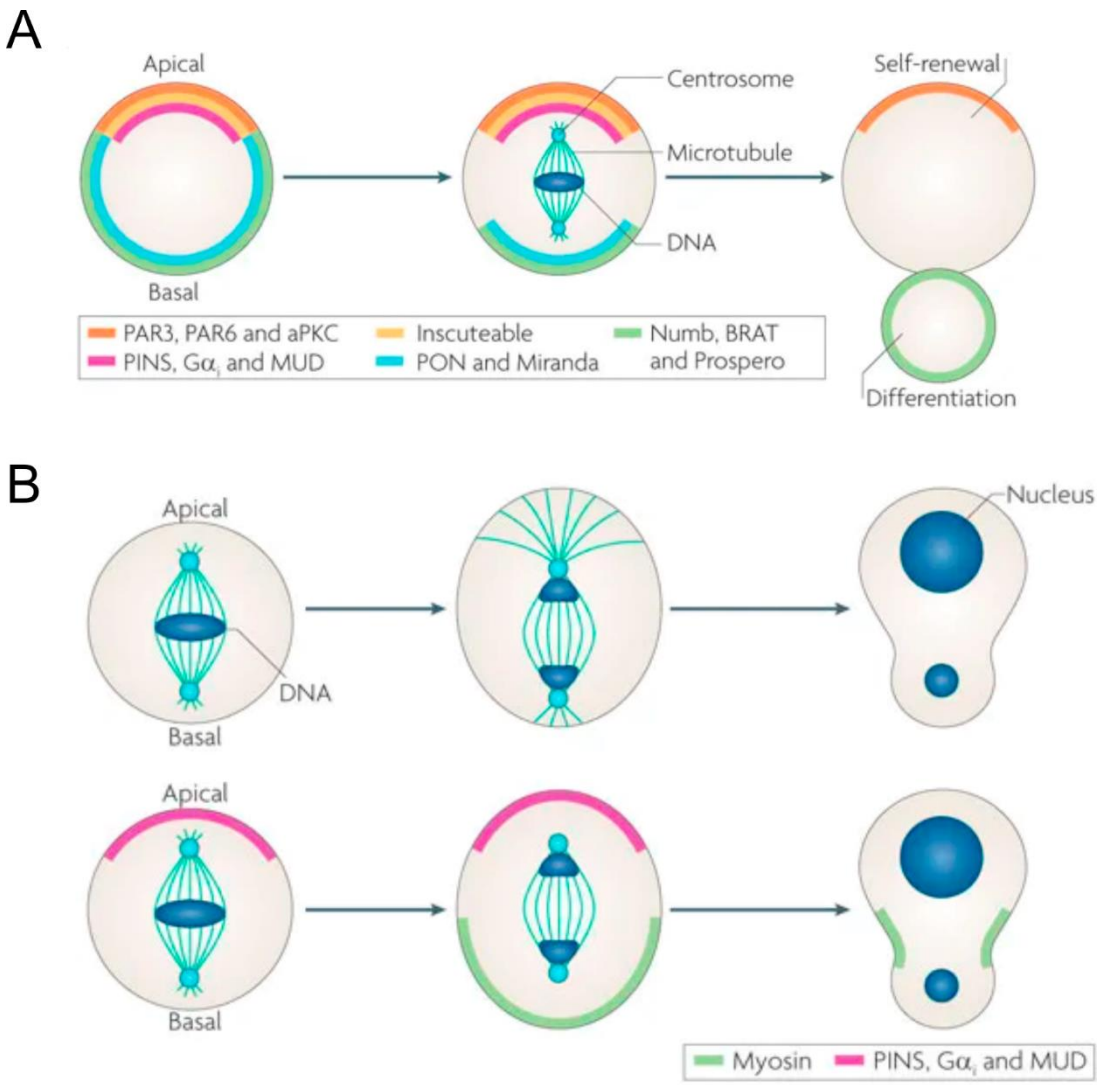

Figure 1.8. Unequal cleavage of *Drosophila* neuroblasts. *A) Polarity in the neuroblast is established by two opposing protein complexes. The two apical complexes are indicated as crescents at the top of the cell, linked by a third band representing the adapter protein Inscuteable. The basal complex is represented in green and is inherited by the smaller daughter which differentiates and becomes a GMC. The larger daughter remains a neuroblast. B) The two parallel mechanisms by which Drosophila neuroblasts generate asymmetric daughter. The first by preferential elongation of the apical spindle microtubules, which moves the cleavage plane basally. The second demonstrating the clearing of myosin firstly from the apical and then the basal cortex, flowing towards the cleavage furrow. (Adapated from Knoblich, 2010).*

1.3.6. Unequal Cleavage in *C. elegans* Neuronal Lineages

In the context of neuronal specification, the study of unequal divisions in *C. elegans* has focused on neuroblast divisions, and in particular on terminal neuroblast divisions producing a smaller daughter cell that it is fated to die. In these contexts the unequal cleavage has been explored by studying regulators that include the MELK kinase homologue, PAR-1 related serine-threonine kinase PIG-1 (Cordes et al., 2006) and the STOX1 transcription factor HAM-1 (Desai et al., 1988; Guenther and Garriga, 1996) and the segregation of apoptotic versus neuronal fate. Whilst widely implicated in such divisions, for example see Teuliere et al, 2018, the role of HAM-1 and PIG-1 as mainly been investigated for its role in three neuroblast lineages which provide different insights into the actions and regulation of both molecules. These are the PVQ/HSN/PHB (Guenther and Garriga, 1996) and NSM neuroblasts (Wei et al., 2017) in the embryo and in the Q lineage neuroblasts during larval development (Teuliere et al., 2014).

In the PVQ/HSN/PHB lineage both *ham-1* and *pig-1* are required for the correct unequal cleavage of the HSN/PHB neuroblast which normally produces a smaller anterior daughter fated to die and a posterior cell which divides to produce PHB and HSN. The cleavage plane is equalised in *pig-1* mutants leading to daughters of equal size (Cordes et al., 2006), and equal or often reversed in *ham-1* mutants (Cordes et al., 2006; Frank et al., 2005; Guenther and Garriga, 1996). This equalisation or reversal is thought to lead to inappropriate survival of the normally dying cell by the incorrect segregation of apoptotic factors (Cordes et al., 2006; Guenther and Garriga, 1996). This leads to the to the adoption of its sister's fate in the inappropriately surviving cell resulting in extra HSN and PHB neurons. Whilst size is affected in almost all mutants the penetrance of either extra or missing neurons is often less than 30%, which is however exacerbated in cell death mutants such as the *ced-3* mutants (Cordes et al., 2006). Furthermore, the reversal of daughter size asymmetry in *ham-1* mutants can result in the absence of HSN and PHB neurons as cells adopt neither neuronal fate nor undergo apoptosis (Cordes et al., 2006; Guenther and Garriga, 1996). *pig-1* appears to be epistatic to *ham-1* in the lineage (Cordes et al., 2006), whilst both must act downstream of the initiation role of proneural gene *hlh-14* in PVQ/HSN/PHB (Frank et al., 2003).

In contrast to the case of the HSN/PHB neuroblast more is understood about the regulation of *pig-1* and its relationship to the control of cell size in the NSM neuroblast division. This division produces a larger daughter which becomes the serotonergic motor neuron NSM and a smaller

sister cell fated to die. Here the bZip transcription factor CES-2, a HLF homologue, acts as a negative regulator of the worm homologue of Snail, *ces-1*, in the NSM lineage (Hatzold and Conradt, 2008). Without repression by CES-2, CES-1 would act as a direct transcriptional repressor of *pig-1* in the NSM neuroblast, leading to cleavage plane equalisation (Wei et al., 2017). This is demonstrated by the equalisation of the cleavage plane resulting from *ces-2* loss of function, *ces-1* gain of function and/or in *pig-1* mutants (Hatzold and Conradt, 2008; Wei et al., 2017). Interesting, although not reported in other lineages, *pig-1* mutants, in addition to *ces-1* and *ces-2*, display a randomisation of cleavage plan orientation in addition to being unequal (Hatzold and Conradt, 2008; Wei et al., 2017). Also unlike other lineages equalisation by *pig-1* has only a very modest effect on the sister cell death of NSM, with only 2.1% inappropriately surviving (Wei et al., 2017), fewer than for inferred for HSN/PHB (Cordes et al., 2006; Frank et al., 2005).

Another well studied lineage in which unequal cleavages are evident is that of the larval Q neuroblast lineage. As described in the section of this introduction concerning proneural genes, Q divides asymmetrically. Q.a also divides asymmetrically producing an anterior cell death and the neuron A/PQR. Q.p divides asymmetrically into a cell which produces the A/PVM and SDL/R neurons and a posterior cell death (Sulston and Horvitz, 1977). An interesting feature of the Q lineage is that the unequal cleavages of Q.a and Q.p are controlled by different mechanisms. At metaphase Q.a has centrally located mitotic spindle yet an anterior bias in the distribution of cortical non-muscle myosin (NMY-2) leading to greater cytoplasmic displacement to the posterior and so a larger posterior daughter. Conversely Q.p has uniform myosin distribution but spindle displacement towards the posterior leading to a posterior biased cleavage plane and smaller posterior daughter (Ou et al., 2010). The result of both of these cases is that it is the smaller daughter which dies (Ou et al., 2010; Sulston and Horvitz, 1977). In Q.a PIG-1 regulates the unequal distribution of NMY-2 in the contractile ring (Ou et al., 2010), requiring transcriptional activation by HAM-1 (Feng et al., 2013). The proneural gene acts either upstream or in parallel to this PIG-1/HAM-1 pathway as *lin-32* mutants demonstrate equalised NYM-2 distribution and Q.a cleavage (Zhu et al., 2014). This correlates with its effect on ectopic A/PQR neurons from the erroneous survival of the would-be apoptotic anterior daughter (Zhu et al., 2014). Also correlating with its lack of impact on terminal Q.p fates, *lin-32* is not required for control of unequal cleavage of Q.p (Zhu et al., 2014), nor is *ham-1* (Feng et al., 2013). In a contrasting role to that in Q.a *pig-1* is required for posterior biased spindle positioning in in Q.p (Chien et al., 2013), with the Q.pa/pp

volume ratio reduced from around 3:1 to 1.2:1 in *pig-1* mutants (Chien et al., 2013; Cordes et al., 2006; Mishra et al., 2018). Whilst PIG-1 mediated control of unequal cleavage is required on both sides of the Q lineage loss of unequal cleavage is far more frequent than the adoption of sister fates in daughters that would normally apoptose indicating that size is not the sole mechanism of fate segregation in either sub-lineage (Mishra et al., 2018; Zhu et al., 2014). Moreover, in Q.p PIG-1 appears to be responsible both for cleavage plane positioning and the establishment of a gradient of mitotic potential towards the anterior, in opposition to the posterior biased *ced-1* dependent apoptotic gradient of CED-3 caspase (Mishra et al., 2018). The loss of this gradient and the equal cleavage plane allows both daughters to divide and produce multiple neurons, a phenotype enhanced by the increased survival in cell death pathway component, *pig-1* double mutants (Mishra et al., 2018). Intriguingly members of the apoptotic pathway also have a *pig-1* independent, yet evidently milder, effect on the degree of unequal cleavage in the Q.p division and thus dual effect on the segregation of mitotic/apoptotic fates (Mishra et al., 2018).

The mechanism by which HAM-1 acts to regulate unequal cleavages is not entirely clear however it has been demonstrated to localise to the cell cortex in a crescent and subsequently be asymmetrically inherited in one daughter, usually that which survives (Frank et al., 2005; Guenther and Garriga, 1996). In addition to cortical localisation the HAM-1 sequence contains two nuclear localisation sequences (Leung et al., 2016) and it is suggested to act as a transcriptional regulator of *pig-1*, being able to bind its promoter region (Feng et al., 2013). Moreover, the interaction between *pig-1* and *ham-1* is not required in all unequal cleavages in which one or the other is implicated. For example correct URX neuron development requires *ham-1* yet not *pig-1* (Romanos et al., 2017), whereas *pig-1* and not *ham-1* is involved in the Q.p divisions (Chien et al., 2013; Feng et al., 2013). Furthermore, whilst to date *pig-1* is the only HAM-1 target identified genetically, *pig-1* is known to be transcriptionally regulated by the SP1 transcription factor SPTF-3, and this regulation is required for AQR, I2 and M4 neurons (Hirose and Horvitz, 2013). As noted above, PIG-1 itself is a kinase which is activated through phosphorylation of its T loop at an evolutionary conserved residue for MELK related kinases (Beullens et al., 2005; Chien et al., 2013; Denning et al., 2012; Lizcano et al., 2004). This phosphorylation occurs through PAR-4, the tumour suppressor kinase LBK1 homologue, which requires STRD-1/STRAD and MOP-25.2/MO25 in complex, as it does in vertebrates (Chien et al., 2013; Denning et al., 2012). Mutation of any of which also causes equalisation of Q.pa/Q.pp

(Chien et al., 2013). However, whilst during Q lineage divisions PIG-1 is seen to localise at centrosomes (Chien et al., 2013), in the one-cell embryo it associates with the cortex where is may be involved in cleavage plane placement by controlling myosin distribution (Pacquelet et al., 2015) in a similar manner to that seen in the Q.a division (Ou et al., 2010).

Part IV

1.4.1. The C Lineage

In this section I will describe the C lineage, the subject of the work in this thesis, in terms of both its lineage pattern and what is known about regulation of fate and neurogenesis in the lineage. The C lineage is so called as it is descended from one of the five somatic founder blastomeres of the *C. elegans* embryo; AB, MS, E, C and D, with the germline descending from P4 (Laufer et al., 1980; Nigon et al., 1960) (Figure 1.9) The style of this nomenclature was established during the very beginnings of nematode embryology (Boveri, 1899).

The patterns and timings of divisions in the C lineage were first elucidated during studies in the 1970s and 1980s, being finalised in the seminal work of John Sulston and colleagues in characterising the entire cell lineage of the embryo (Deppe et al., 1978; Krieg et al., 1978; Sulston et al., 1983). The initial division of the C blastomere produces two daughters, Ca and Cp which give rise to the two halves of what is a near-bilaterally symmetric lineage. Ca produces descendants for the left-hand side of the body whereas Cp produces a near bilaterally symmetrical set of cells for the right-hand side (Schierenberg, 1986; Sulston et al., 1983). The first division of both daughters of the C blastomere represents the segregation of fate between hypodermal in the anterior half and muscle in the posterior half. Cpa undergoes three rounds of symmetric division yielding four pairs of hypodermal cells of which seven cells eventually fuse as part of the hyp7 syncytium (Podbilewicz and White, 1994; Sulston et al., 1983), with the last cell, hyp11, a separate tail hypodermal cell. In contrast, the Cpp lineage comprises eight pairs of muscles cells produced from four rounds of division (Sulston et al., 1983). The bilaterally homologous half of the lineage descended from Ca is nearly identical to that of Cp save two neurons, DVC and PVR, and a cell death in place of three of the hypodermal cells. Both neurons descend from the same branch of the would-be all hypodermal part of the Ca lineage, Caap. Caapaa and Caapap become DVC and its sister cell death respectively, PVR arising from Caappa whose sister is a hyp7 hypodermal cell, rather than hyp11 as with its bilateral Cp homologue. An additionally asymmetry evident only in the Ca lineage is the elongated cell cycle duration of the DVC neuroblast Caapa, resulting in it dividing around thrice as late as either its bilateral homologue or other hypoblasts (Sulston et al., 1983) (Figure 1.10).

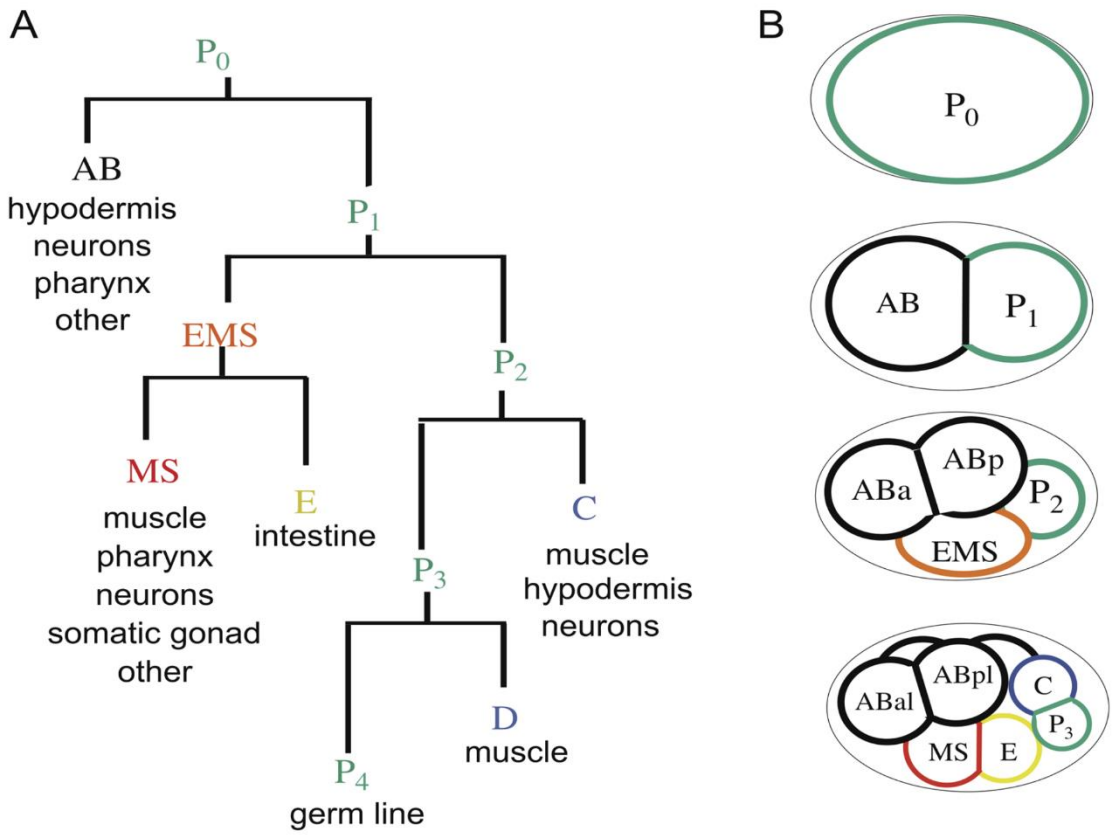

Figure 1.9. Founder blastomeres and cell lineages of *C. elegans.* *A) Lineage diagram illustrating the relative birth times of the founder blastomeres and their mother cells. Cell types that arise from each lineage are listed below each founder cell. B) Illustration of blastomere positions in the developing C. elegans embryo. The coloured outline and name of the blastomere correspond to the lineage diagram in A). (Adapted from Wormbook)*

1.4.2. Specification of the C Blastomere

The identity of the C blastomere is specified by the homeobox transcription factor PAL-1 (Hunter and Kenyon, 1996), the *C. elegans caudal* homologue and known regulator of posterior fates including in worms, i.e. (Edgar et al., 2001; Hunter and Kenyon, 1996; Waring and Kenyon, 1990). PAL-1 activity is restricted C and D blastomeres through a series of interactions between a number of maternally deposited factors.

Maternally deposited *pal-1* mRNA is uniformly distributed in embryos until the latter part of the 4-cell stage when it is becomes restricted to EMS and P2 (Hunter and Kenyon, 1996). This restriction is achieved though *pal-1* 3'UTR mediated translational repression by the regulator of AB fate, the KH domain protein MEX-3 (Hunter and Kenyon, 1996; Pagano et al., 2009). AB fate requires MEX-3, with the eight AB great-granddaughters transformed into C-like cells in the *mex-3* mutants. This repression is spatiotemporally limited to the AB blastomere as in the 1-cell embryo both *mex-3* mRNA and MEX-3 protein accumulate in the anterior of the cell and are preferentially segregated to the AB blastomere yet both are lost after four cell stage (Draper et al., 1996; Hunter and Kenyon, 1996).

In EMS, repression of PAL-1 is achieved through the regulator of EMS fates the bZIP transcription factor SKN-1 which first accumulates at higher levels in the P1 nucleus and is preferentially segregated to the same posterior blastomeres and lost by the eight cell stage (Bowerman et al., 1992; Bowerman et al., 1993). This repression is spatiotemporally regulated to EMS by repression of SKN-1 itself by the germline fate determinant PIE-1 (Mello et al., 1992). PIE-1 is segregated into the posterior most blastomeres by sequential divisions and is thus variously active in P1, P2, P3 and P4 (Mello et al., 1996). Importantly this segregation is accompanied by inhibition of zygotic gene expression (Seydoux et al., 1996). Therefore, at the four-cell stage the EMS/P2 division segregates PIE-1 to P2 and allows active SKN-1 to initiate EMS fates and to repress PAL-1 in EMS (Bowerman et al., 1992; Hunter and Kenyon, 1996; Mello et al., 1992; Mello et al., 1996). At the eight-cell stage PAL-1 is derepressed in C by a combination of PIE-1 segregation to P3 and the degradation of SKN-1 at the eight-cell stage, thus allowing PAL-1 activity in C and its descendants (Bowerman et al., 1993; Hunter and Kenyon, 1996; Mello et al., 1996).

The zygotic expression of *pal-1* begins at the 24 cell stage where is enriched in the daughters of the C blastomere Ca and Cp (Hunter and Kenyon, 1996), is activated by maternal PAL-1 (Baugh et al., 2005a) and maintained in C descendants until the end of gastrulation (Edgar et al., 2001).

1.4.3. The Hypodermal/Muscle Fate Decision in the C Lineage

The patterning of these fates in the C lineage appears to be cell autonomous and downstream of PAL-1 in its role in specifying the C blastomere. Given the near functional and lineal symmetry of the C lineage there has been little insight into what distinguishes Ca from Cp, with single cell transcriptomic studies showing little agreement in supposed informative transcripts and/or often unable to distinguish Ca from Cp (Cao et al., 2017; Hashimshony et al., 2012; Murray et al., 2012; Packer et al., 2019; Tintori et al., 2016; Xu and Su, 2014).

In contrast much work has focussed on the hypodermal vs muscle fate decisions at the Caa/Cap and Cpa/Cpp divisions. A crucial distinction between the lineages is the *C. elegans* Wnt/β-catenin asymmetry pathway described earlier in this chapter in controlling binary fate choices. In asymmetric divisions anterior daughters accumulate nuclear POP-1 and posterior daughters cytoplasmic POP-1 (Kaletta et al., 1997). Low levels of nuclear POP-1 are required for PAL-1 dependent myogenesis in the posterior lineages Cap and Cpp (Fukushige and Krause, 2005). This myogenesis is controlled by the *C. elegans MYOD1* homologue, the bHLH transcription factor *hlh-1* which is expressed in all body wall muscle (Chen et al., 1994; Krause et al., 1990) and was demonstrated to be sufficient to initiate a muscle like programme using a heat-shock inducible promoter (Fukushige and Krause, 2005). Expression of *hlh-1* is directly downstream of *pal-1* with expression first detected at the 8C cell stage in the Cap and Cpp daughters (Baugh et al., 2005a; Fukushige and Krause, 2005) and declining at the 31C cell stage (Yanai et al., 2008). Following initiation by PAL-1, HLH-1 binds the same enhancer in its own regulatory region to maintain its own expression (Lei et al., 2009). This autoregulation forms part of a stable regulatory module for muscle specification involving two more *pal-1* targets, bHLH transcription factor *hnd-1* and the MADS family transcription factor *unc-120* which are also expressed beginning at the 4C and 8C cells stage respectively and are synthetically lethal (Baugh et al., 2005a; Baugh et al., 2005b; Mathies et al., 2003; Yanai et al., 2008). Whilst the precise topology is unclear, RNAi knockdown of the components of the module in turn suggest that *hlh-1* positively regulates itself,

hnd-1 and *unc-120*, that these negatively regulate *hlh-1,* and that *hnd-1* is temporally upstream of initial *hlh-1* expression (Baugh et al., 2005a; Fukushige et al., 2006; Yanai et al., 2008).

Importantly the muscle module discussed above demonstrates mutual repression with an epidermal module which acts to specify the hypodermal branches Caa and Cpa (Yanai et al., 2008). This epidermal module centres on a the factor that specifies the embryonic epidermis, the GATA transcription factor *elt-1*, which is initially expressed in all four C granddaughters at the 8C cell stage and is only maintained in Caa an Cpa and their descendants (Page et al., 1997). As with the muscle module, *elt-1* is a downstream target of *pal-1* (Baugh et al., 2005a; Yanai et al., 2008) and its loss in the muscle branches is likely due to transcriptional repression by the muscle module transcription factors. This is because their knockdown results in the upregulation of ELT-1 targets (Yanai et al., 2008). These direct downstream targets are the GATA transcription factor *elt-3*, nuclear receptor *nhr-25* and ZF transcription factor *lin-26* and are expressed at the 8C cell stage, one cell cycle after *elt-1* (Baugh et al., 2005a; Yanai et al., 2008). These form a module in which enact hypodermal specification (Yanai et al., 2008). In this role LIN-26 acts to maintain hypodermal fate, its loss causing hypodermal disorganisation and eventually non-apoptotic necrosis (Labouesse et al., 1994). NHR-25 likewise appears to have a non-essential role for initial specification of hypodermal specification (Asahina et al., 2000; Gissendanner and Sluder, 2000) with its predicted targets implicating it in maintenance of hypodermal fate (Shao et al., 2013). Furthermore, whilst expressed in body wall muscle and sufficient to drive hypodermogenesis, deletion of *elt-3* demonstrates a non-essential role (Gilleard and McGhee, 2001; Gilleard et al., 1999).

How POP-1 interreacts with these modules directly is currently unconfirmed and it could conceivably act to repress the muscle module genes in the anterior or activate them in the posterior cell at the hypodermal/muscle switch. However, as POP-1 has putative binding sites in the regulatory regions for *hnd-1, hlh-1* and *unc-120* (Yanai et al., 2008), this interaction may be direct.

Patterning of the lineage is further refined in an anterior-posterior manner. Expression of the homeobox transcription factor and *eve* homologue *vab-7* is required in the lineage to impart posterior fates in both hypodermal and muscle branches and is expressed in Caap, Capp, Cpap and Cppp and their daughters. Its loss in hypodermal branches results in the transformation to more anterior yet still hypodermal fates, and to muscle disorganisation (Ahringer, 1996). The

expression of *vab-7* is controlled downstream of *pal-1* (Baugh et al., 2005a) and positively regulated by the redundant T-box transcription factors *tbx-8/9* (Pocock et al., 2004; Yanai et al., 2008) which have an additional later role in correct dorsal intercalation of hypodermal cells (Andachi, 2004; Pocock et al., 2004).

1.4.4. Neurogenesis in the C Lineage

The proneural gene required for neurogenesis in the lineage is the bHLH transcription factor and *achaete-scute* homologue, *hlh-14* (Frank et al., 2003). Expression of *hlh-14* is detected in Caappa (PVR) itself following the division of Caapp and in the DVC neuroblast Caapa after around a third of the cell cycle which persists in both daughters Caapaa and Caapap after division (Frank et al., 2003; Poole et al., 2011). *hlh-14* mutants demonstrate an obvious loss of neurogenesis in the C lineage with the would-be neuroblasts and cell death adopting a hypodermal fate and indeed migrating laterally to sit adjacent to the endogenous hypodermal cells. In addition to adopting hypodermal fate the would-be neuroblast Caapa divides precociously at a similar time to the other hypoblast divisions suggesting that either *hlh-14* directly or some aspect of the neuronal fate regulates division timing (Poole et al., 2011) (Figure 1.11)

The direct downstream targets of *hlh-14* expression in the C lineage neuroblasts and how these relate to later stages of neurogenesis are currently unknown. Recently however, expression of *ztf-11*, the *C. elegans* homologue of *Myt1*, has been reported in the C lineage (Lee et al., 2019a). *Myt1* is a known repressor of non-neuronal fates in vertebrates through the inhibition of Notch signalling. *ztf-11* is expressed in the Caapa, the DVC neuroblast, from about a third of the way through its cell cycle and in the PVR precursor, Caapp, beginning at the same time just prior to its division (Lee et al., 2019a). This timing of expression is similar to the onset of *hlh-14* expression, especially in the DVC neuroblast (Poole et al., 2011), and whilst not tested for HLH-14, *ztf-11* was confirmed to be a target of another proneural bHLH transcription factor LIN-32 (Lee et al., 2019a), suggesting similar regulation by HLH-14 in the C lineage.

Further downstream, classification of DVC as glutamatergic based on the expression of *eat-4/VGLUT* and thus its terminal identity are known to be controlled by the LIM-homeodomain transcription factor *ceh-14* (Cassata et al., 2000; Kagoshima et al., 2013; Pereira et al., 2015; Serrano-Saiz et al., 2013). Downstream of this terminal selector a few members of the DVC

terminal transcriptional cascade have been identified, although their regulatory relationships remain unclear. Expression of the homeodomain transcription factor *ceh-63* is downstream of *ceh-14,* and another unidentified compensatory factor, with the loss of either leading to the loss of the helix-turn-helix transcription factor *mbr-1.* No targets further downstream of this network have been identified (Feng et al., 2012). Functionally, whilst DVC has long been known to be an interneuron with its cell body within the dorsal-rectal ganglion (White et al., 1986), its specific function had proven elusive (Feng et al., 2012). More recently DVC has been shown to be excitatory to reversal behaviour through studies employing optogenetic activation of DVC (Ao et al., 2019) and disruption of *eat-4/VGLUT* (Ardiel and Rankin, 2015). DVC does not receive inputs from sensory neurons (White et al., 1986). However, expression of mechano-sensation channel *trp-4* and a large array of *C. elegans* gap junction innexins *inx-4/5/7/9/10/11/13/17/18, unc-7a/b* and *unc-9* along its process suggest it may integrate mechano-sensation signals from across the length of the animal's body (Altun et al., 2009; Ardiel and Rankin, 2015; Bacik et al., 2016).

The other C lineage neuron PVR is also a tail neuron, with its cell body situated in the right-lumbar ganglion (White et al., 1986). PVR is of uncertain function but may be part of the touch sensitivity circuit (Chalfie et al., 1985). Like DVC, PVR is a glutamatergic neuron, as confirmed by the expression of *eat-4/VGLUT* (Lee et al., 1999; Serrano-Saiz et al., 2013). PVR also shares a terminal selector with DVC, with its terminal identity controlled by expression of *ceh-14* (Cassata et al., 2000; Kagoshima et al., 2013; Serrano-Saiz et al., 2013), in a redundant fashion with the POU transcription factor *unc-86* (Serrano-Saiz et al., 2013). Expression of *unc-86* follows asymmetric division of the PVR neuroblast (Finney and Ruvkun, 1990) and is maintained for the lifetime of the cell illustrating its role in maintaining terminal identity (Finney and Ruvkun, 1990; Serrano-Saiz et al., 2013). The expression of FMRFamide neuropeptides *flp-10* and *flp-20* (Kim and Li, 2004; Ringstad and Horvitz, 2008) is downstream of the terminal selectors *unc-86* and *ceh-14* and are also known as terminal markers of PVR fate (Serrano-Saiz et al., 2013).

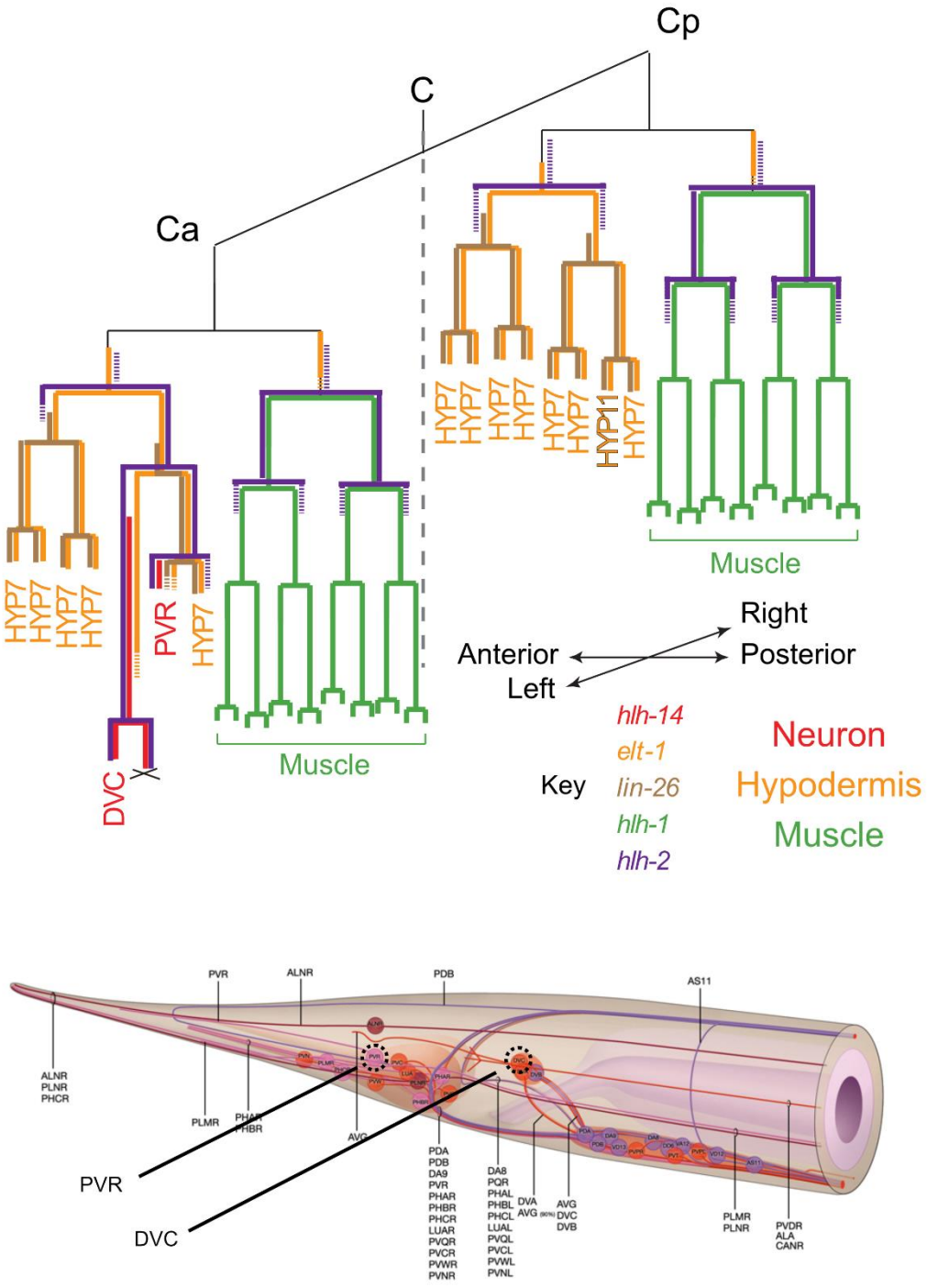

Figure 1.10. The C lineage and C lineage neuron positions. *The lineage diagram for the C lineage with known expression patterns. Terminal fates are indicated underneath terminal branches. Lengths of branches are indicative of relative division timings. Concurrent expression is depicted with one offset with respect to another in order for both to be visible. The two halves of the lineage are offset on an angle as to demonstrate the near bilateral symmetry of the lineage, the dotted line illustrates the mirror line. The lineages divide at the same time despite the offset depiction. A diagram of the tail of a hermaphrodite adult with the positions of the C lineage neurons DVC and PVR highlighted. (Partly adapted from WormAtlas.com)*

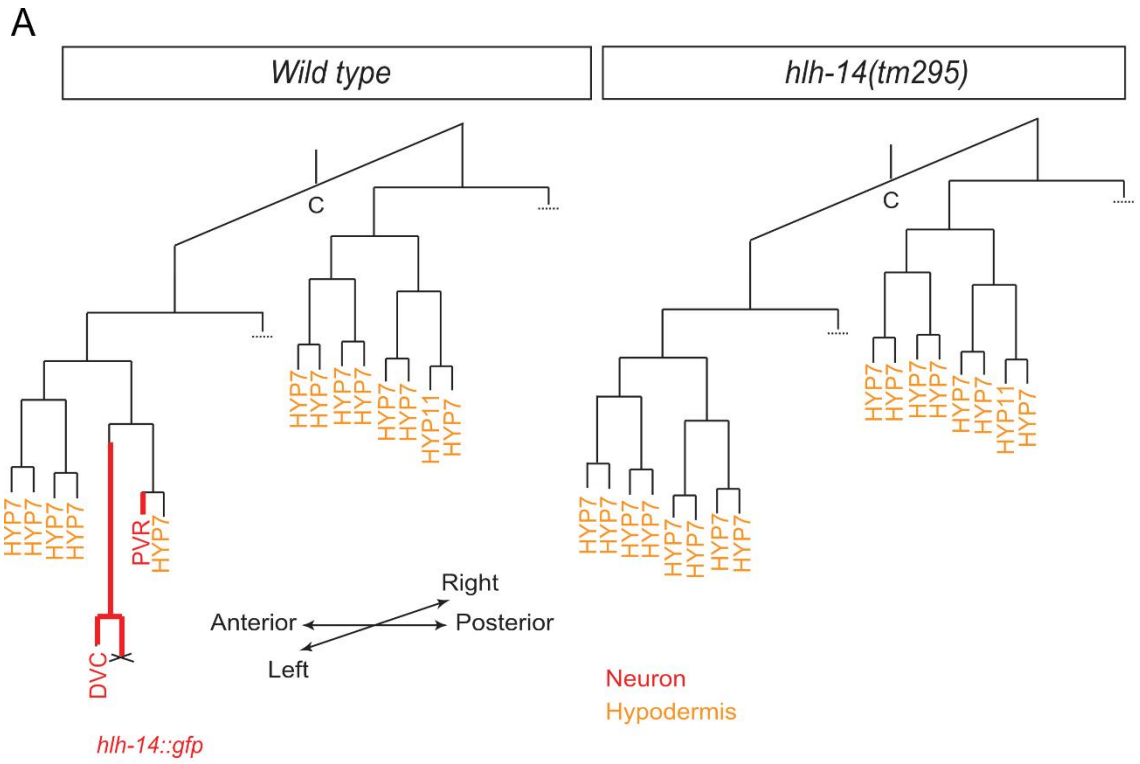

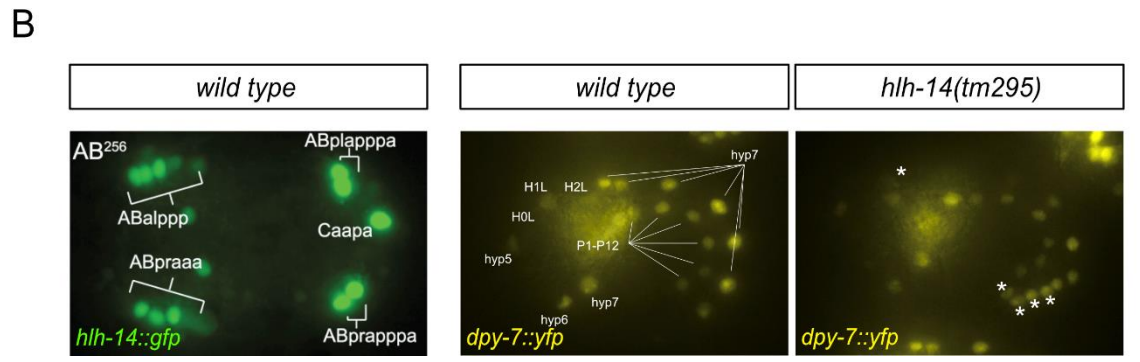

Figure 1.11. C lineage phenotypes of *hlh-14* mutants. *A) lineage diagrams indicating the precocious division of Caapa (the would-be DVC neuroblast). Only hypodermal branches are depicted. Horizontal dotted lines indicate that the lineage beyond that point is not shown. B) A maximum intensity projection of the wild type expression pattern of the hlh-14::gfp transgene gmIs20, embryos in a dorsal-ventral view at the bean stage.. The position of the DVC neuroblast Caapa is indicated. The expression pattern of the hypodermal mark dpy-7::yfp in wild types and hlh-14 mutants. Embryos are in a lateral view at the comma/1.5 fold stage. White stars indicate extra hypoderm cells in the mutant. (Adapted from Poole., et al 2011).*

1.4.5. The C Lineage as a Model for Studying Proneural Gene Regulation and Unequal Cleavages

In contrast to the elucidation of the decision between hypodermal and muscle fates in the C lineage almost nothing is known about the decision between neural and hypodermal fates on the left of the lineage, the Ca lineage. In the lineage this decision appears to occur at the Caaa/Caap given that the descendants of Caaa are four hypodermal cells and those of Caap, the two neurons, a hypodermal cell and a cell death (Sulston et al., 1983). Specifically, this is the first division preceding branches in which the expression of the proneural gene *hlh-14* expression is detected and its two daughters are a neuroblast and hypo-neuroblast (Poole et al., 2011). Whilst evidently the segregation of neuronal fate is refined further by the fact that the mother of PVR is a hypo-neuroblast, this division demonstrates a key decision point in the lineage for the initial segregation of neuronal fates.

Being the only neuronal branch in the C lineage, which is otherwise bilaterally symmetric, the Caap branch therefore represents an attractive model for addressing a number of questions. An obvious question concerns how and when symmetry is broken in the C lineage to result in neurogenesis in the left-hand side of the lineage only. Further to this is the question of how neuronal potential is segregated to the Caap branch downstream of the hypodermal/muscle decision at Caa/Cap. Specifically, the single neuronal branch allows the question of by what mechanism is the expression of the proneural transcription factor *hlh-14* initiated and regulated in the lineage.

Furthermore, this single neuronal branch highlights the C lineage as an attractive model for the study of proneural gene regulation in worms more generally. The small number of neurons allows for rapid assessment of neuronal fate at the level of an entire founder lineage, something not so feasible in the AB lineage. This, and the fact that they are descended from a single branch within an otherwise bilaterally symmetric lineage allows for investigation of fate regulation a multiple lineage levels leading to a defined neuronal branch.

The invariant cell lineage of the worm provides us with the ability to study the decisions leading to proneural gene expression at single cell resolution. This therefore allows investigation of individual asymmetric divisions and how they impact on fate outcome. One aspect of many asymmetric divisions, as discussed in previous sections, is unequal cleavage leading to

asymmetric daughter size. Also as discussed previously, little is known about how fate interfaces with this aspect of cell division. At any given division, unequal cleavage could conceivably be the outcome of an asymmetric division with to-be segregated fate determinants controlling the cleavage or could be controlled separately upstream to bring about an asymmetric division. Indeed, how resultant cell size impacts fate decisions is unclear, yet evidence exists from vertebrate mesenchymal stem cell studies that control of cell volume can direct particular differentiation programs (Bao et al., 2017; Guo et al., 2017; Padovan-Merhar et al., 2015). Is the same true in some of the cleavage divisions of the *C. elegans* embryo? Is unequal cleavage controlled to asymmetrically segregate fate determination factors? Does resultant daughter cell volume direct particular fates with or without asymmetrically localised fate regulators? Once again, the C lineage provides a model to address these questions. Therefore, the general question of the relationship between unequal cleavage, cell volume and cell fate can be asked in the context neuronal fate segregation and the regulation of *hlh-14* in the C lineage.

Part V

1.5.1. Aims of the Project

Given the questions surrounding the initiation of *hlh-14* expression in the C lineage and the outlined advantages of the lineage for studying neurogenesis and the relationship between unequal cleavages/cell volume and cell fate segregation the aims of the project were as follows.

With respect to the C lineage specifically:

1. Confirm whether neurogenesis, and so symmetry breaking, in the C lineage is controlled by lineage-intrinsic or -extrinsic mechanisms.
2. Identify upstream molecular regulators of *hlh-14* in the C lineage.
3. Investigate the role of unequal cleavages in segregating neuronal fate in the C lineage.
    a. Investigate the role of unequal cleavage and cell size on the expression of *hlh-14.*
    b. Determine whether neuronal fate, through HLH-14 itself, controls unequal cleavage.
    c. Investigate whether the same factors that control unequal cleavages control cell fate in the lineage.

By addressing these aims, I sought to further understanding of more general questions.

1. How are proneural genes regulated?
2. What is the role of unequal cleavage in cell fate decisions?
3. Why control cell volume in cleavage divisions if not for fate decisions?

Materials and Methods

Chapter 2

2. Materials and Methods

2.1. General Husbandry and Genetics

2.1.1. Maintenance of *C. elegans* Strains

Maintenance of *C. elegans* strains was undertaken in accordance with established practice in the field, for example see (Stiernagle, 2006). Additional details are as follows. Plates for the maintenance of worm stocks were made with 12ml NGM (Nematode Growth Medium, Recipes section 2.14.) in 55mm diameter petri plates (Gossein), poured using a New Brunswick MP-1000 PourMatic (New Brunswick Scientific) automatic peristaltic plate pourer. A lawn of cultured OP50 strain *E. coli* was used as a food source.

Non-temperature sensitive strains were maintained at 20°C in a temperature-controlled room whilst temperature sensitive strains were maintained in 15°C incubators (Leec).

Picking tools for the transfer of individual worms were fashioned from 0.25mm diameter platinum wire flattened into a shovel at one end with a Pasteur-pipette acting as a handle. A flame was used to gently melt the glass as to seal the wire in place. Worms were transferred using a small amount of OP50 as an adhesive agent on the underside of the flattened shovel-end of a pick to lift them from the plates.

Stocks were passed by one of two methods. Using the chunking method, every 3-4 days for strains at 20°C and every 5-7 days for strains at 15°C, a square of agar was cut from an older plate using a flame-sterilised, steel spatula and placed on the bacterial lawn of a fresh plate. Using the picking method 20 worms of various stages were transferred to a fresh plate every 6-7 days for strains at 20°C and 9-10 days for strains at 15°C.

2.1.2. Generation of Novel *C. elegans* Strains via Crosses

Crosses where performed with a ratio of males to hermaphrodites of 4:1. A small lawn of OP50 was added to the centre of the plate using a pick in place of the large 40µl lawn used on a standard plate.

2.1.3. Population Synchronisation and Cleaning

2.1.3.1. "Egg Prep"

Synchronisation of populations via bleaching was performed using plates full of gravid hermaphrodites. A few ml of 1X M9 buffer was used to wash worms off the plates and collect them into 15 ml falcon tube. Worms were sedimented via centrifugation at 3000 rpm for 2 min. The M9 was aspirated leaving a pellet of worms. In the case that the plates were particularly contaminated this M9 step was repeated as appropriate. 5ml of Egg Prep Solution (Recipes 2.14.) was added to the falcon tube and the tube vortexed at 2 min intervals for a total of 10 mins or until the majority of the adult worms had visibly dissolved. The 15ml falcon tube was filled to maximum with M9 to quench the bleaching reaction. The tube was centrifuged at 3000 rpm for 2 mins to pellet the eggs and the supernatant aspirated. To wash any remaining Egg Prep Solution from the eggs the tube was filled with M9, the tube inverted to dislodge the eggs and re-centrifuged as above. This final washing step was repeated thrice to ensure removal of bleach. Following final aspiration, a glass pipette was used to transfer eggs onto empty, unseeded plates and left to incubate at 20°C. Given the lack of food available on such plates, animals arrested at the L1 stage and were transferred to seeded plates.

2.1.3.2. "Egg Drop"

Population synchronisation/cleaning on a smaller scale was performed via the Egg Drop method. 20 µl drops of a 1:1 solution of 1M NaOH:bleach were added to the surface of an unseeded plate. 10-20 gravid adult hermaphrodites were transferred to the drops via picking. The plates were incubated overnight at 20°C to allow the bodies of the adults to dissolve and eggs to hatch. As with the Egg Prep method, in the absence of a food source larvae arrested at the L1 stage and were subsequently transferred to seeded plates.

2.1.4. Long-term Strain Storage and Freezing of *C. elegans* Strains

Strains were stored cryogenically in 1.8 ml cryotubes both in -80°C freezers and in liquid N_2 using 800µl M9 and 800µl Freezing Solution (M9 Buffer with 30% glycerine (v/v)). See Recipes section 2.14. for M9 Buffer Recipe.

2.1.5. Embryo Collection and Mounting

For general imaging, 4D lineage recordings, laser ablations and slide-based phenotype scoring, embryos were collected using the same method.

For temperature-sensitive strains the following was performed over ice and for non-temperature-sensitive at 20°C. Gravid hermaphrodites were suspended in a 20 µl drop of M9 buffer and bisected using either a scalpel or razor blade through the vulval area around of the body which released embryos into the liquid. Embryos of the appropriate stage were selected and manipulated using an eyelash tool. The eyelash was attached using strong adhesive to a handle of either a narrow piece of doweling or a glass Pasteur pipette. To clean embryos of bacterial and worm debris they were transferred to another 20 µl drop of M9 buffer using a mouth pipette with a hand-pulled ~50 µm (roughly the length of the embryonic long axis) diameter borosilicate tip.

To make a pad for mounting embryos, a drop of either melted 2% agar or agarose (Sigma Aldrich) was flattened between two 76 mm x 26 mm x 1 mm glass microscope slides (Thermo Scientific or Fisherbrand) and the upper slide slid away to leave a smooth pad. The amorphous pad was cut into a square of 5mm x 5mm or smaller using a razor blade to facilitate finding of embryos in a smaller area. Embryos were transferred to, and excess M9 removed from, the pad using a mouth pipette. A 18mm x 18mm coverslip (Fisherbrand) was gently lowered onto the embryos as not to crush them. ~15µl M9 buffer was pipetted under the coverslip to ensure hydration of the embryos leaving a corner of the coverslip unfilled to allow gas exchange between the buffer and air. In order to prevent evaporation of the buffer melted petroleum jelly (Vaseline) was used to seal the coverslip to the microscope slide, applied using a cotton bud.

2.2. Lethality Scoring

The degree of lethality caused by a mutation was assessed via one of two methods.

2.2.1. Embryo Mounting

Embryos were mounted as described in section 2.1.5. and incubated overnight at the appropriate temperature, often at 25°C, the non-permissive temperature for temperature-sensitive mutants. The following day embryos were scored for whether they had either hatched or died and/or arrested during embryogenesis. In order to assess the population, between 50-200 embryos were scored in this manner.

2.2.2. Egg Laying Method

3-5 L4 stage hermaphrodites were singled onto NGM plates and allowed to lay progeny for one day whilst incubated the temperature at which lethality was being assessed. As in the embryo mounting method this was often 25°C for temperature sensitive mutants. L4 larvae were used as to not have any eggs or embryos already within the mother subject to the temperature conditions not being assessed. Following incubation, the now gravid adult was removed and the progeny on each plate assessed for whether they had hatched or arrested and/or died during embryogenesis.

2.3. Laser Ablation

Laser ablations were performed in accordance with a relatively standard protocol, see (Bargmann and Avery, 1995). An Andor Micropoint laser system (Oxford Instruments) was mounted on an Axioplan 2 (Carl Zeiss) imaging microscope and laser firing controlled by a foot pedal trigger. Blastomeres where ablated in the nucleus, moving the stage in the X, Y and Z planes in order to operate on the whole nucleus. Ablation continued until the first signs of bubbling and disintegration could be seen in the nucleus itself. This was sufficient to achieve arrest, continuation beyond this point being too great an insult to the embryo as a whole. Precise aiming was achieved by controlling fine movement of an LEP Bioprecision 99S008-N23 motorised stage with a joystick, controlled by a LEP Modular Automation Controller 2002 control unit (all Ludl Electronic Products). An EXFO X-Cite 120 fluorescence lamp illuminator (Excelitas Technologies) was used to ensure the light path of unobstructed prior to laser ablation. Successful ablation was scored when the targeted blastomere, or its immediate daughters failed to divide; this was scored within around an

hour of operation. Over-ablation was evident if, following overnight incubation, the entire embryo was “bubbling” with cytosolic components clearly exhibiting a large amount of kinetic energy and the entire embryo misshapen and arrested.

2.4. Microscopy and Imaging

2.4.1. General Microscopy

General *C. elegans* work including strain maintenance and crosses were performed using a Nikon SMZ2745 dissecting microscope (Nikon).

2.4.1.1. General Fluorescent Microscopy

Strain maintenance and crosses requiring visualisation of fluorescent reporters were performed using either a Nikon SMZ18 with a P2-SHR Plan Apo 1.6x objective or Nikon SMZ1000 with a P-HR Plan Apo 1.6x objective both using a Nikon Intensilight C-HGFI epi-fluorescence illuminator (all Nikon).

2.4.1.2. Imaging and Image Acquisition

DIC and fluorescent imaging was performed using one of two Zeiss Axio Imager.M2 upright microscopes (Carl Zeiss). Either the Colibri.2 (Carl Zeiss) or Cool LED pE-2 (Cool LED) LED illumination systems were used for epi-fluorescent illumination. Images were acquired using either a mounted pco.sensicam (PCO) or pco.edge 3.1 (PCO) sCMOS camera.

A bespoke image acquisition software, Caenotec (Ralf Schnabel, TU Braunschweig), was employed to control the microscope and acquire images. Embryos were imaged using a 100x/1.3 oil immersion objective with the camera rotated to orient the embryo with the anterior end of the embryo to the left-hand side.

2.4.2. 4D Lineage Recording Acquisition (Movies)

For lineaging analysis of mutant and wild type strains and reporter lines embryos were mounted in the same fashion. Between one and four embryos of the one-cell to four-cell stage were mounted as described in section 2.1.5. Collection and Mounting of Embryos.

As for general imaging lineage recording were acquired using a Zeiss Axio Imager.M2 and pco.sensicam (PCO) or pco.edge 3.1 (PCO) sCMOS camera controlled by the bespoke software TimeToLive Update.

Embryos were arranged and cameras oriented so that the anterior-posterior axis lay from left to right. Using the 100x/1.3 oil objective, differential interference contrast microscopy (DIC, Nomarski) images were acquired as Z-stacks of 25 slices 1µm apart with the top of the embryo set in the software. Slices were acquired at 35 seconds intervals for 750 scans (07:17:35) for recordings at 25°C and 1500 scans (14:35:00) for recordings at 15°C to account for the differing speed of development at the two temperatures to reach completion of embryogenesis. Fluorescent channel scans for either GFP or RFP were programmed for specific scans during the recording.

Temperature of the microscope microenvironment was achieved using water circulated from either a Corio CD-200F or F12-ED Refrigerated/Heating Circulator (both Julabo) to a bespoke copper collar surrounding the 100x/1.3 oil objective. The temperature was verified using a temperature probe.

2.4.3. 4D Lineage Recording Analysis (Lineaging)

4D lineage analysis of embryos was performed manually using the bespoke *C. elegans* lineaging software Simi BioCell 4.1 (Simi). Division times, patterns, number and cell positions were obtained using this software.

2.5. Temperature Shift Experiments

2.5.1. Slide Based Shifts

Temperature shift experiments with temperature sensitive mutants where shifting between permissive and non-permissive temperature was required were performed by moving mounted embryos between incubators of the appropriate temperature (LEEC).

2.5.2. 4D Recordings

2.5.2.1. Copper Collar Method

During 4D recording a change in temperature was input using the Julabo water circulation system. To aid rapid upshift in temperature from 15°C to 25°C 200-500ml of 90°C water was added to the water bath which achieved a ramp time of ~10-15s over an unaided ramp time of ~35s. Rapid downshifts were aided by the addition of two handfuls of ice achieving a ramp time of ~15s over an unaided ramp time in order of minutes.

2.5.2.2. Microfluidic Slide Method

Temperature shifts were conducted with greater precision during 4D recording using a microfluidic chip (Cherry Biotech). Embryos were mounted on the chip above the microfluidic chamber as if on slides using 2% agarose pads as described above with the omission of pad trimming to avoid damage to the microfluidic chip. Temperature and circulation of the "Thermalisation Solution" was controlled by a Cherry Temp Dual Channel Temperature Controller and Cherry Loop Fluid Control and Stability unit (Cherry Biotech). Cherry Biotech software was used to set and change temperature achieving a ramp time of under 10s between 15-25°C.

2.6. Cell Volumetric Measurements

Cell volumes were calculated as pseudo-volumes from cell areas through z-stack images. Single DIC z-stacks from 4D recordings were obtained a few frames (35-140s) after the completion of cytokinesis for each measured volume. Comparison of multiple frames either side of the division in the Simi BioCell 4.1 lineaging software were assessed and only images in which the cell boundaries could be reliably delineated were used.

Z-stacks were constructed in the image processing software Fiji (a distribution of ImageJ from the University of Wisconsin-Maddison and MPI-CBG Dresden) (Rueden et al., 2017; Schindelin et al., 2012). In a single stack, the area of a cell in each slice in which it was present was traced using the "Polygon selections" tool and measured using the "Measure" function to record an area measurement in pixels.

The volume between each pair of slices moving down through the stack was calculated in Microsoft Excel as that of a truncated cone with circular faces of areas equal to those of the cell in the respective slices. As all slices were set at 1µm intervals the height of the truncated cones could reliably be taken to be 10.26031 pixels as measured using a microscope graticule. A

truncated cone was chosen over a cylinder to better account for the changing area over the relatively large distance between slices of 1µm. Volumes between all slices were summed and a volume ratio expressed as volume of the anterior daughter with respect to the posterior daughter set as one; 1.4 expressing 1.4:1 A:P and 0.9 expressing 0.9:1 A:P (equal to 1:1.12).

The volume of a truncated cone:

$$V = \frac{\pi}{3}(r_1^2 + r_1 r_2 + r_2^2)h$$

Here r_1 is the radius of slice 1 and r_2 that of slice 2, h is the distance between two slices, completing the truncated cone (Figure 2.1).

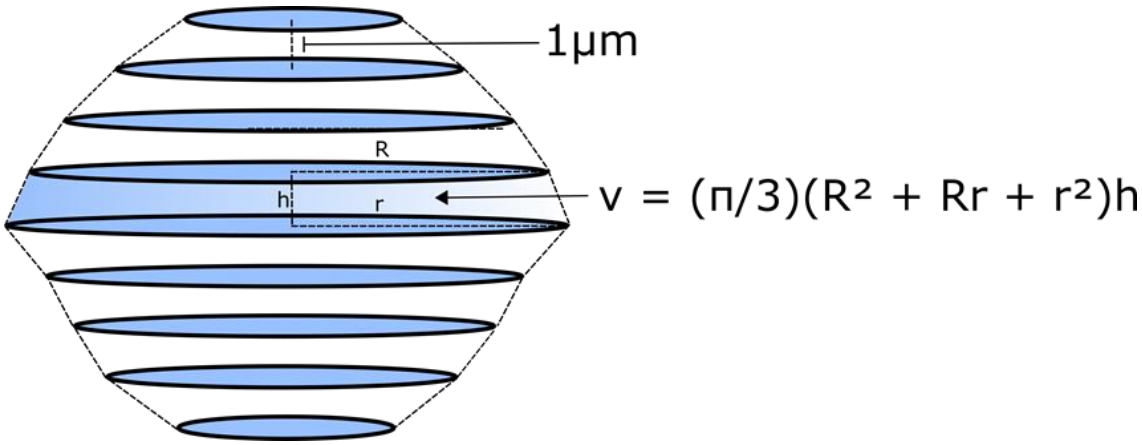

Figure 2.1. Method for volumetric measurement of cells from Z-stacks

2.7. Division Orientation Angle Measurements

2.7.1. Division Angle Along Anterior-Posterior Axis

Using the Fiji "Rectangular" tool, a box was drawn around an embryo so that the short edges were perpendicular to the long axis and long edges parallel. Given the embryos are not perfect ovoids, these angles were judged as to also divide the embryo into approximately equal halves whilst maintaining the axis. This was not done with respect to the line of E cells, as these are offset with respect to the embryo as a whole.

To establish a point from which to measure the division angle a line parallel to the long edge of the box was drawn using the “Straight” tool between the two short edges and positioned to bisect the anterior daughter cell through the centre of the nucleus forming the reference line.

To measure the angle of division with respect to its deviation from the A-P axis the “Angle” tool was used, with one line overlaying the reference line and the other terminating at the centre of the nucleus of the posterior daughter cell. Accounting for the fact that embryos could have either a left or right-hand view all angles were converted to those a in a left-hand view. The left-hand view is the standard diagrammatic view with the A-P axis running left to right and the EMS blastomere at the bottom at the four-cell stage.

Angles were expressed in the context of 90° being parallel to the A-P axis with theoretical minimum angle of 0° up and the maximum of 180° down on the image. These extremes are theoretical as 0° and 180°C would be indistinguishable. If the posterior daughter lay above the reference line in a left-hand view or below it in a right-hand view the angle measured in Fiji was subtracted from 90° to reflect the acute angle. Conversely if the posterior daughter lay below the reference line in a left-hand view or above it in a right-hand view the measured angle was added to 90° to reflect the obtuse angle. This is summarised below:

View	**Posterior Daughter Position with Respect to Reference Line**	**Operation for Final Angle**
Left-hand	Above	90° - θ
	Below	90° + θ
Right-hand	Above	90° + θ
	Below	90° - θ

2.7.2. Division Angle Along Dorsal-Ventral Axis

The division angle in the dorsal-ventral (D-V) axis was measured using the deviation from the plane of the Z-stack containing the centre of the anterior daughter’s nucleus. The Z-stack and defined distance between slices allowed the use of trigonometric functions to calculate the distance between sister nuclei and the angle of division.

Calculations were based around a right-angled triangle; one side was formed by the horizontal distance between sister nuclei with the anterior nucleus in focus, another by the vertical distance

through the stack between planes in which the centre of each sister nucleus was in focus and the hypotenuse between them. The horizontal distance between the sister nuclei was measured by drawing a line between the centre of the nuclei using the Fiji “Straight” tool followed by the “Measure” function. The vertical distance was taken as the number of slices between the respective nuclear focal planes in µm, given that all stacks were taken with µm intervals.

Pythagoras’ Theorem was just to calculate the hypotenuse of the triangle, the distance in three dimensions between the centres of the sister nuclei (Figure 2.1):

$$a^2 + b^2 = c^2$$

$$horizontal\ distance\ between\ nuclei^2\ +\ vertical\ distance\ between\ focal\ planes^2$$
$$= 3D\ distance\ between\ nuclei^2$$

In the triangle the division angle was formed by the hypotenuse and the horizontal distance between nuclei. This angle was calculated from the inverse tangent using the lengths of the sides of the triangle, performed using the “ATAN” inverse tangent function in Microsoft Excel. As Excel operates in radians the “DEGREES” function was employed to convert the output to degrees; “DEGREES(ATAN(a/b))”.

$$tan^{-1}\left(\frac{opposite}{adjacent}\right) = \emptyset$$

$$tan^{-1}\left(\frac{vertical\ distance\ between\ focal\ planes}{horizontal\ distance\ between\ nuclei}\right) = division\ angle$$

All measured embryos displayed a ventral view at the top of the stack however the position of the posterior daughter cell varied between being above and below the plane of the anterior cell. Therefore, final angles were expressed as relative to divisions in-plane being 90°; acute angles reflecting posterior daughters on higher planes and obtuse reflecting posterior daughters at lower planes. The theoretical minimum of 0° and maximum of 180° would be indistinguishable as with the A-P axis angles. This is summarised here:

View	Posterior Daughter Position with Respect to Plane of Anterior Daughter	Operation for Final Angle
Ventral	Above	90° - θ
	Below	90° + θ
Dorsal	Above	90° + θ
	Below	90° - θ

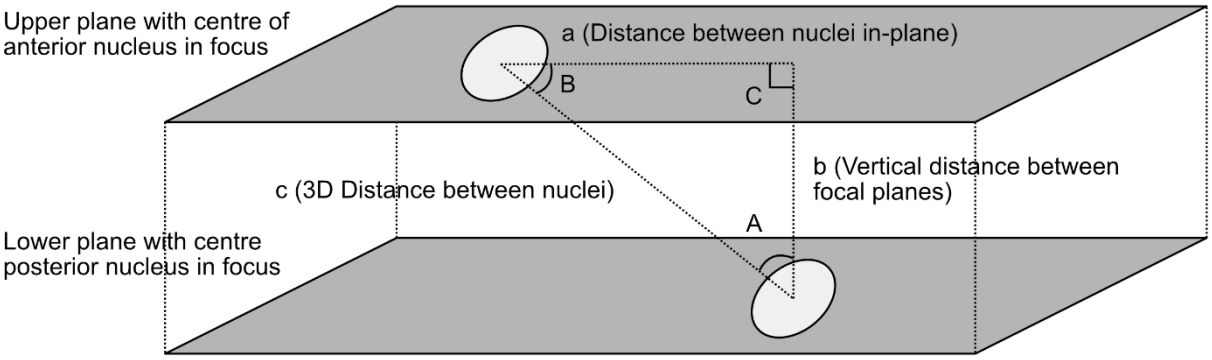

Figure 2.2. Schematic of method used to measure division angle in the DV axis

2.8. Molecular Methods

2.8.1. Miniprep

Minipreps were performed using the QIAprep Spin Miniprep Kit (QIAGEN) as per the manufacturer's instructions. Final elution of samples was performed with miliQ H_2O.

2.8.2. PCR Cleanup

PCR products were purified using the UltraClean PCR Cleanup Kit (QIAGEN) as per the manufacturer's instructions. Final elution of samples was performed with miliQ H_2O.

2.8.3. Assessment of Nucleic Acid Sample Quality

Sample quality was assessed for all molecular applications using a NanoDrop 1000 Spectrophotometer (Thermo Fisher Scientific).

2.9. Genotyping

2.9.1. Primer Design

All primers were designed either manually using the sequence analysis software ApE – A plasmid Editor (jorgensen.biology.utah.edu/wayned/ape/) or the online tool Primer 3 (http://primer3.ut.ee/). Primers were then checked for non-target binding within the *C. elegans* genome using the BLAST tool within the *C. elegans* community website WormBase (www.wormbase.org/tools/blast_blat). All primers were synthesised by Sigma Aldrich.

2.9.2. Polymerase Chain Reactions

Polymerase Chain Reactions (PCR) were conducted using PCRBio HiFi Polymerase, PCRBio 5x PCR Buffer (PCRBiosystems). A typical reaction is outlined below.

Reagent	**Volume per reaction (µl)**
Forward Primer 10µM	1
Reverse Primer 10µM	1
PCRBio HiFi Polymerase (PCRBiosystems)	0.3
PCRBio 5x PCR Buffer (PCRBiosystems)	5
DNA (worm lysate or PCR product)	2
Nuclease Free H_2O (Sigma Aldrich)	15.7
	25

2.9.3. Genotyping *ham-1(n1438)* and *pig-1(gm344)*

2.9.3.1. Genotyping by PCR

As *ham-1(n1348)* and *pig-1(gm344)* are deletion alleles, there presence in constructed strains could be identified via PCR. Following crosses to introduce reporters to the mutant strains, full plates of worms seeded with a single F2 daughter of F1 cross progeny were lysed.

Genotyping primers for the *ham-1(n1438)* and *pig-1(gm344)* lesions were designed around the deletions with the length of the PCR product indicative of the presence or absence of mutant alleles.

As the *n1438* allele constitutes a 238 base pair deletion in the *ham-1* locus the predicted product length for the outer and inner primer pair respectively was 524 and 485. These differences in length were easily distinguishable from the *wild type* products of 762 and 723 respectively when run on 2% agarose gel (Sigma Aldrich).

For *pig-1*, the *gm344* deletion removes 524 base pairs as so the predicted product length with the outer primer set was 535 compared to the *wild type* length of 1059. Difficulty in designing the inner pair without off-target sequences resulted in the inner fragment length of considerably shorter length; 86 base pairs for the mutant and 610 for the *wild type*. As with *ham-1(n1438)* the difference in length of the mutant and *wild type* band was easily discernible on a 2% agarose gel (Sigma Aldrich).

Nested primers were used as to minimise the effect of any off-target loci not picked up in BLAST, with the outer pair used first.

The PCR programme used for genotyping of *ham-1(n1438)* and *pig-1(gm344)* was as follows.

Step	**Temperature (°C)**	**Duration (min)**	**Cycles**
Initial Denaturation	95	5	1
Denaturation	95	1	30
Annealing	62	1	
Extension	72	0.5	
Final Extension	72	10	1
Hold	10	∞	1

2.9.4. Genotyping *lin-5(ev571)*

2.9.4.1. Genotyping by PCR and Restriction Digest

As *ev571* is a temperature-sensitive lethal allele, following crosses to reporter stains F2 descendent populations were identified as suspected homozygotes by lethality at 25°C and homozygosed for the appropriate reporters over subsequent generations.

As the *ev571* lesion is a 9 base pair deletion and thus too small a difference to resolve easily on a gel by product length and so a restriction enzyme digest was undertaken to confirm the genotyping from the lethality assessments.

No novel restriction sites were introduced by the *ev571* lesion. However, using the sequence analysis software ApE a restriction site was identified as disrupted by the *ev571* lesion; the BglII restriction site 5'---A/GATCT---3'.

Lysate from suspected homozygous populations was used to perform PCR to amplify DNA for the digestion assay. The programme used was as follows.

Step	**Temperature (°C)**	**Duration (min)**	**Cycles**
Initial Denaturation	95	5	1
Denaturation	95	1	30
Annealing	56	0.5	
Extension	72	0.5	
Final Extension	72	10	1
Hold	10	∞	1

Restriction digestion was performed using both BglII and its isoschizomer BstYI (New England BioLabs) on the *lin-5(ev571)* reporter containing strains, the positive control reporter strain and negative control *lin-5(ev571)* strain. Reactions were performed at a final volume of 50µl and incubated at the appropriate temperature in an incubator.

The digestions were performed as follows.

Reagent	**Volume per reaction (µl)**
Restriction Enzyme BglII (NEB)	1
Buffer B3.1 (NEB)	5
DNA 1µg	X
Nuclease Free H_2O (Sigm Aldrich)	to 50µl
Reagent	**Volume per reaction (µl)**
Restriction Enzyme BstYI (NEB)	1
Buffer B2.1 (NEB)	5
DNA 1µg	X
Nuclease Free H_2O (Sigm Aldrich)	to 50µl

2.9.4.2. Genotyping by Sequencing

The genotyping by restriction digest method for *lin-5(ev571)* used the disruption of a restriction site and so lack of enzyme activity as the indication of the presence of the allele rather than the introduction of a novel site. To mitigate for the chance that lack of shorter bands could be due to poor enzyme activity rather than lack of a cut site, worm populations were also sequenced for the *lin-5* locus.

Samples were sequenced by Eurofins Scientific using the same primers as used for *lin-5* PCRs.

2.10. Mutant Mapping by Whole Genome Sequencing

Mutant mapping was performed using the “Hawaiian Cross” method (Doitsidou et al., 2016). Mutant strains were crossed to the CB4856 strain, isolated from Hawaii, which is highly polymorphic compared to the standard laboratory N2 strain containing $>10^5$ single nucleotide polymorphisms (SNPs). Linkage between adjacent and causal loci was apparent from the over representation of N2 SNPs in a particular genomic region as recombination at loci with increasing proximity to the loci are increasingly unlikely.

2.10.1. “Hawaiian” (HA) Crosses and Recombinant Collection

Crosses were performed between HA and the mutant strains with ~10 cross plates employed to ensure successful crossing.

The healthiest cross plate was selected and ten F1 heterozygous, hermaphrodite, larval cross progeny (preferably L4 stage) were picked to a single plate at 15°C. F1s were picked to 15°C to ensure the survival of F2 homozygous animals.

The F1s were incubated for five to seven days so that a large number of L3 and L4 stage progeny were present on the plate. ~400 F2 recombinant hermaphrodites were singled and placed at the non-permissive temperature of 25°C. 400 F2s were singled given that the expectation from Mendelian genetics was that only 100, or one quarter, would be homozygous at the mutant locus. ~100 recombinant, homozygous allows for both contaminated plates and those of ambiguous zygosity to be discarded whilst leaving enough recombinants for tight mapping.

Singled F2 L4s were incubated and allowed to throw progeny for one day. As the mutants in question were temperature sensitive, homozygous, recessive lethal, homozygous plates were identified as those which only produced dead and arrested embryonic progeny at 25°C

Clean homozygous F2 plates were removed to 15°C and allowed to throw progeny for seven to ten days, or until the plate was full of worms; F3s and F4s. At this stage a small number of F2s were unable to “recover” and failed to produce progeny, again highlighting the importance to picking F2s in excess.

Full recombinant plates were washed with a few ml of M9 buffer and suspended worms pooled into 15ml Falcon tubes using a glass Pasteur pipette.

Worms were sedimented via centrifugation at 3000 rpm for 2 min and the M9 buffer aspirated leaving a worm pellet. Fresh M9 was used to fill the tube and the wash step repeated three times.

Fresh M9 buffer was again added to fill the tube and the tubes left on a nutator shaker for at least 2 hours to clean worms of bacteria and debris.

The wash step was performed twice more or repeated until M9 was visibly clear.

The M9 buffer was aspirated off and the pelleted worms store at -20°C until genomic extraction as required.

2.10.2. Genomic DNA Preparation

Pelleted worms were removed from -20°C and thawed at 20°C. Genomic DNA extraction was performed using a Gentra Puregene Tissue Kit (Qiagen) following the manufacturers supplemental protocol, “Purification of archive-quality DNA from nematodes or nematode suspensions using the Gentra Puregene Tissue Kit”.

The DNA concentration of the final pooled sample was assessed using a NanoDrop 1000 Spectrophotometer (Thermo Fisher Scientific) and stored at -20°C until required.

2.10.3. Whole Genome Sequencing

Genomic library preparation and sequencing was performed in-house by the UCL Genomics team at the UCL Great Ormond Street Institute of Child Health.

2.10.4. Sequence Analysis and Mapping

Analysis of mutant genomes were performed using the CloudMap pipeline as described in (Minevich et al., 2012). The pipeline was run using a Galaxy web server (Afgan et al., 2018) called Nucleolus hosted by UCL and maintained by Dr. Richard Poole.

Heterozygosity maps were produced by the pipeline indicating the region in linkage with the causal mutation. To narrow down the number of variants within these regions a number of variant list subtractions were performed; a list of HA variants, a list of causal mutants previously identified in the lab and a list of causal mutants previously identified in the Hobert Lab at Columbia University.

2.11. Statistical Analysis

T-tests between single mutant and control strains were conducted using Excel (Microsoft). Comparisons of multiple mutant and control strains at once using ANOVA and subsequent post-hoc tests to uncover which strains varied significantly were performed using Excel (Microsoft) or Prism 7 or 8 (GraphPad). Post hoc tests were carried out following ANOVA in order to identify which genotypes difference significantly. When all samples were compared to each other Tukey’s HSD was employed and the Holm-Sidak correction in cases when only certain strains were compared (for example to the control strain and between temperature conditions).

2.12. Figure Production

2.12.1. Image Processing

Fluorescent images were compiled into the stacks using the ImageJ Plugin “Image5D”, part of the Fiji distribution. As fluorescent reporters often expressed in cells of interest across multiple slices of a Z-stack the fluorescent channels of the stack were used to construct flattened maximum intensity projections across all slices in cases where this was appropriate. This is performed using the “Maximum intensity” option in the “Z-project” function within the “Image5D”.

2.12.2. Graph Construction

Scatter and boxplots were produced using one of either the statistical analysis software Prism 7 or 8 (GraphPad) or the programming environment R (R Foundation for Statistical Computing).

Bar charts were produced using Excel (Microsoft).

2.12.3. Final Figure Production

Figures were designed and produced using the graphic design software Affinity Designer (Serif) or the opensource vector graphic software Inkscape (https://inkscape.org/).

2.13. Primers List

Gene(allele)	Purpose/Name	Sequence
lin-5(ev571)	Fwd Genotyping Primer Inner	AGAAGTCTGGAGGAAGCTGAC
lin-5(ev571)	Rev Genotyping Primer Inner	TTGTTCCTGGAGGTCAGC
lin-5(ev571)	Fwd Genotyping Primer Outer	CGAATGACGTTGAGATCCGAG
lin-5(ev571)	Rev Genotyping Primer Outer	CTCCGGTAAGTTGTTCCTGG
ham-1(n1438)	Fwd Genotyping Primer Inner	GCCTTGTAGGCAGTCAGGA
ham-1(n1438)	Rev Genotyping Primer Inner	CACAACGGCTAAGTAGGTCATG
ham-1(n1438)	Fwd Genotyping Primer Outer	GTCGTAGGTACGAGTCGCC
ham-1(n1438)	Rev Genotyping Primer Outer	TTCTTGGCTTTTGGTCCGTT
pig-1(gm344)	Fwd Genotyping Primer Inner	CAACAAACTCACTCCAAGCTGC
pig-1(gm344)	Rev Genotyping Primer Inner	TTTCATTCGCGTCCTGACAC
pig-1(gm344)	Fwd Genotyping Primer Outer	TTTGAACTCGCGGCAGGT
pig-1(gm344)	Rev Genotyping Primer Outer	CTACTAATCTCCGGGTCGTGTT

2.14. Recipes

Recipe for KPO_4 Buffer

Reagents for 100ml	
1M KH_2PO_4	76ml
1M K_2HPO_4	24ml

Recipe for NGM (Nematode Growth Media)

Reagents for 1 L	
NaCl (Sigma-Aldrich)	3g
Agar (Sigma-Aldrich)	17g
Bactopeptone (BD Biosciences)	2.5g
mQ H_2O	975ml
Autoclave	
1M KPO_4 (Fluka-Honeywell)	25ml
1M $CaCl_2$ (Sigma-Aldrich)	1ml
Cholesterol (5mg/ml in EtOH) (Sigma-Aldrich)	1ml
Nystatin (10mg/ml in H_2O) (Sigma-Aldrich)	2.5ml

Recipe for 'Egg Prep' Solution

Reagents for 10ml	
Bleach(Mexcel)	2ml
10M NaOH (Sigma-Aldrich)	0.5ml
mQ H_2O	7.5ml

Recipe for 'Egg Drop' Solution

Reagents for 10ml	
Bleach(Mexcel)	5ml
1M NaOH (Sigma-Aldrich)	5ml

M9 Buffer

Reagents for 1L	
KH_2PO_4	3g
Na_2HPO_4	6g
NaCl	5g
1 M $MgSO_4$	1ml
H_2O	to 1L

2.15. Software and Web Resources List

Name	Purpose	Web Link
Caenotec (Ralf Schnabel, TU Braunschweig)	Image and 4D recording acquisition	n/a
BioCell (Simi Reality Motion Systems)	Embryo lineaging	http://www.simi.com/en/products/cell-research/simi-biocell.html
Fiji (ImageJ)	Image processing	https://fiji.sc/ https://imagej.net/Fiji/Downloads
Prism 7/8 (GraphPad)	Statistical analysis, graph production	https://www.graphpad.com/scientific-software/prism/
R (The R Project for Statistical Computing)	Statistical analysis, graph production	https://www.r-project.org/
RStudio (RStudio)	GUI for R	https://www.rstudio.com/
Excel (Micsosoft)	Data analysis, statistical analysis, graph production	https://products.office.com/en-gb/excel
Galaxy (Galaxy Community)	WGS data analysis workflow system	https://galaxyproject.org/
BLAST (NIH)	Sequence analysis	https://blast.ncbi.nlm.nih.gov/Blast.cgi https://wormbase.org/tools/blast_blat
ApE – A plasmid Editor (M. Wayne Davis, University of Utah)	Sequence analysis, primer design	http://jorgensen.biology.utah.edu/wayned/ape/
Primer 3 (Whitehead Institute for Biomedical Research)	Primer design	http://bioinfo.ut.ee/primer3/
WormBase	Reference	https://www.wormbase.org
WormAtlas	Reference	https://www.wormatlas.org/
WormBook	Reference	http://www.wormbook.org/
Affinity Designer	Figure production	https://affinity.serif.com/en-gb/designer/

2.16. Strain List

Strain Number	Genotype
CB4856	*Hawaiian*
CHL28	*stIs10166 [dpy-7p::HIS-24::mCherry + unc-119(+)]; let-19(t3200) gmIs20 [hlh-14prom::hlh-14::gfp rol-6(+)] II; otIs458 [ceh-63::gfp] III*
CHL29	*hlh-2(drp6) gmIs20[hlh-14prom::hlh-14::gfp rol-6(+)] II; otIs458 [ceh-63prom::gfp] III; stIs10166 [dpy-7p::HIS-24::mCherry,unc-119(+)]*
CHL31	*stIs10166 [dpy-7p::HIS-24::mCherry + unc-119(+)]; gmIs20 [hlh-14prom::hlh-14::gfp rol-6(+)] II; otIs458 [ceh-63::gfp] III*
CHL45	*mex-3(zu155) egl-30(n686)/+ I; gmIs20 [hlh-14prom::hlh-14::gfp rol-6(+)] II*
CHL46	*gmIs20 [hlh-14prom::hlh-14::gfp rol-6(+)] II; otIs458 [ceh-63::gfp] III; and-7(t3224) IV*
CHL47	*stIs10166 [dpy-7p::HIS-24::mCherry + unc-119(+)]; otIs458 [ceh-63::gfp] III; and-7(t3224) IV*
CHL48	*and-8 II; otIs458 [ceh-63::gfp] III*
CHL49	*t3462; otIs458 [ceh-63::gfp] III*
CHL50	*stIs10166 [dpy-7p::HIS-24::mCherry + unc-119(+)] I; lin-5(ev571) gmIs20 [hlh-14prom::hlh-14::gfp rol-6(+)] II; otIs458 [ceh-63::gfp] III; tubulin::gfp*
CHL51	*gmIs20 [hlh-14prom::hlh-14::gfp rol-6(+)] II; otIs458 [ceh-63::gfp] III; pig-1(gm344) IV*
CHL52	*stIs10166 [dpy-7p::HIS-24::mCherry + unc-119(+)]; gmIs20 [hlh-14prom::hlh-14::gfp rol-6(+)] II; otIs458 [ceh-63::gfp] III, pig-1(gm344) IV*
CHL53	*stIs10166 [dpy-7p::HIS-24::mCherry + unc-119(+)]; gmIs20 [hlh-14prom::hlh-14::gfp rol-6(+)] II; otIs458 [ceh-63::gfp] III; ham-1(n1438) IV*
CHL54	*let-19(t3273) II gmIs20 [hlh-14prom::hlh-14::gfp rol-6(+)] II*
CHL55	*let-19(t3273) II; otIs458 [ceh-63::gfp] III*
DR466	*him-5(e1490) V*
FM102	*lin-5(ev571) II; tubulin::gfp*
FX1238	*cdk-8(tm1238) I*
GE4421	*let-19(t3200) II*
GE4634	*let-19(t3273) II*
GE5038	*Unmapped*
GE5039	*and-7(t3224) IV*
GE5315	*Unmapped*
GE5651	*t3462*
GE5691	*and-8(t3294) II*
GE5697	*Unmapped*
GE5880	*t3461*
GE6048	*Unmapped*
GE6057	*Unmapped*
GE6436	*Unmapped*
GE6507	*t3463*

GE6534	*t3464*
GE6566	*t3465*
HS445	*dpy-22(os38) X; osEx89[col-10::GFP + dpy-22(+)]*
HS458	*let-19(os33)/mIn1 [dpy-10(e128) mIs14] II*
JJ478	*mex-3(zu155) egl-30(n686)/hT1 I; +/hT1 V*
MD2822	*ces-2(bc213) I; bcIs66*
MD3397	*ces-1(tm1036) I*
MD3876	*pig-1(gm344) IV*
MD3998	*bcSi43[pig-1::gfp] II; unc-119(ed3) III*
MT1506	*ces-1(n703sd) I*
MT3351	*ham-1(n1438) IV*
N2	*wild type*
NG4280	*hlh-14(tm295)/mln1 II [mIs14 dpy-10(e128)]*
OH11974	*otIs458 [ceh-63::gfp] III*
SD1546	*stIs10166 [dpy-7p::HIS-24::mCherry + unc-119(+)]*
	gmIs20 [hlh-14prom::hlh-14::gfp rol-6(+)] II

Results

Chapter 3

3. Characterisation of the C Lineage

3.1. Characterisation of C Lineage Division Times

As mentioned in Chapter 1 the precocious division of the DVC precursor Caapa displayed by *hlh-14* mutants is a very clear phenotype accompanying the loss of neurogenesis and conversion to hypodermal fate. As I intended to make extensive use of lineage analysis during the project precise understanding of timings in the wild type lineage and how this relates to lineage aberrations, particularly this precocious division, was invaluable.

As stated in the introduction, the *wild type* division pattern and relative timings of the C lineage were elucidated during early work on *C. elegans* embryogenesis in 1960s and 1970s culminating in Sulston's landmark work reporting the entire embryonic cell lineage published in 1983 (Sulston et al., 1983). However, these timings were calculated as an average of a number of embryos, with terminal division timings not explicitly stated (Sulston et al., 1983). Additionally, given that a degree of variability in embryonic division timings is apparent (Schnabel et al., 1997) and that my recordings were taken at 25°C, I endeavoured to characterise timings in the *wild type* lineage until the terminal division producing the DVC neuron and its sister cell death.

Nine *wild type* embryos were manually lineaged at 25°C in order to extract division timings from the five rounds of division from the birth of the C blastomere to the terminal division of the neuronal branch of the C lineage, the division of Caapa and the birth of DVC (Caapaa). These timings were expressed as cell cycle durations calculated from the birth of a cell until its division (± standard deviation). An initial observation from this analysis is that cell cycle duration elongates progressively throughout the development of the C lineage; C 21 ± 1 min, Ca 23 ± 1 min, Caa 30 ± 1 min, Caap 44± 3 min and Caapa 129 ± 19 min (Figure 3.1). The greatest contrast is evident between the first division, that of C, 21 min, and the terminal division of Caapa, 129 min. The first three rounds of division in the lineage are all relatively short, displaying cell cycle durations of under 30 min. The increase in duration therefore is also increase in magnitude of difference as evidenced by the relative differences between a cell's cell cycle duration and that of its mother

expressed as ratio form; Ca vs C 1.10, Caa vs Ca 1.31, Caap vs Caa 1.47, Caapa vs Caap 2.89 (Figure 3.1).

In addition to greater duration and magnitude of increase in duration, the variability in cell cycle duration between embryos also increases as the lineage progresses, in agreement with previous reports (Schnabel et al., 1997). The first four divisions show smaller degrees of variation as can be seen from the standard deviation values; C, Ca, Caa all ± 1 min, Caap ± 3. The greatest degree of variation is seen in the final division of the neuronal branch, Caapa ± 19 min. As *C. elegans* has an invariant cell lineage an appropriate assumption is that animals from a near-isogenised laboratory strain would show little variation in developmental timing and as such one would expect a low value for the coefficient of variance ($CV=\sigma/\mu$). The respective CV values for the five divisions of 4.88%, 5.93%, 3.83%, 6.74% and 14.6% again demonstrate the trend of an increasing degree of variation and in particular highlights the far greater variation in the Caapa cell cycle with respect of all other cells measured.

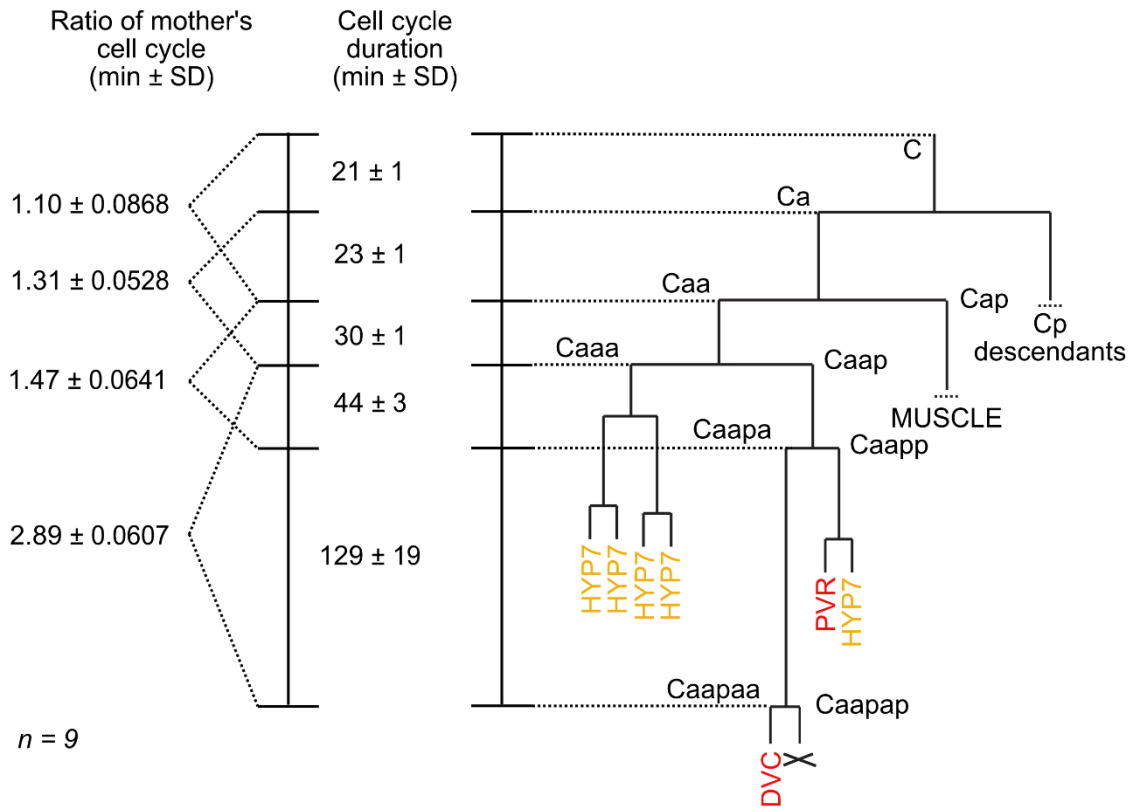

Figure 3.1. Characterisation of division timings in the C lineage neuronal branch (at 25°C). *Cell cycles are defined as from the completion of the division and are expressed as the mean ± standard deviation for the sample analysed. The ratio of daughter vs mother cell's cell cycle was calculated using the daughters cell cycle/mother's cell cycle for each embryo and expressed as the mean ± standard deviation for the sample as a whole. A short dotted line underneath a lineage indicates that descendant cells are not depicted.*

3.2. The C Lineage Demonstrates Two Dramatically Unequal Cleavages Preceding *hlh-14* Expression

As described in Chapter 1 a distinct feature of the C lineage is its near left-right symmetry. This is broken in terms of fate by the two neurons, DVC and PVR, and the cell death and in division pattern by the elongated cell cycle duration of Caapa compared to both its sister and cousin branches and its bilateral homologue. These neurogenesis events clearly present the lineage with fate decisions in the Ca lineage not present in Cp. At the Caa division there is a decision between an anterior hypodermal branch and hypodermal and neuronal posterior branch. At the next division, of Caap, a decision between an anterior neuronal branch and a posterior hypodermal and neuronal branch. The bilaterally homologous divisions of Cpa and Cpap lack these decisions with all descendants adopting hypodermal fate.

Through my own lineage analysis, I observed that in addition to being asymmetric these two divisions also demonstrate dramatic unequal cleavages with Caaa clearly around twice as large as Caap and Caapp twice that of Caapa (Figure 3.2 A). Although, early literature noted that P lineage cleavages show more size asymmetry that those of AB, to this author's knowledge these two divisions have not been specifically highlighted before. The unequal size, or volumetric asymmetry, of daughter cells at these apparently key divisions prompted further investigation of the size of daughter cells in the C lineage more generally. Quantification of cell volumes and thus volumetric asymmetries were calculated from either four or ten embryos for both divisions in the neurogenic branch and their bilateral homologues.

Expressed as the volume of the anterior daughter divided by the volume of the posterior daughter, the majority of measured divisions displayed either an "equal" cleavage with no strong bias or an "unequal" cleavage with a very small bias towards the anterior daughter (Figure 3.2 B). This is in agreement with previous studies finding that in the C lineage, as in the embryo on a whole, the majority of divisions measured featured small anterior bias in volume (Arata et al., 2015; Fickentscher and Weiss, 2017).

The initial division of the C blastomere, Ca/Cp, defines the two halves of the lineage and displays an equal cleavage with a volumetric ratio of 1.01 ± 0.0937 (A/P (3 significant figures) ± standard deviation (3 significant figures)). The next division, defining the hypodermal and muscle parts of the lineage, Caa/Cap, displays a ratio of 1.34 ± 0.168. The ratio of the bilateral homologous

division, Cpa/Cpp, whilst defined as a small anterior bias, shows a significantly larger anterior bias of 1.59 ± 0.165 (two-tailed T-test, p = 0.0257). Caaa/Caap, which I confirmed to be the first greatly unequal cleavage in the lineage, displays a ratio of 2.30 ± 0.266 which is the largest measured asymmetry and significantly greater than its bilateral homologue Cpaa/Cpap, 1.62 ± 0.268 (two-tailed T-test, p = 0.00101). The second identified unequal cleavage Caapa/Caapp is the only division to demonstrate a large bias to the posterior daughter, 0.430 ± 0.101, and is significantly different to the bilaterally homologous division Cpapa/Cpapp, 1.33 ± 0.266 (two-tailed T-test, p = 0.0288). The divisions in the same round which produce only hypodermal descendants on both sides of the lineage are both equal cleavages and do not differ significantly; Caaaa/Caaap 1.01 ± 0.198 vs Cpaaa/Cpaap 0.969 ± 0.0581 (two-tailed T-test, n.s., p = 0.717).

Even though Caa/Cap 1.34 ± 0.168 differs significantly from its bilateral homologue, both divisions display what can be considered the same kind of asymmetry and anterior bias. In contrast Caaa/Caap 2.30 ± 0.266 and Caapa/Caapp 0.430 ± 0.101 are the two most clearly equal cleavages and most overtly dissimilar to their bilateral homologues coinciding with differing fates to those homologues, immediately preceding the expression of *hlh-14* in the neurogenic branches. Therefore, these two divisions were identified for further study with respect to the relationship between unequal cleavage and fate decisions in the lineage.

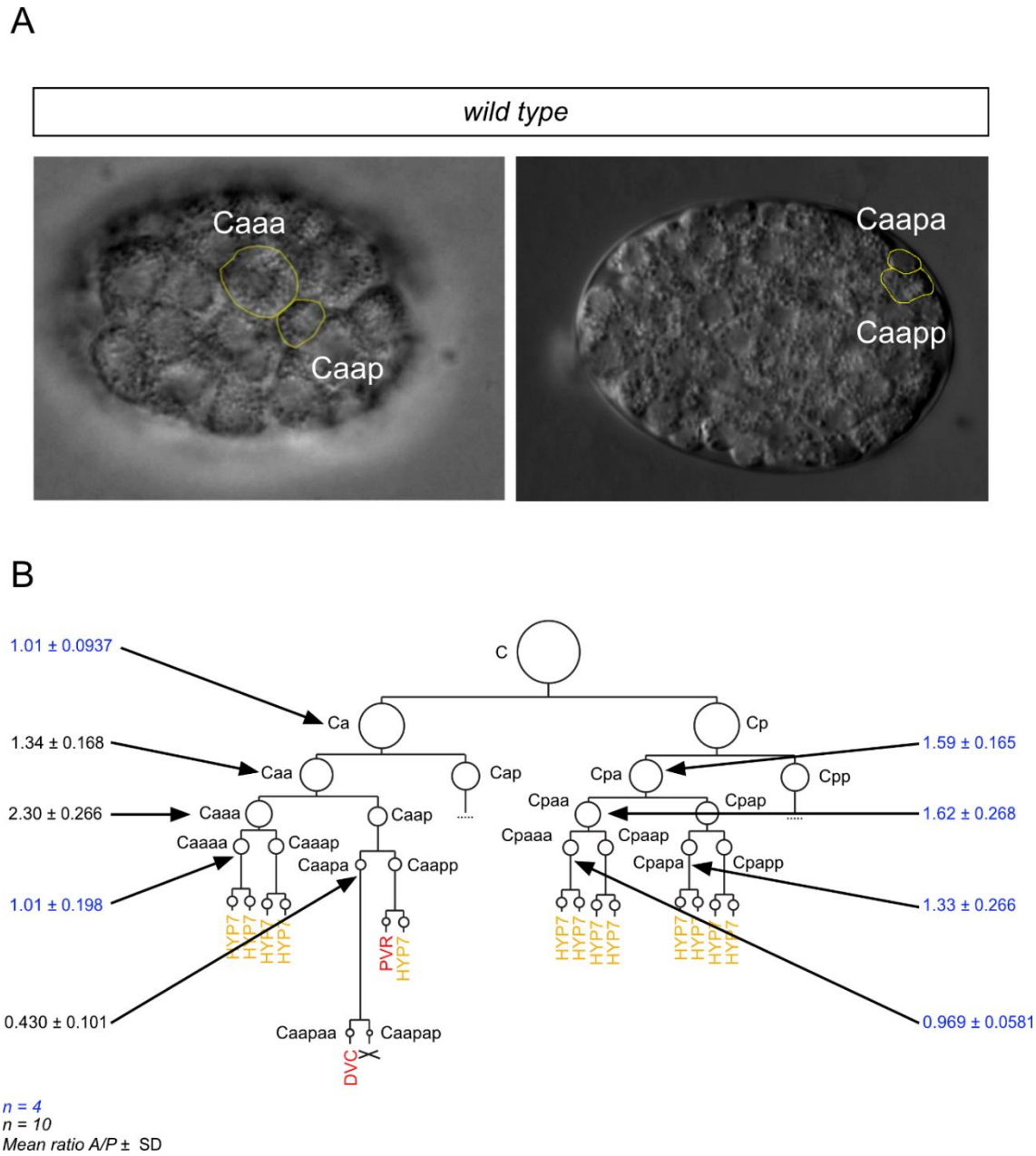

Figure 3.2. Characterisation of unequal cleavages in the C lineage. *Arrows indicate the anterior daughter of the division in question. Numbers express the cell size asymmetry as the volume of the anterior cell divided by the posterior cell. Blue numbers, measured embryos n = 4. Black numbers, n =10. Circles are illustrative of general cell differences between cells and are not based on exact values. HYP7 = hypodermal cell, DVC and PVR = neurons, X = cell death.*

3.3. Neurogenesis in the C lineage is Under Lineage-intrinsic Control

As mentioned in previous sections, an apparent feature of the C lineage is that it is nearly completely left-right symmetric save the neurons arising on the left side. In the previous section I characterised a further feature of this neuronal branch in the Ca lineage, revealing that two unequal cleavages precede or coincide with the onset of *hlh-14* expression and are not seen on the bilateral homologous part of the Cp lineage. Considering this clear asymmetry in an otherwise symmetric lineage I sought to determine whether lineage intrinsic mechanisms confined neurogenesis to the Caap branch or whether lineage inductive extrinsic signalling mechanisms.

With regards to early embryonic signalling C contacts MS and E, known Notch signalling cells (Shelton and Bowerman, 1996) but has not been shown to respond to such signals. Conversely, C has been revealed to be a signalling cell, for example orienting spindle of ABar through proteoglycan SND-1 mediated contact dependent Wnt signalling (Dejima et al., 2014). Additionally, the mother of C, P2, expresses a *C. elegans* Notch ligand APX-1 and signals to ABp which leads to the activation of REF in its descendants (Mickey et al., 1996; Priess, 2005).

To investigate the possibility of a missed early acting inductive signal asymmetrising the C blastomere I chose to employ a classical embryological approach in *C. elegans*, that of laser ablation. Ablation of blastomeres in the early embryo would remove inductive and/or inhibitory signals from other founder and early blastomere to the C blastomere and allow it to develop in relative isolation. A unique marker of the DVC neuron *ceh-63*, part of the terminal transcriptional cascade (Feng et al., 2012), was employed in ablation experiments. This was done using an integrated transcriptional reporter driving GFP[S65C] from the *ceh-63* promoter. Presence or loss of expression in a single characteristically tear shaped DVC cell was taken to be indicative of whether neurogenesis was abolished. In *wild type* unablated embryos a single *ceh-63::gfp* expressing DVC neuron (n = 12) was present in pre-hatching embryos observed at 16-18 hours. Embryos in which ablation of all other blastomeres was performed as they were born also displayed a single *ceh-63::gfp* positive cell (n = 19). Successful ablation was evidenced by groups of large cells from arrested lineages and smaller cells from the developed C lineage. Ablation of the C blastomere itself resulted in embryos with no *ceh-63::gfp* expressing cells (n = 5). The C blastomere was often identifiably arrested suggesting the lack of expression arose from the lack of C lineage progression. (Figure 3.3.)

Ablation of all blastomeres other than C results in its development in the absence of other intact lineages and any signals from therein and suggests the lack of a requirement for an early acting signal for neurogenesis. This operation however could potentially result in the removal of both inductive and inhibitory signals which in combination could be required for *wild type* blastomere fates. To account for this possibility ablation of two blastomeres which contact P2 (the mother of C) ABp and EMS were performed. These operations removed both signals from the ablated blastomeres to P2 but also from ABpl, ABpr and E all of which contact C. In both cases (ABp; n = 13, EMS; n = 4) a single *ceh-63::gfp* positive DVC cell was observed in all operated embryos as with the ablation of all blastomeres. This was also the case for the ablation of the sister cell of ABp which does not contact P2, ABa (n = 11). Addressing the possibility that a signal may be required following the first division in the embryo the AB blastomere was also ablated. This operation resembled all other ablations in that a single DVC was observed in all embryos by the expression of *ceh-63::gfp* (n = 6) (Figure 3.3). Taken together these ablation experiments suggest that neurogenesis in the C lineage does not require a lineage extrinsic signal and is intrinsically part of the specified C lineage program.

Whilst the laser ablation experiments suggest the lack of a required signal for C lineage neurogenesis a caveat remains in that arrested blastomeres can still make membrane contact with the C blastomere and descendants. As such any signalling molecules present at those membranes could still continue to fulfil their roles. In order to address this, I sought to use a genetic approach to compliment the blastomere ablations.

Mutants carrying null alleles of the KH (hnRNP K homology) domain protein MEX-3 are maternally lethal and display gross lineage transformations caused by the misexpression of *C. elegans* Caudal homologue *pal-1* in anterior lineages (Draper et al., 1996; Hunter and Kenyon, 1996). This causes the eight AB great-granddaughters to adopt a C like fate producing the anterior pairs of hypodermal and posterior pairs of muscles cells (Draper et al., 1996). The C lineage proper in these mutants is reported as unaffected with PVR adopting correct neuronal fate, however the fates of cells in the branch to DVC were not determined (Draper et al., 1996). The expected number of ectopic *ceh-63::gfp* positive DVC neurons in these mutants was therefore unclear, yet eight transformed lineages would suggest eight. Assessing these mutants thus served to answer two questions, the first being; does the adoption of C fate in *mex-3(-)* embryos extend to the

neuronal branches? Secondly, as transformed blastomeres have adopted a C lineage like fate; does the endogenous C lineage require AB derived neurogenic signals?

Homozygous *mex-3(zu155)* mutants displayed a variable number of *ceh-63::gfp* positive cells (Figure 3.4 A). 4D lineage analysis of embryos from DIC recordings was performed on *mex-3(zu155)* mutants, however lineage transformations presented considerable challenges for full lineage analysis thus making it difficult to determine the lineal origin of ectopic DVC neurons. In agreement with previous reports however (Draper et al., 1996) 2/2 *mex-3(zu155)* embryos C displayed the *wild type* division pattern with Caapaa (DVC) expressing *ceh-63::gfp*.

Assessment of *ceh-63::gfp* expression in non-lineaged *mex-3(zu155)* embryos confirmed a variable number of *ceh-63::gfp* expressing DVC cells (Figure 3.4 B, C). In no embryo, 0/43 (0%), was the expected number of nine (eight ectopic) GFP positive cells observed. 10/43 (23.3%) displayed the *wild type* number of one, presumably from the endogenous C lineage given the lineage data, and thus no ectopic cells. The highest proportion of the embryos, 13/43 (30.2%) displayed two GFP positive cells one being ectopic. Three and four GFP positive cells were present in similar proportions; 8/43 (18.6%) and 7 (16.3%) respectively. The greatest number of GFP positive cells observed was five, four ectopic, in 4/43 (9.30%) embryos. One embryo had no GFP positive cells, although it arrested prior to the on-set of *wild type ceh-63* expression, explaining the absence.

This absence is a potential explanation for the variability in the number of ectopic DVCs. It is possible that transformed lineages are arresting prior to the expression of *ceh-63* in a similar manner to the zero GFP animal above (Figure 3.4 C). A further possibility is that *pal-1(+)* expression in *mex-3(-)* is not entirely sufficient for complete fate transformations of AB lineages into C (and so the generation of ectopic DVCs), something that would not have been realised by Draper et al., 1996 as they did not determine fate in the DVC branch in lineaged animals.

Whilst the degree to which AB lineages are truly transformed into C lineages in *mex-3(zu155)* is a somewhat separate issue, the fact that the endogenous C lineage produces a *ceh-63::gfp* positive DVC when isolated from AB lineages suggests that it does not require an inductive signal from AB lineages. This supports the conclusion from the blastomere ablation experiments indicating that regulation of neurogenesis is lineage intrinsic in the *wild type* C lineage.

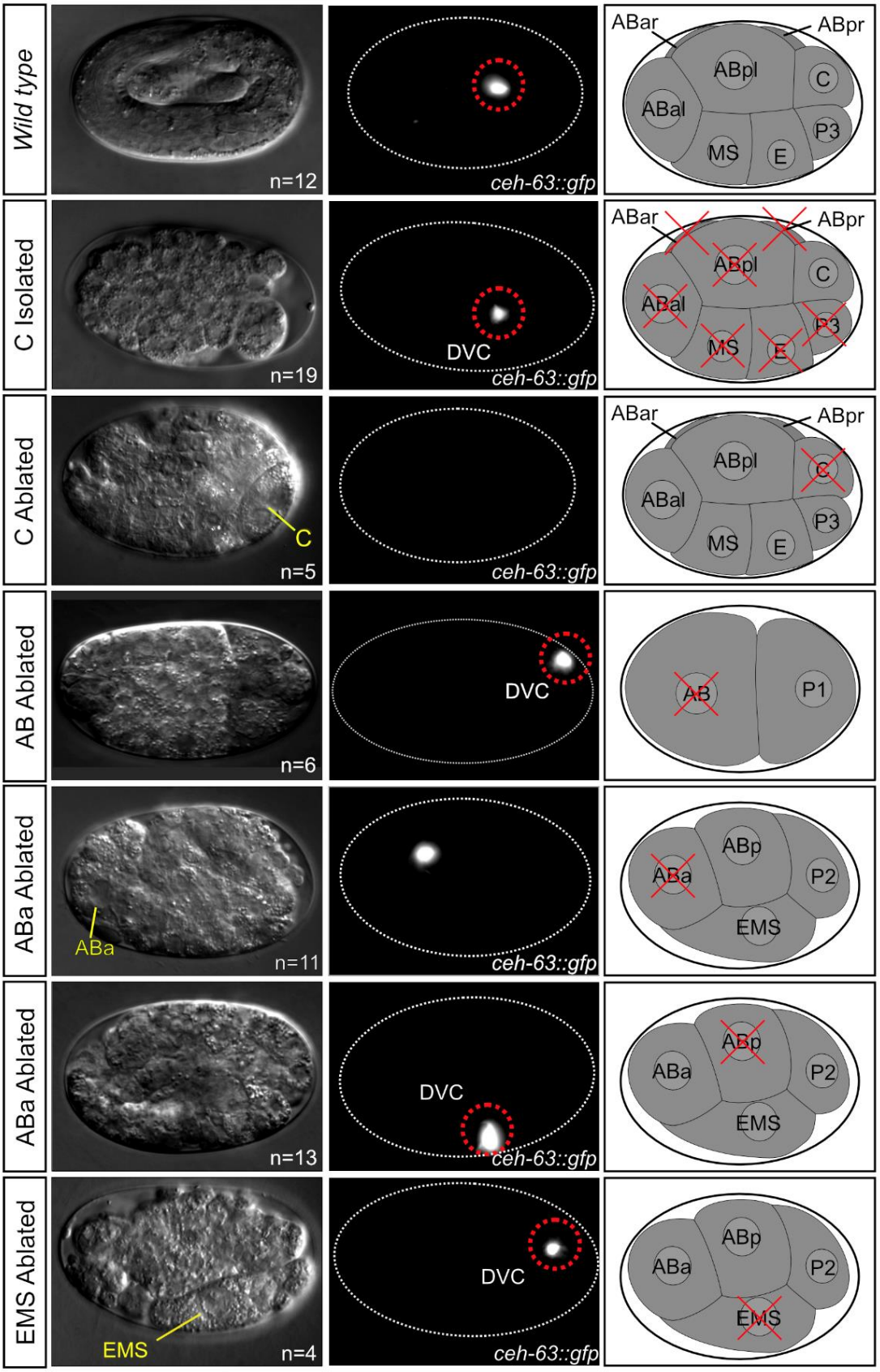

Figure 3.3. Blastomere laser ablation. *The presence of a DVC neuron is evidenced by the expression of the ceh-63::gfp reporter, often with the characteristic tear-shaped cell body. When readily identifiable arrested early blastomeres are indicated in the DIC images. Schematics indicate the blastomere ablated with a red cross with the embryo stage depicted indicative of the timing of the ablation.*

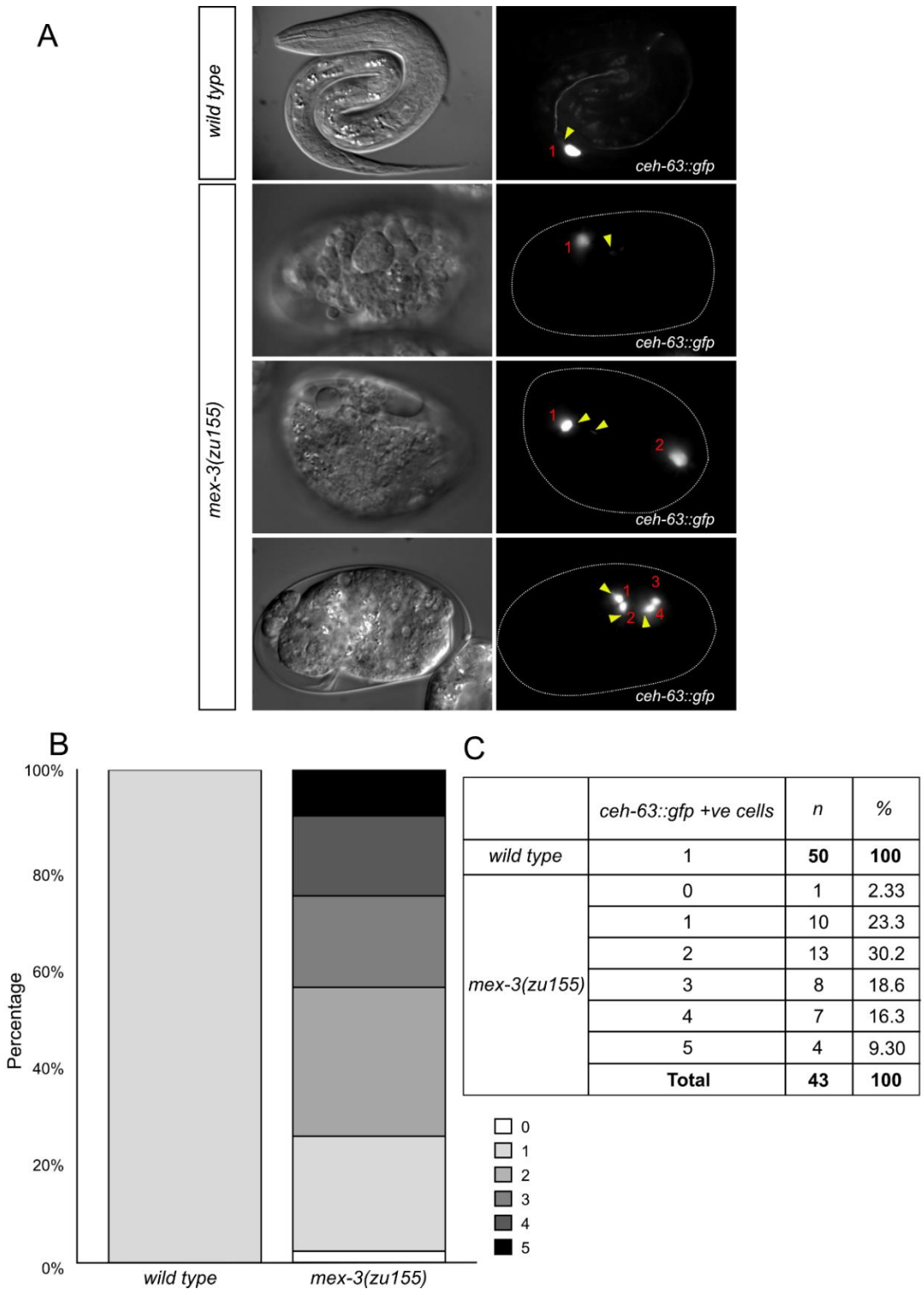

C

	ceh-63::gfp +ve cells	*n*	*%*
wild type	1	**50**	**100**
mex-3(zu155)	0	1	2.33
	1	10	23.3
	2	13	30.2
	3	8	18.6
	4	7	16.3
	5	4	9.30
	Total	**43**	**100**

Figure 3.4. Scoring for the presence of DVC neurons in *mex-3(zu155)* mutants. *A) DIC and GFP images of representative mex-3(zu155), ceh-63::gfp embryos used for scoring of the presence of DVC. Red number = number of neurons, yellow arrow = clear neuronal process. B) Stacked bar chart of the number of DVC neurons in slide scored mex-3(zu115), ceh-63::gfp embryos and wild type embryos. C) Table of number of DVC neurons in slide scored mex-3(zu115), ceh-63::gfp embryos.*

Chapter 4

4. Investigating the Role of Unequal Cleavage in the Acquisition of Neuronal Fate

4.1. Manipulation of Spindle Position with *lin-5(ev571ts)*

As discussed in Chapter 3, the observation that two clearly unequal cleavages occur prominently, immediately preceding the onset of detectable *hlh-14* expression in the neurogenic branches of the C lineage leads to a number of exciting questions. Does this unequal cleavage, and the subsequent asymmetry in daughter cell size, impact on fate decisions and in particular the regulation of *hlh-14* expression? Or rather is the asymmetry in cell size indicative of a fate choice having occurred and thus an output of said choice? As stated in the introduction section an absence of growth in the *C. elegans* embryo means that unequal cleavage is the only method by which size asymmetry can be generated and the relationship between cell size and fate remains understudied in the field.

To address these questions, a method to manipulate the size of daughter cells in a manner independent of polarity was required. Daughter cell size is known to be regulated through either spindle positioning or cortical tension, or a combination thereof with different divisions relying on either one to varying extents, for example (Lorson et al., 2000; Ou et al., 2010; Pacquelet et al., 2015). As the C lineage has to date not been studied with regards to unequal cleavage, it was unknown which was of primary importance in the lineage. However, as neuronal precursor divisions in *C. elegans* often display non-centralised cleavage planes, manipulation of spindle position was undertaken as a first approach.

Caap, the grandmother of both DVC and PVR, is the posterior daughter of the first of the two unequal cleavages in the C lineage. It marks the part of the lineage from which the neuronal branches descend as its descendants, Caapa (the mother of DVC) and Caappa (PVR) are the first cells in which *hlh-14* expression can be detected (Poole et al., 2011; Sulston et al., 1983). Being upstream of *hlh-14* expression the Caaa/Caap division potentially marks a key neuronal fate decision. I therefore sought to symmetrise the cleavage plane in this division resulting in

daughters of equal size, in order to address the crucial questions of whether unequal cleavage was required to asymmetrically segregate an upstream regulator of *hlh-14* expression and if daughter cell size impacted on the acquisition of subsequent neuronal fate.

In order to have temporal control over the manipulation I employed a temperature sensitive mutant of *lin-5,* the *C. elegans* NuMa homologue. Both the temperature sensitive allele *ev571* and RNAi knockdown of *lin-5* cause either a block of or delay in cytokinesis, or equalisation of cleavage in the one-cell embryo (Lorson et al., 2000).

Live lineaged embryos were incubated at the permissive temperature of 15°C until just prior to the beginning of cytokinesis and shifted to the non-permissive temperature of 25°C to disrupt the division using the CherryTemp temperature-controlled stage, described in the Materials and Methods section of this thesis. 2/4 *lin-5(ev571)* embryos shifted for a few minutes prior to the onset of division were blocked in cytokinesis, the cells skipping the round of division. 2/4 embryos demonstrated a dramatic equalisation of the daughter size (Figure 4.1 A) with a mean Caaa/Caap ratio of 1.21 compared to 2.30 ± 0.266 (n = 10) in *wild types* (Figure 4.1 B). This had a variable effect on the asymmetry in daughter size on the next division with the Caapa/Caapp ratio reversed from *wild type* in one embryo and equalisation in another with a mean ratio of 2.05 (n = 2) (Figure 4.1 B). Shifted embryos also displayed a precocious division of Caapa with its cell cycle duration resembling *hlh-14* mutants in that it divided at the same time as Caapap and their hypoblastic cousins (Figure 4.1 A). No assessment of fate was made in these embryos as they did not carry GFP reporters.

Assessment of *hlh-14* expression was performed using an integrated translational fusion of HLH-14 and GFP[265C] driven from the *hlh-14* promoter (Frank et al., 2003). However, the Caaa/Caap division was equalised in 0/16 shifted embryos which carried the reporter, 12/16 not showing visible cleavage plane disruption. Cytokinesis was blocked in the remaining 4/16 embryos (Figure 4.2 A). In these blocked embryos cells visibly stopped attempting to divide after a few minutes, after which they were shifted down to the permissive temperature once more. Following downshift, Caa divided in time with the next round of division when Caaa and Caap would normally divide. In 2/16 embryos “Caaa” and “Caap” then proceeded to divide when the terminal hypoblast divisions occur in *wild type*, this was the final round of division meaning that a loss of a division round occurred in these embryos (Figure 4.2 A). 2/16 embryos displayed an anterior “Caaa” anucleate cell which did not divide and an “Caap” cell which displayed a division pattern of the

wild type Caaa. This cell's daughters divided at the same as *wild type* hypoblasts and also divided once more themselves (Figure 4.2 A). In 4/4 embryos in which the Caaa/Caap division was blocked Caa and "Caap" contained two sets of spindle just prior to their respective divisions (Figure 4.2 B). This suggested that multinuclearity persisted into division rounds after those which were blocked.

In the 12/16 embryos in which the Caaa/Caap division was not blocked, the expression of *hlh-14* in Caapa was unaffected. Conversely, blocking the Caaa/Caap division resulted in a lack of *hlh-14* expression in the remaining 4/16 (Figure 4.2 C). Given both the anucleate/multinucleate nature of descendants of the blocked Caaa/Caap divisions and that in some cases the skipped round of division was not recovered, it is difficult to interpret the significance of the lack of *hlh-14* expression in the C lineage in these embryos. The question arises as to the identity and fate of these cells and whether they are attempting a developmental programme akin to that of their division round to be completed or as if the blocked division had occurred. What is clear however is that a division must occur for the onset of *hlh-14* expression.

Given that assessment of *hlh-14* expression following equalisation of Caaa/Caap was the express purpose of the *lin-5(ev571)* experiments, the fact that that equalisation in the *lin-5(ev571) hlh-14::gfp* strain was unachievable meant that an alternative more explicitly genetic approach was initiated in its place.

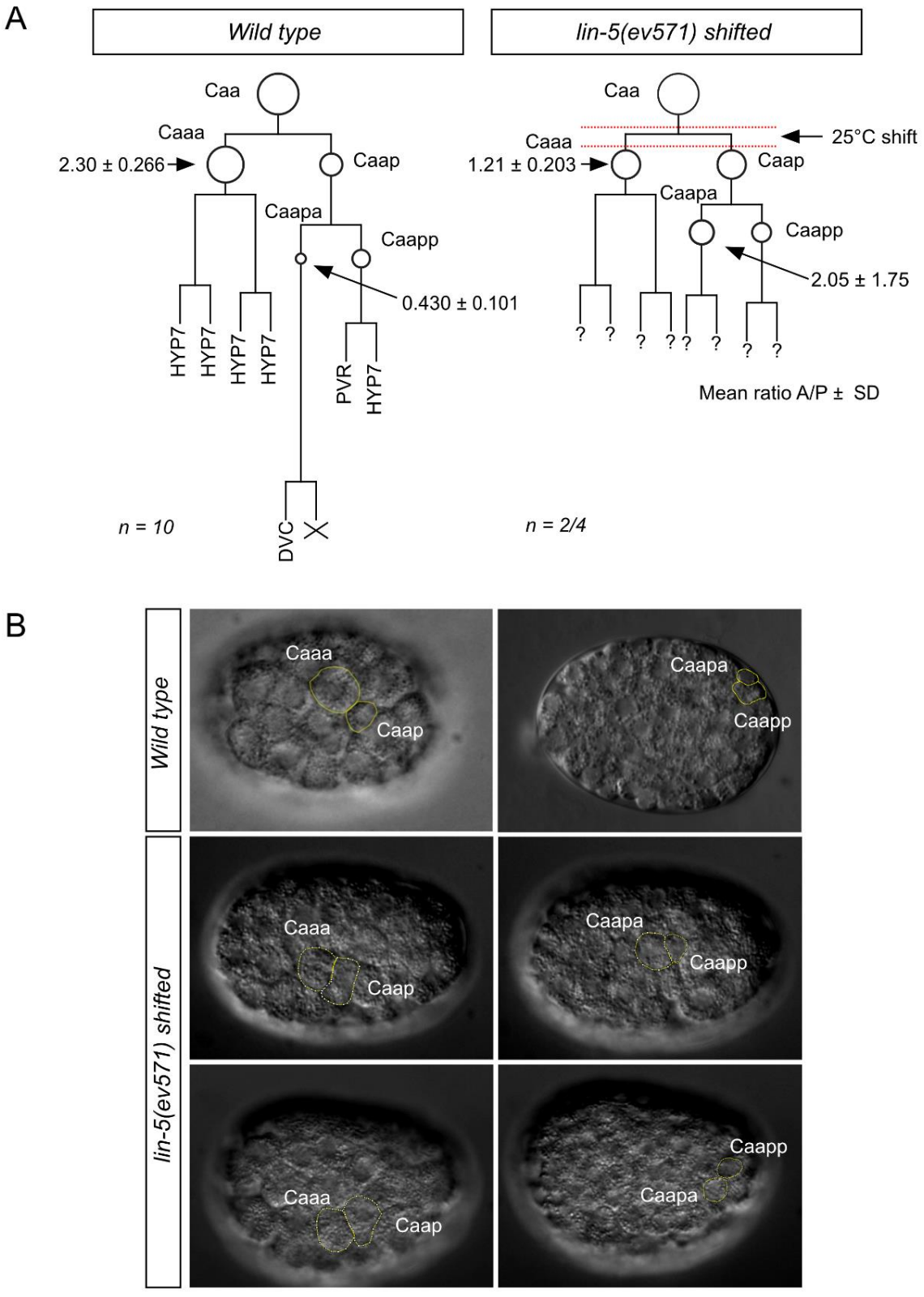

Figure 4.1. Equalisation of C lineage cleavages in *lin-5(ev571ts)* mutants. *A) A schematic representation of the temperature shift experiments of lin-5(ev571) temperature sensitive mutants and lineage consequences. Embryos were incubated at 15 °C, outside of the indicated 25°C shift period. Arrows indicate the anterior daughter of the division in question. Numbers express the cell size asymmetry as the volume of the anterior cell divided by the posterior cell. B) DIC images of wild type and lin-5(ev571) embryos indicating equalisation of Caa/Caap and Caapp/Caapp cleavages.*

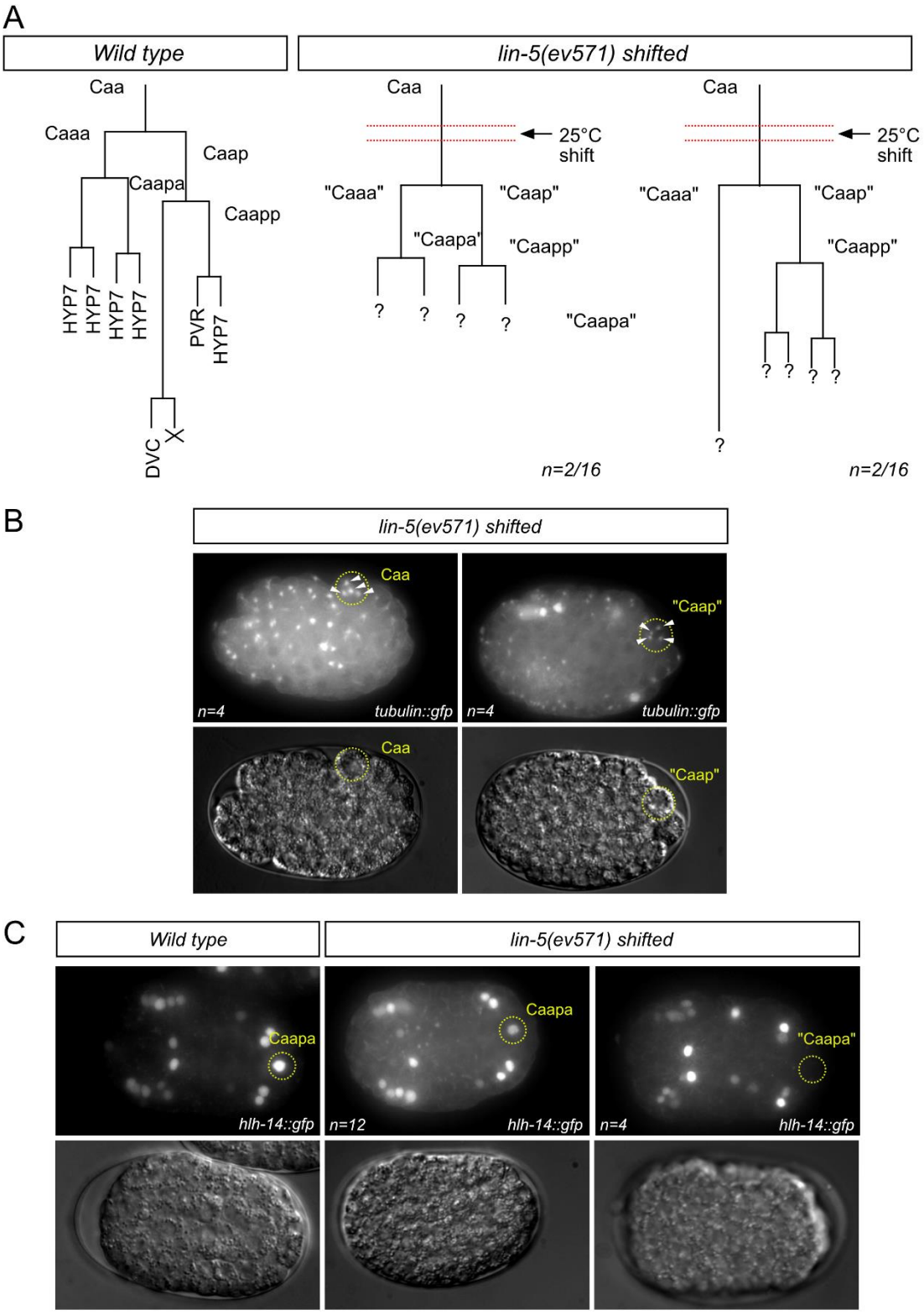

Figure 4.2. Multiple spindle and *hlh-14* expression in *lin-5(ev571ts)* hlh-14::gfp mutants with blocked . *A) A schematic representation of the temperature shift experiments of lin-5(ev571) temperature sensitive mutants and lineage consequences. Embryos were incubated at 15 °C, outside of the indicated 25°C shift period. Cell names in quotation marks indicate that a cell is the product of a previously blocked division. B) DIC and GFP images of indicating multiple sets of mitotic spindle lin-5(ev571) embryos as indicated by tubulin::gfp. Yellow circles = position of indicated cell. White arrows = mitotic spindle. C) hlh-14 expression pattern in wild type and lin-5(ev571) using gmIs20.*

4.2. The role of PIG-1 and HAM-1 in C lineage Unequal Cleavages

As discussed in the introduction chapter the *C. elegans* MELK kinase homologue PIG-1 is involved in asymmetric neuroblast divisions (Cordes et al., 2006). The transcription factor HAM-1 is a known upstream regulator of *pig-1* in a number of these neuronal lineages (Feng et al., 2013; Frank et al., 2005), in particular being implicated in asymmetric and unequal divisions in which a smaller anterior daughter is fated to undergo apoptosis (Teuliere et al., 2018). Whilst not previously implicated in the C lineage and mainly investigated for roles in terminal divisions, I hypothesised that they may play a role in unequal cleavages further up in lineages. This was due to the indication of a more general role in unequal cleavage due to *pig-1*'s recently described roles in the one-cell embryo and EMS blastomere divisions (Liro et al., 2018; Pacquelet et al., 2015). Mutants of *pig-1* and *ham-1* were thus assessed for unequal cleavage phenotypes in the C lineage. As described in the following sections I find that certain C lineage cleavages are equalised in these mutants. This demonstrated that the mutants could be used as a genetic tool for the crucial assessment of whether the equalisation of dramatically unequal cleavages impacted on the initiation of the proneural gene *hlh-14* in the lineage.

4.2.1. Equalisation of Caaa/Caap and Caapa/Caapp in *pig-1(gm344)*

Investigation of *pig-1* was undertaken using the null allele, *gm344,* which has been used in many studies of neuroblast and early embryonic divisions. 28/28 *pig-1(gm344)* mutants display equalisation in both the Caaa/Caap and Caapa/Caapp divisions, clearly revealed from DIC imaging (Figure 4.3 A). This therefore demonstrates that PIG-1 must play a role in regulating the two unequal cleavages in the C lineage.

Of the 21 measured *pig-1(gm344)* embryos, all displayed dramatic reductions in size asymmetry for the Caaa/Caap division. This yielded a daughter size asymmetry ratio of 1.17 ± 0.275 (A/P ± standard deviation) which is significantly different to that of the *wild type* 2.30 ± 0.266 ($p<0.0001$) (Figure 4.3 B; 4.4 A). The degree to which the daughter size asymmetry was reduced in *pig-1(gm344)* mutants ranged from two embryos with comparatively smaller reductions with ratios of 1.77 and 1.75 to those in which the posterior daughter was slightly larger than the anterior with a ratio of around 0.850, for example 0.864 and an outlier of 0.687. However, the majority of the 21 measured embryos displayed ratios that can be considered clearly equalised with respect to *wild*

type clustering around a ratio of 1.2 (Figure 4.4 A). As would be expected this equalisation results in an increased absolute volume of Caap which ranges in a similar manner to the range in ratio. This increase was found to be significant with a mean value of 356693 voxels larger than that of the *wild type* 245549 ($p<0.01$) (Figure 4.4 B).

For Caapa/Caapp 21/21 embryos exhibited reductions in daughter size asymmetry with ratios all outside of the *wild type* range and a mean value of 0.949 ± 0.183 (Figure 4.3 B). This is a significant equalisation with respect to the *wild type* value of 0.430 ± 0.101 (Figure 4.3 B; 4.4 A) ($p<0.0001$). As with Caaa/Caap, values for individual embryos clustered around the mean, in this case at 0.9, save outliers of larger, 1.40 and smaller effect, 0.629 (Figure 4.4 A). As with the previous division, this equalisation also results in a larger absolute volume for Caapa. Being the product of two equalised division the difference to the *wild type* volume is even greater than for Caaa/Caap being measured at 184757 voxels compared to the *wild type* 57659 ($p<0.0001$) (Figure 4.4 B).

4.2.2. *pig-1* is Expressed in Caa and Caap

Following the finding that *pig-1(gm344)* mutants display equalisation of the Caaa/Caap and Caapa/Caapp divisions the question arose as to whether PIG-1 was acting within the dividing cells in controlling daughter size. Despite its widespread expression pattern, expression of *pig-1* in both Caa and Caap was confirmed using the transgene *bcSi43*, a full length, MosSCI single insertion, transcriptional GFP reporter using the *pig-1* promoter. The signal was clearer in Caap but in both cells nuclear expression was evident (Figure 4.5). It is therefore expressed at the right time and place to be potentially acting cell-autonomously.

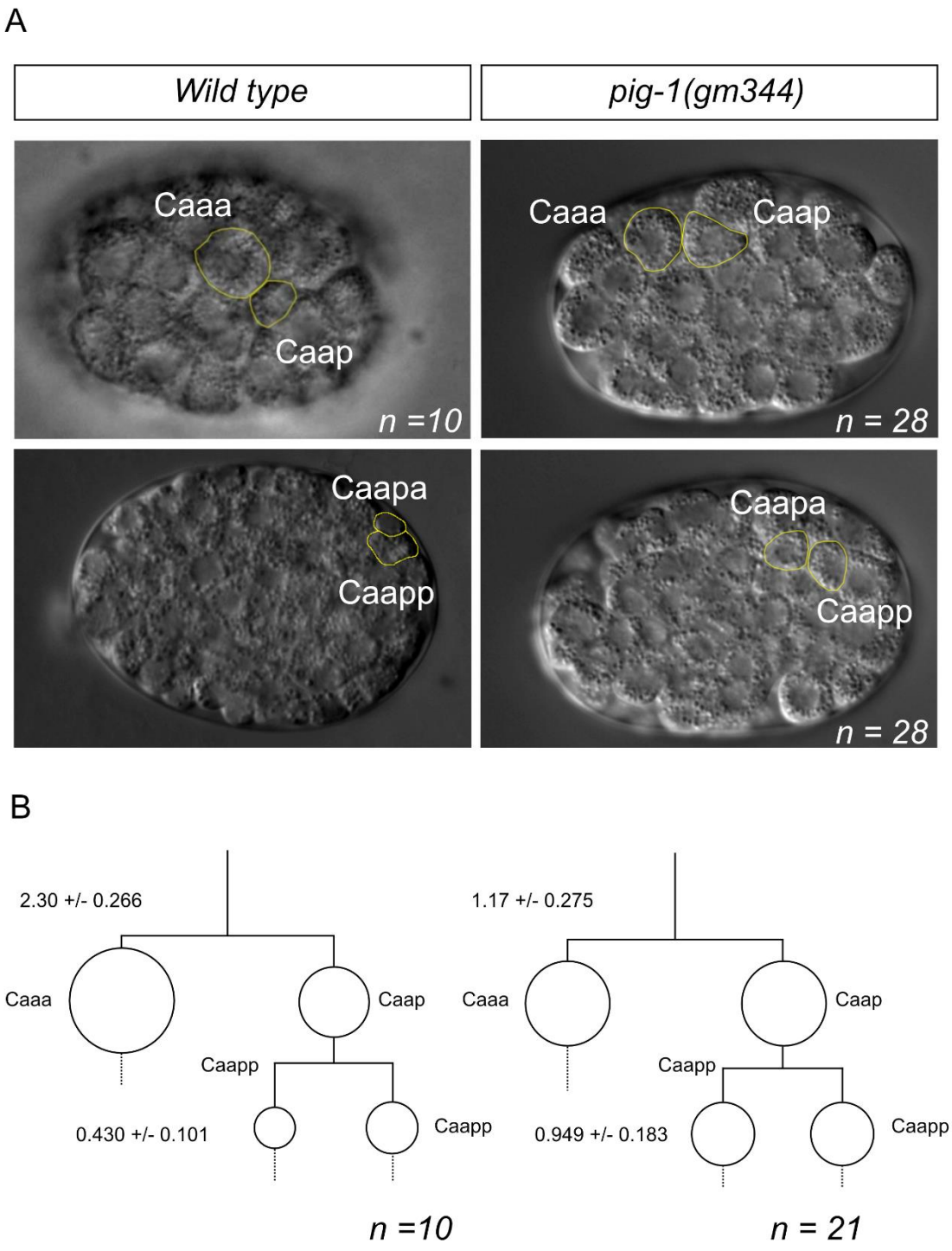

Figure 4.3. C lineage cleavage equalisation phenotypes in *pig-1(gm344)*. *A) DIC images of wild type and pig-1(gm344) embryos showing indicative equalisation of cell size following the Caaa/Caap and Caapa/Caapp cleavages. B) Partial C lineage diagrams depicting the loss of daughter size asymmetry at the Caaa/Caap and Caapa/Caapp cleavages. Circles are illustrative of relative differences in cell size. Volume ratios are expressed as volume of anterior daughter/ volume of posterior daughter +/- standard deviation. Dotted lines indicate that the lineage belong this point is not depicted in the diagram.*

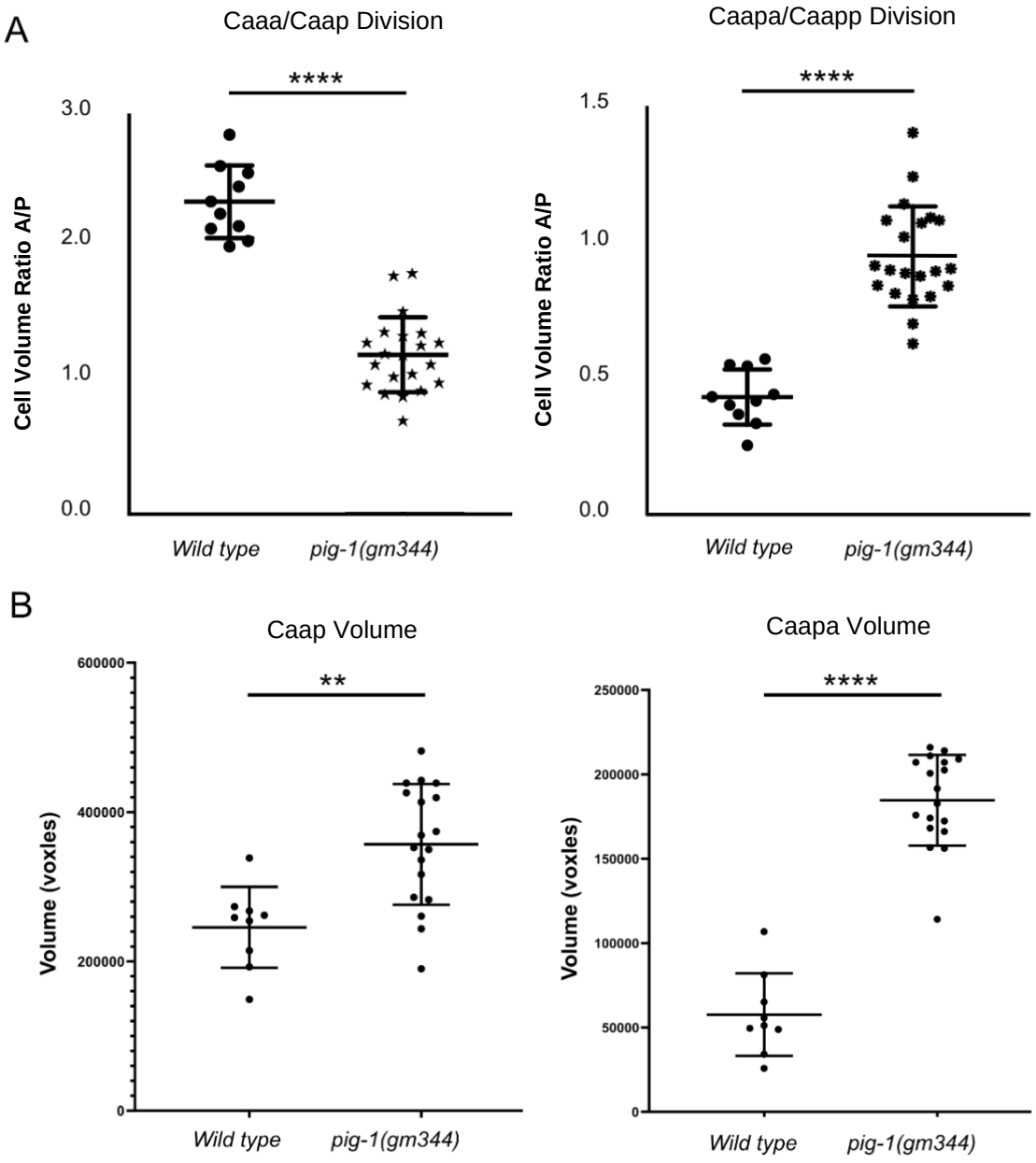

Figure. 4.4. Quantification of Caaa/Caap, Caapa/Caapp volume ratios in *pig-1(gm344)* mutants. *A) Scatter dot plot illustrating cell volume ratios following the Caaa/Caap and Caapa/Caapp cleavages in wild type and pig-1(gm344) embryos. Plots include mean ± standard deviation. B) Boxplots of absolute volume of Caap and Caapa in wild type and pig-1(gm344) embryos. Plots include mean ± standard deviation. ** = p < 0.01, **** = p < 0.0001, One-way ANOVA, with Holm-Sidak post hoc test for multiple comparisons.*

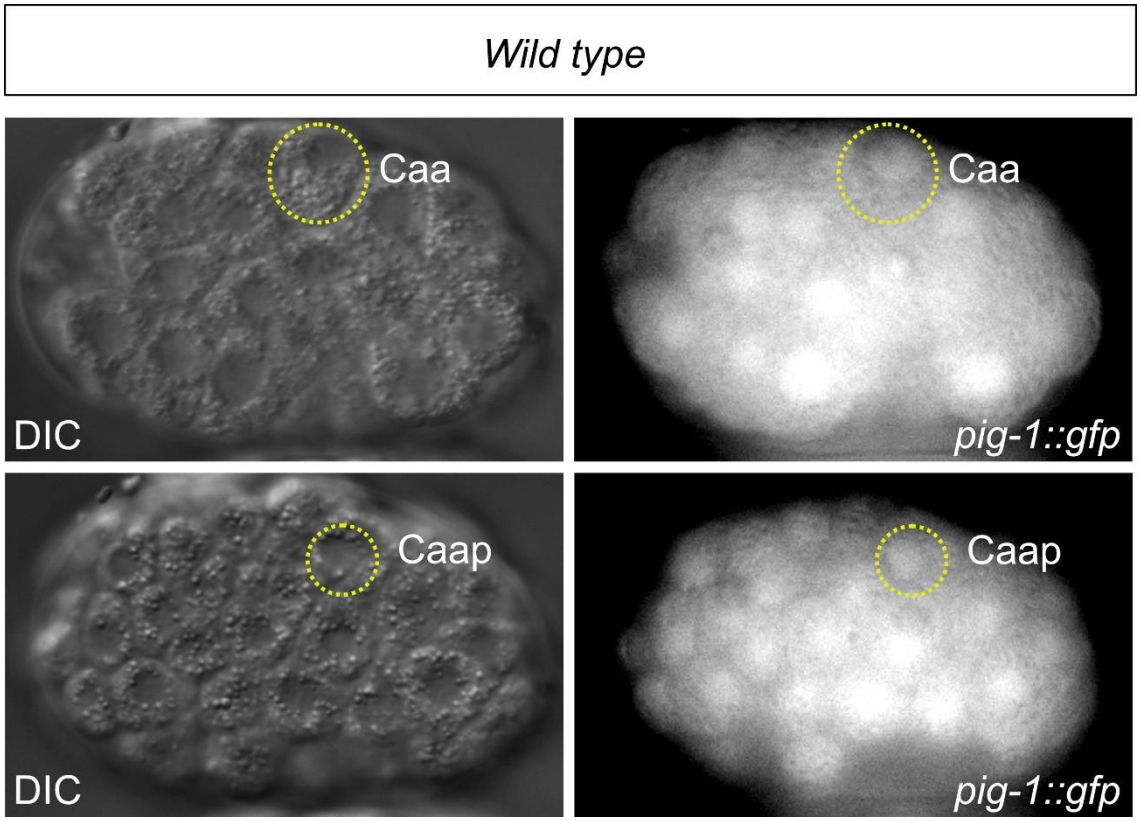

Figure 4.5. Expression of *pig-1::gfp* in Caa and Caap. *Expression pattern of pig-1 in wild type embryos as indicated using the bcSi43 transgene. Yellow circles mark the position of the indicated cell.*

4.2.3. Equalisation of Caaa/Caap and Caapa/Caapp in *pig-1(gm344)* Mutants Has no Effect on the Initiation of *hlh-14* Expression

4D lineage analysis was employed using the *hlh-14::gfp* reporter *gmIs20* and the unique DVC marker *ceh-63::gfp*. Crucially this revealed that as in a *wild type* embryo, *hlh-14* was expressed initially in Caapa and following division, in its daughters Caapaa, which will become DVC and Caapap, fated to apoptose, in 24/26 (92.3%) of lineaged embryos (Figure 4.6). The scarcity of the loss of *hlh-14* phenotype demonstrates that the equalisation of daughter size has little impact on the initial expression of *hlh-14* and thus that size is neither the sole nor most important factor in determining the segregation of its expression. Importantly, this is supported by the observation that ectopic *hlh-14::gfp* from the *gmIs20* transgene was not detected in either the hypodermal branch from Caaa or in Caapp, the sister branch of Caapa. Expression in all cases arose in the Caapa branch as in *wild types,* with extra expression resultant from extra cells in this branch.

The remaining 2/26 embryos lacked expression in the C lineage with Caapaa and Caapap displaced laterally, rather than in their central location in *wild type* embryos (Figure 4.6 A). This positioning places the cells adjacent to their hypodermal cousins and could be indicative of the adoption of at least a partial hypodermal fate.

4.2.4. *pig-1(gm344)* Mutants Display Ectopic *hlh-14* Expression due to Extra C lineage Divisions

Despite this lack of impact on the initial expression of *hlh-14, pig-1(gm344)* mutants display a number of intriguing phenotypes downstream of this event. Later in the bean stage 5/24 *hlh-14* expressing embryos displayed ectopic expression of the proneural gene (Figure 4.6 A). 4D lineage analysis revealed that this ectopic expression was due to extra divisions of either both or one of Caapaa and Caapap (Figure 4.7 A). 3/26 (11.5%) embryos overall expressed *hlh-14* in three cells following said extra divisions. 2/26 (7.69%) displayed four *hlh-14* expressing cells (Figure 4.6 B, C, Figure 4.7 A), namely the supernumerary cells Caapaaa, Caapaap, Caapapa and Caapapp such as the embryo in Figure 4.6 A. In *wild type* development *hlh-14* expression is initially detected in Caapap but quickly ceases as the cell undergoes apoptosis. In *pig-1(gm344)* this cessation of expression was observed in 9/19, or 9/26 (34.6%) overall, of those embryos displaying the *wild type* expression pattern. Expression persisted in the other 10/19 embryos

leaving two expressing cells at the end of the bean stage, Caapaa and Caapap; 10/26 (38.5%) (Figure 4.6 B, C). In all embryos in which ectopic expression was detected, all cells demonstrated persistent expression of *hlh-14::gfp.* The persistence of expression suggests that both supernumerary cells and Caapap are surviving and not undergoing apoptosis in these embryos. This is consistent with the observation that a clear cell death was only evident in 3/28 (10.7%) embryos. Although newly described for the C lineage, this is also consistent with PIG-1's known role in apoptotic-neuroblast divisions where loss of PIG-1 either results in loss of (Cordes et al., 2006) or delay in apoptosis (Wei et al., 2017)

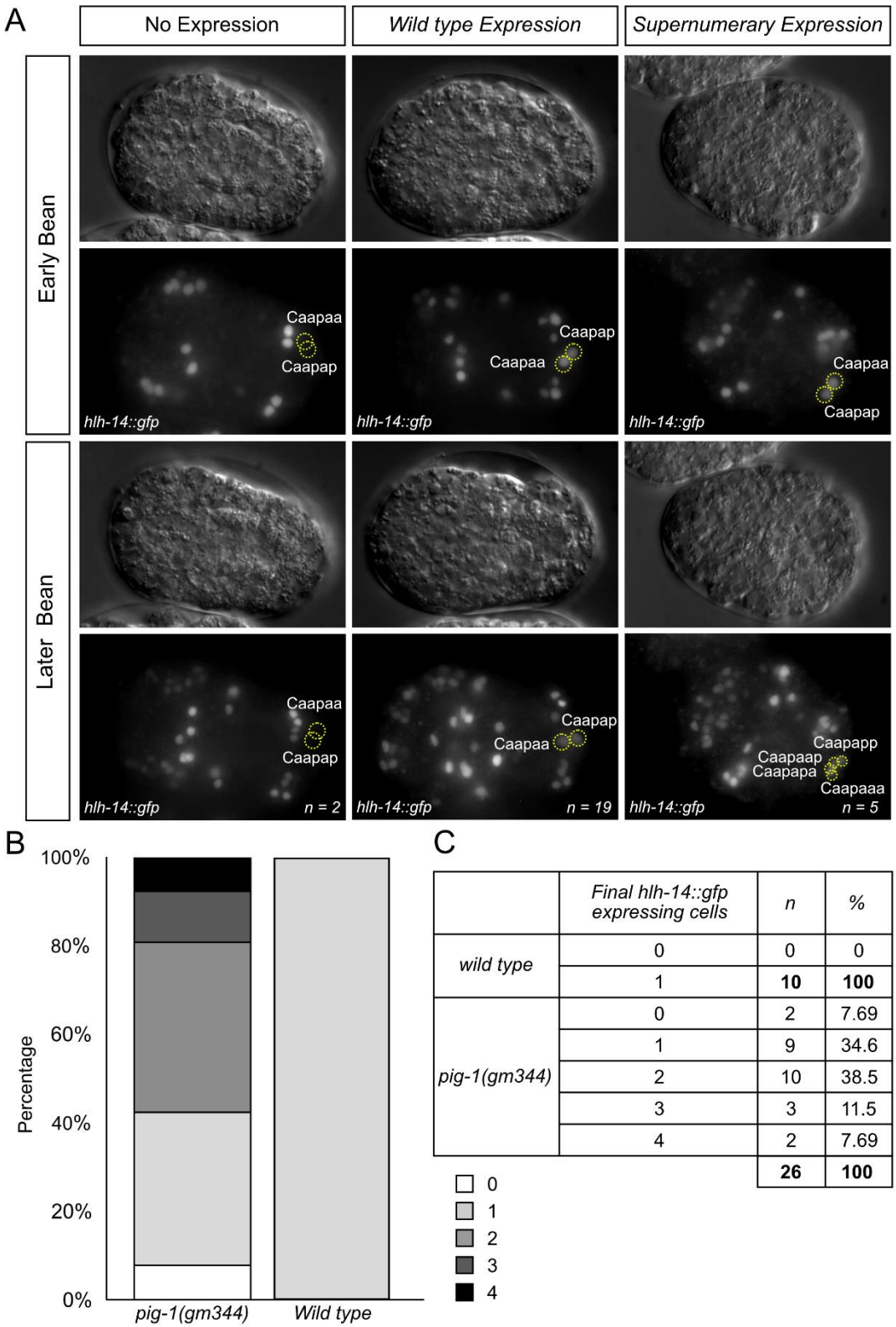

	Final hlh-14::gfp expressing cells	*n*	*%*
wild type	0	0	0
	1	**10**	**100**
pig-1(gm344)	0	2	7.69
	1	9	34.6
	2	10	38.5
	3	3	11.5
	4	2	7.69
		26	**100**

Figure 4.6. *hlh-14* expression pattern in *pig-1(gm344)* mutants. *A) DIC and GFP images of hlh-14::gfp expression at the bean stage in pig-1(gm344) mutants. Yellow circles = position of indicated cell. B) Stacked bar chart representing proportions of embryos with different numbers of hlh-14 expressing cells at the end of the bean stage. Number in the coloured boxes indicate the number of expressing cells. C) Table of data in B). "Final hlh-14::gfp" refers to the fact that expression does not persist in all cells.*

4.2.5. Supernumerary DVC Neurons Arise from Extra C Lineage Divisions in *pig-1(gm344)*

The occurrence of extra divisions in the C lineage and thus supernumerary expression of *hlh-14* was not indicative of the number of cells that would undergo neurogenesis. Neither was there an apparent link between whether a cell underwent an extra round of division and whether its descendant become a DVC neuron.

The two embryos lacking *hlh-14* expression divided early, in time with the hypoblast divisions and reminiscent of the precocious Caapa division of *hlh-14* mutants. As expected these embryos did not show *ceh-63::gfp* expression and lacked neurogenesis. 10/28 (35.7%) embryos displayed a *wild type* division pattern with Caapa dividing around twice as late as Caapp and the C lineage hypoblast divisions (Figure 4.7 A). However, Caapaa became DVC in only 5/10 of these embryos with Caapap, normally fated to die, becoming DVC in 2/10 embryos. In 3/10 despite either a *wild type* expression pattern of *hlh-14* or maintained expression in Caapap, neither cell became DVC (as evidenced by *ceh-63::gfp* expression). Despite a *wild type hlh-14* expression pattern, Caapa divided precociously in 10/28 embryos, displaying an otherwise *wild type* division pattern. DVC arose from Caapap in 4/10 of these embryos, both Caapaa and Caapap in 1/10, Caapaa in 4/10 embryos and was absent in 2/10 (Figure 4.7 A). Caapaa underwent an extra division following the precocious division of Caapa in 2/28 embryos with the resultant supernumerary cells Caapaaa and Caapaap becoming DVC in 1/2 and Caapap doing so in 1/2 embryos (Figure 4.7 A). 2/28 embryos displayed an extra division of Caapap only. Caapaa became DVC in both embryos, despite expression of *hlh-14* in the supernumerary Caapapa and Caapapp (Figure 4.7 A). The most severe division phenotype was displayed by 2/28 embryos in which Caapa divided precociously and its daughters both erroneously divided, yielding four *hlh-14* expressing cells. Despite this *hlh-14* expression in 2/2 of these embryos the daughters of the anterior branch, Caapaaa and Caapaap became DVC neurons (Figure 4.7 A).

Summarising the lineal origin of DVC neurons in *pig-1(gm344)* mutants, 7/28 lineaged embryos lacked a DVC neuron despite only two of these embryos lacking expression of the *hlh-14* (Figure 4.7, B, C). The most frequent lineal identity of DVC was Caapaa, as it is in *wild type*; 9/28 (32.1%) embryos displayed a single DVC identified as Caapaa (Figure 4.7 B). This was true of both embryos with a *wild type* C lineage division pattern and those with either just a precocious Caapa division or those with an extra division (Figure 4.7 A). 8/28 (28.6%) embryos had a DVC neuron arising solely from Caapap, (Figure 4.7 B) the sister cell of DVC in *wild types*, indicating a reversal

of the division. Caapaa and Caapap became DVC in 1/28 (3.57%) embryo. Caapaaa and Caapapa, the supernumerary daughters of the would-be DVC adopted DVC fate in 3/28 (10.7%) embryos (Figure 4.7 B).

The division pattern defects in *pig-1(gm344)* evidently show a great degree of variability which also leads to variability in the *hlh-14* pattern and therefore which cells undergo neurogenesis to become DVC. A few things are apparent from this data. An initial observation is that *pig-1(gm344)* affects three divisions, the first and second unequal cleavages, Caaa/Caap and Caapa/Caapp, and the terminal DVC neuroblast division Caapaa/Caapap. The mutants can therefore be seen as belonging to three broad categories with respect to their lineage phenotypes and fate consequences; those affecting *hlh-14* expression, those with extra divisions and so supernumerary cells, and those with only terminal division phenotypes and loss of apoptosis. Whether there is an identifiable difference between these would-be classes and so whether they are meaningful is unknown. Moreover, when grouped in this way they do not differ significantly in terms of daughter size ratio for the first of the unequal cleavages Caaa/Caap; 1.22 ± 0.0657 (A/P ± standard deviation), 1.07 ± 0.192 and 1.23 ± 0.332 respectively (Figure 4.8 A). The same is true for second unequal cleavage Caapa/Caapp with the ratio not being shown to differ significantly; 1.15 ± 0.353, 0.867 ± 0.148 and 0.969 ± 0.152 respectively (Figure 4.8 B). Therefore, any biologically relevant difference that would confirm the classes is not due to daughter cell sizes.

Another observation is that the expression of the proneural gene in these mutants is not sufficient to drive neurogenesis in all cells expressing it. A potential explanation for this could be that the segregation of an apoptotic signal to Caapap may not be greatly affected by the increased volume of Caapa. When considering the lineage pattern of these mutants it is also clear that there is an anterior bias in which cells become DVC even when expressing *hlh-14*. It is therefore possible that the apoptotic signal is still mainly inherited by Caapap and any descendants thereof in these mutants, and that this competes with HLH-14 with neither enough to fully realise either fate.

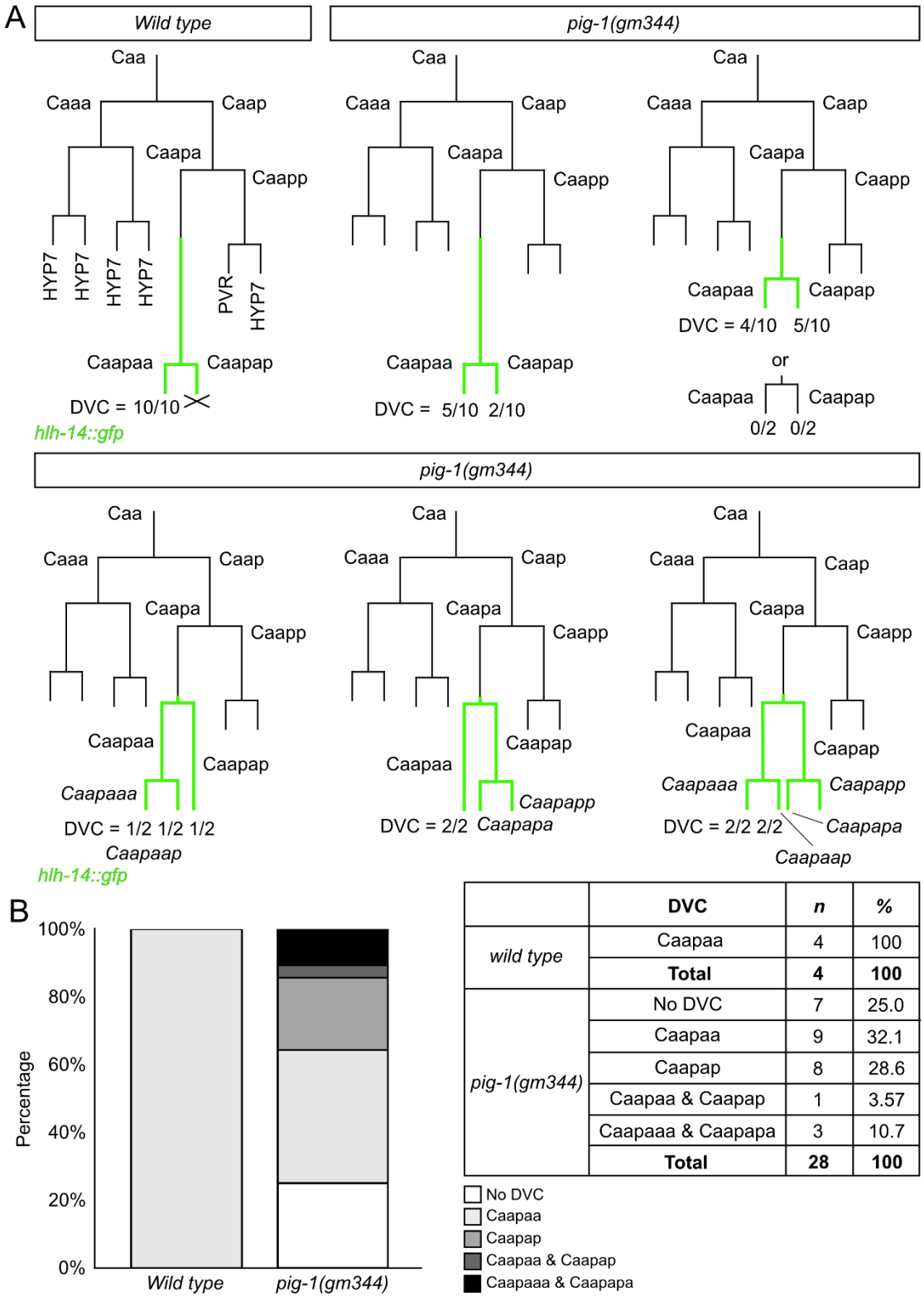

	DVC	*n*	%
wild type	Caapaa	4	100
	Total	**4**	**100**
pig-1(gm344)	No DVC	7	25.0
	Caapaa	9	32.1
	Caapap	8	28.6
	Caapaa & Caapap	1	3.57
	Caapaaa & Caapapa	3	10.7
	Total	**28**	**100**

Figure 4.7. Lineage analysis of *pig-1(gm344)* mutants. *A) Illustrative lineage diagrams of different observed lineage patterns. Line length are indicative of cell cycle duration. Green lines indicate hlh-14::gfp expression as scored using the gmIs20 transgene. Numbers under terminal branches indicate both the number of embryos with the observed pattern, and which hlh-14::gfp expressing cells within all embryos displaying that pattern became a DVC neuron. B) Stacked bar chart and table indicating the proportion of embryos in which particular cells became a DVC neuron, rather than cells scored individually as in A).*

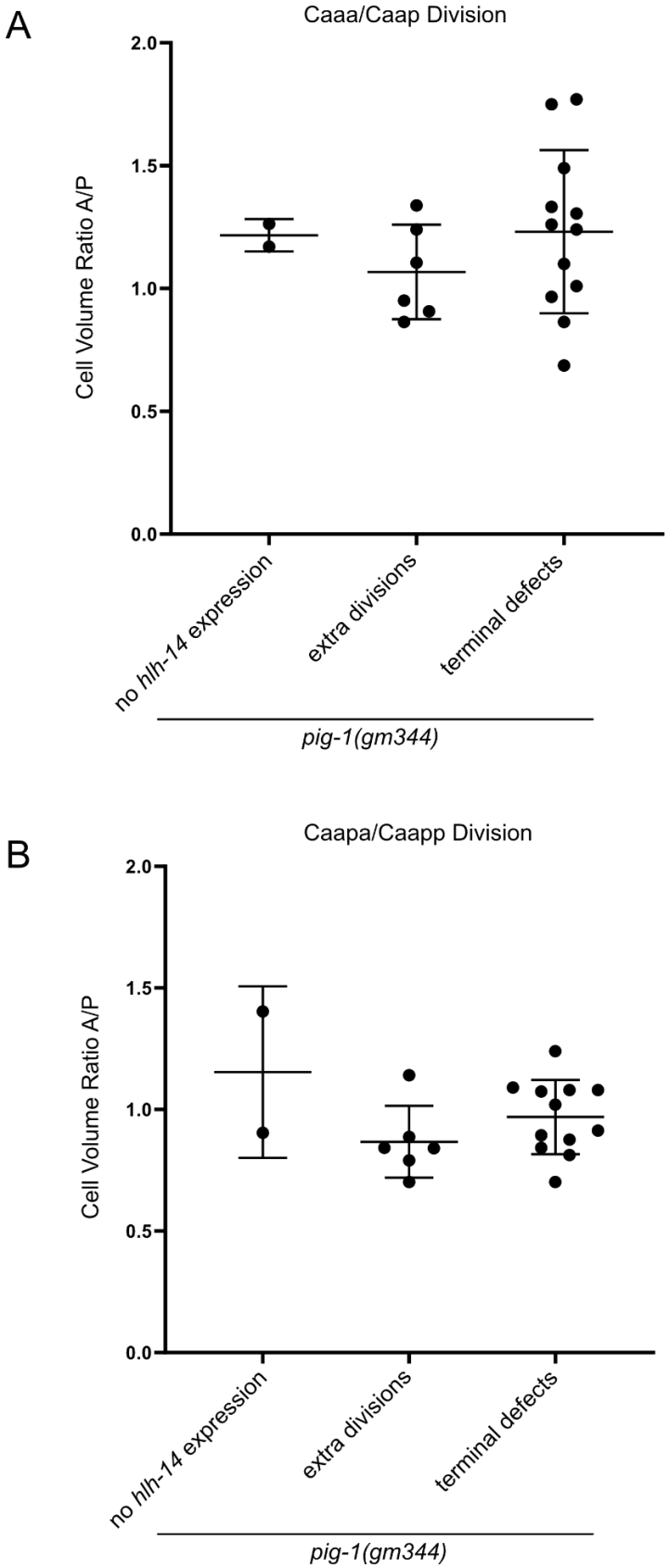

Figure 4.8. Quantification of Caaa/Caap, Caapa/Caapp volume ratios in *pig-1(gm344)* mutants grouped as phenotypic classes. *A) Scatter dot plot illustrating cell volume ratios following the Caaa/Caap cleavages in pig-1(gm344) embryos grouped in phenotypic classes. B) Scatter dot plot for Caapa/Caapp Plots include mean ± standard deviation. Not significant, One-way ANOVA, with Tukey HSD post hoc test due to all possible comparisons.*

4.2.6. *pig-1(gm344)* Mutants Display a loss of, and Ectopic, DVC Neurons

I also sought to better assess the penetrance of the ectopic and loss of DVC phenotypes in *pig-1(gm344)* revealed through lineage analysis. To achieve this, embryos were mounted on slides and scored for the presence or absence of DVC using its unique maker *ceh-63::gfp*.

This analysis revealed that both a loss of and ectopic expression of the *ceh-63* (Figure 4.9 A), indicating both the loss of neurogenesis and the presence of extra neurons in agreement with the lineaging data. A small fraction of embryos mounted and scored on slides displayed no GFP positive cells, 8/94 (8.51%) indicating the lack of neurogenesis (Figure 4.9 B). 67/94 (71.3%) of the embryos displayed the *wild type* number of a single DVC, whilst two neurons were present in 18/94 (19.1%) of embryos (Figure 4.9 B). A single embryo, 1/94 (1.06%) had three neurons (Figure 4.9 B). A larger proportion of embryos displayed a lack of DVC than those scored via 4D lineage recordings of which 6/27 (22.2%) had no GFP positive cells (Figure 4.9 B). However as indicated by said lineaging, the loss in slide mounted animals is not necessarily due to the loss of initial *hlh-14* expression. Similar proportions of embryos displayed either one or two DVCs in 4D recordings as in those scored *en masse* on slides; 17/27 (63%) and 4/27 (14.9%) (Figure 4.9 B).

pig-1(gm344) is known to display a variable degree of embryonic lethality, which in this study was scored at 8% at 15°C, 18.3% at 20°C and 6.67% 25°C from embryos laid on plates (Figure 4.10 A). This was increased when scored in reporter carrying strains on slides at 25°C as 84/105 (80%) (Figure 4.11 A, B). However, loss of, or ectopic neurogenesis was not linked to whether the embryo arrested or completed embryogenesis as all phenotypes were observed in both cases (Figure 4.9 A). Furthermore, the array of phenotypes from a loss of DVC to extra neurons being present is also reflected in adult animals, indeed embryos scored here came from mothers of all types.

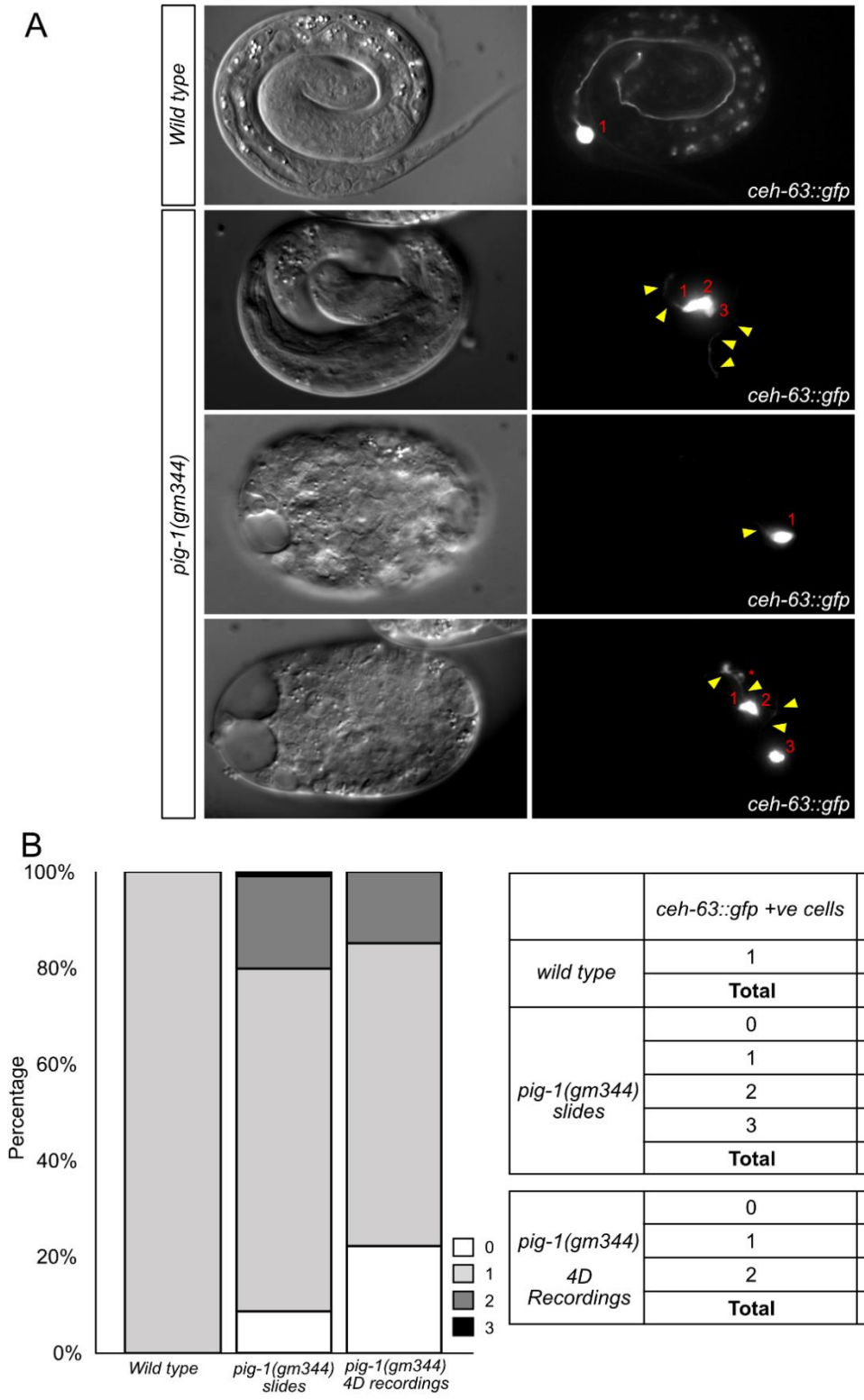

	ceh-63::gfp +ve cells	*n*	*%*
wild type	1	62	100
	Total	**62**	**100**
pig-1(gm344) slides	0	8	8.51
	1	67	71.3
	2	18	19.1
	3	1	1.06
	Total	**94**	**100**
pig-1(gm344) 4D Recordings	0	6	22.2
	1	17	63.0
	2	4	14.8
	Total	**27**	**100**

Figure 4.9. Scoring for the presence of DVC neurons in *pig-1(gm344)* embryos. *A) DIC and GFP images of representative. DIC images demonstrate that some embryos arrest, whilst other hatch. The presence of DVC neurons is evidenced by the expression of ceh-63::gfp, often with the characteristic tear-shaped cell body. Red numbers = the number of DVCs. Yellow arrows = clear neuronal processes. B) Stacked bar chart representing the number of DVC neurons in wild type and pig-1(gm344), ceh-63::gfp embryos from both mounted and lineaged embryos. A table detailing the scored number of DVC neurons in embryos.*

A

pig-1(gm344)

Temperature	Lethality	*n*	*%*
15C	Hatched	23	92.0
	Arrested	2	8.00
	Total	**25**	**100**
20C	Hatched	178	81.7
	Arrested	40	18.3
	Total	**218**	**100**
25C	Hatched	98	93.3
	Arrested	7	6.67
	Total	**105**	**100**

B

ham-1(n1438)

Temperature	Lethality	*n*	*%*
15C	Hatched	19	100
	Arrested	0	0
	Total	**19**	**100**
20C	Hatched	152	91.6
	Arrested	14	8.43
	Total	**166**	**100**
25C	Hatched	113	90.4
	Arrested	12	9.60
	Total	**125**	**100**

Figure 4.10. Lethality scoring for *pig-1(gm344)* and *ham-1(n1438)* embryos from hatching assays. *A) A table detailing the lethality for pig-1(gm344) embryos as assessed through hatching assays at three temperatures; 15°C, 20°C, 25°C. "Arrested" refers to death or arrest at any embryonic for larval stage. B) The same table for ham-1(n1438) embryos.*

A

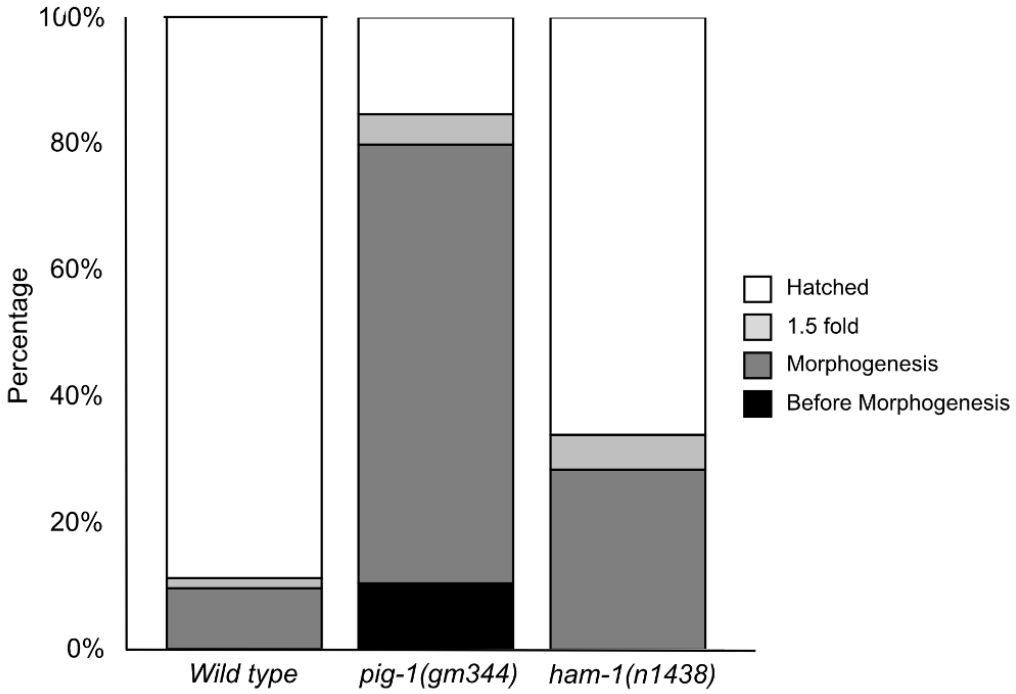

B

	Stage of Development Reached	*n*	*%*
wild type	Before morphogenesis	0	0.00
	Morphogenesis	6	9.68
	1.5-fold	1	1.61
	Hatched	55	88.7
	Total	**62**	**100**
pig-1(gm344)	Before morphogenesis	11	10.5
	Morphogenesis	73	69.5
	1.5-fold	5	4.76
	Hatched	16	15.2
	Total	**105**	**100**
ham-1(n1438)	Before morphogenesis	0	0.00
	Morphogenesis	16	28.6
	1.5-fold	3	5.36
	Hatched	37	66.1
	Total	**56**	**100**

Figure 4.11. Lethality scoring for *pig-1(gm344)* and *ham-1(n1438)* embryos from mounting assays at 25°C. *A) Stacked bar chart indicating the proportion of embryos either hatching or reaching the indicated stage of development before arresting when mounted on slides and incubated at 25°C overnight. B) A table detailing the same data.*

4.2.7. Equalisation of Caaa/Caap and Caapa/Caapp is not Corelated with Caapa Division Timing in *pig-1(gm344)*

As described above, *pig-1(gm344)* mutants displayed a variety of C lineage division patterns. These included a *wild type* pattern, precocious Caapa (DVC neuroblast) division, or extra divisions. In the case of extra divisions, the Caapa division also often occurred precociously. This resulted in a range of cell cycle durations, some within the *wild type* range at around 120 mins, and another proportion similar to the precocious divisions in *hlh-14* mutants of around 60 mins. This range was observed despite the equalisation of both divisions, suggesting that the timing of division was not linked to the size of the cell. Expressed in both actual minutes and as a ratio of the Caapa/Caap (mother/daughter) cell cycles, *pig-1(gm344)* mutants demonstrate significant reductions in the mean Caapa division time at 25°C; 83 mins ± 25 (n = 30) vs 129 mins ± 19 (n = 9) ($p<0.0001$) or 1.81 ± 0.499 vs 2.98 ± 0.599 ($p<0.0001$) (Figure 4.12 A, B).

4.2.8. Caaa/Caap Division Orientation is not Significantly Affected in *pig-1(gm344)* Mutants

Mutations in *pig-1* are thought to cause the randomisation of spindle orientation in some of the neuroblast divisions in which it was been implicated, particularly NSM (Wei et al., 2017). The variability of the C lineage phenotypes seen in *pig-1(gm344)* therefore prompted investigation of the division angles in the C lineage divisions in these mutants.

Division angles were measured using 3D stacks of embryos immediately following division. Angles in the AP axis were defined as a deviation from the line of the AP axis. Additional description of the method used to calculate these angles can be found in the Materials and Methods section of this thesis. A division in line with the axis was designated as an angle of 90° with orientations perpendicular to the line tending towards either 0° or 180° depending on the position of the posterior daughter. In *wild type* embryos the Caaa/Caap division angle was 125° ± 11.4 (n = 6) (Figure 4.13 A). Considering *pig-1(gm344)* in the classes introduced above, the angle for those embryos which lack *hlh-14* expression was 145° ± 4.7 (n = 2), those with extra divisions 118° ± 28.7 (n = 3) and those in which only terminal division were affected 120° ± 20.4 (n = 3) (Figure 4.13 A, B). Whilst embryos lacking *hlh-14* demonstrate the greatest difference compared to *wild type* this difference was found to not be significant ($p>0.05$) (Figure 4.13 B).

This is also true embryos with extra divisions and those affecting terminal divisions only, in additional to all *pig-1(gm344)* classes compared between themselves (p>0.05) (Figure 4.13 B).

Division angles with respect to deviation in and out of the imaging plane were used to define deviations from the DV axis. Divisions with daughters both in the imaging plane were assigned the angle of 90° with those in and out of the plane tending towards either 0° or 180° depending on whether the posterior daughter was out of the plane (higher) with respect to the anterior cell, to into it (lower). The *wild type* angle was measured at 96.4° ± 13.1 (n =6) (Figure 4.13 A). In a similar manner to that of the AP angle, the class of embryos lacking *hlh-14* expression demonstrated the greatest appreciable deviation from the *wild type* with an angle of 114° ± 18.3 (n = 2), which once again was found to be not statistically significant (p>0.05) (Figure 4.13 C). Also like the situation for the AP angle the other two phenotypic classes of *pig-1(gm344)* mutants displayed division angles very similar to that in *wild type* with those with extra divisions dividing at 99.0° ± 16.4 (n = 3) and those with only terminal defects at 96.8° ± 6.2 (n =3).

This would suggest that there is not a meaningful difference between these *pig-1(gm344)* groups. When treated as an entire sample the *pig-1(gm344)* Caaa/Caap division angle in the AP axis was 126° ± 22.4 and in the DV axis 102° ± 14 (n = 8). As when separated, these were found to not differ significantly from that of the *wild type.*

Whilst statistical analyses suggest that the embryos in which *hlh-14* expression is absent in the C lineage do not have Caaa/Caap division angles that differ significantly from either other *pig-1(gm344)* mutants or *wild type* they still present the largest deviation. It is possible that given the rarity of this phenotype and this the low *n* that a possible difference is overlooked here.

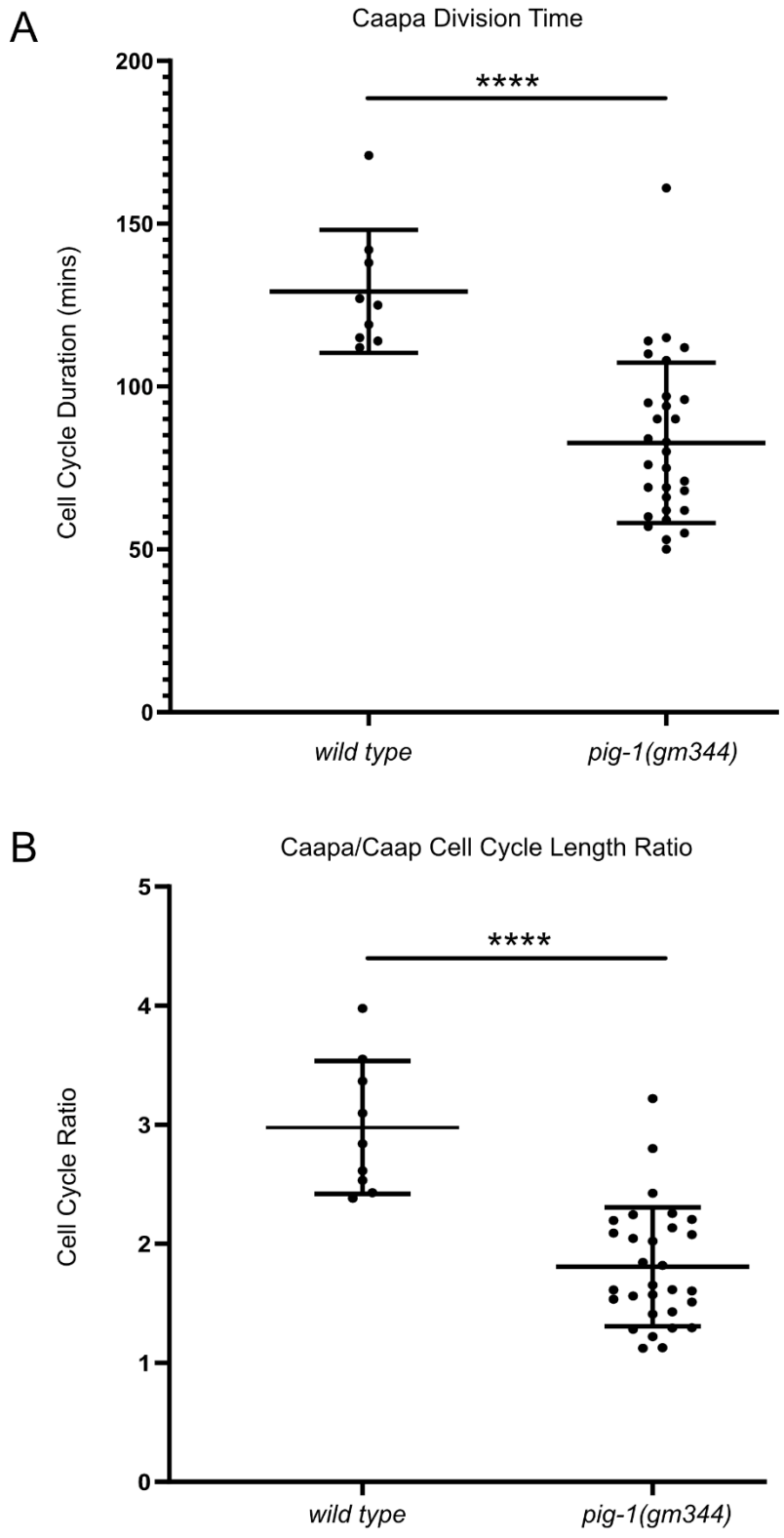

Figure 4.12. Quantification of Caapa cell-cycle duration in *pig-1(gm344)* embryos. *A) Scatter dot plot of Caapa cell-cycle duration in minutes for wild type and pig-1(gm344) lineaged at 25°C. B) Scatter dot for Caapa cell-cycle duration expressed as a proportion of its mother's cell-cycle duration. All charts include mean values ± standard deviation. **** = p < 0.0001, one-way ANOVA, with Holm-Sidak post hoc test for multiple comparisons.*

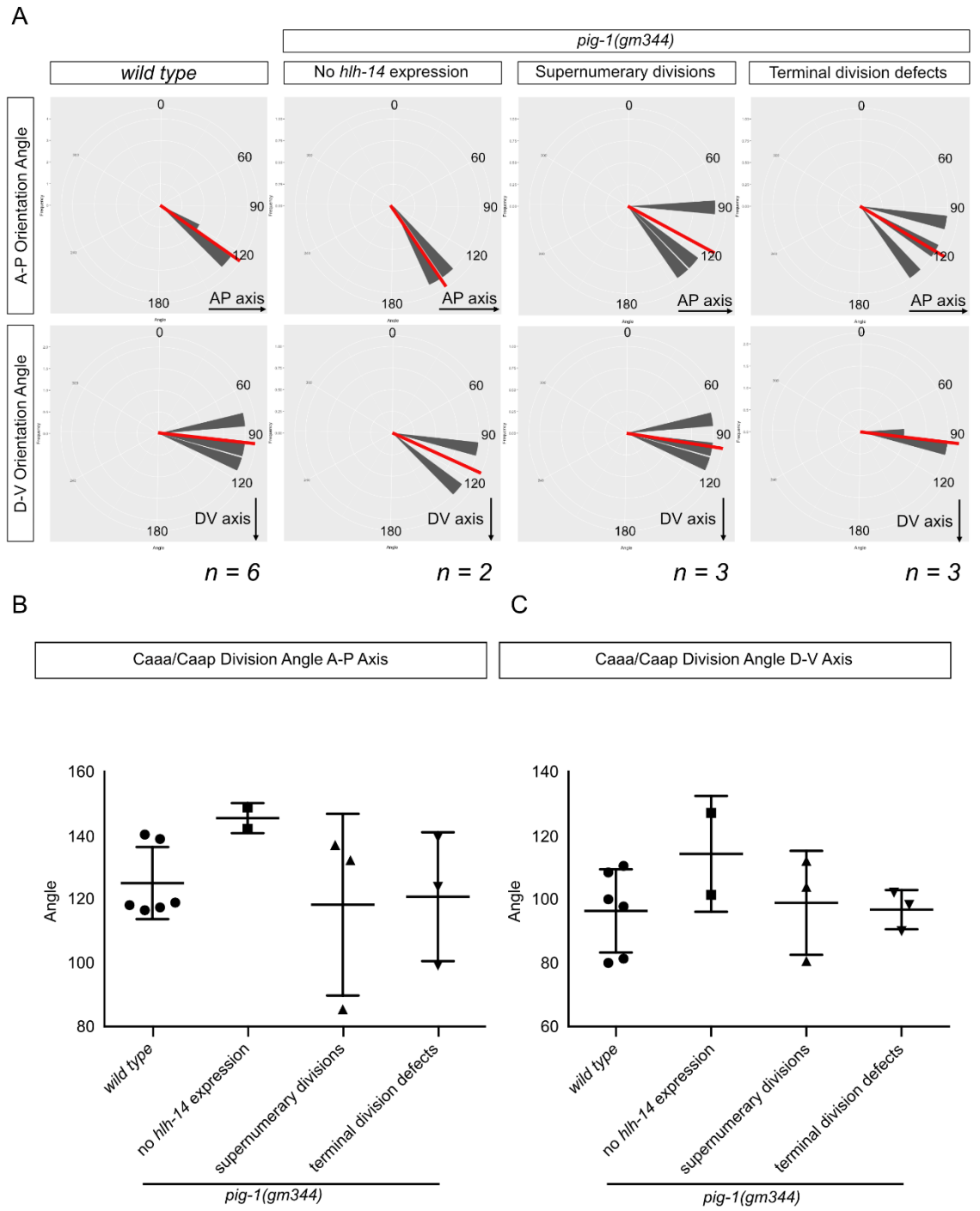

Figure 4.13. Caaa/Caap division orientation with respect to AP and DV axes in *pig-1(gm344)* embryos. *A) Rose plots for the division angles in 10° bins for Caaa/Caap in wild type and pig-1(gm344) embryos grouped into phenotypic classes. AP plots are plotted to display the angle at which the posterior cell is displaced away if the anterior daughter is imagined to be in the centre of the plot. DV angles are plotted as if viewing a Z-stack from the side and the 90° line as cells dividing in plane. i.e. Acute angles indicate the posterior daughter was on a higher plane. The length of the grey triangles indicates the number of divisions occurring at the indicated angle. Red line = mean division angle. Black arrow = indication of the line of the axis in question, i.e. along the AP axis = 90°. B) Scatter dot plots for the same division angles, plotted with mean values ± standard deviation. Not significant, one-way ANOVA, with Tukey HSD post hoc test due to all possible comparisons.*

4.3. Equalisation of Caapa/Caapp in *ham-1(n1438)* Mutants

The transcription factor HAM-1 is a known to act upstream of *pig-1* in a number of neuroblast divisions. Therefore, in order to understand how PIG-1 may be regulated in its role in controlling unequal cleavages in the C lineage *ham-1(n1438)* mutants were initially analysed for similar division defects.

In 13/13 *ham-1(n1438)* embryos the Caaa/Caap division displayed a clear anterior bias with a larger anterior daughter in all cases (Figure 4.14 A). The ratio of this division was similar to that in *wild type* animals leading to a mean value of 2.80 ± 0.742 (A/P ± standard deviation) (Figure 4 B), which was found to not significantly differ from the *wild type* 2.30 ± 0.266 (Figure 4.14 B; 4.15 A). Whilst there is not a significant difference between *ham-1(n1438)* mutants and *wild type* ham-1 mutants show a greater degree of variability in the daughter size asymmetry at this division (Figure 4.15 A). This is evident from outliers with a smaller ratio that in the *wild type* range; 1.65 and 1.72. Furthermore, whilst found to be not significant *ham-1(n1438)* mutants display a tendency to a larger anterior bias in the Caaa/Caap size ratio with indeed two embryos demonstrating ratio of 3.80 (Figure 4.15 A). This is reflected in the fact that the mean volume of Caap is on average slightly smaller than in *wild type* embryos but that this difference is not significant, 206883 voxels (n = 13) vs 245549 (n = 9) (Figure 4.15 B). Given the maintenance of the unequal cleavage this suggests that HAM-1 does not have a significant role in controlling the division and as the phenotype differs from that in *pig-1(gm344)* that it does not regulate it at this division.

Contrastingly a clear tendency towards equalisation in the Caapa/Caapp division is seen in *ham-1(n1438)* mutants (Figure 4.14 A). The ratio of daughter size asymmetry in *ham-1(n1438)* of 0.847 ± 0.252 (n = 13) is significantly lesser than that of the *wild type* 0.430 ± 0.101 (n = 10) ($p<0.0001$) (Figure 4.15 A). This equalisation phenotype is not as strong as in *pig-1(gm344)* mutants and indeed 2/13 divisions displayed ratios within the *wild type* range; 0.419 and 0.683 (Figure 4.15 A).

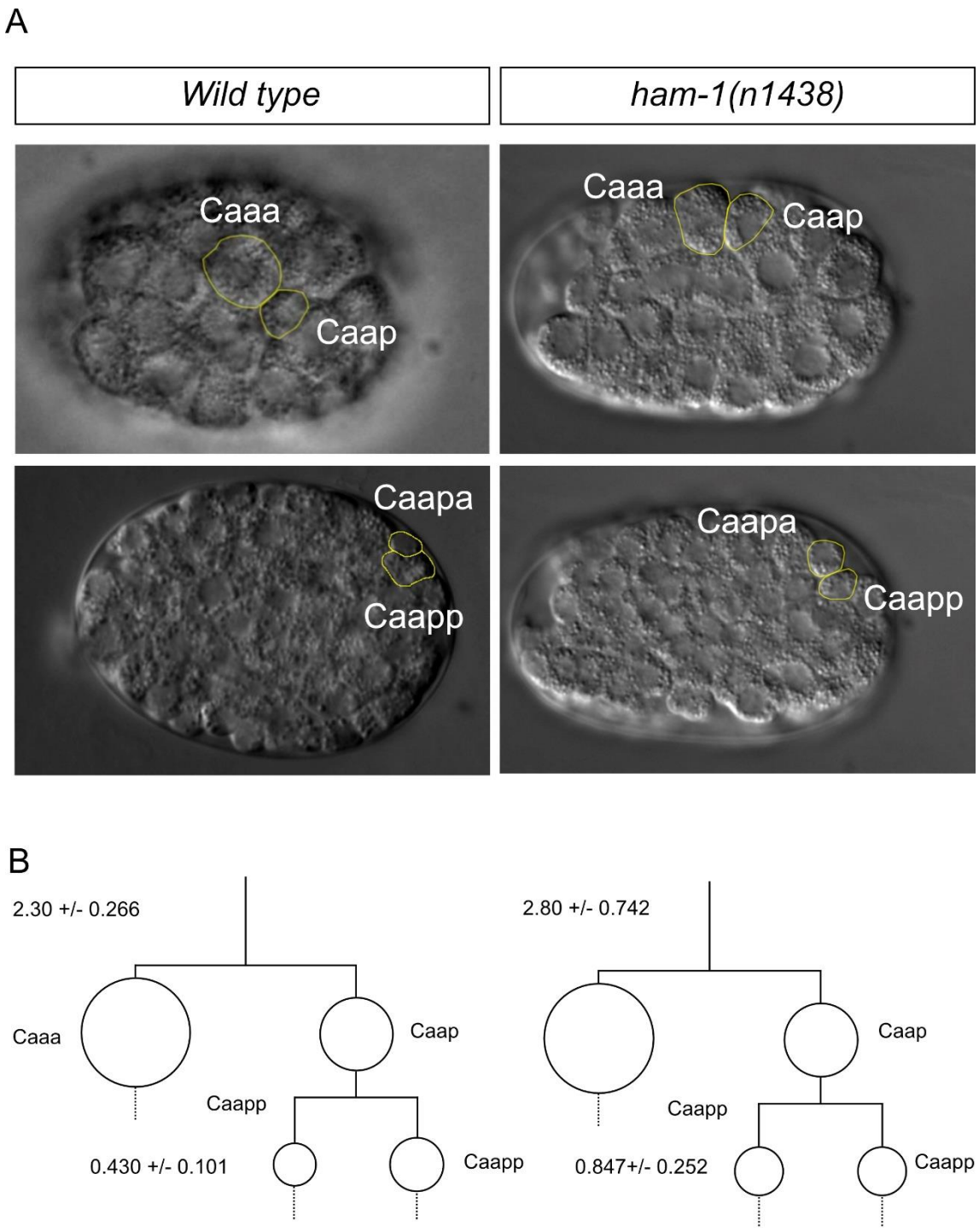

Figure 4.14. C lineage cleavage equalisation phenotypes in *ham-1(n1438)* embryos *A) DIC images of wild type and ham-1(n1438) embryos showing indicative equalisation cell size following the Caaa/Caap and Caapa/Caapp cleavages. B) Partial C lineage diagrams depicting the loss of daughter size asymmetry at the Caaa/Caap and Caapa/Caapp cleavages. Circles are illustrative of relative differences in cell size. Volume ratios are expressed as volume of anterior daughter/ volume of posterior daughter +/- standard deviation. Dotted lines indicate that the lineage belong this point is not depicted in the diagram.*

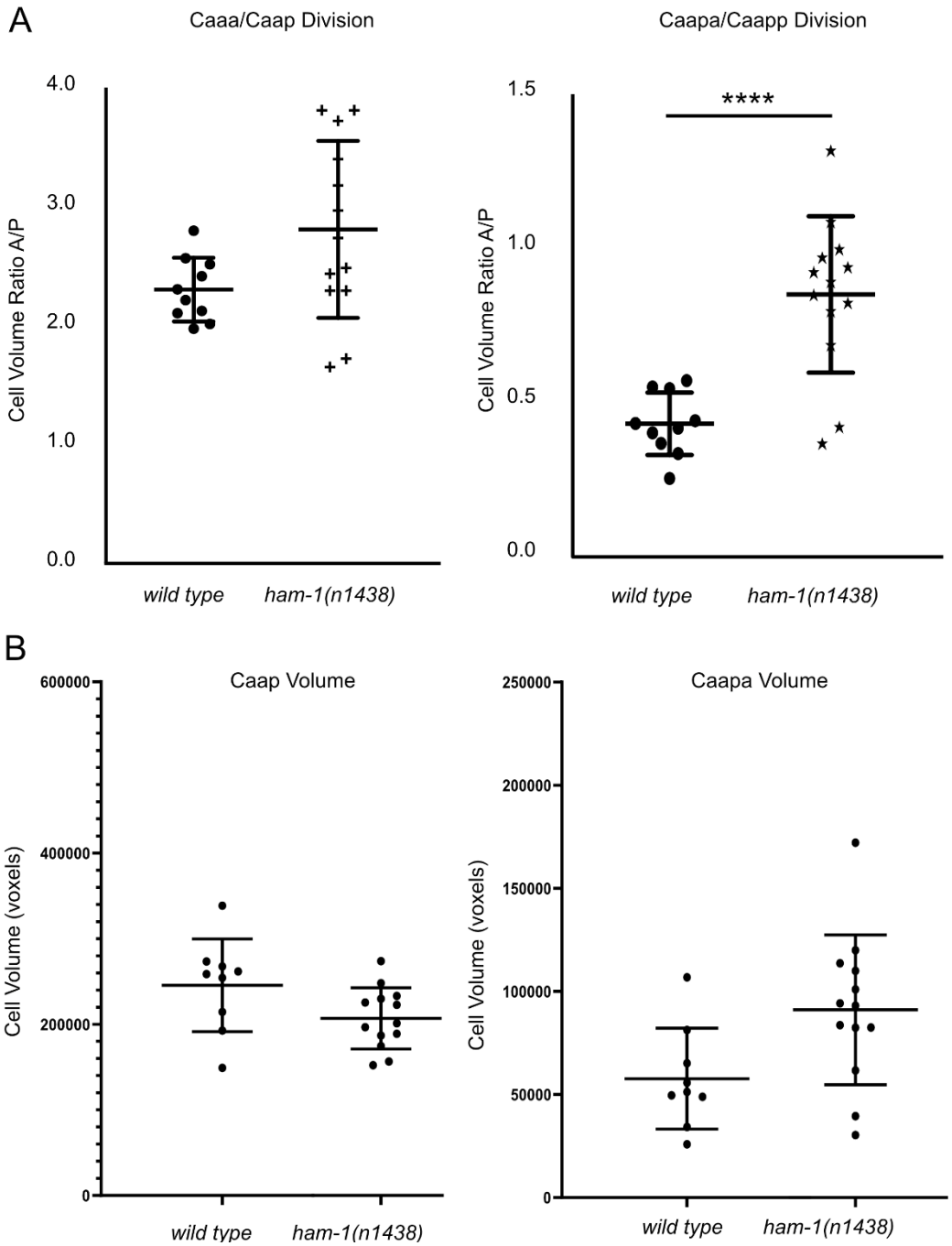

Figure. 4.15. Quantification of Caaa/Caap, Caapa/Caapp volume ratios in *ham-1(n1438)* mutants. *A) Scatter dot plot illustrating cell volume ratios following the Caaa/Caap and Caapa/Caapp cleavages in wild type and ham-1(n1438) embryos. Plots include mean ± standard deviation. B) Boxplots of absolute of volume of Caap and Caapa in wild type and ham-1(n1438) embryos. Plots include mean ± standard deviation. **** = p < 0.0001, One-way ANOVA with Holm-Sidak post hoc test for multiple comparisons.*

4.3.1. Equalisation of Caapa/Caapp in *ham-1(n1438)* Has no Effect on Initiation of *hlh-14*

As in *pig-1(gm344)* mutants, expression of *hlh-14* was not lost in *ham-1(n1438)* mutants despite equalisation of the second unequal cleavage in the lineage, Caapa/Caapp. Through 4D lineaging it was apparent that the majority of *ham-1(n1438)* embryos feature a *wild type*-like C lineage division with Caapa dividing later than Caapp, as in *wild types*. A further 2/10 embryos displayed a precocious Caapa division in time with the hypoblast divisions like that of *hlh-14* mutants (Figure 4.16 A). Due to the combination of both a *wild type* and precocious division *ham-1(n1438)* mutants exhibit non-significant reduction in mean Caapa cell cycle duration but a significant reduction in the Caapa/Caap cell cycle ratio; 1.80 ± 0.824 (n = 14) vs the *wild type* 2.98 ± 0.558 (n =9) ($p<0.0001$) (Figure 4.17).

4.3.2. *ham-1(n1438)* Displays a Weak Ectopic and loss of DVC Phenotype

In both lineaged embryos with the precocious division *hlh-14* was expressed in both Caapaa and Caapap with Caapaa later expressing *ceh-63* and adopting DVC fate, as it does in *wild type* (Figure 4.16 A). In 6/8 embryos with the *wild type* Caapa cell cycle, Caapaa became DVC, Caapap doing so in the other 2/8 (Figure 4.16 B). Overall Caapaa became DVC in 8/10 embryos and in 2/10 the Caapap cell, which would normally undergo apoptosis became DVC instead (Figure 4.16 A).

In this way *ham-1(n1438)* resembles most closely the group of *pig-1(gm344)* mutants with equalised Caapa/Caapp divisions but only defects in the neuron/death fate decisions in the terminal Caapaa/Caapap division. Thus, it is possible that *ham-1* acts upstream of *pig-1* to control the unequal cleavage at Caapa/Caapp and then later again in the terminal DVC neuroblast division resulting in the loss of apoptosis.

Although not revealed in lineage analysis presumably due to a lower *n*, *ham-1(n1438)* displayed a both a loss of DVC and ectopic supernumerary DVC phenotype. This was of very low penetrance and was assessed with the unique DVC marker *ceh-63::gfp* as in 4D-lineage recordings. As indicated from the lineage analysis, the majority of *ham-1(n1438)* embryos have a single DVC neuron (Figure 4.18 A). 52/56 (92.9%) slide mounted embryos had a single DVC neuron with only a single embryo lacking the neuron, 1/56 (1.79%). A small proportion of embryos displayed two DVCs, indicating the presence of a single ectopic neuron, 3/56 (5.36%) (Figure 4.18 B). The weakness of this phenotype is also demonstrated in 4D lineaged embryos with 10/10

having a single DVC (Figure 4.18 B). 28.6% of these embryos arrested during morphogenesis (Figure 4.18) however as with *pig-1(gm344)*, the loss of or extra neurons is not linked this phenotype with both arrested and hatched embryos displaying all DVC phenotypes (Figure 4.18 A).

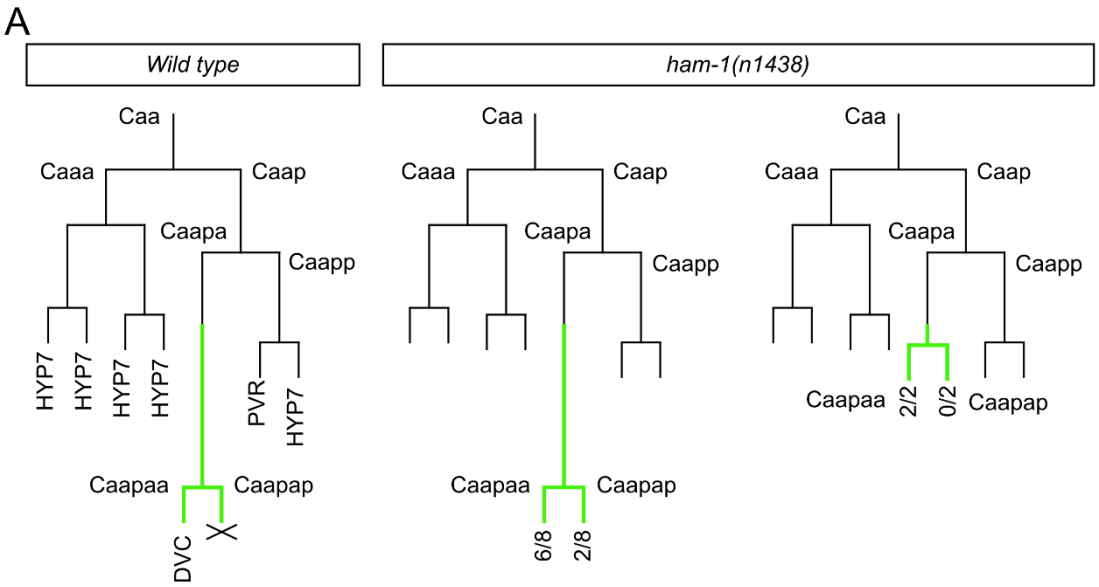

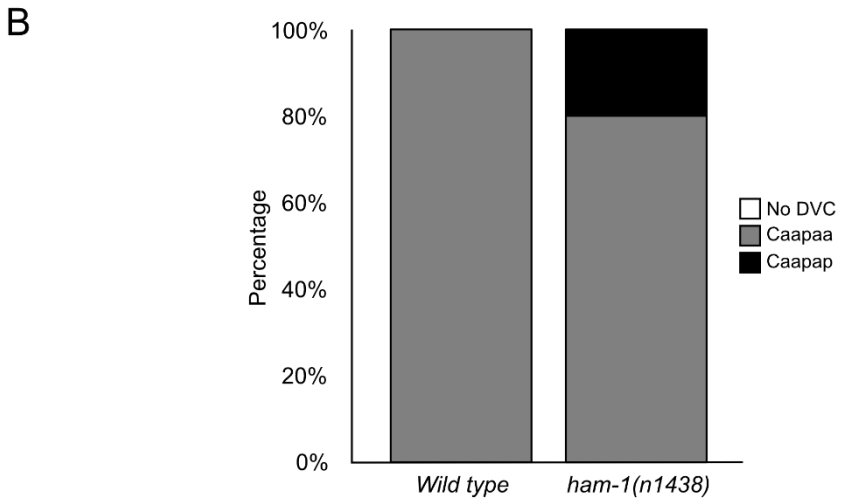

	DVC	*n*	%
wild type	Caapaa	4	100
	Total	**4**	**100**
ham-1(n1438)	No DVC	0	0.00
	Caapaa	8	80.0
	Caapap	2	20.0
	Total	**10**	**100**

Figure 4.16. Lineage analysis of *ham-1(n1348)* embryos. A) Illustrative lineage diagrams of different observed lineage patterns. Line length are indicative of cell cycle duration. Green lines indicate hlh-14::gfp expression as scored using the *gmIs20* transgene. Numbers under terminal branches indicate both the number of embryos with the observed pattern, and which *hlh-14::gfp* expressing cells within all embryos displaying that pattern became a DVC neuron. B) Stacked bar chart and table indicating the proportion of embryos in which particular cells became a DVC neuron, rather than cells scored individually as in A).

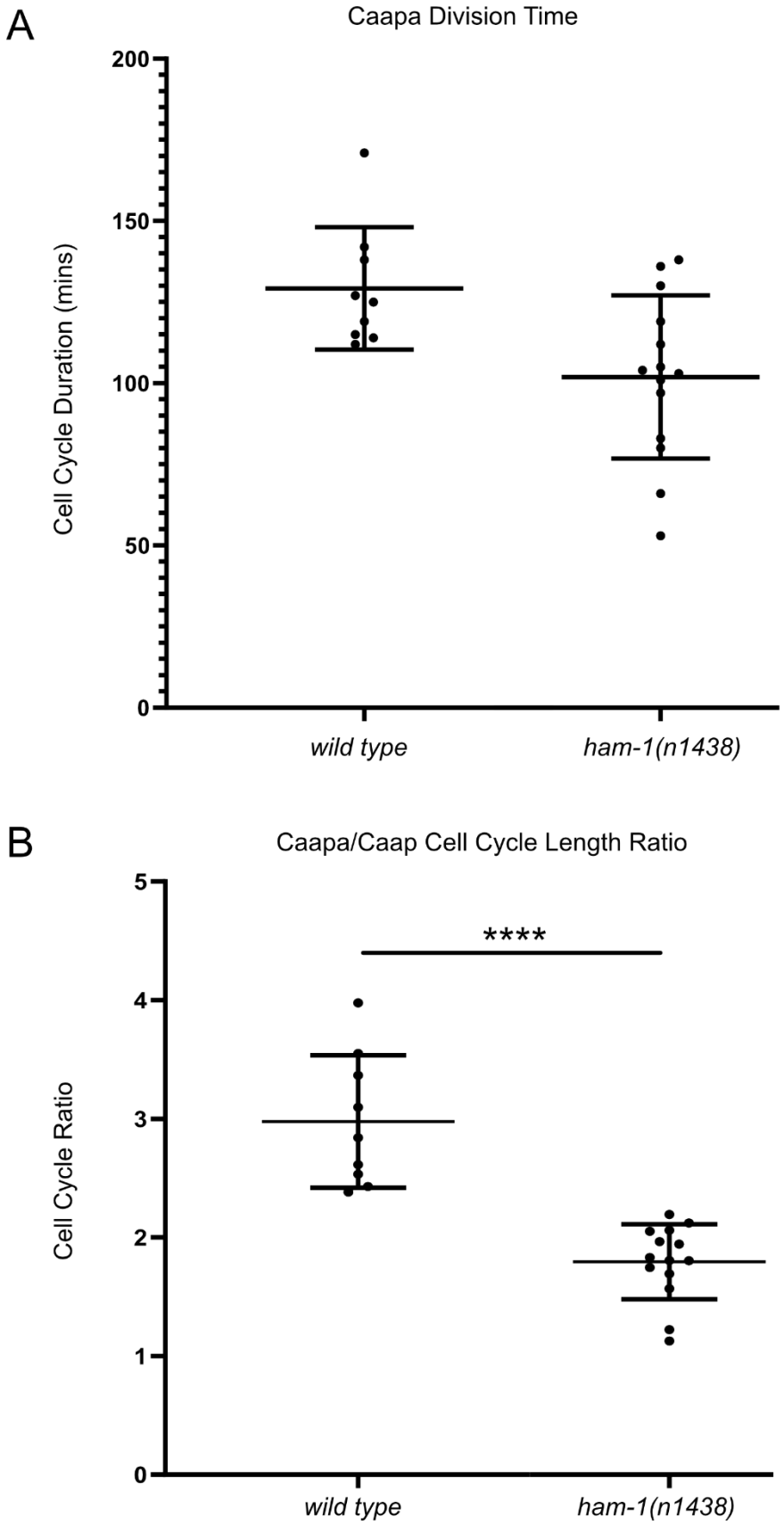

Figure 4.17. Quantification of Caapa cell-cycle duration in *ham-1(n1438)* embryos. *A) Scatter dot plot of Caapa cell-cycle duration in minutes for wild type and ham-1(n1438) lineaged at 25°C. B) Scatter dot for Caapa cell-cycle duration expressed as a proportion of its mother's cell-cycle duration. All charts include mean values ± standard deviation. **** = p < 0.0001, one-way ANOVA with Holm-Sidak post hoc test for multiple comparisons.*

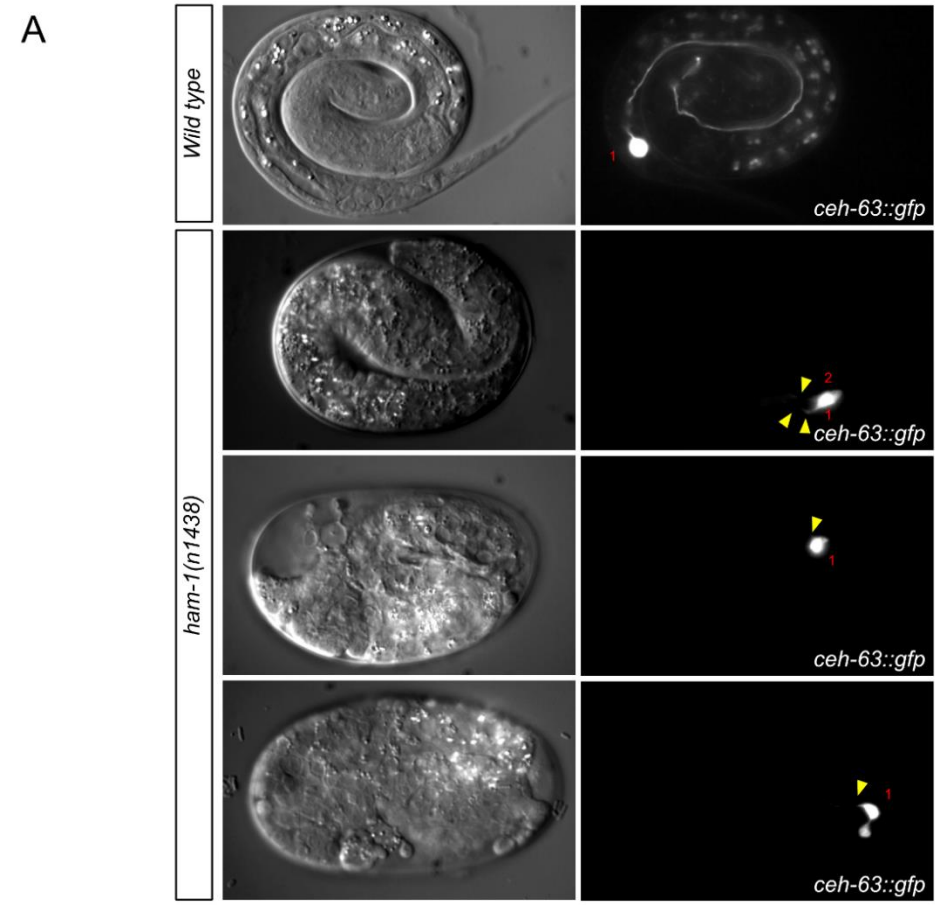

B

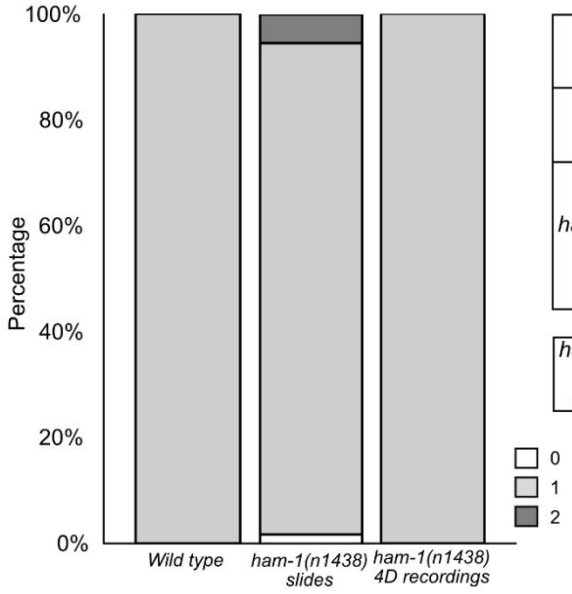

	ceh-63::gfp +ve cells	n	%
wild type	1	62	100
	Total	**62**	**100**
ham-1(n1438) slides	0	1	1.79
	1	52	92.9
	2	3	5.36
	Total	**56**	**100**
ham-1(n1438) 4D Recordings	1	10	100
	Total	**10**	**100**

Figure 4.18. Scoring for the presence of DVC neurons in *ham-1(n1438)* embryos. *A) DIC and GFP images of representative. DIC images demonstrate that some embryos arrest, whilst other hatch. The presence of DVC neurons is evidenced by the expression of ceh-63::gfp, often with the characteristic tear-shaped cell body. Red numbers = the number of DVCs. Yellow arrows = clear neuronal processes. B) Stacked bar chart representing the number of DVC neurons in wild type* and *ham-1(n1438), ceh-63::gfp embryos from both mounted and lineaged embryos. A table detailing the scored number of DVC neurons in embryos.*

4.3.3. C lineage Unequal Cleavages are not Affected in *ces-1(tm1036), ces-1(n703sd)* or *ces-2(bc213)*

The finding that *ham-1(n1438)* only affects the second unequal cleavage, Caapa/Caapp, suggested that *pig-1(gm344)* is regulated by different mechanisms in the first unequal cleavage, Caaa/Caap. Given that *ham-1(n1438)* may be a transcriptional regulator of *pig-1(gm344)* in Caapa/Caapp I sought to assess other known transcriptional regulators of *pig-1(gm344)* for a role in Caaa/Caap. *ces-1/Snail* and its upstream repressor *ces-2/HLF* have recently been described as having role in negative regulation of *pig-1* in the NSM neuroblast (Wei et al., 2017). Although not measured, mutants with either a *ces-1* loss or gain of function allele, or a *ces-2* loss of function allele displayed *wild type* unequal cleavage patterns division and Caapa divisions times (Table 4.1). Therefore, this suggests that *ces-1* is not required for the regulation of *pig-* in the C lineage.

Gene	Allele	Nature of Allele	Caaa/Caap Cleavage	Caapa/Caap Cleavage	Precocious Caapa Division (%)	n Assessed
ces-1	*tm1036*	Loss of function	Unequal, *wild type*	Unequal, *wild type*	0	2
ces-1	*n703sd*	Gain of function	Unequal, *wild type*	Unequal, *wild type*	0	3
ces-2	*bc213*	Loss of function	Unequal, *wild type*	Unequal, *wild type*	0	3

Table 4.1. Summary of *ces-1* and *ces-2* C lineage phenotypes.

4.4. How are the C Lineage Unequal Cleavages Coordinated with Neurogenesis?

pig-1 and *ham-1* were found to have little impact on the initial expression of *hlh-14* whilst evidently sequentially regulating both fate decisions downstream and controlling the unequal and asymmetric divisions of Caaa/Caap, Caapa/Caapp and the terminal division produced DVC, Caapaa/Caapap.

These findings raise the question of how these factors are regulated in order to coordinate unequal cleavages, particularly *pig-1*. Moreover, another question concerns how the control of daughter cell size through unequal cleavages is regulated and interacts with the overall neurogenic programme in order to produce cells of both the correct size and transcriptional fate.

A potential answer to how size is regulated in the neuronal branches of the lineages comes from the factors previously found to be involved in regulating the explicitly neuronal aspects of the C lineage.

4.4.1. *let-19* Mutants Demonstrate C Lineage Neurogenesis Defects

In Chapter 5 I will describe the characterisation of three mutants from a 4D lineage-based screen of temperature sensitive, embryonic lethal mutants (generated by collaborators in the lab of Ralf Schnabel) to uncover upstream regulators of *hlh-14*. As will be outlined in that chapter the initial basis of identification of mutants from the screen was a phenocopy of the precocious division of the DVC neuroblast, Caapa, as seen in *hlh-14* mutants.

From this screen a previous PhD student in the lab, Terry Felton, identified an allele of the Mediator Complex Kinase Module subunit *let-19, t3273,* as displaying this precocious division (Felton, 2019). Former Masters students in the lab, Janis Tam and Justina Yeung, also characterised *t3273* and another allele, *t3200*, confirming the loss of neurogenesis expected of an upstream regulator of *hlh-14* (Tam, 2015; Yeung, 2016). Both alleles were found to be missense point-mutations in 4th exon of *let-19.* Rescue experiments using three independent lines carrying the WRM061cD04 fosmid rescued the 89% embryonic lethality of *t3273* at the non-permissive temperature: reducing it to 22%, 32% and 10% respectively. Importantly, no other loci covered by the fosmid were found to contain variants in the whole genome sequencing and mapping of *t2373.* Assessment of dominance effects demonstrated that both *t3273* and *t3200* are

recessive alleles with respect to embryonic lethality with the heterozygous embryos displaying 9% and 15% lethality at the non-permissive temperature (Felton, 2019). The *t3200* allele had previously been confirmed to be that of *let*-19 (Schnabel, pers, comms.) and complementation tests revealed *t3273* to be another allele of *let-19* with *t3200/t3273* heterozygous embryos demonstrating 76% lethality. As neurogenesis phenotypes correlated with lethality in both mutants, it was reasoned that assessing lethality phenotypes in terms of both dominance and complementation was sufficient to assume the same for neurogenesis (Felton, 2019).

Phenotypes in *let-19(t3273)* were found to be highly variable. For example the precocious division of Caapaa, the DVC neuroblast, was observed in 13/17 (76.5%) embryos at the non-permissive temperature of 25°C. *let-19(t3200)* embryos on the other hand displayed the precocious division in 17/17 (100%) cases. *let-19(t3273)* additionally displayed a highly variable extra division phenotype in the C lineage in 10/25 (40%) of embryos (Tam, 2015).

At 25°C *hlh-14* expression in the C lineage was lost in 4/10 (40%) *let-19(t3273)* (Tam, 2015) and 13/19 (68%) let-19*(t3200)* lineaged embryos carrying the *gmIs20* transgene (Felton, 2019; Tam, 2015)

Hypodermal fate was assessed with a nuclear histone HIS-24::mCherry fusion driven by the promoter of the hypodermal gene *dpy-7* (Liu et al., 2009). For *let-19(t3200)* embryos also carrying *dpy-7::rfp*, of those lacking *hlh-14* expression at 25°C. 7/7 (100%) were found to express *dpy-7::rfp* in Caapaa the would-be DVC, indicating conversion to hypodermal fate in the absence of the proneural gene. In none of these embryos however was expression detected in PVR (Felton, 2019). The highly variable division phenotype of *let-19(t3273)* yielded a highly variable *dpy-7* expression pattern including the loss of expression from would-be hypodermal cells in the 10/25 (40%) embryos with extra divisions and in 5/25 (20%) embryos without extra division. The expression of *hlh-14* and *dpy-7* was not assessed in the same *let-19(t3273)* embryos and so it is difficult to know in what proportion of those embryos lacking *hlh-14* Caapaa (DVC) and indeed Caappa (PVR) adopted hypodermal fate. However, in only 5/25 (20%) lineaged embryos was *dpy-7* expression detected in Caapaa (DVC) and never in Caappa (PVR) (Tam, 2015).

Assessing the fate of Caapaa,, 7/7 (100%) *let-19*(*t3200)* lineaged embryos lacked expression of *ceh-63* and thus lacked neurogenesis (Felton, 2019). Again demonstrating greater variability,

slide mounted *let-19(t3273)* embryos displayed on an 8% loss of DVC, 16% with two DVCs, 4% with three and 72% with the *wild type* single neuron (n = 102) (Tam, 2015)

Given the far more varied and less penetrant phenotypes of *let-19(t3273)* it was evident that *let-19(t3200)* represented a far cleaner allele and was thus preferred for future study in the lab. Most critically, *let-19(t3200)* displays the three key phenotypes in common with *hlh-14* mutants; precocious division of DVC neuroblast, loss of *hlh-14* expression and the conversion of would-be neurons to a hypodermal fate (Felton, 2019; Poole et al., 2011).

4.4.2. Equalisation of Caaa/Caap in *let-19(t3200)* and *let-19(t3273)* Correlates with C lineage Neurogenesis Defects

Whilst studying DIC images during 4D lineaging of *dpy-7::rfp*, *let-19(t3200) hlh-14::gfp, ceh-63::gfp* embryos myself, I observed that the Caaa/Caap division displayed a striking equalisation in cell size at the non-permissive temperature of 25°C (Figure 4.19 A), in addition to its neurogenesis defects outlined above. This phenotype was not apparent at the permissive temperature of 15°C (Figure 4.19 A), again as with its other phenotypes. Quantification of the equalisation was confirmed using 4D lineage recordings from 16 embryos, yielding a value of 1.17 ± 0.197 compared to the *wild type* 2.30 ± 0.266 (Figure 4.19 B). As mentioned above, previous work in the lab had established that at 25°C *let-19(t3200)* does not show a 100% loss of *hlh-14* expression. Reassessing this phenotype with the addition of my own 4D recording data I realised that this phenotype was in fact more complicated, with some embryos presenting initial expression of *hlh-14* that was not maintained. In these embryos, expression of *hlh-14* was detected in Caapa prior to its precocious division and then was either lost following the division or only briefly expressed in the daughters Caapaa and Caapap. In all cases neurogenesis did not occur in these embryos (n = 7). Despite this initial expression however, the ratio of daughter cell sizes for the Caaa/Caap division in these embryos of 1.28 ± 0.122 (n = 7), does not differ significantly to embryos in which no there is no *hlh-14* expression; 1.10 ± 0.214 (n = 5.). Both groups differ significantly from the *wild type* (both $p<0.0001$) (Figure 4.20 A). The equalisation phenotype is rescued at 15°C with a ratio more akin to that in *wild type* embryos of 1.88 ± 0.322 (n = 4), that whilst smaller, does not differ significantly to the *wild type* but does to both groups of *let-19(t3200)* embryos at 25°C (both $p>0.05$) (Figure 4.20 A). This is in agreement with the

findings for *pig-1(gm344)* and indicates that the unequal cleavage of Caaa/Caap is not instructive of *hlh-14* expression.

let-19(t3273) also displayed a significant equalisation of Caaa/Caap of 1.22 ± 0.287 (n = 5, p<0.001) in those embryos displaying its aforementioned lineage and neurogenesis phenotypes (Figure 4.20 A). This phenotype correlates exactly with these phenotypes in that the proportion of *let-19(t3273)* embryos that did not show lineage or neurogenesis defects exhibited a *wild type* ratio significantly differing from those embryos with said defects, 2.29 ± 0.407 (n = 5, p< 0.01) (Figure 4.20 A).

As a result of this equalised cleavage the volume of Caap in absolute terms is significantly increased with respect to the *wild type* in *let-19(t3200)* embryos with or without the initiation of *hlh-14* expression and in *let-19(t3273)* embryos lacking expression. These respective increases compared to the *wild type* 245549 (n =9), 399910 (n =7, p<0.001), 381934 (n = 9, p<0.01) and 399571 (n = 5, p<0.01) are evidently similar to each other (Figure 4.21 A). Whilst not significant, an increased volume of Caap was also evident in *let-19(t3200)* at the permissive temperature of 15°C, due to the reduced but non-significantly lesser Caaa/Caap size ratio of 1.88 described above (Figure 4.21 A).

4.4.3. Caapa/Caapp Unequal Cleavage is not Affected in *let-19(t3200)* and Weakly in *let-19(t3273)*

Interestingly the size asymmetry of Caapa/Caapp is not significantly affected in *let-19(t3200)*, displaying a ratio of 0.553 ± 0.112 at 25°C and 0.355 + 0.0727 at 15°C compared to the *wild type* 0.430 ± 0.101 (Figure 4.19 A, B). As with the Caaa/Caap division there was no significant difference between those embryos with initial expression of *hlh-14* 0.495 ± 0.0955 (n = 7), and those without, 0.599 ± 0.126 (n = 9) (Figure 4.19 B).

Contrastingly *let-19(t3273)* demonstrated a variable equalisation of the division in embryos with neurogenesis defects; Caapa/Caapp was equalised in 2/5 embryos and divided with the *wild type* asymmetry in 3/5 (Figure 4.20 B). This resulted in a mean ratio of 0.802 ± 0.315 (n = 5) which differed significantly from the *wild type* (p > 0.05) (Figure 4.20 B), on account of the equalised divisions. *let-19(t3273)* embryos presenting no C lineage defects were also *wild type* for the Caapa/Caapp size ratio, 0.549 ± 0.157 (n = 5).

Despite the unequal cleavage of Caapa/Caapp the equalisation of the preceding division, Caaa/Caap, results in the increased volume of Caapa in these embryos from the *wild type* volume of 57659 voxels (n = 9) (Figure 4.21 B). For *let-19(t3200)* a volume of 109569 voxels with initial *hlh-14* expression and 119684 without was found to be significant (n = 7, 9, p<0.01). *let-19(t3273)* embryos, which display either one or two equal cleavages exhibited the expected range in Caapa volume and thus significant difference to that of the *wild type*; 193534 voxels (n = 5, p<0.001) (Figure 4.21 B).

4.4.4. Precocious Caapa Division is Correlated with the Caaa/Caap Equalisation in *let-19(t3200)* but not *let-19(t3273)* and not with *hlh-14* expression

As mentioned above, previous characterisation of *let-19* mutants in the lab revealed a precocious Caapa division phenotype like that seen in *hlh-14* mutants. Analysing the timing of the Caapa division, this differed significantly from the *wild type* ratio of 2.98 ± 0.558 (n = 9) due to an elongated Caapa cell cycle. *let-19(t3200)* mutants exhibit a clearly reduced Caapa/Caap cell cycle ratio irrespective of initial *hlh-14* expression; 1.25 ± 0.120 (n = 7, p<0.0001) in embryos with initial *hlh-14* expression and 1.06 ± .0208 in those without (n = 9, p<0.0001). This was also true for *let-19(t3273)* embryos lacking *hlh-14* with a precocious Caapa division, yielding a Caapa/Caap cell cycle ratio of 1.18 ± 0.0931 (p<0.0001). In all these mutants a precocious division of the Caapa neuroblast was preceded by an equalised Caaa/Caap cleavage. However, 5/7 *let-19(t3273)* embryos exhibiting no neurogenesis or cleavage defects exhibited a precocious Caapa division (Figure 4.22 A). The Caapa/Caap cell cycle ratio thus demonstrates a clear bimodal distribution and significantly differs from *wild type*; 1.71 ± 0.626 (n = 7, p<0.0001) (Figure 4.22 B). This indicates that the both the unequal cleavage and expression of *hlh-14* in these cells is not instructive of Caapa division timing.

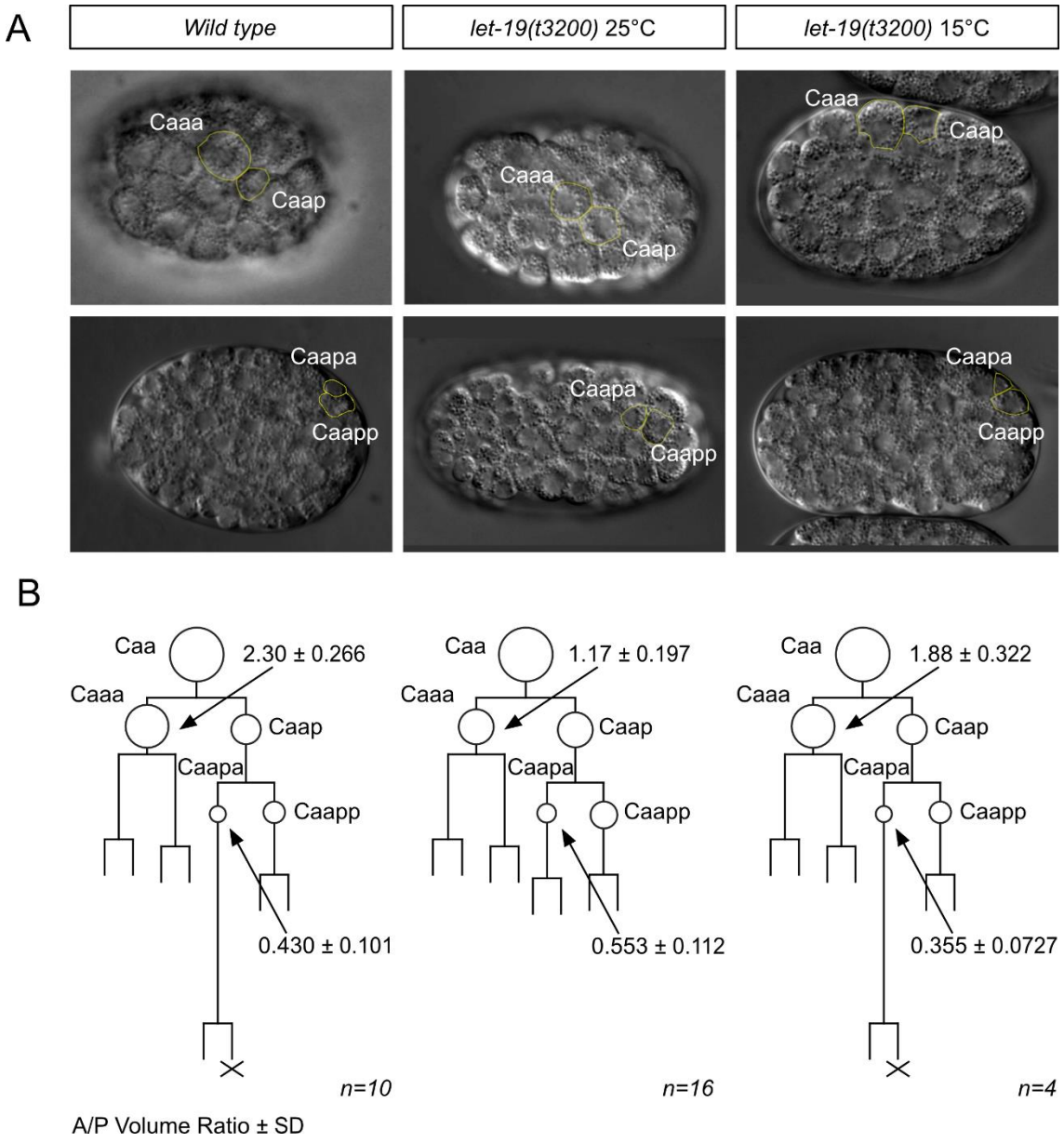

Figure 4.19. C lineage cleavage equalisation phenotypes in *let-19(t3200)* embryos *A) DIC images of wild type and let-19(t3200) embryos showing indicative equalisation cell size following the Caaa/Caap and Caapa/Caapp cleavages. B) Caa lineage diagrams depicting the loss of daughter size asymmetry at the Caaa/Caap and Caapa/Caapp cleavages. Circles are illustrative of relative differences in cell size. Volume ratios are expressed as volume of anterior daughter/ volume of posterior daughter +/- standard deviation and the division in question indicated by an arrow pointing to the anterior daughter of the division.*

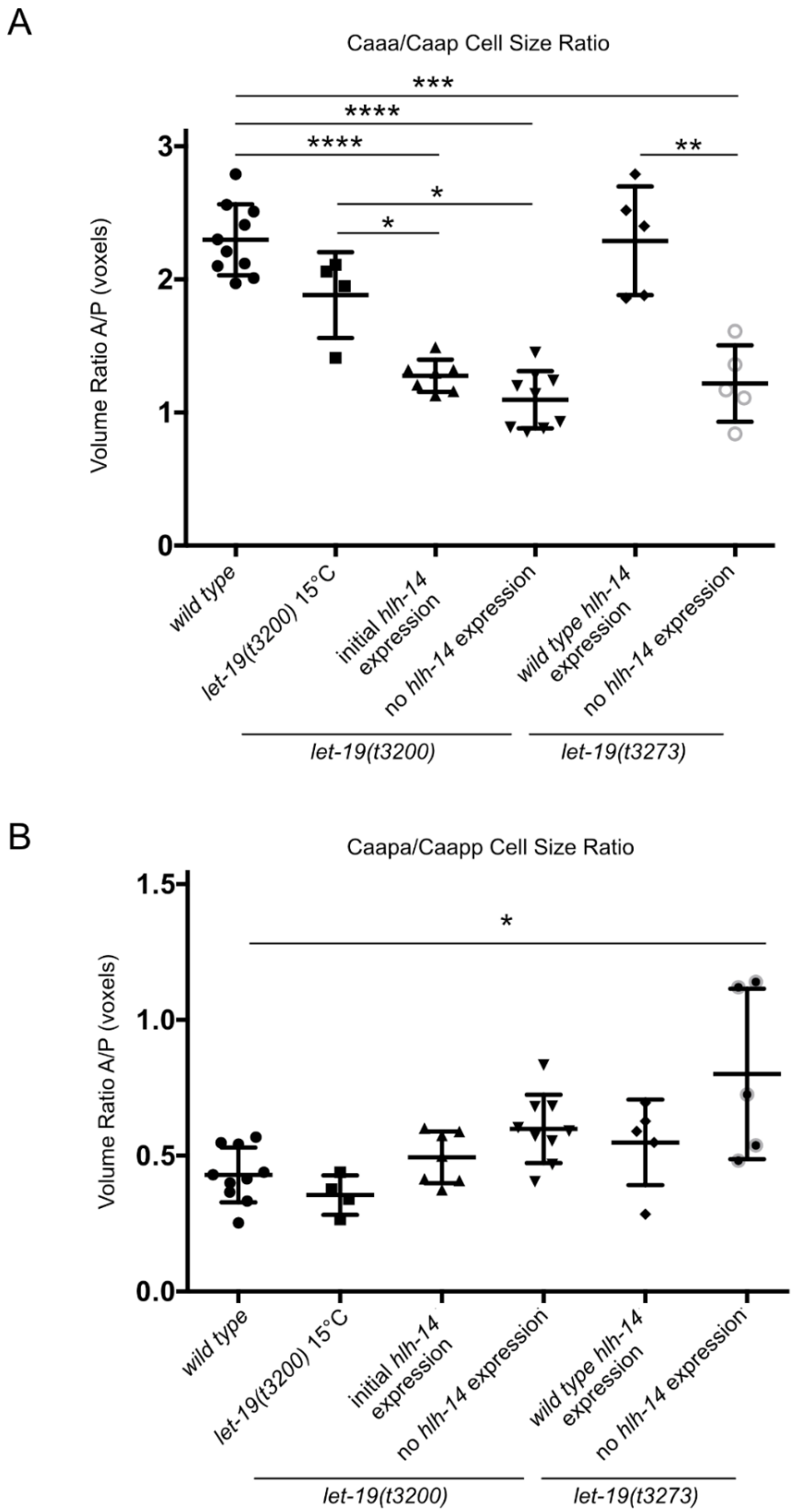

Figure 4.20. Quantification of Caaa/Caap and Caapa/Caapp volume ratios in *let-19(t3200)* and *let-19(t3273)* mutants. *A) Scatter dot plots illustrating cell volume ratios following the Caaa/Caap cleavage in wild type and mutant embryos at 25°C, unless otherwise stated. B) Scatter dot plot for the Caapa/Caapp division Plots include mean ± standard deviation. * = p < 0.05, *** = p < 0.001, **** = p < 0.0001, One-way ANOVA with Holm-Sidak post hoc test due to multiple, yet not all, comparisons.*

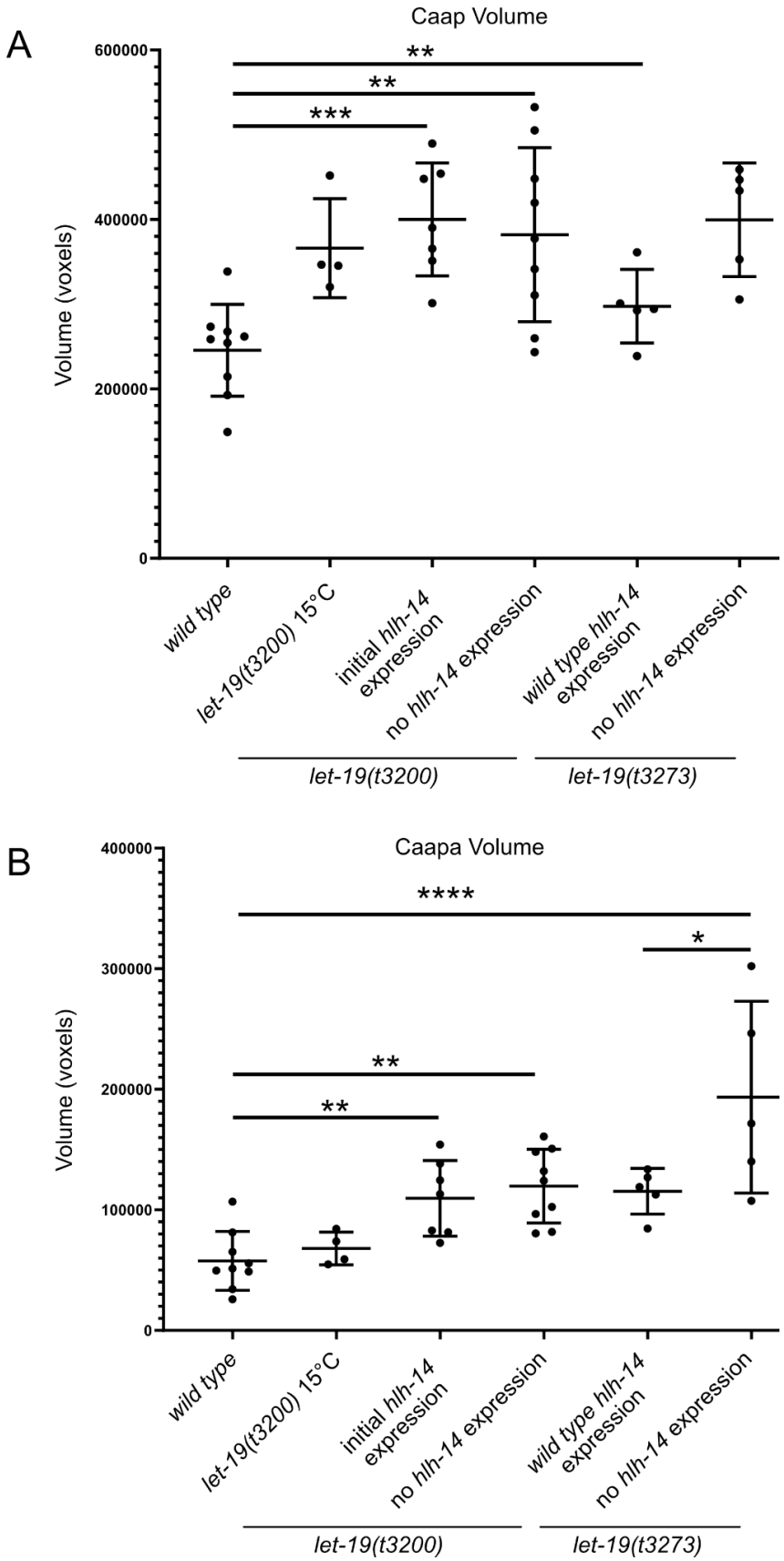

Figure 4.21. Quantification of absolute Caap and Caapa volumes in *let-19(t3200)* and *let-19(t3273)* mutants. *A) Scatter dot plots illustrating Caap cell volume following the Caaa/Caap division in wild type and mutant embryos at 25°C, unless otherwise stated. B) Scatter dot plot for Caapa following the Caapa/Caapp division Plots include mean ± standard deviation. * = p < 0.05, ** = p < 0.01, *** = p < 0.001, **** = p < 0.0001, One-way ANOVA with Holm-Sidak post hoc test due to multiple, yet not all, comparisons.*

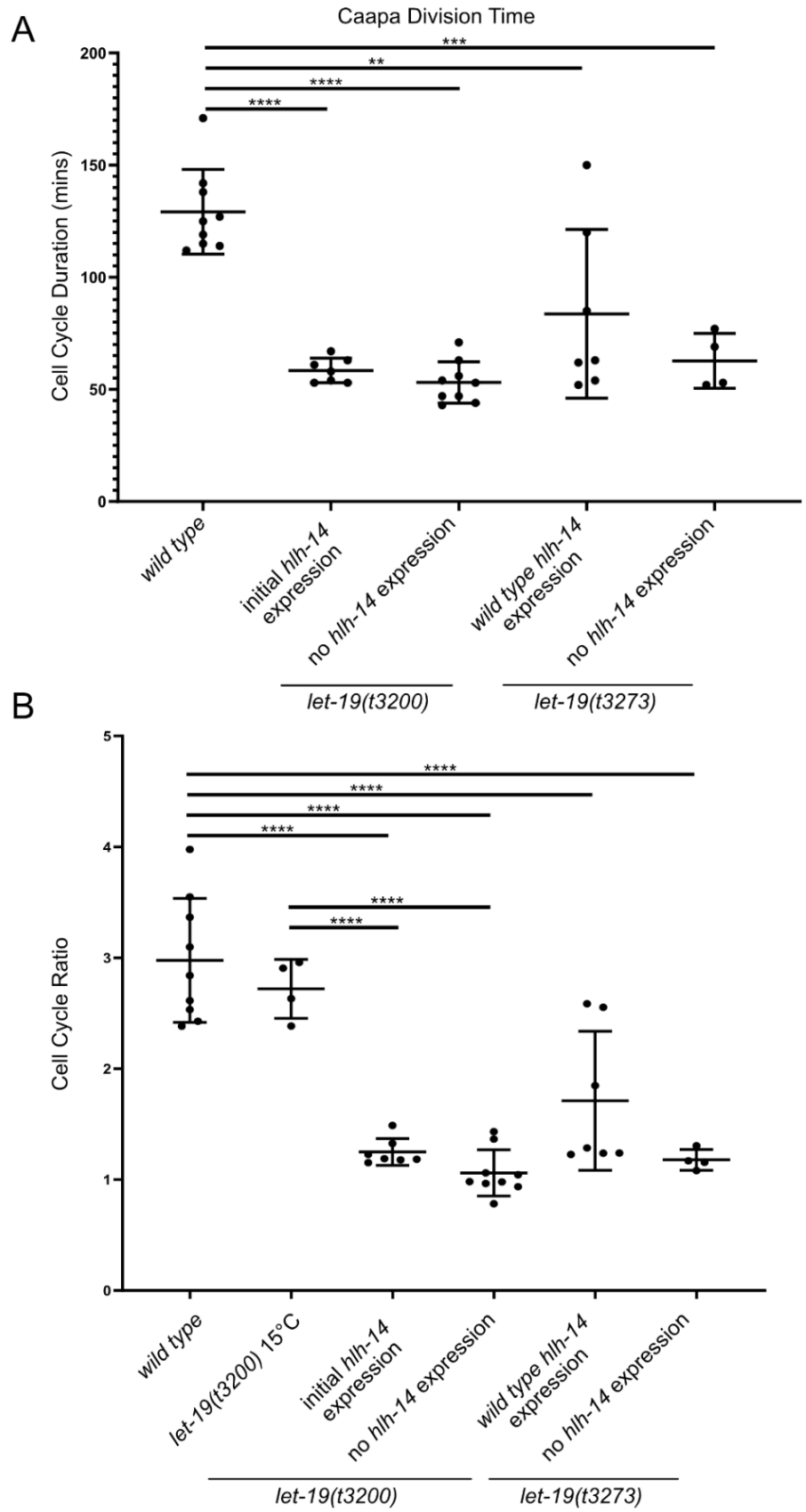

Figure 4.22. Quantification of Caapa cell-cycle duration in *let-19(ts)* embryos. *A) Scatter dot plot of Caapa cell-cycle duration in minutes for wild type and mutant lineaged at 25°C unless otherwise stated. B) Scatter dot for Caapa cell-cycle duration expressed as a proportion of its mother's cell-cycle duration. All charts include mean values ± standard deviation. ** = p < 0.01, *** = p < 0.001, **** = p < 0.0001, one-way ANOVA with Holm-Sidak post hoc test due to multiple, yet not all, comparisons.*

4.4.5. C lineage Unequal Cleavages are not Affected in Other Mediator Complex Kinase Module Mutants

Given that two alleles of *let-19* cause defects in C lineage neurogenesis and the unequal cleavage of Caaa/Caap it was reasoned that it was doing so in its capacity as a member of the Mediator Complex kinase module. It was therefore sought to analyse other members of the kinase module.

Firstly, I analysed an available reported null allele of *let-19*, *os33,* reported to be larval lethal or embryonic lethal (Yoda et al., 2005). Embryos were thus identified by the loss of the *mIn1* balancer. Surprisingly, these embryos did not reveal obvious defects in the C lineage unequal cleavages (not measured). Neither did those of another member of the kinase module, *dpy-22(os38)* (Table 4.2).

The known viable null mutant of a third member of the Kinase module, *cdk-8(tm1238)*, also displayed *wild type* unequal cleavages for both Caaa/Caap, 2.69 ± 0.485 (n = 4) and Caapa/Caapp 0.469 ± 0.109 (n = 4) (Figure 4.23).

Gene	Allele	Nature of Allele	Caaa/Caap Cleavage	Caapa/Caap Cleavage	Precocious Caapa Division (%)	n Assessed
let-19	*os33*	Null, nonsense	Unequal, *wild type*	Unequal, *wild type*	25	4
dpy-22	*os38*	Substitution	Unequal, *wild type*	Unequal, *wild type*	25	4
cdk-8	*tm1238*	Deletion	Unequal, *wild type*	Unequal, *wild type*	0	4

Table 4.2. Summary of other Mediator Complex Kinase Module subunits

4.4.6. *let-19(os33)* Displays a Weak Precocious Caapa Division Phenotype

Neither *cdk*-8 nor *dpy*-22 mutants displayed highly penetrant precocious divisions of Caapa. 4/4 *cdk-8(tm1238)* lineaged embryos displayed a *wild type* Caapa/Caap division with a cell cycle ratio of 2.47 ± 0.482 (n =4). *dpy-22(os38)* mutants also displayed a *wild type* cell cycle ratio of 2.47 ± 0.824 (n = 4) (Figure 4.24).

In contrast Caapa divided slightly precociously in *let-19(os33)* mutants with a resultant Caapa/Caap cell cycle ratio of 2.01 ± 0.448 (n = 4) that was significantly different to that of the *wild type* ($p<0.05$) (Figure 4.24).

Given the absence of or low penetrance of both precocious Caapa division or defects in the unequal cleavage of Caaa/Caap or Caapa/Caapp in these other Mediator mutants, assessment of neurogenesis with fate markers was not undertaken. For the same reason the fourth subunit of the kinase module *cic-1*, was also not assessed.

The low penetrance of C lineage phenotypes in the null allele *let-19(os33)* is surprising when compared to the TS alleles *t3200* and *t3273.* This could be suggestive of a repressive event caused by the faulty LET-19 protein in the TS mutants that does not normally occur and so is unaffected in a null mutant.

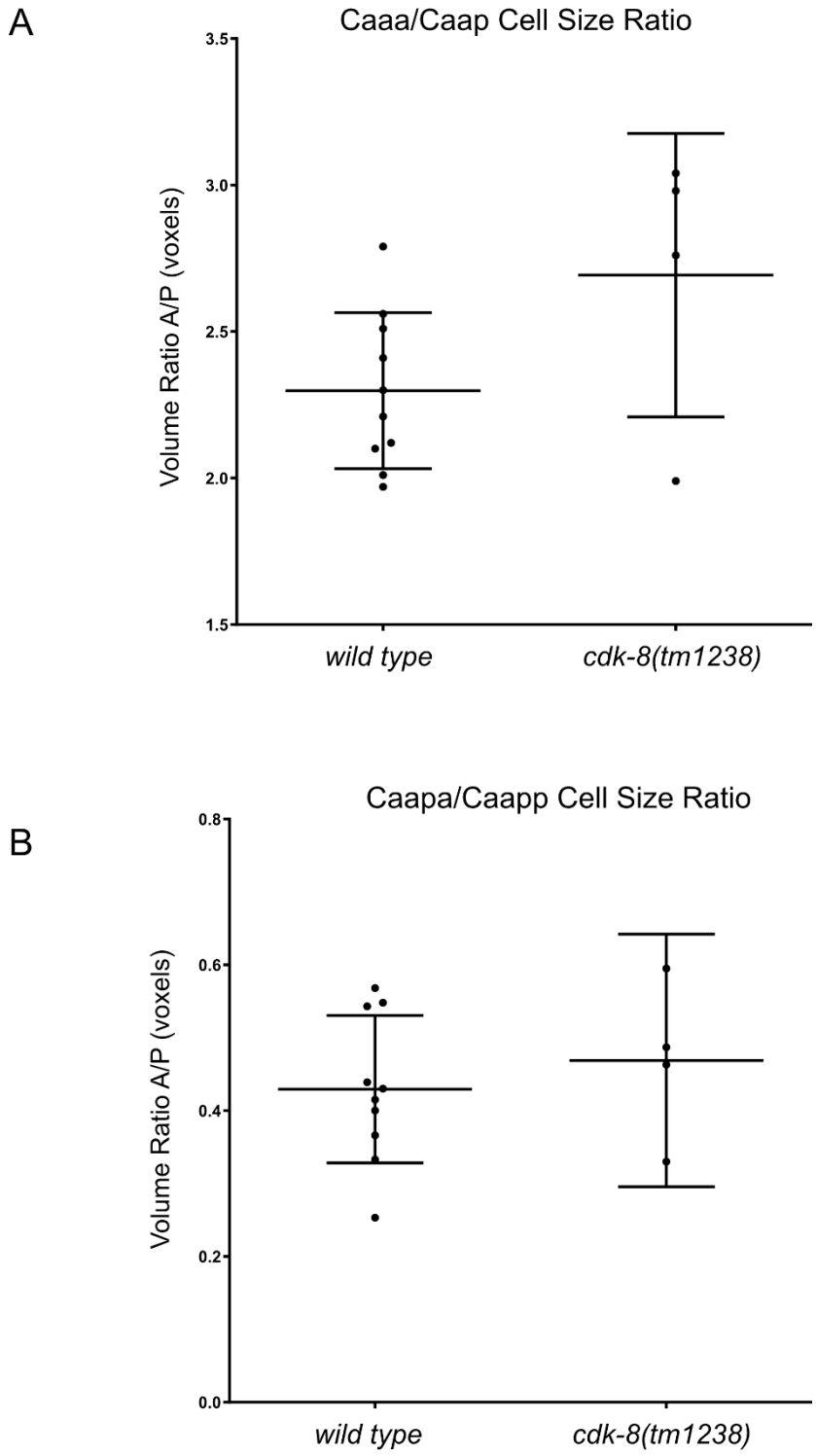

Figure 4.23. Quantification of Caaa/Caap and Caapa/Caapp volume ratios in *cdk-8(tm1238).* ***A)*** *Scatter dot plots illustrating cell volume ratios following the Caaa/Caap cleavage in wild type and mutant embryos at 25°C. B) Scatter dot plot for the Caapa/Caapp division Plots include mean ± standard deviation. Not significant, One-way ANOVA, with Holm-Sidak post hoc test.*

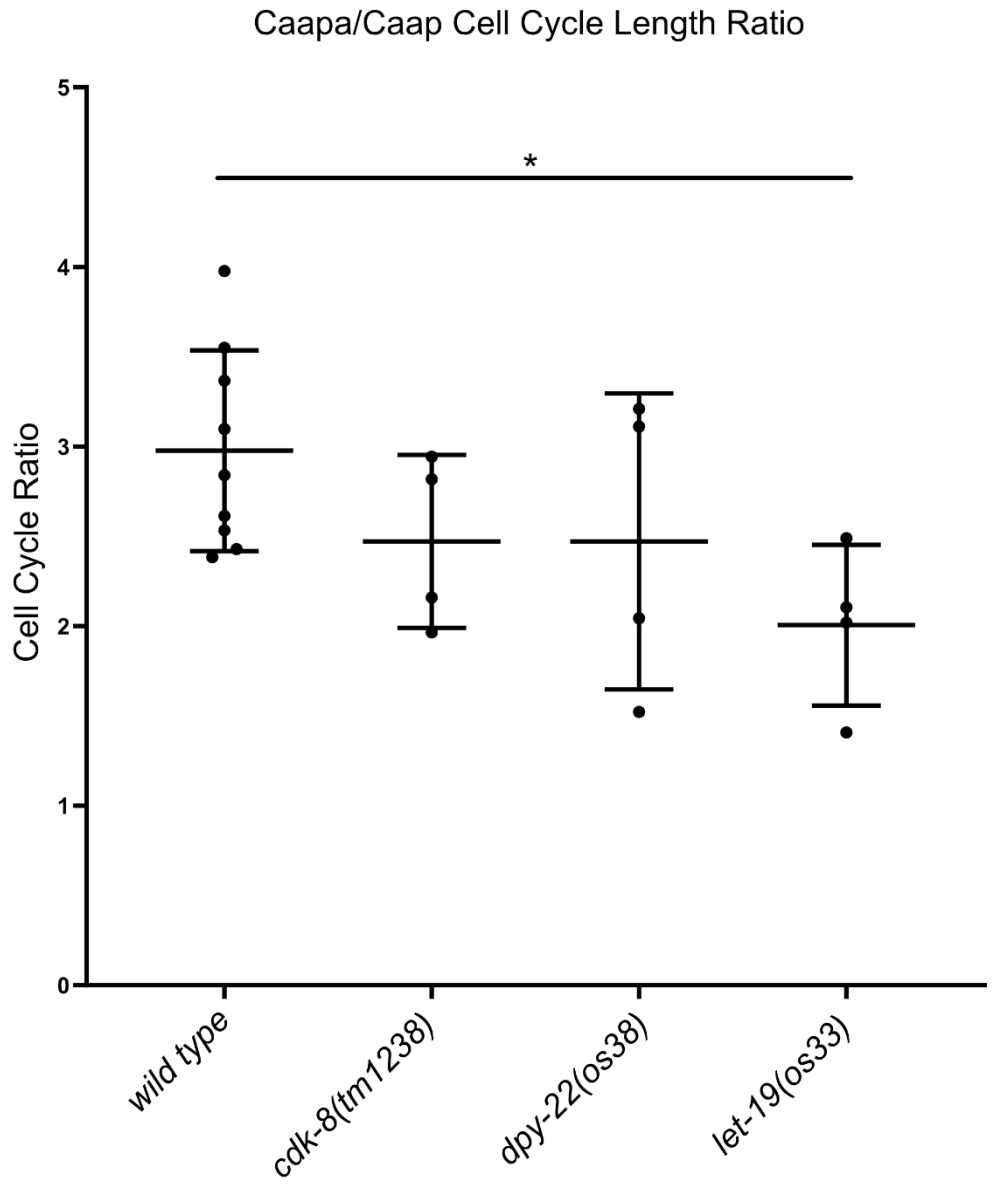

Figure 4.24. Quantification of Caapa cell-cycle duration in Mediator complex kinase module mutant mutants. *Scatter dot for Caapa cell-cycle duration expressed as a proportion of its mother's cell-cycle duration at 25°C. All charts include mean values ± standard deviation. * = $p < 0.05$, one-way ANOVA with Holm-Sidak post hoc test due to multiple comparisons.*

4.4.7. Caapa/Caapp is Equalised in *hlh-14(tm295)*

Given that *let-19* acts upstream of *hlh-14* and that the loss of the unequal cleavage of either Caaa/Caap or Caapa/Caapp appears not to be instructive of *hlh-14* expression, I investigated whether unequal cleavages were affected in *hlh-14* mutants themselves particularly that of Caapa/Caapp which precedes detectable *hlh-14* expression. As *hlh-14* null mutants are larval lethal, null embryos were identified by the loss of the *mIn1* balancer.

In contrast to *let-19(t3200),* Caaa/Caap divided with a *wild type* size ratio of 2.27 ± 0.610 (n = 4) in *hlh-14(tm295)* embryos (Figure 4.25 A, B). Conversely, the Caapa/Caapp division demonstrated a dramatic change in the cell size ratio when compared to *wild type* (Figure 4.25 A). In *hlh-14(tm295)* embryos Caapa/Caapp divides with an anterior bias of 1.36 ± 0.232 (n = 4) which is significantly different (p>0.001) to the *wild type* 0.430 ± 0.101 (n = 9) and almost a reversal of its size ratio (Figure 4.26 A). This is rescued in balanced embryos where the ratio does not significantly differ from the *wild type,* 0.516 ± 0.104 (Figure 4.26 A).

The absolute volume of Caapa in *hlh-14(tm295)* embryos is significantly increased with respect to *wild type* (p<0.0001), as would be expected from a near reversal of size ratio in the Caapa/Caapp division. The increased volume of 93682 voxels (n = 4) is almost twice that of the *wild type,* 57659 (n = 9) and is rescued in balanced embryos, 59096 (n = 4) (Figure 4.26 B).

As *hlh-14(tm295)* demonstrates an equalisation of Caapa/Caapp, HLH-14 it must be acting to regulate the unequal nature of the cleavage. This is intriguing because the fact that HLH-14 regulates this cleavage indicates that it must to acting in Caap, which is prior to the detectable expression using the *gmIs20* transgene.

4.4.8. C Lineage Unequal Cleavages are Unaffected in *hlh-2(drp6)*

Following the discovery that the proneural bHLH transcription factor HLH-14 regulates the second unequal cleavages, Caapa/Caapp, I wondered whether this action require the ubiquitous binding partner for bHLH transcription factors, HLH-2 (Grove et al., 2009) . Previous work in the lab had already established the expression of *hlh-2* was required for *hlh-14* expression in the C lineage and that *hlh-2* expression was regulated by LET-19 (Felton, 2019).

Unlike in *hlh-14*, both the first and second unequal cleavages (Caaa/Caap and Caapa/Caapp) are unaffected in *hlh-2(drp6)* mutants, displaying ratios of 2.59 ± 0.397 (n = 4) and 0.570 ± 0.131 (n = 4) respectively (Figure 4.27 A, B; 4.26 A). The absolute volume of both Caap and Caapa is also unaffected (Figure 4.26 B) as one would expect from unaffected cleavages. As *hlh-2(dr6)* mutants do not affect the unequal cleavage of Caapa/Caapp, the presence of HLH-2 is evidently not required for ability of HLH-14 to regulate the cleavage, but it is required for HLH-14's regulation of neurogenesis.

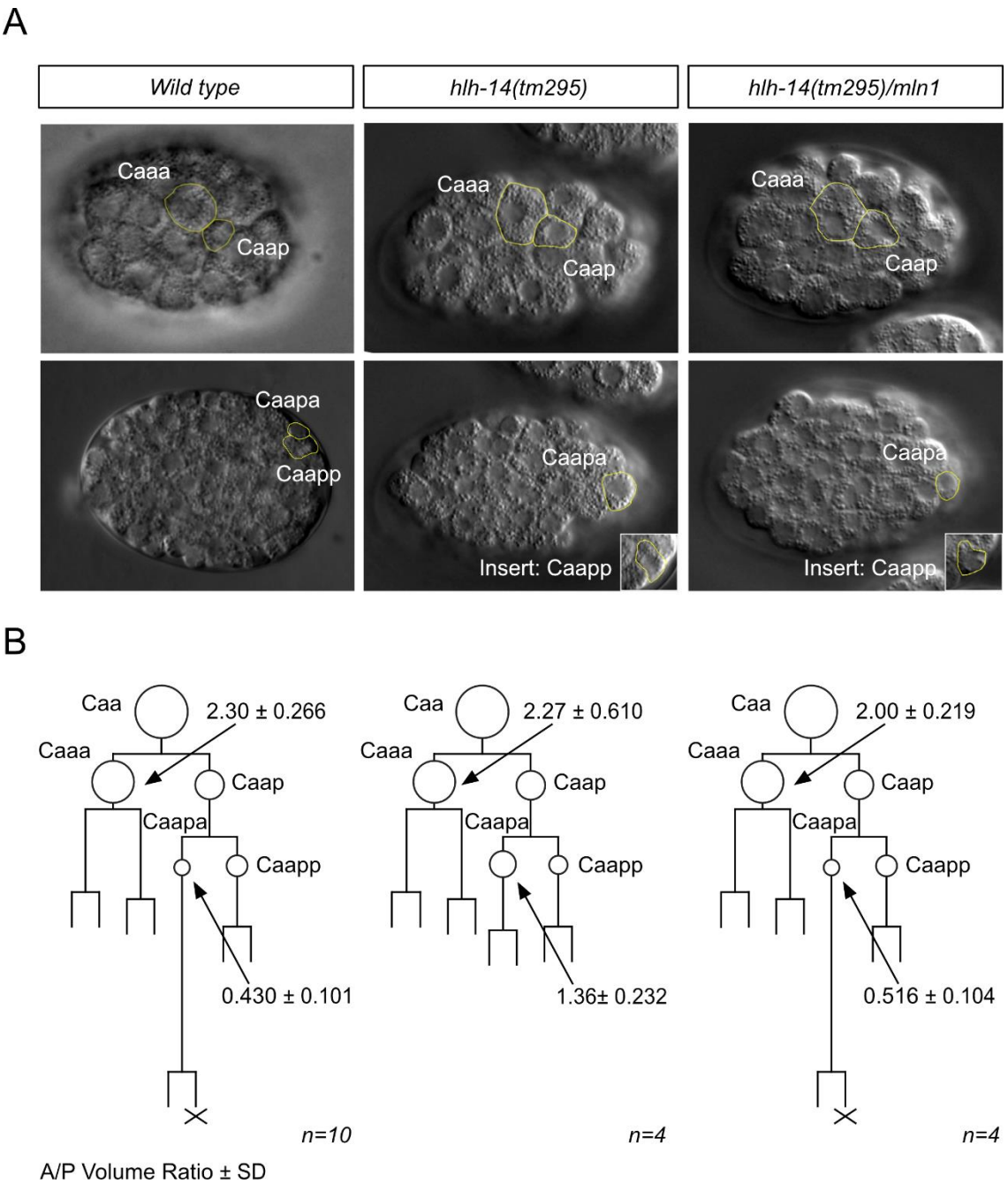

Figure 4.25. C lineage cleavage equalisation phenotypes in *hlh-14(tm295)* embryos *A) DIC images of wild type and mutant embryos showing indicative equalisation cell size following the Caaa/Caap and Caapa/Caapp cleavages. B) Caa lineage diagrams depicting the loss of daughter size asymmetry at the Caaa/Caap and Caapa/Caapp cleavages. Circles are illustrative of relative differences in cell size. Volume ratios are expressed as volume of anterior daughter/ volume of posterior daughter +/- standard deviation and the division in question indicated by an arrow pointing to the anterior daughter of the division.*

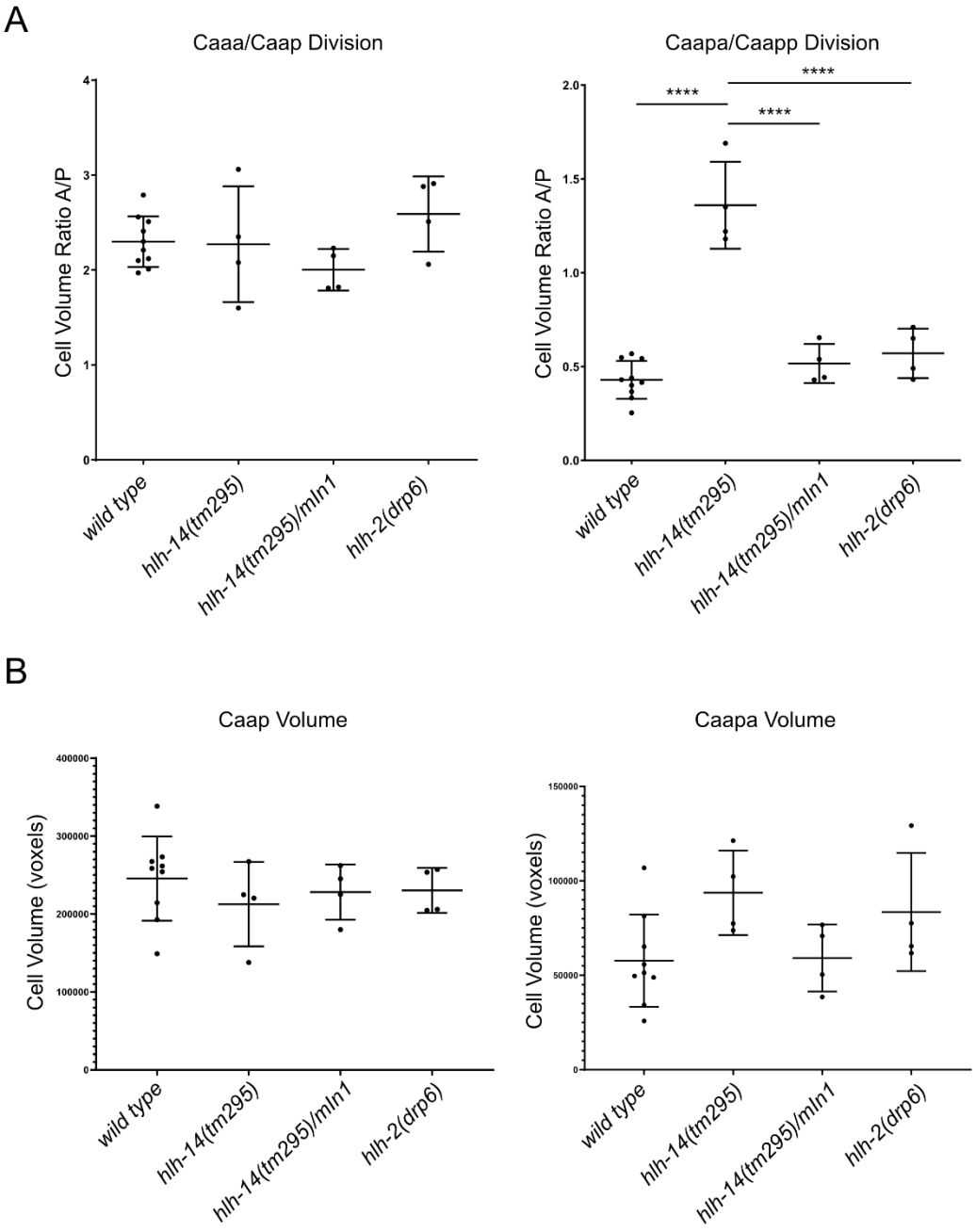

Figure. 4.26. Quantification of Caaa/Caap, Caapa/Caapp volume ratios in *hlh-14(tm295)* and *hlh-2(drp6)*. *A) Scatter dot plot illustrating cell volume ratios following the Caaa/Caap and Caapa/Caapp cleavages in wild type and mutant embryos. Plots include mean ± standard deviation. B) Boxplots of absolute of volume of Caap and Caapa in wild type hlh mutant embryos. Plots include mean ± standard deviation. **** = p < 0.0001, One-way ANOVA, with Holm-Sidak post hoc test due to multiple, but not all, comparisons.*

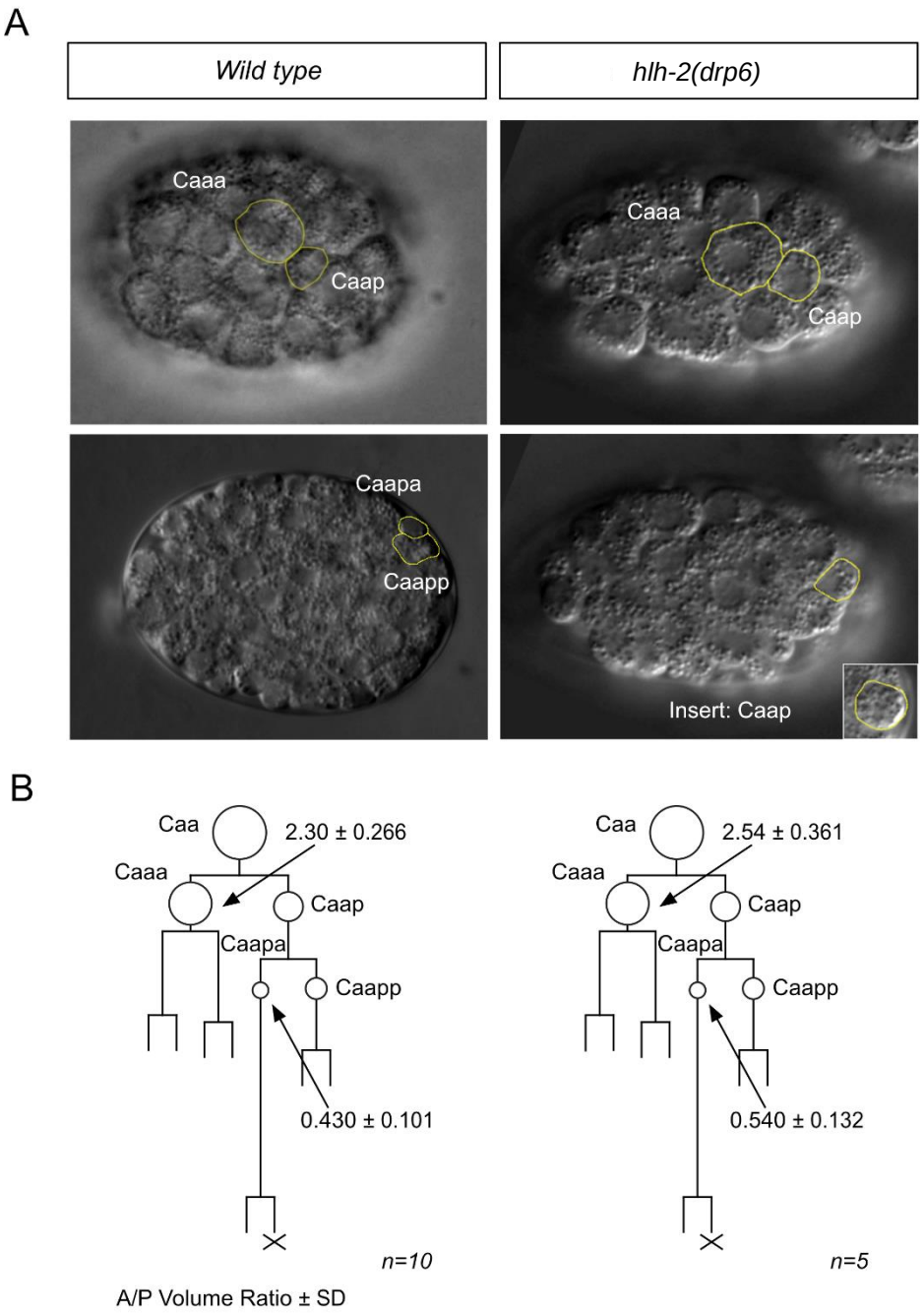

Figure 4.27. C lineage cleavage equalisation phenotypes in *hlh-2(drp6)* embryos *A) DIC images of wild type and mutant embryos showing indicative equalisation cell size following the Caaa/Caap and Caapa/Caapp cleavages. B) Caa lineage diagrams depicting the loss of daughter size asymmetry at the Caaa/Caap and Caapa/Caapp cleavages. Circles are illustrative of relative differences in cell size. Volume ratios are expressed as volume of anterior daughter/volume of posterior daughter +/- standard deviation and the division in question indicated by an arrow pointing to the anterior daughter of the division.*

Chapter 5

5. 4D-Lineage Based Screen of Temperature Sensitive, Embryonic Lethal Mutants for Upstream Regulators of *hlh-14*

5.1. A 4D-lineage Screen

An aim of the project was to increase understanding of the molecular regulation of neurogenesis with a focus on the initial steps which lead to the onset of proneural gene expression. As *hlh-14* is known to be the proneural gene expressed in the C lineage I sought to identify its upstream regulators in the C lineage.

hlh-14 null mutants display a characteristic precocious Caapa division, so it was reasoned that the loss of factors acting upstream would also exhibit such a phenotype. Taking advantage of the invariant cell lineage of *C. elegans* I led a still ongoing 4D lineage based genetic screen to uncover such mutants in a lineage-based manner. In this endeavour I was assisted at various times by Masters students Richard Wademan and Imaan Tamini and Undergraduate students Osama Kasem, Priya Barot and Vlad Arimia.

The screen employed a collection of 4D recordings of embryos of over 1000 temperature sensitive, embryonic lethal mutants generated by a collaborator, Ralf Schnabel, based the TU Braunschweig, Germany. These mutants were specifically collated from a larger EMS screen as those which display a large degree of differentiation as to attempt to exclude factors acting in the earliest stages of embryogenesis in favour of those with more cell type or lineage specific actions. The temperature sensitive nature of the mutants is advantageous as it allows for later identification of the timing of action of the factor in question. In relation to *hlh-14* regulation as *hlh-14* mutations cause early and mid-larval lethality it is plausible that some upstream regulators would have broad early acting pleiotropic effects causing embryonic lethality.

These recordings were manually lineaged and following initial identification as displaying a precocious Caapa division, or other aberration of the C lineage, the mutant strain itself was obtained and further characterisation undertaken in our own hands. Mutants uncovered in this

way were classed as *and* mutants for ***a****symmetric* ***n****eurogenesis* ***d****efective*, on account of neurogenesis only occurring in the left side of the C lineage in a *wild type* animal.

A total of over 83 mutant strains have thus far been screened; 45 of which were lineaged principally by me, the remainder secondarily screened by me following identification by the referenced indicated above. 15/83 strains of interest displayed a precocious Caapa division and were subsequently obtained. To date 11/15 of these strains have been further lineaged in a secondary screen using 4D recordings made using our own facilities at the non-permissive temperature of 25°C. This was done to both reconfirm the phenotype and as to obtain recordings of a higher image quality than the originals. Of these eleven strains, 8/11 or 8/83 overall were confirmed as exhibiting the precocious Caapa division indicating a hit rate of 9.64% with respect to the precocious division phenotype. A summary of this can be found in Table 5.1 (bold indicating a mutant identified by me).

5.2. Characterisation of Mutants from the Screen

In this next section I will discuss 6/11 mutants that I have characterised to differing extents with a particular focus on three of those mutants.

Three strains exhibited sufficiently high penetrance for the precocious Caapa division to warrant further investigation. All embryos of the strains GE5039 (4/4) and GE5691 (2/2) and 50% of GE5651 (2/4) displayed the phenotype. The remaining three strains exhibited low penetrance of the precocious division phenotype; 33% (1/3) in GE5880, 25% (1/4) in GE6436 whilst GE5315 lacked the precocious division in all three lineaged embryos (0%, 0/3) (Table 5.1, Figure 5.1). Considering this, further characterisation was not undertaken for these strains in favour of GE5039, GE5691 and GE5651. The allele numbers for GE5039, GE5691 and GE5651 are *t3224, t3294* and *t3462* respectively and will be referred to as such hereafter.

Strain Name	*and* number or Gene name and Allele (if assigned)	Lineaged	Precocious Caapa Division Confirmed in Secondary Screen	Precocious Caapa % at 25°C
GE6566	*t3465*	**Yes**	No	0
GE6534	*t3464*	**Yes**	Yes	100
GE6507	*t3463*	**Yes**	Yes	66
GE6436	tbc	**Yes**	Yes	25
GE6057	tbc	**No**	n/a	n/a
GE6048	tbc	No	n/a	n/a
GE5880	*t3461*	**Yes**	Yes	33
GE5697	tbc	No	n/a	n/a
GE5691	*and-8(t3294)*	**Yes**	Yes	100
GE5651	*t3462*	Yes	Yes	50
GE5315	tbc	**Yes**	No	0
GE5039	*and-7(t3224)*	**Yes**	Yes	100
GE5038	tbc	No	n/a	n/a
GE4421	*let-19(t3200)*	Yes	Yes	100
GE4634	*let-19(t3273)*	Yes	Yes	76.5

Table 5.1 Summary of mutants identified in the 4D lineage screen. *The "lineaged" column refers to whether the strain has been lineaged from 4D recording made with our own facilities. Bold entries in this column indicate that I was the one to have lineaged said embryos. A question mark indicates that an allele number is yet to be assigned by the Schnabel lab, or that we currently do not know it.*

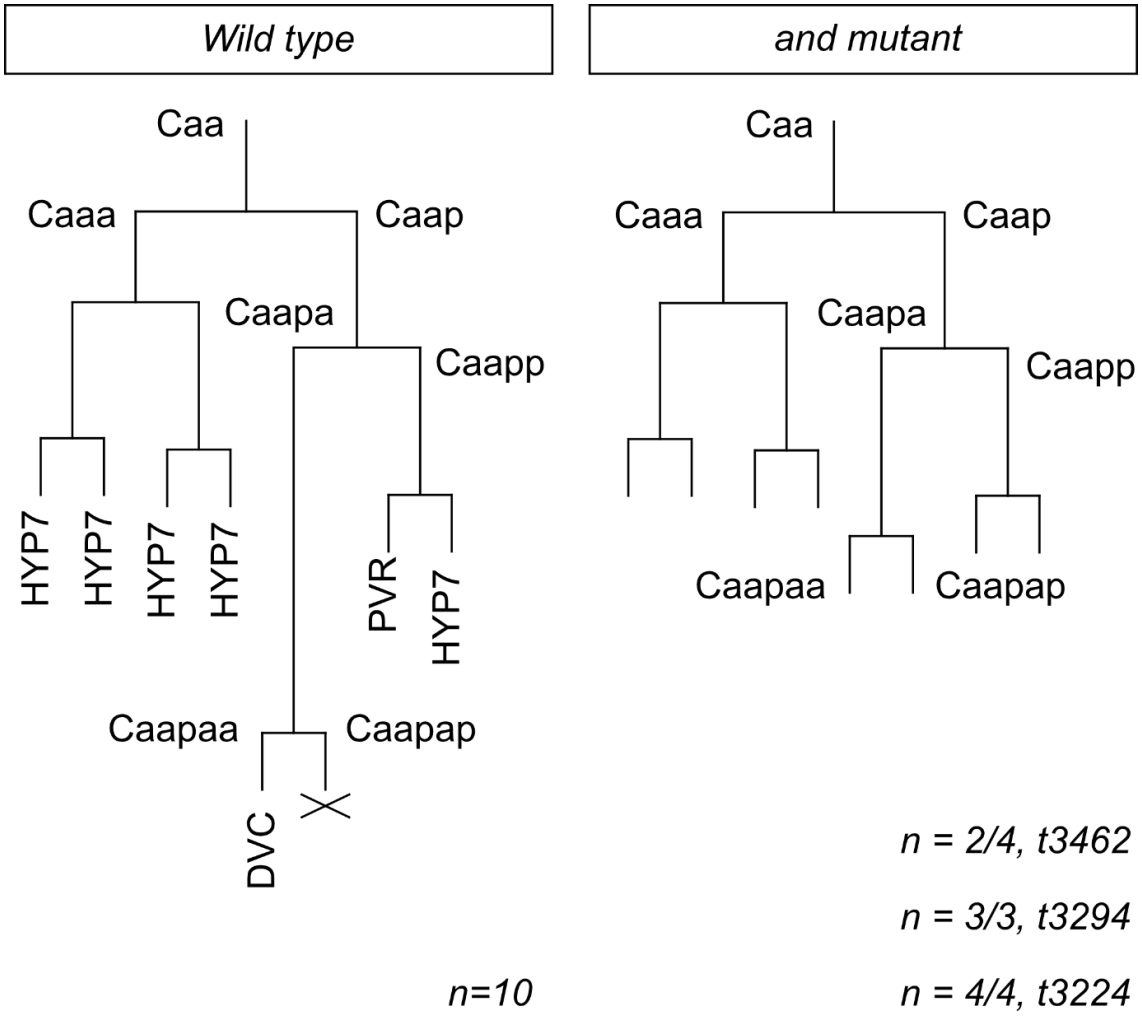

Figure 5.1. Summary of precocious Caapa divisions in and mutants identified from the 4D lineaging TS screen. *Wild type and mutant lineages detailing the recapitulation of the precocious division of the DVC neuroblast Caapa, for which the mutants were identified. Branch lengths are indicative of cell cycle duration and thus division time. The mutant lineages lack indication of fate as these were not assessed in initial 4D lineaging recordings.*

5.3. *and-7(t3224)* Displays a Variable Lineage Transformation and Ectopic DVC Phenotype

In addition to the C lineage division phenotype, *t3224* display lineage aberrations in the posterior most lineages, D and P4. Characterised in conjunction with Masters student Richard Wademan, 15/17 embryos were found to exhibit aberrations differing considerably from the *wild type* division pattern (Figure 5.2 A). This phenotype was highly variable with almost every embryos lineaged displaying a different division pattern; 10 different patterns were recorded across the 15 embryos, seven of which were unique to an individual embryo (Figure 5.2 B, C). 9/17 embryos displayed aberrations in the D lineage only, with a *wild type* P4 division pattern. In all cases the division pattern did not appreciably resemble that of a *wild type* D lineage, with multiple rounds of division missing in all embryos resulting in far fewer than the 20 cells following the terminal divisions, ranging from 4-9/20 with modal number being 6/20 (Figure 5.2 B). The remaining 6/17 embryos exhibited lineage aberrations in the P4 lineage in addition to D. In *wild type* animals P4 divides once to produce the germline precursors Z3 and Z4 which do not divide again until post-embryonic development. *t3224* mutant embryos that have aberrant P4 lineages display multiple divisions producing between 6-12 descendants of indeterminant fate with the modal number of eight present in 3/6 embryos (Figure 5.2 C). The great degree of variability and partial nature of these D and P4 lineage aberrations makes it difficult to determine if particular lineage swaps are occurring and thus the fates adopted by the blastomeres. Indeed, there is a lack of consistency in the aberrant lineages in that there are several different patterns adopted and these do not resemble other founder lineages fully as they do not include enough rounds of division.

With respect to neurogenesis in the C lineage *t3224* demonstrate ectopic expression of *ceh-63::gfp*, a unique DVC marker, at the non-permissive temperature indicating ectopic DVC neurons (Figure 5.3 A). Whist 100% (118/118) of mutant embryos scored arrested in or during morphogenesis, 88/118 (74.6%) present a single DVC with 22% (26/118) and 3.39% (4/118) of embryos presenting two (one ectopic) and three (two ectopic) DVCs respectively (Figure 5.3 B).

A

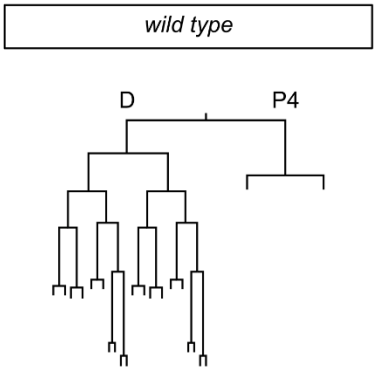

Gross Lineage aberrations	n	%
No	2	11.8
Yes	15	88.2
	17	**100**

B

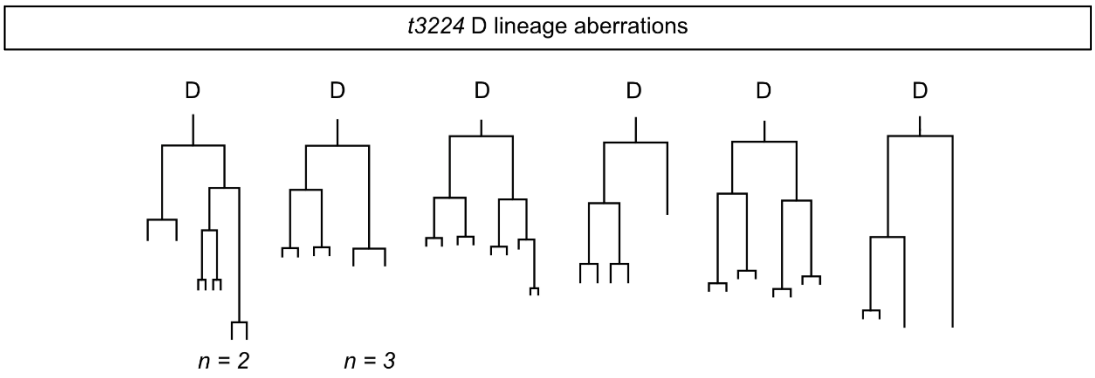

C

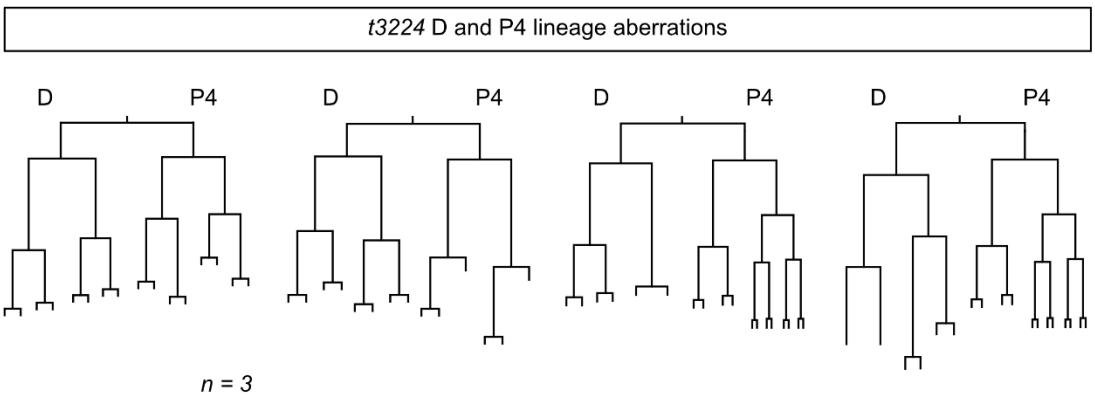

Figure 5.2. Gross lineage aberrations in the D and P4 lineages in *and-7(t3224)*. *A) Wild type reference lineages for the D and P4 lineages. A table scoring the occurrence of D and P4 lineages defects in 4D lineaged and-7(t3224) embryos. B) Division patterns observed in and-7(t3224) mutants for the D lineage. n = 1 unless otherwise stated. n values here include embryos in which the depicted D lineage pattern was observed, irrespective of whether they displayed P4 defects. C) Division patterns observed in and-7(t3224) mutants with defects in both D and P4. n = 1 unless otherwise stated. n numbers refer only to the P4 lineage with the n values for the D lineage include in section B).*

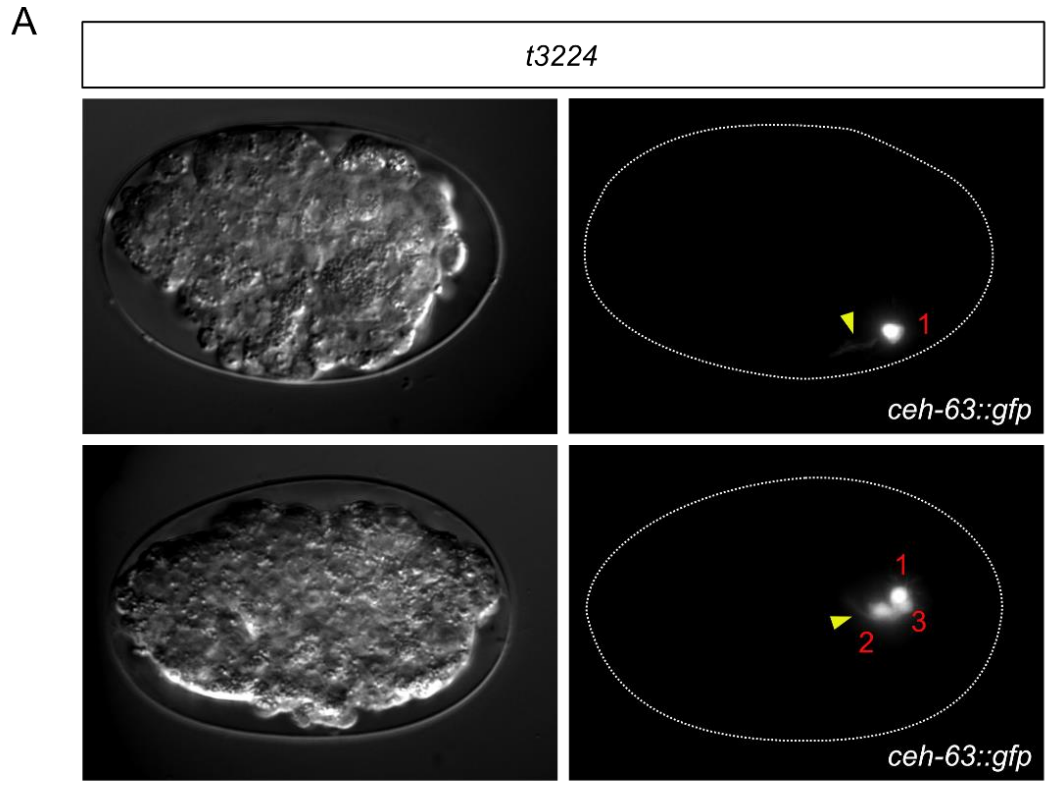

B

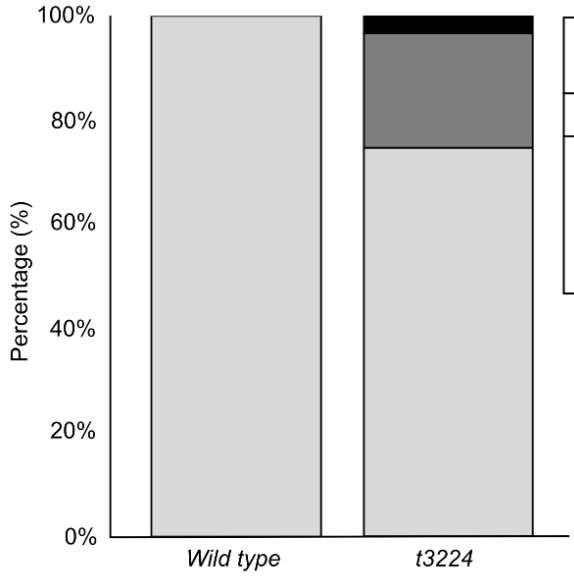

	ceh-63::gfp +ve cells	*n*	*%*
wild type	1	**52**	**100**
t3224	1	88	74.6
	2	26	22.0
	3	4	3.39
	Total	**118**	**100**

Figure 5.3. Scoring for the presence of DVC neurons in *and-7(t3224)* *A) DIC and GFP images of representative and-7(t3224) embryos. DIC images demonstrate that embryos arrest during morphogenesis. The presence of DVC neurons is evidenced by the expression of ceh-63::gfp, often with the characteristic tear-shaped cell body. Red numbers = the number of DVCs. Yellow arrows = clear neuronal processes. B) Stacked bar chart representing the number of DVC neurons in wild type and and-7(t3224), ceh-63::gfp embryos. A table detailing the scored number of DVC neurons in embryos.*

In light of the gross lineage aberrations in *t3224* mutants 4D lineage recordings where employed to ascertain the origin of these ectopic DVC neurons. Ectopic expression of *ceh-63::gfp* was observed in 7/13 (53.8%) lineaged embryos (Figure 5.4 A). Lineage analysis demonstrated that there was a great variability in the lineal origin of DVC neurons as evidenced by *ceh-63::gfp* expression and a clear neuronal process. Whilst this origin is varied it is restricted to the AB (4/13), MS (1/13), C (8/13) and D (2/13) lineages with the E and P4 lineages not exhibiting an ectopic DVC (Figure 5.4 B). This would suggest that the as yet indeterminant fate swap of P4 in some *t3224* mutants is not to that of C, in agreement with the lineage analysis. Furthermore, embryos in which a single DVC neuron was evident did not necessarily have it arising from the C lineage (Figure 5.4 B, C). This demonstrates that the 74.6% of embryos with a single neuron recorded during the previous analysis (Figure 5.3) likely do not all represent *wild type* expression. DVC arose from the C lineage in only 6/10 lineaged embryos with a single DVC neuron (Figure 5.4 C). Furthermore, it is evident that embryos with extranumerary DVC neurons also do not always have one arising from the C lineage, as 1/3 embryos exhibited two neurons from the MS and D lineages (Figure 5.3 C).

Having described this ectopic DVC phenotype the question arose as to whether these ectopic DVCs were generated from a complete recapitulation of the DVC branch of the C lineage. Such a recapitulation would require the expression of the proneural gene *hlh-14* prior to the onset of *ceh-63* expression as part of the DVC transcriptional cascade. Confirming that these ectopic neurons were indeed caused by recapitulation of the DVC branch, in 4/4 *and-7(t3224); ceh-63::gfp; hlh-14::gfp* embryos *hlh-14::gfp* expression was detected as preceding *ceh-63::gfp* in cells arising from both the *wild type* C lineage and ectopic lineages (Figure 5.5 A). An example being that of the MS lineage derived cell demonstrated in Figure 5.5 B.

A

ceh-63::gfp expression	**n**	**%**
ectopic	7	53.8
wild type	6	46.2
	13	**100**

B

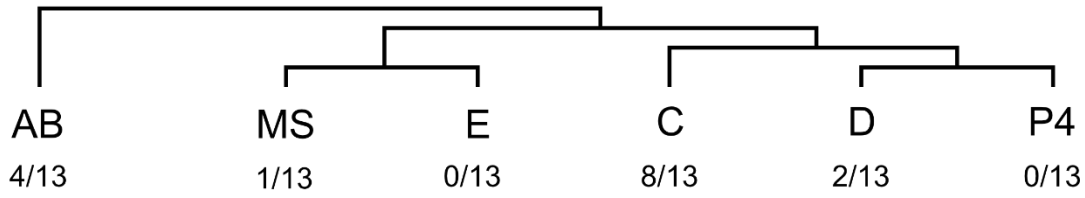

C

Blastomere origin of *ceh-63::gfp +ve* cells	**n**	**%**
AB	3	23.1
MS	0	0.00
E	0	0.00
C	6	46.2
D	1	7.69
P4	0	0.00
AB + C	1	7.69
MS + C	1	7.69
MS + D	1	7.69
	13	**100**

Figure 5.4. Summary of the lineal origin of DVC neurons in *and-7(t3224).* *A) Table scoring whether a lineaged embryo displayed a DVC neuron arising from an ectopic lineage. B) Summary of which founder lineage from which DVC neurons arose in lineaged embryos. C) Summary of the founder blastomere from which DVC arose in each individual lineaged embryo.*

A

hlh-14::gfp* expression preceding ectopic *ceh-63::gfp	**n**	**%**
No	0	0
Yes	4	100
		100

B

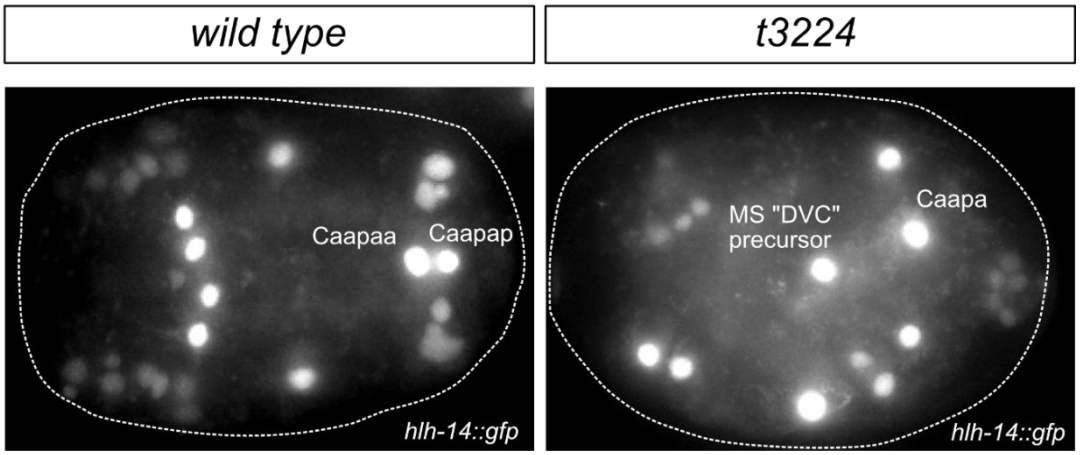

Figure 5.5. Expression of *hlh-14::gfp* in lineaged *and-7(t3224)* embryos. *A) Table summarising whether hlh-14::gfp expression was detected in ectopic DVC neurons prior to the expression of ceh-63::gfp. B) Representative hlh-14::gfp expression pattern in wild type and and-7(t3224) embryos at the bean stage of development. The greatly perturbed expression pattern in and-7(t3224) mutants is evident. Expression in the ectopic MS lineage derived DVC precursor is indicated.*

5.4. Mapping of *and-7*(*t3224)*

In order to identify the causal mutation for the *t3224* phenotypes mapping was conducted via the mapping by sequencing method (Doitsidou et al., 2018; Minevich et al., 2012). The highly polymorphic Hawaiian strain was used to outcross the mutants. A linkage region was identified by a region of increased N2 homozygosity on chromosome IV from 4.5-13 mega-bases (Figure 5.6). Both the size of the region and the fact that the homozygosity value for Hawaiian alleles did not reach zero in the region indicated that the mapping was of poor quality. This was possibly due to heterozygous animals being present in pooled samples used to genome extraction. The region however, whilst large, could be narrowed down by several factors.

The region contained only 56 unique lesions of which 45/56 are of the type expected from EMS mutagenesis, G>A or C>T. Only 13/56 lesions of the type expected from EMS mutagenesis had a mutant homozygosity value of over 0.5. Values between 0.5-1 would be expected in a sample that was contaminated by heterozygous animals as the value would be reduced from one in the heterozygotes that are evidently present in the sample. The most promising candidate from this list is a C>T transition, a missense mutation in *let-99* at position 12569664, which is located near the steepest part of the curve. *let-99* is also an interesting candidate for *and-7* given that in the one-cell embryo LET-99 localises in cortical bands excluding the ternary complex and therefore dynein. This uncouples microtubules from the cortex in these bands resulting in asymmetric pulling forces (Krueger et al., 2010; Wu and Rose, 2007). This thus affects asymmetric divisions which could lead to fate choice defects and lineage swaps in the early and later embryo as seen in the mutant. Validation of *let-99* was not undertaken during the project and so this and further candidates remain to be tested in future.

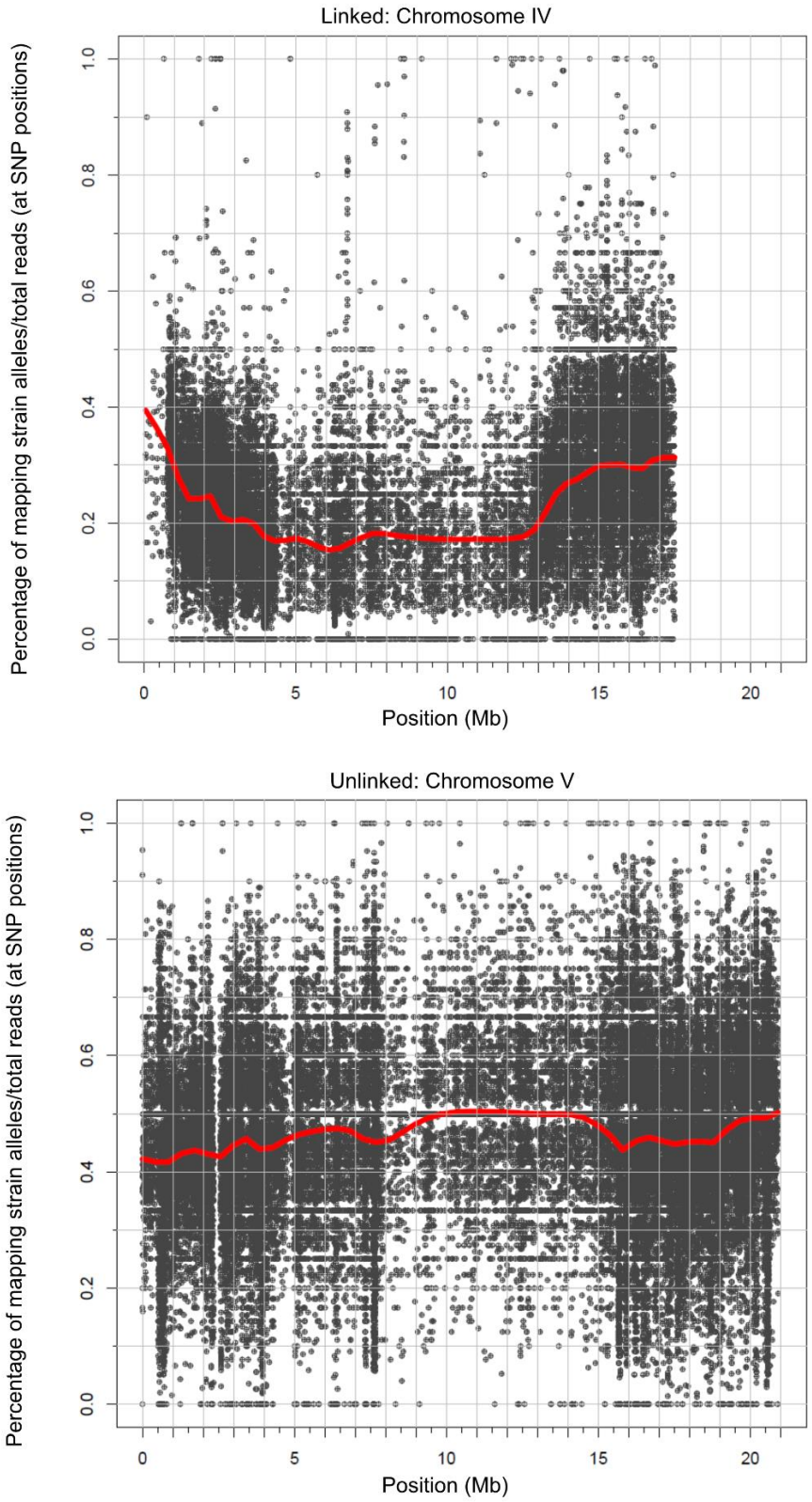

Figure 5.6. Linkage plots from mapping of *and-7(t3224).* *Mapping plots for the linked chromosome, Chromosome IV and an unlinked chromosome, Chromosome V. The linked region on Chromosome IV from 4.5-13 Mb is evidenced by decreased percentage of HA SNPs and thus homozygosity less than the 0.5 expected from random segregation. The fact that this region does not reach zero on the y axis is suggestive of poor mapping. The unlinked chromosome has homozygosity for HA alleles of around 0.5, indicating random segregation*

5.5. *and-8(t3294)* Displays Loss of DVC Phenotype

The second mutant that I characterised from the temperature sensitive screen is that of *and-8(t3294).* Unlike the gross lineage aberrations displayed by *and-7*(*t3224)* described in the previous section*, and-8(t3294)* resembles the typical lineage mutant that was sought during the screen; the precocious division of the DVC neuroblast Caapa mirroring *hlh-14* mutants. As previously stated, this precocious division phenotype was displayed by 3/3 embryos lineaged indicating a highly penetrant phenotype (Table 5.1, Figure 5.1).

As is the case with most of the mutants screened during the temperature sensitive lineage screen the majority of *and-8(t3294)* embryos arrest or die during morphogenesis at 25°C, 59/67 (80.60%) with a small fraction not reaching this stage 5/67 (7.46%). A further fraction of embryos arrest during elongation, 3/67 (4.48%). A small proportion, 5/57 (7.46%) do not arrest during embryogenesis and developed into 3-fold animals. These hatched animals however display an abnormal head morphology with a bulbous outgrowth adjacent to the posterior bulb of the pharynx (Figure 5.7 A) indicating phenotypes outside the C lineage. This head phenotype was not investigated further in favour of interrogation of the mutant's C lineage phenotype.

As 100% of *and-8(t3294)* mutants displayed the precocious Caapa division reminiscent of that seen in *hlh-14* mutants, confirmation was sought as to whether this division phenotype correlated with the lack of neurogenesis also seen in *hlh-14* mutants. Embryos were therefore scored using *ceh-63::gfp*, with both GFP expression and the evidence of a neuronal process indicating the presence of DVC. The lack of DVC was evident in 26/62 (41.9%) of scored embryos, with 36/62 (58.1%) containing the *wild type* single neuron (Figure 5.7 B) confirming that *t3294* causes a C lineage neurogenesis phenotype. Absence of neurogenesis in this 41.9% of embryos however showed no relation to the morphogenesis phenotype of these mutants. Both those embryos arrested in morphogenesis and those hatching with head defects displayed either a single or absence of a neuron (Figure 5.7 A).

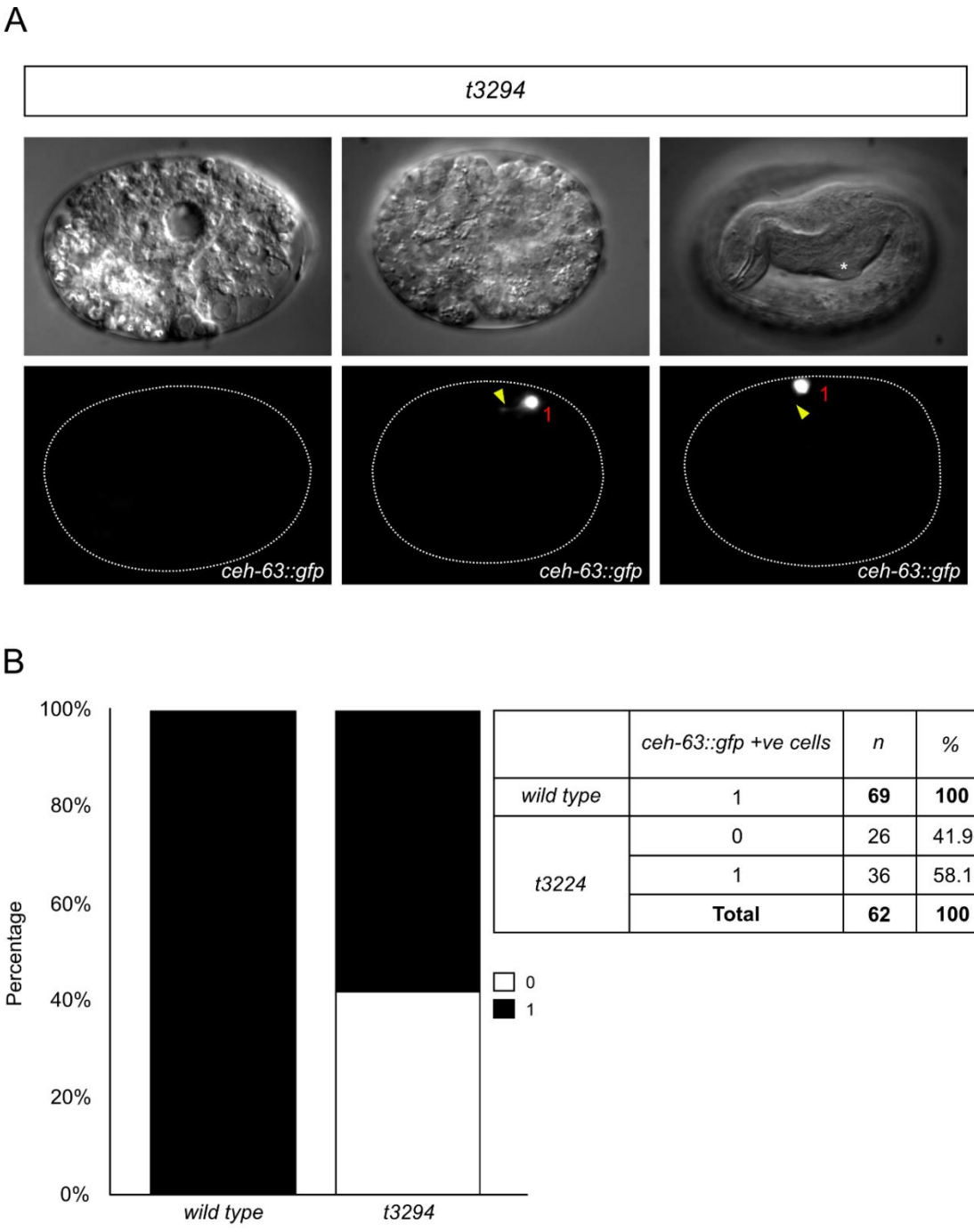

	ceh-63::gfp +ve cells	*n*	*%*
wild type	1	**69**	**100**
t3224	0	26	41.9
	1	36	58.1
	Total	**62**	**100**

Figure 5.7. Scoring for the presence of DVC neurons in *and-8(t3294)* *A) DIC and GFP images of representative and-8(t3294) embryos. DIC images demonstrate that some embryos arrest during morphogenesis whilst other hatch. In hatched embryos the bulbous outgrowth adjacent to the pharynx is indicated by an asterisk. The presence of DVC neurons is evidenced by the expression of ceh-63::gfp, often with the characteristic tear-shaped cell body. Red numbers = the number of DVCs. Yellow arrows = clear neuronal processes. B) Stacked bar chart representing the number of DVC neurons in wild type and and-8(t3294), ceh-63::gfp embryos. A table detailing the scored number of DVC neurons in embryo.*

In addition to being separable from the morphogenesis phenotype it is apparent that the neurogenesis defect caused by *t3294* is also not entirely corelated with the precocious Caapa neuroblast division. Two embryos were lineaged to initially identify *and-8(t3294)* as a mutant of interest with a further three lineaged using our own facilities. In 3/3 of these a precocious division was observed. Whilst the embryos analysed for lineage defects were not the same as those for *ceh-63::gfp* expression, the fact that a neurogenesis defect was observed in only 41.9% of these embryos presumes that they also undertook such a division. This therefore suggests that the precocious division in of the DVC neuroblast as seen in *hlh-14* mutants is not an entirely accurate predictor of neurogenesis and thus parallel and upstream regulators of *hlh-14*. Moreover, this in turn suggests that the precocious division in *hlh-14* mutants itself could be separable from its effect on neuronal fate decisions.

5.6. Mapping *and-8(t2394)*

As with *t3224* above, in order to identify the genetic lesion, *t3294* mutants were mapped using the mapping by sequencing method employing the highly polymorphic Hawaiian strain (Doitsidou et al., 2018; Minevich et al., 2012). The mapping quality was again poor with a large region of linkage on chromosome II revealed between 4-12 megabases along the chromosome (Figure 5.8). This large region was again likely caused by the inclusion of heterozygous mutants in the genome extraction samples. The region contains 619 unique lesions of which 421/619 are G>A or C>T transitions, the type expected from EMS mutagenesis. Of these only 20/421 have a homozygosity value of over 0.5. The majority of these are uncharacterised loci and as such it is difficult to identify targets of particular intrigue. However, potential targets for investigation include DNJ-5, a co-chaperone for heat-shock proteins Hsp70 and Hsp90 possibly linked to the temperature sensitive nature of the mutation, TRR-1 due its involvement in chromatin remodelling and antagonism to ras signalling in vulval development (Ceol and Horvitz, 2004) and NSY-1, an orthologue of the human MAP kinase kinase kinase MAP3K15, given its role in asymmetric fate decision in the AWC neuron pair downstream of UNC-43 (Sagasti et al., 2001).

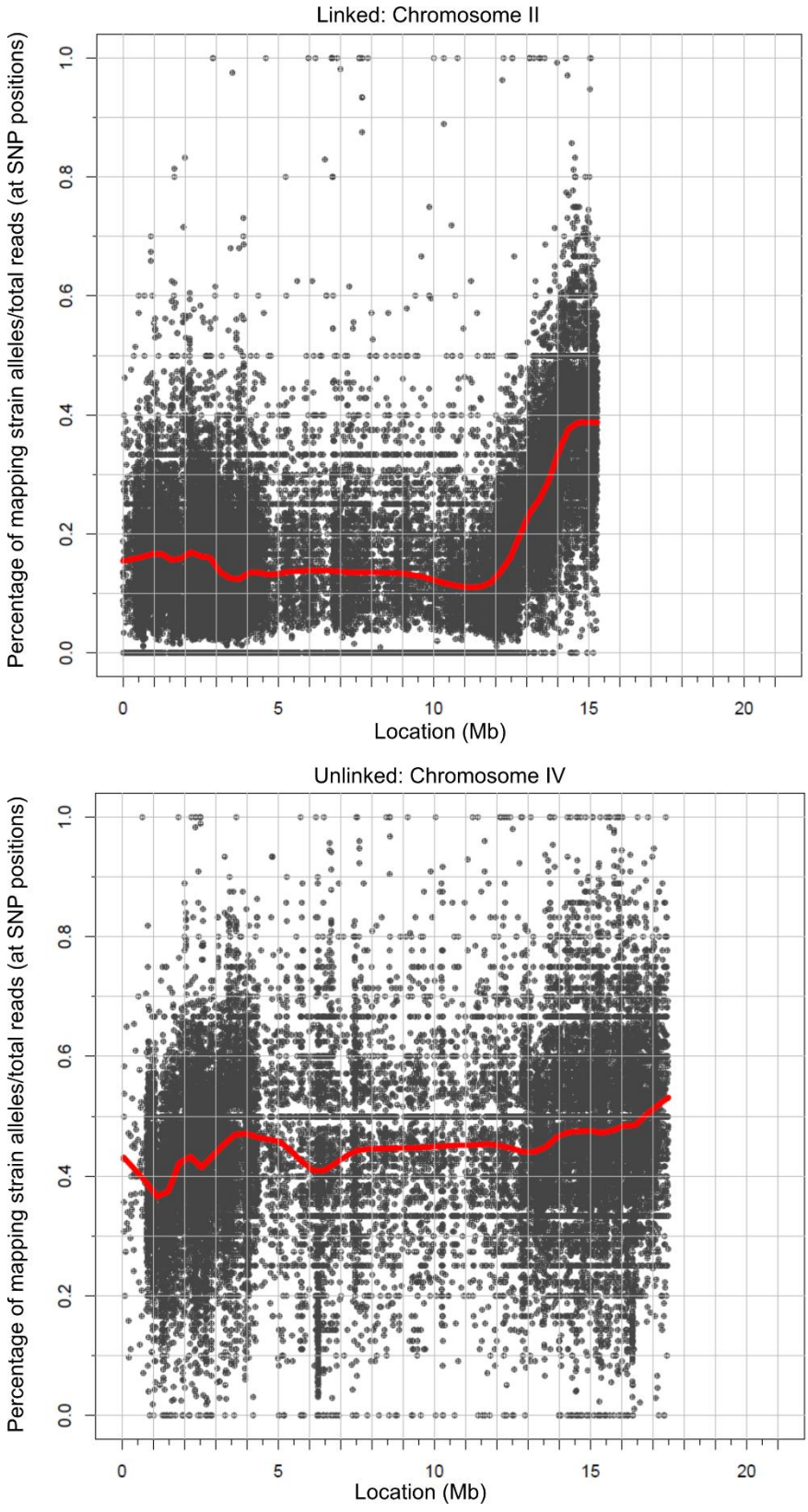

Figure 5.8. Linkage plots from mapping of *and-8(t2394).* *Mapping plots for the linked chromosome, Chromosome II and an unlinked chromosome, Chromosome V. The linked region on Chromosome IV from 4-12 Mb is evidenced by decreased percentage of HA SNPs and thus homozygosity less than the 0.5 expected from random segregation. The fact that this region does not reach zero on the y axis is suggestive of poor mapping. The unlinked chromosome has homozygosity for HA alleles of around 0.5, indicating random segregation.*

5.7. *and-9(t3462)* Mutants Displays a Loss of and Ectopic DVC Phenotype

The third mutant characterised following confirmation of the precocious division phenotype was *and-9(t3462)*. Of the three, this mutant is the least characterised. In common with the majority of *and* mutants recovered from the screen, *and-9(t3462)* mutants arrest during either morphogenesis (65.79%, 50/76) or elongation (13.16%, 10/76), as evidenced in the DIC images in (Figure 5.9 A).

In terms of a DVC neurogenesis phenotype *and-9(t3462)* displays a reasonably penetrant loss of DVC as indicated by the loss of *ceh-63::gfp* expression when scored in mounted embryos at 25°C. 44/72 (61.1%) of the embryos that developed to the stage at which *ceh-63* is expressed in a *wild type* lacked expression (Figure 4.9 B). In addition to this loss of DVC a weak ectopic DVC phenotype was observed in which embryos displayed a single extra DVC neuron, 4/72 (5.66%) (Figure 4.9 B). Lineaging of embryos carrying the *ceh-63::gfp* transgene was not undertaken and so the source of this extra DVC neuron in these rare cases was not determined. Furthermore, assessment of *hlh-14::gfp* expression was not made in *and-9(t3462)* mutants embryos and so confirmation that the loss of *ceh-63::gfp* and DVC neurogenesis is caused by the loss of proneural gene expression remains to be undertaken.

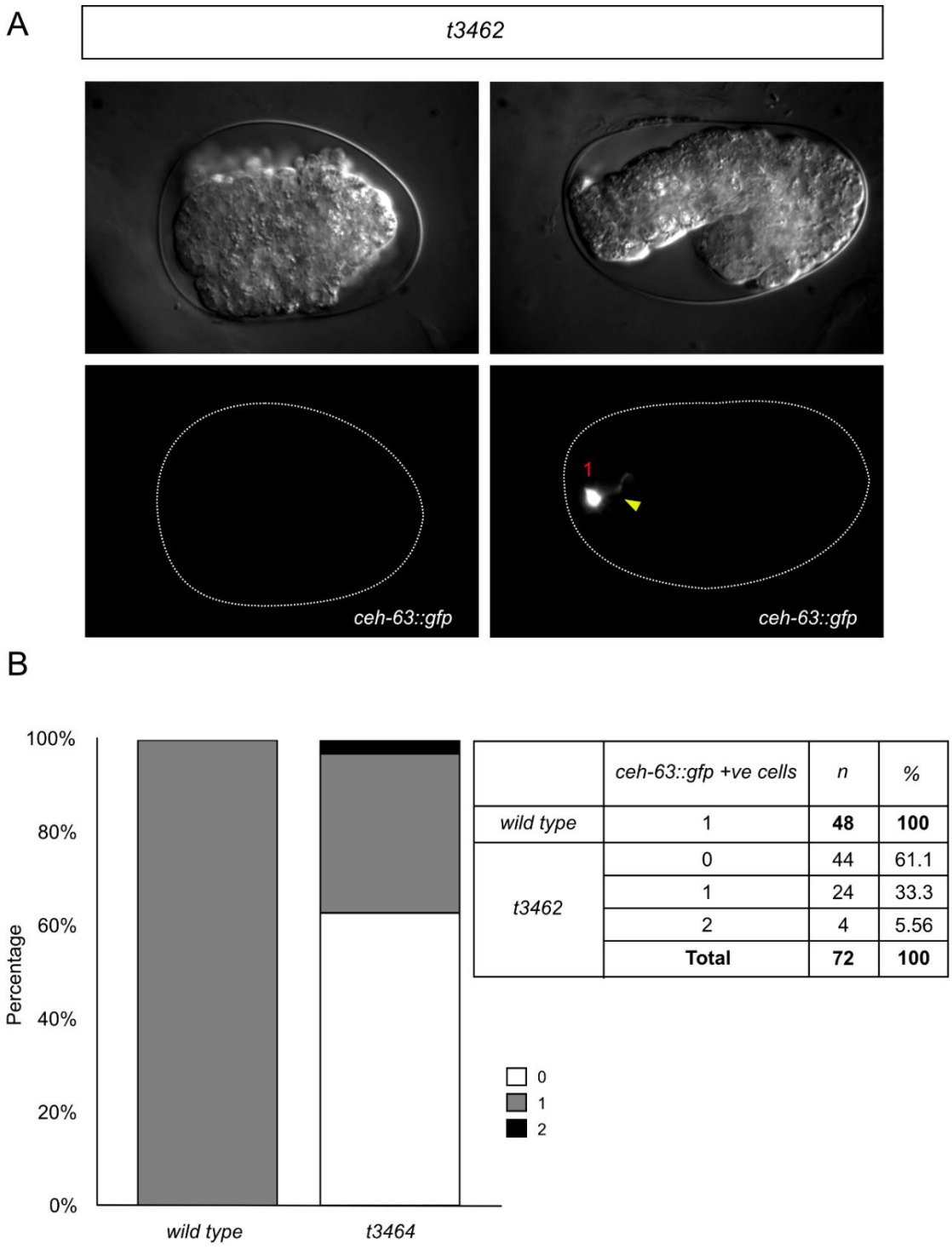

	ceh-63::gfp +ve cells	n	%
wild type	1	**48**	**100**
t3462	0	44	61.1
	1	24	33.3
	2	4	5.56
	Total	**72**	**100**

Figure 5.9. Scoring for the presence of DVC neurons in *and-9(t3462)* *A) DIC and GFP images of representative (t3462) embryos. DIC images demonstrate that embryo both arrest during early morphogenesis and the during elongation. The presence of DVC neurons is evidenced by the expression of ceh-63::gfp, often with the characteristic tear-shaped cell body. Red numbers = the number of DVCs. Yellow arrows = clear neuronal processes. B) Stacked bar chart and table representing the number of DVC neurons in wild type and scored embryos.*

Discussion

Chapter 6

6. Discussion

6.1. The 4D-lineage Screen is Effective in Uncovering Upstream Regulators of HLH-14

As outlined in my introduction the upstream molecular regulators involved in initiating proneural gene expression are poorly understood in most model systems, with this being particularly true in *C. elegans.* During this thesis I have described a 4D lineage-based screen as the method by which I attempted to identify these novel upstream regulators for *hlh-14* expression in the C lineage. As previously stated, this screen is designed around a key C lineage phenotype of *hlh-14* mutants, the precocious division of the DVC neuroblast (Poole et al., 2011). The rationale behind this design being that regulators both immediately and further upstream will phenocopy this aspect of *hlh-14* mutants due to the loss of action by HLH-14. To date over 100 strains have been screened in this manner. Of the 83 strains screened since I began to lead the screen, eight have demonstrated this precocious division with a higher enough penetrance to be identified. This hit rate of 9.64% for the discovery of such mutants and that around half of these display neurogenesis phenotypes in subsequent analysis, demonstrates that it is a method with a reasonable degree of efficiency. Adding to this is the fact at an allele of *let-19* described in this thesis, *(t3273),* was also identified as part of a previous phase of the screen, thus highlighting that key regulators of *hlh-14* expression can be uncovered through this method

As will be discussed in following sections, *let-19* likely acts in the cell and/or mother of the cell in which *hlh-14* is expressed. Highlighting that the lineage screen will also uncover factors acting further upstream than this, and so earlier in the lineage decisions that lead to *hlh-14* expression, is the identification of the and-7(*t3224). and-7* was originally identified due to the high penetrance of its precocious DVC neuroblast division, however subsequent analysis revealed that it this was caused by lineage duplications and or swaps leading to ectopic and supernumerary DVC neurons. This thus suggests that the processes affected in *and-7* are potentially early acting. The highly variable nature of the lineage aberrations in *and-7* mutants made the identification of precise lineage identity changes challenging. These defects are somewhat reminiscent of those seen in Wnt mutants and in fact one of the *and-7* candidates is the Wnt repressor, non-receptor tyrosine

kinase *frk-1*. Mutations in which cause embryonic lethality, loss of asymmetric seam cell divisions and over-proliferation phenotypes (Mila et al., 2015; Putzke and Rothman, 2010; Putzke et al., 2005). Other mutations in Wnt signalling pathways often lead to sub-lineage and branch duplications due to disruption of fate acquisition caused by defects in pathways such as the Wnt/β-catenin pathway. These defects however are, whilst still showing variation, often stereotyped and easily identifiable. A good example of this is demonstrated in *lit-1* mutants in which posterior fates within lineages which develop lineage-autonomously, such as C, are lost and so branches adopt the fate of more anterior sister branches (Kaletta et al., 1997; Schnabel, 1995). In the early embryo inductive Wnt signalling is required for the adoption of endoderm fate in the E blastomere over that of its sister MS (Calvo et al., 2001; Kaletta et al., 1997; Maduro et al., 2005; Thorpe et al., 1997), yet whilst the C blastomere is a source of Wnt signals (Dejima et al., 2014), it has not shown to be receptive to them (reviewed in Sawa and Korswagen, 2013). Another candidate for *and-7* is *let-99,* a DEP protein required for the exclusion of the ternary complex from the cortex and thus contributing to unequal cleavage and asymmetric division of the one-cell embryo (Krueger et al., 2010; Wu and Rose, 2007). Although *let-99* is maternal-effect lethal as a null and is required in the one-cell embryo (Rose and Kemphues, 1998; Tsou et al., 2002), the use of temperature sensitive alleles and RNAi has revealed a similar role in division in AB and EMS (Liro and Rose, 2016; Price and Rose, 2017). It is thus not inconceivable that *t3224* could have a weak effect on these early divisions that has an impact on later fate decisions or that the nature of the lesion caused defects in later divisions than previously described. This would have to be tested through precisely timed discrete temperature shift experiments to pinpoint the timepoint and divisions affected in such a way. Therefore, whilst not immediately obvious both *frk-1* and *let-99* do provide potential candidates to be tested in future.

The lineage phenotypes of the other mutants identified in the 4D lineage screen discussed in this thesis appear to be restricted to the C lineage and the precocious DVC neuroblast division. They thus represent the kind of mutants the screen was designed to uncover. However, the investigation of *pig-1* and *ham-1* mutants demonstrates that this phenotype will lead to false-positives in the first screening step. Around a third of *pig-1* mutants demonstrate a precocious DVC neuroblast division as their only C lineage aberration as do a fifth of *ham-1* mutants. This was not accompanied by neurogenesis defects or the loss of *hlh-14* expression in *ham-1* mutants and only 2/12 such *pig-1* mutants lacked *hlh-14* expression, being the only 2/28 to do so. This

illustrates that using the precocious division was a marker will also cause mutants that affect the timing of the division which are not upstream of *hlh-14* to be selected. This must be borne in mind for the future continuation of the screen and its impact on its efficiency.

6.2. Neurogenesis is in the C Lineage is Controlled by Lineage-Intrinsic Mechanisms

The asymmetry of the C lineage, with neurons arising from only the left-hand side, leads to the question of whether this symmetry breaking neurogenesis is lineage-intrinsic or requires a lineage-extrinsic signal. To address this question, I performed laser ablation experiments of other founder blastomeres to isolate the C lineage. Through these experiments I have demonstrated that neurogenesis in the C lineage does not require lineage-extrinsic signals as in ablated embryos the DVC is clearly evident and produces a neuronal projection. This is consistent with previous reports suggesting that specification of the C blastomere and subsequent downstream specification of hypodermis and body-wall muscle is blastomere- and then lineage-intrinsic (Draper et al., 1996; Hunter and Kenyon, 1996; Schnabel, 1994; Sulston et al., 1983). The results in this thesis also confirm that this is also true for C lineage neurons. This had seemingly only been assumed previously though incomplete lineage analysis of the PVR branch and not the DVC branch in transformed “C like” lineages in *mex-3* mutants (Draper et al., 1996).

This is also consistent with a lack of requirement for early Notch signalling in the C lineage. Although P2, the mother of C, expresses the Notch ligand APX-1/Delta and is required to signal to ABp to activate REF-1 family bHLH transcription factors and specify ABp fates (Mickey et al., 1996; Moskowitz et al., 1994; Neves and Priess, 2005), C itself does not express GLP-1/Notch or APX-1/Delta (Evans et al., 1994; Mickey et al., 1996). Furthermore, although MOM-2/Wnt signalling from P2 to EMS is required for correct E fates (Rocheleau et al., 1997; Thorpe et al., 1997), and from C to ABpar for spindle orientation (Dejima et al., 2014; Walston et al., 2004), C has not been identified as responsive to Wnt signals (reviewed in Sawa and Korswagen, 2013).

To complement the ablation experiments I analysed lineage transformation mutants in which AB descendants are transformed into “C like” cells, isolated the endogenous C blastomere from potential AB-derived signals. Analysis of *mex-3(-)* mutants revealed that they may have an incomplete lineage transformation. Based on (Draper et al., 1996), the expected number of extra DVC neurons should match that of the eight transformed AB great-granddaughters. Using a *ceh-*

63::gfp transgene to mark DVC, I did not observe this number, with far fewer extra DVCs present. One interpretation of this is that these transformed “C like” cells are in fact of mixed fate and so are not true recapitulations of the C blastomere. This is at least partially true given the observation that GLP-1/Notch and APX-1/Delta are expressed in the *wild type* spatial pattern in *mex-3(-)* mutants (Draper et al., 1996), although whether they are in any way responsive to such signals is unknown and would require investigation. The generation of those signals is theoretically possible given that the E is untransformed in *mex-3* mutants (Draper et al., 1996) and whose descendants are the source of Notch signalling to AB lineages (Neves and Priess, 2005). Lineage analysis was challenging in *mex-3* mutants due to the gross transformations causing changes in the placement and movements of cells and so confirmation of which AB great-granddaughters the extra DVCs arose from was not achieved. It would be interesting to revisit the problem and assess if there is any lineage or spatial bias with respect to which AB descendants do or do not express *ceh-63::gfp*.

Importantly however, the endogenous C blastomere always demonstrated a *wild type* division pattern and expression of *ceh-63::gfp* which combined with blastomere ablation confirms that neurogenesis in the lineage does not require lineage-extrinsic inductive signalling.

6.3. Unequal Cleavage and Subsequent Daughter Cell Size Asymmetry is Controlled by *ham-1* and *pig-1* but is not a Main Driver of the Initiation of *hlh-14* Expression

One of the key findings of the work described in this thesis is that the unequal cleavages are not a mechanism by which the expression of the proneural gene is segregated into the neurogenic branches of the C lineage. One method by which I assessed this was in mutants of *ham-1* and *pig-1* which are known regulators of other asymmetric and unequal neuroblast cleavages. This analysis revealed a novel role of *ham-1* and *pig-1* in the C lineage and as will be discussed, provides insight into the regulation of unequal cleavages in the lineage. Importantly *pig-1* is required for the unequal cleavage of both Caaa/Caap and Caapa/Caapp and *ham-1* for Caapa/Caapp; neither of which has been described before.

In *pig-1* mutants equalisation of Caaa/Caap, at which the hypodermal/neuronal decision is made in the lineage, does not result in the loss of *hlh-14* expression in Caapa, the DVC neuroblast. Importantly this equalisation does not lead to ectopic expression in Caaa descendants further

illustrating the unequal cleavage is not responsible for the correct segregation of an as-yet unidentified regulator into Caap or its exclusion from Caaa. The second unequal cleavage in the lineage, that of Caapa/Caapp, also appears not to be required for correct expression of *hlh-14* in the DVC neuroblast, Caapa, as equalisation of this division in both *pig-1* and *ham-1* mutants has little to no effect on its expression nor induces ectopic expression. As would be expected the absolute volume of Caap is almost twice as large in *pig-1* mutants as in *wild types* as a result of an equalised cleavage that would otherwise produce a Caap half the volume of its sister. In *wild types* the reverse is true for the following division, where Caapa is smaller. The overall volume of Caapa in *pig-1* mutants is therefore around three times that of a *wild type* as the result of consecutive equalised divisions. The increased volume of either cell however has no impact on the correct onset of *hlh-14* expression. Overall, this leads to the conclusion that unequal cleavage is not required for segregation of an *hlh-14* regulator nor is it required to produce a particular volume of cell needed for specific reaction kinetics leading to *hlh-14* expression.

However, two embryos of the 28 assessed for *hlh-14* expression in this study failed to express and so lacked neurogenesis. The cause of this is not entirely clear given that these two embryos display daughter volume ratios within the range of *hlh-14* expressing *pig-1* embryos for both Caaa/Caap and Caapa/Caapp suggesting that they do not have a unique unequal cleavage phenotype. The same is true for their Caap and Caapa absolute volumes. However, because the *pig-1(gm344)* mutant used in this study is a null mutant and affects both cleavages assessed, it is difficult to judge when a potentially divergent phenotype may have occurred. The orientation of the Caaa/Caap division in these embryos is also not significantly different to expressing *pig-1* mutants for *wild type* embryos and so this is possibly not causal. However, it could be telling that although not statistically significant, the orientation in these embryos clearly deviated from *wild type.* It is possible that the low *n* of two for this phenotype resulted in the non-significance, but it also highlights that it is a very rare phenotype. Revisiting this by analysing more *pig-1(gm344); hlh-14::gfp* embryos would reveal how rare a phenotype it is and if the orientation defect reoccurs, provide more numbers for more powerful statistical analysis. Due to time constraints the orientation of the Caapa/Caapp was not assessed for any *pig-1* mutants, and as such this may also provide an answer, indeed randomisation of cleavage plane orientation has been observed in *pig-1* mutant NSM neuroblasts (Wei et al., 2017).

This consideration leads into the discussion of the appropriateness of using *pig-1* to assess unequal cleavage. This is because it has been argued that *pig-1* may also be required for the polarisation of fate determinants in addition to the control of the cleavage plane during divisions that produce a neuron or neuroblast and a cell death. This interpretation is based on the observation that although cleavage plane position is affected in nearly all *pig-1* and *ham-1* mutants, the penetrance of ectopic neuronal fate in surviving daughter does not correlate, for example (Cordes et al., 2006; Feng et al., 2013; Guenther and Garriga, 1996). However as these phenotypes are enhanced by mutations in cell death genes and that *pig-1* has been demonstrated as required for cleavage plane positioning, segregating a caspase gradient in the NSM neuroblast (Mishra et al., 2018), another interpretation is that it is required for the segregation of apoptotic rather than neuronal fate in these instances. Furthermore, the lack of a phenotype preceding *hlh-14* expression in the C lineage described in this thesis suggests that the polarity in terms of whatever initiates *hlh-14* expression is unaffected.

Another method by which I attempted to equalise C lineage cleavages was through the disruption of spindle pulling forces though the use of a temperature-sensitive allele of *lin-5/NuMa.* As mentioned in the results section this method was technically challenging and unsuccessful after the addition of *hlh-14::gfp* and *ceh-63::gfp* transgenes. However, in order to address any potential caveats surrounding the possible loss of *wild type* polarity in *pig-1* mutants the disruption of cleavage plane positioning in a more overtly mechanical way may be desirable. Recent advances in optogenetic tools allow for the photo-inactivation or localisation of engineered transgene products and present a rapidly acting tool with which to disrupt components of cell division (Fielmich et al., 2018; Johnson and Toettcher, 2018). Disruption of *lin-5* or *nmy-2* in this manner could potentially overcome the technical limitations of the temperature sensitive alleles.

ham-1 is known to mainly affect divisions in which the anterior daughter is smaller (Teuliere et al., 2018), and this is also true in the C lineage, in which it affects the unequal cleavage of Caapa/Caapp which displays such an asymmetry and not Caaa/Caap which displays the opposite. Interestingly, the observation that *ham-1* only affects specific C lineage divisions is also in agreement with the finding that *ham-1* mutants do not affect the expression of the now known to be terminal selector *unc-86* in PVR (Desai et al., 1988; Guenther and Garriga, 1996). As *ham-1* mutants have only a weak DVC phenotype and a seemingly *wild type* PVR branch in my own analysis, this partially explains why its role in the C lineage has so far gone undescribed.

Although not the main focus of analysis in this study *pig-1* and *ham-1* are also required in their well-established role in neuroblasts dividing to produce a neuron and a cell death in the C lineage. this is evidenced by the near total loss of death in the DVC sister and its adoption of DVC fate in many cases in *ham-1* and *pig-1* mutants. The fact that the description of this role is novel comes from the fact that only specific sets of neurons were assessed in previous studies (Cordes et al., 2006; Frank et al., 2005), that they did not assess the C lineage directly and that the *hlh-14* expressing cells of the C lineage were not confirmed at such until later (Poole et al., 2011).

An additional phenotype displayed by around 20% of *pig-1* mutants is the extra rounds of division of Caapaa (DVC) and Caapap, its surviving sister. That *pig-1* may be involved in the segregation of "mitotic potential" during terminal neuroblast divisions has recently been proposed to explain how undead QL.p daughters are sometimes able to erroneously divide and produce two rather than one ectopic SDQL neuron (Mishra et al., 2018). In the C lineage such mitotic potential should not need to be segregated as Caapaa does not divide and instead differentiates into the DVC neuron. However, a recent transcriptional and proteomic study of *pig-1* null mutants demonstrated that *pig-1* targets at the transcriptional and phosphorylation levels include factors implicated in the control of cell division and cell cycle (Offenburger et al., 2017). Given that this extra division phenotype is restricted to the Caapa branch this would suggest that *pig-1* may be involved in repressing the ability of Caapa descendants to divide.

Although originally implicated only in generating daughters of different sizes in neuronal divisions producing one apoptotic daughter, recent findings have demonstrated a wider role for *pig-1* in unequal cleavages. My results for earlier divisions of the C lineage add to the body of evidence for this wider role which include the redundant requirement in both the one-cell embryo (Pacquelet et al., 2015) and in the division of the EMS blastomere (Liro et al., 2018). The requirement for *pig-1* in the unequal cleavages of Caaa/Caap, Caapa/Caapp and Caapaa/Caapap also strengthens the evidence of this wider role. Importantly this is also to the author's knowledge the first demonstration of roles for *pig-1* in multiple rounds of division in the same lineage. It will be intriguing to see how wide a role *pig-1* plays in the unequal cleavage in the *C. elegans* embryo and particularly whether this more general role is also required in other neuronal lineages in which its involvement in neuroblast/apoptotic divisions is already well characterised. It would also be important from a mechanistic viewpoint to ascertain by which method *pig-1* and *ham-1* control unequal cleavage in the C lineage. Assessment of spindle positioning and the localisation of NMY-

2 are both readily achievable through transgenes in *C. elegans* and their disruption in *pig-1* and *ham-1* the mutants would be informative.

6.4. Unequal Cleavages are Controlled by Regulators of C Lineage Fates

Whilst the unequal cleavages and the resultant daughter cell size asymmetries in the C lineage do not contribute to *hlh-14* expression, they nevertheless must be actively regulated given how much they differ from the symmetric divisions in the lineage. I have demonstrated that *pig-1* is required to control these unequal cleavages and that in Caapa/Caapp it may be under the control of the transcription factor *ham-1*, as it is a number of lineages such as Q.a (Feng et al., 2013).

Several lines of evidence suggest that *pig-1* could be regulated at the transcriptional level in the C lineage and by novel regulators. In the NSM neuroblast *pig-1* is regulated at the transcriptional level by CES-2/HLF repression of a *pig-1* repressor, CES-1/Snail (Wei et al., 2017). However, unlike in the NSM lineage, *pig*-1 does not appear to be regulated by this mechanism and loss and gain of function mutants for *ces-1* and *ces-2* are *wild type* for C lineage cleavages.

However, the first unequal cleavage requiring *pig-1* expression is also equalised in *let-19(t3200)* and *let-19(t3273)* mutants. LET-19 is required for the correct expression of proneural genes *hlh-14* and *hlh-2*, to be discussed below. As a member of the Mediator Complex LET-19/Mdt-13 most likely enacts this control over *pig-1* in a transcriptional manner (Grants et al., 2015; Grants et al., 2016; Wang et al., 2004). Given that the unequal cleavage defects and that absolute volumes of Caaa/Caap in *let-19* and *pig-1* mutants are remarkably similar and display a similar range of values, I propose that transcriptional regulation of *pig-1* in Caa is mediated by LET-19. Mediator complex components have been previously demonstrated to mediate asymmetric divisions in conjunction with POP-1 asymmetry is response to Wnt signalling in the hyp7/T blast cell (Yoda et al., 2005). Assessing other members of the Mediator complex kinase module such as *dpy-22/Mdt-12*, *cdk-8/CDK8* and a supposed null allele of *let-19,* revealed that the cleavage phenotype is peculiar to *let-19* and curiously not observed in the null allele of *let-19.* Although at first unintuitive, that the same process would be differently affected by mutations in different kinase module components has been widely noted. For example, control of cell cycle genes in vulval precursor cells is more dependent on *dpy-22, let-19 and cdk-8* than on the fourth member of the module *cic-1/CyclinC* (Clayton et al., 2008). Moreover, in a neuronal context it has more recently been

reported that HLH-3 driven neurogenesis of the I4 neuron requires both functional CDK-8 and DPY-22, yet that this is twice as reliant on DPY-22 (Luo and Horvitz, 2017). The lack of a phenotype in the *let-19(os33)* null mutant is however difficult to explain, although it must be noted that they were only assessed for cleavage plane and division time, not neurogenesis phenotypes. However, another member of the kinase module, CDK-8, is known to have weak phenotypes in null mutants so the possibility for a compensatory mechanism for total loss of a component may exist.

A striking feature of the main *let-19* mutants employed in this study is that they demonstrate very specific defects in the expression of *hlh-14,* only affecting the C lineage, and for cleavage phenotypes, affecting only certain cleavages (Caaa/Caap and not Caapa/Caapp). This is particularly true of the *t3200*, with *t3273* having a more pleiotropic effect.

In considering the interpretation of the *let-19(t3200)* and *let-19*(*t3273)* phenotypes, and indeed their relationship to that of the supposed null *let-19(os33),* another important aspect to consider is the nature of the lesions. Both are temperature sensitive missense alleles. Temperature sensitive alleles have been used for decades in the study of gene and protein function in a wide range of taxa (Edgar and Lielausis, 1964; Hartwell, 1967; Horowitz, 1950). Such mutations are almost universally thought to result in mutant phenotypes at non-permissive temperatures by nature of being missense lesions. Their phenotypes are therefore thought to be due to either loss of, or reduced, protein function resulting from protein instability or disrupted protein-protein interactions (Peck Justice et al., 2020; Sahni et al., 2015; Sugaya, 2018). The assumption of destabilisation however has recently been challenged by a study in yeast finding that only 130 proteins of over 3000 tested displayed destabilisation at higher temperatures (Peck Justice et al., 2020), suggesting interactions may be more important. This is supported by that fact that although certain regions of protein sequences, particularly those residues buried deep within protein structures, are thought to contribute most to stability (Kellis et al., 1989; Pakula and Sauer, 1989), it remains difficult to predict which residues would contribute temperature sensitivity.

As mentioned above, as a member of the Mediator complex kinase module, it remains likely that the LET-19 protein is present and functional at the permissive temperature with the lesions only affecting the modulation of certain transcriptional events once shifted to the non-permissive temperature. It is difficult to predict the precise effect of the mutations represented in the *t3200* and *t3273* alleles on the LET-19 protein. Indeed, the 3D structure remains unstudied. What is

known however is that MED13 homologues show deep evolutionary conservation of many domains and predicted structural elements including transcriptional repression and PIWI domains (Bourbon, 2008; Burroughs et al., 2013; Tsai et al., 2014). MED13 is also a conserved subunit which is involved in the interactions between the kinase module and the core Mediator (Tsai et al., 2013) and has extensive interactions with the C terminus of MED12 (DPY-22 in *C. elegans*), which runs along its surface (Li et al., 2021). MED12 itself is a key modulator of kinase module function in transcriptional repression (Grants et al., 2015). Thus it can be seen that whilst the *t3200* and *t3273* alleles do not lie within a currently known domain in LET-19 which would elucidate their precise impact on function (Burroughs et al., 2013; Felton, 2019), it is conceivable that they could disrupt interactions within the kinase module itself or between the kinase module and the core Mediator.

As the kinase module is mainly involved in transcriptional repression (Grants et al., 2015), the consequence therefore could be either the disruption of transcriptional repression or in the inability of the kinase module to de-repress and allow a particular transcriptional event. To reconcile with the supposed null allele *os33* having a *wild type* phenotype for cleavage, the *let-19(ts)* mutations would have to function to not allow de-repression to occur at the non-permissive temperature, whereas in a null the loss of LET-19 would be equivalent to the normal steps in which the kinase module releases repression and allows transcription. It must be remembered however that this speculation is based solely on the cleavage phenotypes as assessment of neurogenesis was not undertaken in the *let-19(os33)* mutants. Furthermore, as discussed elsewhere in this chapter and outlined in the working model at the end of the chapter, it is likely that the kinase module is involved in spatiotemporally distinct transcriptional mediation affecting cleavage and the expression of *hlh-14*.

Another possibility regarding the differing cleavage phenotypes for the temperature sensitive alleles and the supposed null would be that that *let-19(t3200)* and *let-19(t3273)* are neomorphic alleles. This is however unlikely because as noted above that the lesions are in different regions of the protein and not within the transcriptional repression domain (Felton, 2019) so it is unlikely that they would cause the same neomorphic phenotype at the same unequal cleavages. Furthermore, both the non-complementation between them and the recessive nature of both alleles (Felton, 2019) would argue against a neomorphic function as dominance is a feature of neomorphs (Muller, 1932).

Epistasis analyses between *let-19(t3200)* and *pig-1(gm344)* mutants was not possible as both display nearly 100% unequal cleavage phenotypes for Caaa/Caap of near-identical magnitude and so assessment of additive or synergistic effects could not be assessed.

The second unequal cleavage affected by *pig-1* loss, Caapa is under control of the proneural transcription factor required in the lineage, HLH-14. That a proneural gene would have this effect on an unequal cleavage in addition to neurogenesis has been seen in the Q.a lineage where LIN-32 controls both Q neuroblast identity and unequal cleavage of Q.a (Zhu et al., 2014). I hypothesise that HLH-14 regulates *pig-1,* possibly through or in parallel to HAM-1, which would represent a novel regulation of *pig-1* by proneural factors. A question that then arises is that if HLH-14 is an upstream regulator of *pig-1*, why do *pig-1* mutants have additional phenotypes not seen in *hlh-14* mutants and why is the equalisation of the Caapa/Caapp in both mutants not more similar? A potential answer for this could be both temporal and spatial and based on the context of the fate adopted by Caap. In a *wild type*, HLH-14 acts in Caap to confer its neural identity as the precursor of DVC/PVR/hyp7 rather than as a hypoblast. One of the consequences of this identity, or indeed in parallel, is the regulation of the cleavage plane through *pig-1* and results in unequal cleavage in which Caapa is smaller and Caapp larger. In a *pig-1* null mutant transcriptional control by HLH-14 would have no effect in Caap and so the cleavage is equal whilst HLH-14's other action in conferring the correct neural identity is unaffected. In an *hlh-14* mutant Caap adopts a hypodermal lineage identity and thus the cleavage plane is positioned appropriately for such a fate with a slight anterior bias. As this Caap divides symmetrically to produce two hypoblasts, this is very likely PIG-1 independent and so would explain why it does not resemble the *pig-1* mutant. Essentially, the hypothesis is therefore that the absence of PIG-1 in a context in which it is required would not resemble a context where it is not required. The assessment of an *hlh-14, pig-1* double mutant is needed to confirm this, but more importantly is assessment of *pig-1* expression in an *hlh-14* mutant to confirm the proposed transcription link between them.

Overall this leads to the critical conclusion that the transcriptional program that is required for the correct expression of proneural genes and the acquisition of neuronal fate in the lineage are is required to control successive unequal cleavages. LET-19 is required for neurogenesis and unequal cleavage of Caaa/Caap and the proneural transcription factor itself HLH-14, is required for neurogenesis and the unequal cleavage of Caapa/Caapp. That unequal cleavage is not

instructive of fate demonstrates that this control is in parallel to the control of neuronal fate by these factors. Therefore, these factors coordinate acquisition of neuronal fate and terminal embryonic cell size in space and time.

6.5. The Regulation and Action of *hlh-14* in C Lineage Neurogenesis is Best Explained in the Context of Unequal Cleavage

The finding that *let-19* is required for unequal cleavage of Caaa/Caap and not Caapa/Caapp, that *hlh-14* is required for unequal cleavage of Caapa/Caapp and not Caaa/Caap and that *hlh-2* is required for neither is initially confusing.

let-19 was originally identified as an upstream regulator of *hlh-14* expression (Felton, 2019) and so one could reasonably expect *let-19* to phenocopy *hlh-14* mutants in that regard. The fact that the two mutants have opposite effects in terms of which unequal cleavages they effect is not however unreconcilable. I posit that closer scrutiny of the *let-19* phenotype with regards to *hlh-14* expression and of *hlh-2* and *hlh-14* mutants with respect to both *hlh-14* expression and unequal cleavage actually allows for greater understanding of the spatiotemporal actions of these factors. The main conclusion of which is that *let*-19 is not in fact a direct regulator of *hlh-14* expression.

Temperature shift analysis defined the window of *let-19* action in C lineage neurogenesis as from the birth of Ca until the birth of Caap as assessed for *hlh-14* and *ceh-63* expression (Tam, 2015; Yeung, 2016). Within this window *let-19* is also required for the expression of *hlh-2* in the lineage (Felton, 2019) and to control the Caaa/Caap cleavage plane (this study). I speculate that it is this control of *hlh-2* expression that is critical for *hlh-14* expression but that this is not required until after the birth of Caapa, the DVC neuroblast. Several aspects of the *let-19* and *hlh-14* phenotypes are suggestive of this. Firstly, *let-19* mutants often display detectable *hlh-14* expression in Caapa which is not maintained and does not lead to neurogenesis. *hlh-14* mutants display the loss of the Caapa/Caapp unequal cleavage despite the fact that its expression not is detected until after this division, with the *gmIs20* transgene This confirms the speculation that *hlh-14* is in fact expressed in Caap. The delay in detection is possibly attributable to GFP maturation, which can in some cases lag two hours behind the onset of expression (Albano et al., 1996; Hazelrigg et al., 1998). Thus, I hypothesise that *let-19* is not responsible for the initiation of *hlh-14* expression. In *let-19* mutants, initiation of *hlh-14* expression would therefore allow it to begin to confer neural identity

on Caap and to control transcriptional events controlling the unequal cleavage of Caapa/Caapp. This would explain the *wild type* cleavage of this division in *let-19* mutants. Also, in Caa and Caap *let-19* is required for the expression of *hlh-2.* That *hlh-2* mutants have no unequal cleavage phenotypes suggests that it also is not required to initiate *hlh-14* expression, and so its role in Caap is unclear. *hlh-2* mutants do however lack the detectable *hlh-14* expression in Caap. The role of *hlh-2* therefore must be to initiate and/or maintain *hlh-14* expression in this cell, rather than at an earlier timepoint. This maintenance is likely to be through HLH-14/HLH-2 heterodimers and/or HLH-2/HLH-2 homodimers given that HLH-2 is a widely utilised dimerization partner of bHLH transcription factors and is required for the autoregulation of *Drosophila* proneural genes and vertebrate *atonal* homologues (Grove et al., 2009; Helms et al., 2000; Sun et al., 1998; Van Doren et al., 1992). *hlh-14* cannot regulate its own expression through HLH-14/HLH-14 homodimers as otherwise expression would not be lost in *let-19* or *hlh-2* mutants. As for the proposed regulation of *hlh-14,* HLH-14/HLH-2 heterodimers are then likely required to activate proneural target genes given HLH-14 requires HLH-2 in order to bind DNA (Grove et al., 2009).

When cleavage and *hlh-14* expression phenotypes are considered together they are therefore suggestive that *let-19* is indirectly required for the expression of *hlh-14* through its control of *hlh-2,* which is required for its continued but not initial expression. The variable penetrance of the detectable burst of *hlh-14* expression in *let-19* mutants is likely due to the nature of the alleles as temperature sensitive. Individual embryos may vary in the degree to which the lesion affects its action, which at the same time will be modulated by variation in the exact temperature of the microenvironment mounted embryos find themselves when at the non-permissive temperature of 25°C.

Similar multi-level regulatory logical controlling expression of a proneural gene beginning with a transcriptional event in the grandmother of the cell in which the proneural gene is detectable has been described for the MI neuron (Nakano et al., 2010). Here the grandmother of MI expresses the Otx transcription factor *ceh-36*, which act in the MI to activate expression of *ngn-1* and *hlh-2* which in turn acts as the proneural heterodimer in MI itself (Nakano et al., 2010). Moreover the role of the Mediator complex in being permissive of proneural gene action rather than as a direct transcriptional activator is reminiscent of the proposed role for the CDK-8 kinase module in interacting with HLH-2 to allow HLH-3 expression by repression of a repressor in the I4 neuron (Luo and Horvitz, 2017).

6.6. The Direct Upstream Mechanism and Transcriptional Regulator of *hlh-14* Remains Elusive

During this thesis I have established that unequal cleavage and resultant cell size is not a primary mechanism controlling initial *hlh-14* expression. This demonstrates that the asymmetric division of Caa leading to the expression of *hlh-14* in Caap is controlled by another mechanism. Therefore, it can be assumed that the segregation of whatever upstream regulator initiates this expression is unaffected by the loss of unequal cleavage. Such a regulator may be polarised such that the loss of unequal cleavage does not affect its segregation. If this as yet unidentified regulator is polarised in Caap, this is also unaffected by the loss of *let-19* despite the loss of unequal cleavage. Such a theoretical regulator could be tethered to the cell cortex in a manner similar to the tethering of fate determinants to the basal cortex by Miranda in *Drosophila* neuroblasts (Matsuzaki et al., 1998; Shen et al., 1997). Indeed, as already stated above, the disruption of unequal cleavage in *Drosophila* neuroblasts by particular G protein mutants doesn't affect the tethering and segregation of these basal fate determinants (Kitajima et al., 2010). It is possible that a similar situation occurs in Caa. This segregated regulator may be represented within the currently unmapped mutants identified by the 4D lineage screen, or of course could be factors involved the mechanism by which it is controlled.

Whatever this regulator is, it must intersect with the Wnt/β-catenin asymmetry pathway described in the introduction section of this thesis to bring about binary fate decisions. The phenotype of *lit-1* mutants demonstrates that Caap evidently normally has posterior fate which is transformed into Caaa (Kaletta et al., 1997). Furthermore, with varying strengths of disruption to the pathway, Cap can adopt Caa and Cpp adopt Cpa fates (Kaletta et al., 1997; Nair et al., 2013). Thus, Caap is the product of particular combinations of anterior and posterior identities within the context of its C lineage history. Both of these are required for neurogenesis in the C lineage. In the work described in this thesis I chose to focus on that lineage context, attempting to find the upstream regulators of *hlh-14* and the mechanism by which they segregated or activated, rather than to focus on the consequences of the disruption of Wnt/β-catenin.

In addition to a potential role in the control of *hlh-14* expression it would be interesting to investigate the role of the pathway downstream because this could in fact be under the control of HLH-14 at the Caapa/Caapp division to generate asymmetry. Caap divides to produce an anterior daughter in which *hlh-14* is detected and which divides to generate DVC and a cell death.

Expression is not detected in the posterior daughter, Caap, but is in its anterior daughter PVR, and not the sister hyp7 cell. Although this lack of expression could be attributed to transcriptional and GFP maturation dynamics as discussed above, it could also be revealing of true expression. The Wnt/β-catenin asymmetry pathway could for example only allow *hlh-14* expression in Caappa (PVR), which allows the otherwise underlying hypodermal fate program to be expressed in Caappp. Such a role for transcription factors in a neuronal lineage would not be unprecedented. Whilst not required for the initial expression, expression of the proneural gene *lin-32* is restricted to anterior branches by low nuclear POP-1 in the RnA ray neuron lineage (Miller and Portman, 2011). Furthermore, the asymmetry of POP-1 in the V5 lineage is downstream of the transcription factor ZTF-6 which leads to the loss of the postdeirid neurons PDE and PVD (Doitsidou et al., 2018).

It would therefore be informative to assess *pop-1* expression in Caapa and Caapp in *hlh-14* mutants to see whether, owing to the symmetry in the division in mutants, levels are equal in mutants.

6.7. Functional Consequences of an Enlarged DVC

An obvious question arises from the finding that unequal cleavage is not used to segregate fate in the C lineage; why control cell size in this manner during embryogenesis?

Cell size has often been thought to be linked to the cell cycle with larger cells exiting the cell cycle earlier and dividing. In multi-cellular organisms the relationship between cell volume and cell cycle duration is established to be a power-law relationship in both *Xenopus* (Wang et al., 2000) and *C. elegans* (Arata et al., 2015) and follows the logic that larger cells have shorter cell cycles. However, in *Xenopus* this size-dependent mechanism is only active after mid-blastula transition, with unequal cleavages occurring synchronously regardless of cell size until the 12th cleavage (Wang et al., 2000), demonstrating that this relationship is not absolute. Furthermore, in *C. elegans* embryos *par-4* mutants display synchronous AB and P1 division despite unequal size (Watts et al., 2000).

The cell cycle duration results described in this thesis demonstrated that the asynchrony in cell-cycle duration between the smaller DVC neuroblast Caapa, and larger Caapp cannot be solely control by size. As stated above, the volume of a *pig-1* mutant Caapa is about thrice that of a *wild*

type yet a third of these cells still divide with the *wild type* timing. Nor can division timing be attributed to fate in the lineage, which is frequently linked to cell size and cell cycle duration, as Caapa is a hypoblast in *hlh-14* mutants and a neuroblast in *pig-1* mutants. Indeed systems-level analysis of division times in *C. elegans* reveals that there is often asynchrony between cells of equivalent fates due to the requirement for differential migration and cellular integration (Ho et al., 2015). This suggests that although coordinated, fate and cell cycle duration are not always mechanistically linked. It therefore seems unlikely that unequal cleavage in the C lineage is solely controlled for the purpose of division timing.

Given that *C. elegans* has an invariant cell lineage and a fixed number of cells the only method of body size control after all terminal divisions have occurred is through cell growth. Therefore, a key question is that following the misregulation of the terminal embryonic size of Caapaa, is the increased size of DVC retained after embryogenesis? The growth rate of *C. elegans* is linear within each larval stage with this rate increasing with body size to yield and exponential rate overall (Knight et al., 2002). The study of growth however has mainly focused on body size and those studies that have focused on cells have only measured hypodermal, intestinal and pharyngeal cells, for example (Dineen and Gaudet, 2014; Nagamatsu and Ohshima, 2004; Watanabe et al., 2005; Watanabe et al., 2007). It is therefore unclear whether neuron cell bodies also grow during this time. However, although not measured as part of this study anecdotal observation suggests that the DVC cell body is indeed larger in *pig-1* larvae and adults than in *wild types.*

If this increased size carries over into adulthood as is anecdotally observed, the question of whether this has any functional consequences for the DVC neuron is an important one. The functional relevance of cell size to different cell types is not entirely clear (Ginzberg et al., 2015). However, what is known is that transcriptional rates increase with cell size to compensate for size heterogeneity in a diverse range of organisms such as mammals and plants (Ietswaart et al., 2017; Padovan-Merhar et al., 2015) and that organelle sizes are scalable with cell size (Reber and Goehring, 2015). In contrast to this isometric scaling, metabolic fitness scales allometrically with cell size, decreasing over a certain size. This establishes an optimal cell size for peak metabolic function (Miettinen and Björklund, 2016). It is therefore possible that an increased volume for the DVC cell body could enlarge it beyond its optimal functional size, although this would require explicit testing of mitochondrial function.

Given the recent confirmation that DVC is required for backward locomotion (Ao et al., 2019), this aspect of DVC function is more readily testable and could be undertaken in *pig-1* mutants. Of course, given the fact that *pig-1* mutants also affect a wide array of other neurons means that it would be preferable to assess such functional consequences in adults in which one precisely affected only DVC. As mentioned in a previous section, targeted photo-inactivation or degradation of components of cell division machinery, such as *nmy-2* or *lin-5*, during embryogenesis and subsequent recovery of the animal to adulthood would be a better experiment to address this.

6.8. The Use of GFP-based Reporter Genes and Alternative Techniques

During the work presented in this thesis the assessment of fate in both mutant and *wild type* embryos was undertaken mainly with the use of GFP reporter strains, with reference to reporters using other fluorescent proteins.

Having originally been identified in the sea jelly *Aequorea victoria* (Morise et al., 1974; Shimomura et al., 1962), reporters using the protein and its derivatives are used range of organisms since pioneering work in the worm and allow spatial and temporal readouts of gene expression (Chalfie et al., 1994). However, an obvious caveat in the use GFP reporters comes from the maturation time of the fluorescent protein in question. This introduces a delay between the onset of endogenous expression and visualisation of the protein. The known maturation time of the original *wild type* GFP at 37°C is relativity slow at around two hours (Heim et al., 1995), whilst more recently engineered fluorescent proteins derived from it have greatly increased maturation efficiency and are tuned to a variety of wavelengths (Balleza et al., 2018; Iizuka et al., 2011). A number of the early modifications to GFP for use in transgenes, such as the S65T and S65C mutations improve the maturation time to closer to 30 minutes and improve fluorescence intensity sixfold respectively (Balleza et al., 2018; Heim et al., 1995; Iizuka et al., 2011). As an example, the S65C variant of GFP is employed in the *gmIs20* transgene in this study to assess the expression of *hlh-14* (Frank et al., 2003).

Discussed in previous sections of this discussion, the potential for this discrepancy is most obviously highlighted in this study by the fact that there is a distinct difference in timing between the first detachable *hlh-14::gfp* expression, in the DVC neuroblast, and the obvious requirement for HLH-14 in the mother cell. This finding coupled with the known caveat of reporter gene delay

necessitates a method to more rapidly visualise expression. Such would not only serve the purpose of elucidating the discrepancy between *hlh-14* mutant phenotypes and reporter expression patterns, but would also confirm whether the burst of *hlh-14::gfp* expression seen in some *let-19* mutants is due to initiation of expression in a greater proportion of embryos than seen.

As a translational fusion, the *gmIs20* transgene used in this study can be used to assess both the expression of the gene and any subsequent segregation of the protein. Even with a single copy array the increase in protein size with the addition of GFP has the potential to affect the mobility, localisation and action of the protein. Thus, this must be born in mind in the assessment of these aspects of reporter expression. However, given that that *gmIs20* transgene can rescue the lethality seen in the *hlh-14(gm34)* mutant (Frank et al., 2003), as least in this case the protein appears to be functional. An obvious caveat with the use of this translational reporter therefore concerns regulatory relationships, particularly those of autoregulatory loops the GFP fusion protein may be involved in. In the case of autoregulation, a GFP fusion could have the potential to sustain its own expression once initiated. This would be of concern in a situation in which the endogenous protein would not normally sustain itself, such as in a mutant. This appears not to be the case for this project however, given that the expression of the *gmIs20* transgene was not sustained in mutants that have an initial burst of expression, namely those of *let-19(t3200).* Similar to the second case outlined for translational reporters, one does not always know if a transgene necessarily contains the complete promoter and necessary regulatory elements to drive all expression. Indeed, as mentioned elsewhere in this thesis the *gmIs20* transgene suffers from this, lacking expression in PVR that is otherwise seen in a full length fosmid (Frank et al., 2003; Poole et al., 2011).

Construction of fluorescent reporters using a faster maturing protein than those used in this study is an obvious option to overcome these issues (Balleza et al., 2018; Iizuka et al., 2011). This would allow assessment of expression as already described in this thesis. On the other hand, clear alternatives to the use of GFP reporters with greater temporal resolution include techniques used to visualise the production of nascent mRNA transcripts. A well-known example of such a technique is single molecule fluorescent in situ hybridisation (smFISH) (Femino et al., 1998). As the name suggests the methods makes use of fluorescent probes to identify individual mRNA transcripts in fixed tissue. The most common protocols are derived from methods employing multiple oligonucleotides of 20-50 bases each, labelled with 1-5 fluorophores (Femino et al., 1998;

Raj et al., 2008), the multiple binding of labelled probes creating visible spots corresponding to individual transcripts. Designing and constructing fluorescent probes for each target transcript of interest can incur great cost and so more recent innovations have included use of secondary fluorescent probes which target a common sequence on an unlabelled probe which itself targets the transcript of interest. This then allows for multiplexing and the assessment of multiple transcripts simultaneously (Chen et al., 2015; Tsanov et al., 2016). An obvious advantage to the method, and in particular these recent advances, is that it allows for not only a qualitative signal of transcription but also for a quantitative assessment of transcript numbers (Chen et al., 2015; Mueller et al., 2013; Tsanov et al., 2016), which is enhanced further with the use of automation and super-resolution microscopy (Titlow et al., 2018; Trcek et al., 2017). For the questions that need to be addressed following introduction this thesis however, super-resolution microscopy would not be a requirement. The use of secondary probes would however be preferable given their greater longer-term utility.

Despite its advantages, a weakness of the technique is its need for fixed samples. This introduces its own challenges in both the precise staging of fixed material but also that it only provides a snapshot of transcription at a single timepoint. As a strength of work in this thesis is the simultaneous assessment of multiple phenotypes in the same live embryo, such approaches would lose this advantage. A further disadvantage is that in situ hybridisation in worm embryos requires freeze-cracking the embryos to permeablise the cuticle and allow fixation, which can introduce structural deformation.

A second alternative approach that would allow greater spatiotemporal resolution without the drawback of requiring fixed tissue is the bacteriophage-derived MCP-MS2 system. This relies on a bacteriophage coat protein, the MS2 coat protein (MCP), and its binding to particular RNA stem-loops called MS2 loops (Bernardi and Spahr, 1972). By creating fusion proteins of MCP with a fluorescent protein and introducing MS2 loops to transcripts of interest, transcription can be visualised as dots in live tissues (Bertrand et al., 1998), with 24 MS2 stem-loops found to be the most efficient for visualisation (Fusco et al., 2003). Fluorescent dots are formed when the multivalent binding of MCP to the MS2 stem-loops brings the fluorophore to the mRNA and are representative of transcription as their intensity will be well above background signal. Depending on the model system the introduction of the required constructs can be achieved via homologous recombination mediated knock-in, retroviral transfection or CRISPR editing, as such the system

has been successfully implemented in a range of model organisms (Bertrand et al., 1998; Pichon et al., 2018; Tutucci et al., 2018; Vera et al., 2019). Using confocal microscopy, the system has recently been used to monitor Notch signalling and transcriptional bursting in *C. elegans* germline stem cells (Lee et al., 2019b). Here the method employed two integrated transgenes; one for MCP::fluorophore driven by a strong promoter in the tissue or lineage in question (here the germline) and another for the target gene under its own promoter, with 24 MS2 loops introduced into 5' UTR (Lee et al., 2019b). An important consideration for this method is therefore the use of the strong tissue or lineage specific promotor. An obvious candidate for use in the C lineage to assess *hlh-14* expression would be *pal-1*, given its zygotic expression in the C descendants (Hunter and Kenyon, 1996; Packer et al., 2019). This expression begins around the 2-4 C cell stage and so should be sufficiently active at the 8-16 C cell stages where *hlh-14* would be assessed in Caap and Caapa (Edgar et al., 2001; Hunter and Kenyon, 1996; Packer et al., 2019). Another potential candidate would be *elt-1*, an epidermal marker expressed in the C lineage from the 2 C cell stage and present in the C lineage hypodermal precursors including the DVC grandmother Caap (Page et al., 1997). However, as it is not clear whether it is still expressed at the Caapa stage it may not be an ideal candidate (Packer et al., 2019).

As previously stated the above two techniques are of particular interest for the work in this study for looking at *hlh-14* expression in a *wild type* animal to reconcile the GFP transgene pattern and *hlh-14(tm295)* mutant cleavage phenotype. Secondly, they would allow the assessment of *hlh-14* expression in *let-19* mutants, to ascertain whether the burst of expression as indicated by GFP reporters is more widespread of a phenotype than would be suggested by the transgene expression.

6.9. Single Cell RNA Sequencing Data in Relation to the C Lineage Phenotypes

Advances in, and increased application of, single cell RNA sequencing (RNA-seq) techniques also allow another angle from which to view gene expression in relation to reporter gene expression. Given the varied design of such studies and their available datasets it is interesting to note that informative transcripts used to differentiate between lineages and blastomeres are often also varied (Cao et al., 2017; Hashimshony et al., 2015; Lorenzo et al., 2020; Packer et al., 2019). For the C lineage in particular this often results in an inability to resolve differences

between the Ca and Cp blastomeres (and if sampled, their descendants) either molecularly or physically through blastomere isolations (Hashimshony et al., 2012; Hashimshony et al., 2015; Tintori et al., 2016). Furthermore, most RNA-seq datasets are concerned with narrow developmental stages. For example, whilst informative of the early embryo, studies such as Tintori et al., 2016 only sampled up to the 16-cell stage, and Lorenzo et al., 2020, was concerned with the neuronal transcriptome of the L2 larval stage. As such they do not focus on the stages of the C lineage of most concern in this thesis.

Despite this variation however, and even without precise identification of cells, studies do identify common informative transcripts for the identification of the C lineage. In studies in which founder blastomeres were isolated and sampling undertaken on their pooled descendants, *hlh-14* is identified as an informative C lineage transcript, being newly expressed in either C itself (Hashimshony et al., 2012) or at the 2C stage, increasing at the 4-8C stages (Hashimshony et al., 2015). This increase corresponds to the same timepoint at which expression is detected in Caapa using the *gmIs20* transgene and to the Caap stage at which *hlh-14(tm295)* mutants display unequal cleavage defects. Contrastingly, this low level expression early in the lineage (in C, Ca or Cp) is not identified with either *gmIs20* used in this study, or when using the full length expression fosmid (Poole et al., 2011).

A recent study has provided the most comprehensive and lineage resolved single cell RNA-seq dataset of the developing *C. elegans* embryo to date (Packer et al., 2019). In contrast to the other studies mentioned above, expression of *hlh-14* was not detected early in the C lineage, with significant expression in the neuronal branch beginning only in the DVC neuroblast and its sister, the mother of PVR and a hyp7 cell (Packer et al., 2019). An important consideration here is the fact that the published expression pattern of *hlh-14* in the C lineage (Poole et al., 2011) was used in the clustering algorithm for this study (Packer et al., 2019). As such it is possible that the lack of reported transcription in the DVC grandmother (Caap) at least partially reflective of this. This is especially true when viewed in conjunction with the mutant phenotype described for Caap in this thesis and previous RNA sequencing datasets indicating heightened expression at the 4-8C stages (that of Caap) (Hashimshony et al., 2015). Similarly, the aforementioned recent transcriptome study of neurons at the L2 stage used *hlh-14* to cluster DVC and PVR (Lorenzo et al., 2020) despite the fact that its expression in these cells is known to end in the embryo. Furthermore, *ceh-63* was not amongst the most enriched DVC transcripts (Lorenzo et al., 2020)

despite continued expression in the neuron reported by the transcriptional reporter used in the work described in this thesis, supported by its unique expression detected in DVC in Packer et al., 2019.

Expression of *hlh-2*, *pig-1*, and *let-19* was found to be high in C lineage cells for all sampled timepoints in Hashimshony et al., 2015 and *let-19* transcripts have specifically been reported as highest in the C lineage in Caa and Caap (Packer et al., 2019). This agrees with the timing of action identified through temperature shift experiments for *let-19(t3200)* in terms of its neurogenesis phenotypes (Yeung, 2016) and with the fact that the unequal cleavages of these cells are those affected by *let-19(t3200)* and *let-19(t3273)*. This would support the conclusion that LET-19 must act specifically within these cells in the C lineage to regulate both phenotypes.

Interestingly, *pig-1* transcripts are either detected at a very low level or not at all in Caa and Caap, the cells for which *pig-1(gm344)* displays cleavage phenotypes. Transcripts are however detected in the anterior daughters of each of these cells and could therefore be suggestive of expression starting in their mother cells and is reminiscent of *pig-1* dynamics recently proposed in the NSM neuroblast lineage (Wei et al., 2020). This would agree with the expression pattern as indicated by the transgene used in this thesis, finding expression in Caa and Caap. An alternative interpretation of expression in Caapa is that is it indicative of its role in the terminal division of this neuroblast as newly described in this thesis.

Interpreting single cell RNA-seq datasets to gain insight into mutant phenotypes especially if assigning higher value to those of greater spatiotemporal resolution such as Packer et al., 2019, can both confirm suspicions regarding expression patterns and raise many questions. Disagreement between transcriptome data, transgene expression patterns and cells affected in mutants highlights this fact. Whilst such data can often reveal expression missed with transgenes using incomplete regulatory sequences, it may likewise report no transcription in cells known to express the gene of interest. An obvious caveat with single cell lineage resolved RNA-seq datasets is that a threshold must be set for transcripts to be informative of a particular cell and as such important transcripts could be underreported. Therefore, such datasets should primarily be used as guides for further investigation. Indeed, many of the specific questions and incongruences highlighted by assessment of transcriptome data in the C lineage prompt investigation. This would be undertaken using alternative techniques such as those described above in the discussion surrounding GFP reporter transgenes.

6.10. A General Working Model

The results described in this thesis therefore lead to the construction of the following working model which summarises the discussion of those results in the previous sections. The model draws on the crucial conclusion of this thesis, that the same factors play spatiotemporally distinct roles to coordinate acquisition of neuronal fate and terminal embryonic cell size in parallel (Figure 6.1). The relationships between the factors implicated in this model that will require future testing have been discussed in the previous sections of this discussion.

1. In Caa LET-19, most likely acting in its role as a member of the Mediator complex, is required for the control of a transcriptional event leading to unequal cleavage of Caa generating a larger anterior daughter Caaa, and a smaller posterior daughter, Caap. This is potentially through the transcriptional regulation of *pig-1*, mutants of which equalise the division.

2. Downstream of this unequal cleavage, in the smaller posterior daughter Caap, LET-19 mediates expression of the bHLH transcription factor HLH-2, the role of which in Caap is unclear. Controlled by an as yet unidentified factor, a separate independent transcriptional event initiates expression of the proneural transcription factor HLH-14. The role of HLH-14 in Caap appears to be two-fold; to establish the neuronal lineage identity, and to control unequal cleavage. The control of unequal cleavage is as an upstream and potentially direct transcriptional regulator of *pig-1* and/or *ham-1,* which are required for unequal cleavage.

3. In the DVC neuroblast, Caapa, continued expression of *hlh-14* requires regulation by HLH-2 and/or autoregulation through heterodimerisation of HLH-14 and HLH-2. Continued expression of HLH-14 allows it to be able to perform its proneural role in the lineage and the differentiation of the DVC neuron. Additionally,, HLH-2 may have very weak proneural activity in Caapa in the absence of HLH-14.

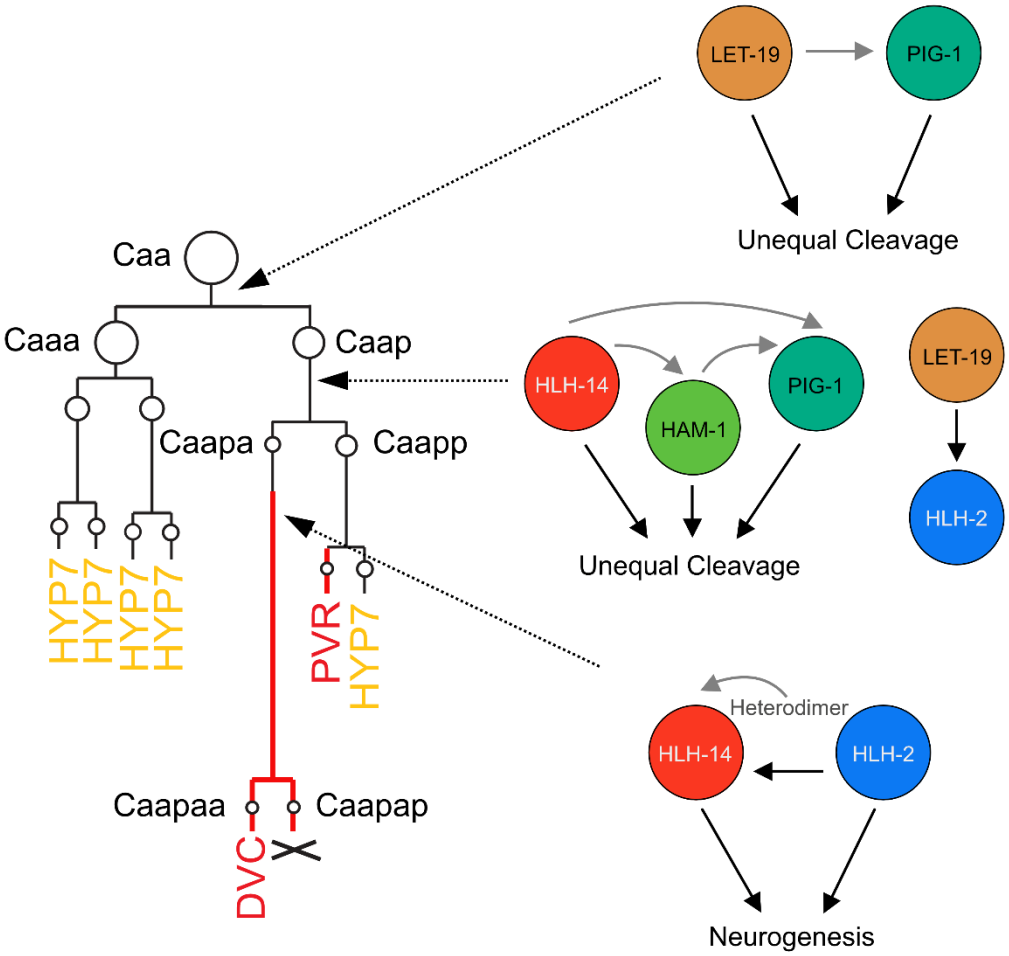

Figure 6.1. General working model for the control of unequal and neurogenesis in the C lineage. *Lineage diagram of the C lineage and potential roles for factors discussed in this work. White circles on the lineage diagram are indicative of relative cell sizes. hlh-14 expression is indicated in red. For each cleavage/cell the factors and their roles are illustrated, with the stage at which they act indicated with a dotted arrow. Black arrows indicate confirmed genetic interactions and phenotypic consequences. Grey arrows illustrate inferred interactions to be tested in future. Arrows do not assume the nature of the interaction, i.e. transcriptional.*

6.11. Conclusions

The aims of this thesis were to investigate the regulation of proneural gene expression in the C lineage with a focus on interrogating the role of unequal cleavages and resultant daughter cell size asymmetry in the initial acquisition of neuronal fate. Although the main conclusion is that unequal cleavage does not play a role and that the upstream regulators of *hlh-14* in the lineage remain elusive, a number of key findings are apparent regarding their coordination.

In summary, in addition to allowing the construction of a model the results presented here allow for the drawing of a number of separate conclusions, which are as follows:

1. Neurogenesis in the C lineage is controlled by lineage-intrinsic mechanisms.
2. Unequal cleavages in the neuronal branches of the C lineage are not required for neuronal fate acquisition or the correct segregation of an upstream regulator of *hlh-14* expression.
3. Unequal cleavages in the C lineage require the MELK kinase *pig-1*, not previously implicated in the lineage.
4. *pig-1* is required to control multiple successively unequal cleavages in the same lineage, both of which produce daughter that both survive; this is a novel finding.
5. Regulators of neurogenesis in the C lineage also regulate unequal cleavage.
6. Regulation of *pig-1* in the C lineage is possibly under transcriptional control.
7. *pig-1* and *ham-1* are required for segregation of apoptotic fate in the DVC neuroblast division; both are novel findings.
8. Cell size, fate and division timing can be genetically uncoupled in the C lineage.
9. The regulation of unequal cleavage is sequentially regulated by the same regulators of neuronal fate acquisition to coordinate terminal embryonic cell size with terminal identity. This is likely required for tissue integrity and cellular function.

Bibliography

Bibliography

Afgan, E., Baker, D., Batut, B., Van Den Beek, M., Bouvier, D., Ech, M., Chilton, J., Clements, D., Coraor, N., Grüning, B. A., et al. (2018). The Galaxy platform for accessible, reproducible and collaborative biomedical analyses: 2018 update. *Nucleic Acids Res.* **46**, W537–W544.

Ahringer, J. (1996). Posterior patterning by the Caenorhabditis elegans even-skipped homolog vab-7. *Genes Dev.* **10**, 1120–1130.

Albano, C. R., Randers-Eichhon, L., Chang, Q., Bentley, W. E. and Rao, G. (1996). Quantitative measurement of green fluorescent protein expression. *Biotechnol. Tech.* **10**, 953–958.

Albertson, D. G. and Thomson, J. N. (1976). The pharynx of Caenorhabditis elegans. *Philos. Trans. R. Soc. Lond. B. Biol. Sci.* **275**, 299–325.

Alicea, B. (2018). The emergent connectome in Caenorhabditis elegans embryogenesis. *BioSystems* **173**, 247–255.

Alper, S. and Kenyon, C. (2001). Ref-1, a protein with two bHLH domains, alters the pattern of cell fusion in C. Elegans by regulating Hox protein activity. *Development* **128**, 1793–1804.

Altun, Z. F., Chen, B., Wang, Z. W. and Hall, D. H. (2009). High resolution map of Caenorhabditis elegans gap junction proteins. *Dev. Dyn.* **238**, 1936–1950.

Amador-Arjona, A., Cimadamore, F., Huang, C. T., Wright, R., Lewis, S., Gage, F. H. and Terskikh, A. V. (2015). SOX2 primes the epigenetic landscape in neural precursors enabling proper gene activation during hippocampal neurogenesis. *Proc. Natl. Acad. Sci. U. S. A.* **112**, E1936–E1945.

Andachi, Y. (2004). Caenorhabditis elegans T-box genes tbx-9 and tbx-8 are required for formation of hypodermis and body-wall muscle in embryogenesis. *Genes to Cells* **9**, 331–344.

Ao, Y., Zeng, K., Yu, B., Miao, Y., Hung, W., Yu, Z., Xue, Y., Tan, T. T. Y., Xu, T., Zhen, M., et al. (2019). An Upconversion Nanoparticle Enables Near Infrared-Optogenetic Manipulation of the Caenorhabditis elegans Motor Circuit. *ACS Nano* **13**, 3373–3386.

Arata, Y., Takagi, H., Sako, Y. and Sawa, H. (2015). Power law relationship between cell cycle duration and cell volume in the early embryonic development of Caenorhabditis elegans. *Front. Physiol.* **5**, 529.

Ardiel, E. L. and Rankin, C. H. (2015). Current Biology Cross-referencing online activity with the connectome to identify a neglected but well-connected neuron. *Curr. Biol.* **25**, 391–408.

Asahina, M., Ishihara, T., Jindra, M., Kohara, Y., Katsura, I. and Hirose, S. (2000). The conserved nuclear receptor Ftz-F1 is required for embryogenesis, moulting and reproduction in Caenorhabditis elegans. *Genes Cells* **5**, 711–23.

Atwood, S. X. and Prehoda, K. E. (2010). Phosphorylation-mediated cortical displacement of fate determinants by aPKC during neuroblast asymmetric cell division. *Mol. Biol.* **19**, 723–729.

Aydin, B., Kakumanu, A., Rossillo, M., Moreno-Estellés, M., Garipler, G., Ringstad, N., Flames, N., Mahony, S. and Mazzoni, E. O. (2019). Proneural factors Ascl1 and Neurog2 contribute to neuronal subtype identities by establishing distinct chromatin landscapes. *Nat. Neurosci.* **22**, 897–908.

Bacik, K. A., Schaub, M. T., Beguerisse-Díaz, M., Billeh, Y. N. and Barahona, M. (2016). Flow-Based Network Analysis of the Caenorhabditis elegans Connectome. *PLoS Comput. Biol.* **12**, e1005055.

Bailey, M. J. and Prehoda, K. E. (2015). Establishment of Par-Polarized Cortical Domains via Phosphoregulated Membrane Motifs. *Dev. Cell* **35**, 199–210.

Baldwin, A. T. and Phillips, B. T. (2014). The tumor suppressor APC differentially regulates multiple β-catenins through the function of axin and CKIα during C. elegans asymmetric stem cell divisions. *J. Cell Sci.* **127**, 2771–81.

Balleza, E., Kim, J. M. and Cluzel, P. (2018). Systematic characterization of maturation time of fluorescent proteins in living cells. *Nat. Methods* **15**, 47–51.

Bao, M., Xie, J., Piruska, A. and Huck, W. T. S. (2017). 3D microniches reveal the importance of cell size and shape. *Nat. Commun.* **8**, 1962.

Bargmann, C. I. and Avery, L. (1995). Laser killing of cells in Caenorhabditis elegans. *Methods Cell Biol.* **48**, 225–50.

Barrandon, Y. and Green, H. (1985). Cell size as a determinant of the clone-forming ability of human keratinocytes. *Proc. Natl. Acad. Sci. U. S. A.* **82**, 5390–4.

Barros, C. S., Phelps, C. B. and Brand, A. H. (2003). Drosophila nonmuscle myosin II promotes the asymmetric segregation of cell fate determinants by cortical exclusion rather than active transport. *Dev. Cell* **5**, 829–840.

Baugh, L. R., Hill, A. a, Claggett, J. M., Hill-Harfe, K., Wen, J. C., Slonim, D. K., Brown, E. L. and Hunter, C. P. (2005a). The homeodomain protein PAL-1 specifies a lineage-specific regulatory network in the C. elegans embryo. *Development* **132**, 1843–1854.

Baugh, L. R., Wen, J. C., Hill, A. A., Slonim, D. K., Brown, E. L. and Hunter, C. P. (2005b). Synthetic lethal analysis of Caenorhabditis elegans posterior embryonic patterning genes identifies conserved genetic interactions. *Genome Biol.* **6**, R45.

Beatty, A., Morton, D. and Kemphues, K. (2010). The C. elegans homolog of Drosophila Lethal giant larvae functions redundantly with PAR-2 to maintain polarity in the early embryo. *Development* **137**, 3995–4004.

Beer, K. B., Fazeli, G., Judasova, K., Irmisch, L., Causemann, J., Mansfeld, J. and Wehman, A. M. (2019). Degron-tagged reporters probe membrane topology and enable the specific labelling of membrane-wrapped structures. *Nat. Commun.* **10**, 3490.

Bernardi, A. and Spahr, P. F. (1972). Nucleotide sequence at the binding site for coat protein on RNA of bacteriophage R17. *Proc. Natl. Acad. Sci. U. S. A.* **69**, 3033–3037.

Bertrand, V. (2016). β-catenin-driven binary cell fate decisions in animal development. *Wiley Interdiscip. Rev. Dev. Biol.* **5**, 377–388.

Bertrand, V. and Hobert, O. (2009). Linking Asymmetric Cell Division to the Terminal Differentiation Program of Postmitotic Neurons in C. elegans. *Dev. Cell* **16**, 563–575.

Bertrand, V. and Hobert, O. (2010). Lineage programming: navigating through transient regulatory states via binary decisions. *Curr. Opin. Genet. Dev.* **20**, 362–8.

Bertrand, E., Chartrand, P., Schaefer, M., Shenoy, S. M., Singer, R. H. and Long, R. M. (1998). Localization of ASH1 mRNA particles in living yeast. *Mol. Cell* **2**, 437–445.

Bertrand, N., Castro, D. S. and Guillemot, F. (2002). Proneural genes and the specification of neural cell types. *Nat. Rev. Neurosci.* **3**, 517–530.

Bertrand, V., Bisso, P., Poole, R. J. and Hobert, O. (2011). Notch-dependent induction of left/right asymmetry in C. elegans interneurons and motoneurons. *Curr. Biol.* **21**, 1225–1231.

Betschinger, J., Mechtler, K. and Knoblich, J. A. (2006). Asymmetric segregation of the tumor suppressor brat regulates self-renewal in Drosophila neural stem cells. *Cell* **124**, 1241–53.

Beullens, M., Vancauwenbergh, S., Morrice, N., Derua, R., Ceulemans, H., Waelkens, E. and Bollen, M. (2005). Substrate specificity and activity regulation of protein kinase MELK. *J. Biol. Chem.* **280**, 40003–11.

Björklund, M. (2019). Cell size homeostasis: Metabolic control of growth and cell division. *Biochim. Biophys. Acta - Mol. Cell Res.* **1866**, 409–417.

Bourbon, H. M. (2008). Comparative genomics supports a deep evolutionary origin for the large, four-module transcriptional mediator complex. *Nucleic Acids Res.* **36**, 3993–4008.

Boveri, T. (1899). Die Entwickelung von Ascaris megalocephala mit besonderer Rücksicht auf die KernverhältnisseNo Title. *G. Fischer, Jena. Festschrift zum Sieben. Geburtstag von Carl von Kupffer* 383–430.

Boveri, T. (1910). Die Potenzen der Ascaris-Blastomeren bei abgeänderter Furchung: zugleich ein Beitrag zur Frage qualitativ-ungleicher Chromosomen-Teilung. *G. Fischer, Jena. Festschrift zum sechzigsten Geburtstag Richard Hertwigs* **3**, 133–214.

Bowerman, B., Eaton, B. A. and Priess, J. R. (1992). skn-1, a maternally expressed gene required to specify the fate of ventral blastomeres in the early C. elegans embryo. *Cell* **68**, 1061–1075.

Bowerman, B., Draper, B. W., Mello, C. C. and Priess, J. R. (1993). The maternal gene skn-1 encodes a protein that is distributed unequally in early C. elegans embryos. *Cell* **74**, 443–452.

Bowman, S. K., Neumüller, R. A., Novatchkova, M., Du, Q. and Knoblich, J. A. (2006). The Drosophila NuMA Homolog Mud Regulates Spindle Orientation in Asymmetric Cell Division. *Dev. Cell* **10**, 731–742.

Brenner, S. (1974). The genetics of Caenorhabditis elegans. *Genetics* **77**, 71–94.

Briscoe, J. and Novitch, B. G. (2008). Regulatory pathways linking progenitor patterning, cell fates and neurogenesis in the ventral neural tube. *Philos. Trans. R. Soc. B Biol. Sci.* **363**, 57–70.

Briscoe, J., Pierani, A., Jessell, T. M. and Ericson, J. (2000). A homeodomain protein code specifies progenitor cell identity and neuronal fate in the ventral neural tube. *Cell* **101**, 435–445.

Burroughs, A. M., Iyer, L. M. and Aravind, L. (2013). Two novel PIWI families: Roles in inter-genomic conflicts in bacteria and Mediator-dependent modulation of transcription in eukaryotes. *Biol. Direct* **8**, 13.

Cabernard, C., Prehoda, K. E. and Doe, C. Q. (2010). A spindle-independent cleavage furrow positioning pathway. *Nature* **467**, 91–4.

Cabrera, C. V, Martinez-Arias, A. and Bate, M. (1987). The expression of three members of the achaete-scute gene complex correlates with neuroblast segregation in Drosophila. *Cell* **50**, 425–33.

Cai, Y., Yu, F., Lin, S., Chia, W. and Yang, X. (2003). Apical complex genes control mitotic spindle geometry and relative size of daughter cells in Drosophila neuroblast and pI asymmetric divisions. *Cell* **112**, 51–62.

Calvo, D., Victor, M., Gay, F., Sui, G., Po-Shan Luke, M., Dufourcq, P., Wen, G., Maduro, M., Rothman, J. and Shi, Y. (2001). A POP-1 repressor complex restricts inappropriate cell type-specific gene transcription during Caenorhabditis elegans embryogenesis. *EMBO J.* **20**, 7197–7208.

Cao, J., Packer, J. S., Ramani, V., Cusanovich, D. A., Huynh, C., Daza, R., Qiu, X., Lee, C., Furlan, S. N., Steemers, F. J., et al. (2017). Comprehensive single-cell transcriptional profiling of a multicellular organism. *Science* **357**, 661–667.

Cassata, G., Kagoshima, H., Andachi, Y., Kohara, Y., Dürrenberger, M. B., Hall, D. H. and Bürglin, T. R. (2000). The LIM homeobox gene ceh-14 confers thermosensory function to the AFD neurons in Caenorhabditis elegans. *Neuron* **25**, 587–597.

Castro, D. S., Martynoga, B., Parras, C., Ramesh, V., Pacary, E., Johnston, C., Drechsel, D., Lebel-Potter, M., Garcia, L. G., Hunt, C., et al. (2011). A novel function of the proneural factor Ascl1 in progenitor proliferation identified by genome-wide characterization of its targets. *Genes Dev.* **25**, 930–945.

Caudy, M., Vässin, H., Brand, M., Tuma, R., Jah, L. Y. and Jan, Y. N. (1988). daughterless, a Drosophila gene essential for both neurogenesis and sex determination, has sequence similarities to myc and the achaete-scute complex. *Cell* **55**, 1061–1067.

Ceol, C. J. and Horvitz, H. R. (2004). A new class of C. elegans synMuv genes implicates a Tip60/NuA4-like HAT complex as a negative regulator of Ras signaling. *Dev. Cell* **6**, 563–576.

Chalfie, M. and Au, M. (1989). Genetic control of differentiation of the caenorhabditis elegans touch receptor neurons. *Science* **243**, 1027–1033.

Chalfie, M., Sulston, J. E., White, J. G., Southgate, E., Thomson, J. N. and Brenner, S. (1985). The neural circuit for touch sensitivity in Caenorhabditis elegans. *J. Neurosci.* **5**, 956–964.

Chalfie, M., Tu, Y., Euskirchen, G., Ward, W. W. and Prasher, D. C. (1994). Green fluorescent protein as a marker for gene expression. *Science* **263**, 802–5.

Chen, L., Krause, M., Sepanski, M. and Fire, A. (1994). The caenorhabditis elegans MYOD homologue HLH-1 is essential for proper muscle function and complete morphogenesis. *Development* **120**, 1631–1641.

Chen, K. H., Boettiger, A. N., Moffitt, J. R., Wang, S. and Zhuang, X. (2015). Spatially resolved, highly multiplexed RNA profiling in single cells. *Science (80-.).* **348**, aaa6090.

Chien, C. T., Hsiao, C. D., Jan, L. Y. and Jan, Y. N. (1996). Neuronal type information encoded in the basic-helix-loop-helix domain of proneural genes. *Proc. Natl. Acad. Sci. U. S. A.* **93**, 13239–13244.

Chien, S. C., Brinkmann, E. M., Teuliere, J. and Garriga, G. (2013). Caenorhabditis elegans PIG-1/MELK acts in a conserved PAR-4/LKB1 polarity pathway to promote asymmetric neuroblast divisions. *Genetics* **193**, 897–909.

Choksi, S. P., Southall, T. D., Bossing, T., Edoff, K., de Wit, E., Fischer, B. E., van Steensel, B., Micklem, G. and Brand, A. H. (2006). Prospero Acts as a Binary Switch between Self-Renewal and Differentiation in Drosophila Neural Stem Cells. *Dev. Cell* **11**, 775–789.

Cimadamore, F., Fishwick, K., Giusto, E., Gnedeva, K., Cattarossi, G., Miller, A., Pluchino, S., Brill, L. M., Bronner-Fraser, M. and Terskikh, A. V (2011). Human ESC-derived neural crest model reveals a key role for SOX2 in sensory neurogenesis. *Cell Stem Cell* **8**, 538–51.

Clark, S. G., Chisholm, A. D. and Horvitz, H. R. (1993). Control of cell fates in the central body region of C. elegans by the homeobox gene lin-39. *Cell* **74**, 43–55.

Clayton, J. E., van den Heuvel, S. J. L. and Saito, R. M. (2008). Transcriptional control of cell-cycle quiescence during C. elegans development. *Dev. Biol.* **313**, 603–613.

Cohen, M., Briscoe, J. and Blassberg, R. (2013). Morphogen Interpretation: The Transcriptional Logic Of Neural Tube Patterning. *Curr. Opin. Genet. Dev.* **23**, 423–428.

Conklin, E. G. (1905). The Organization and Cell-lineage of the Ascidian Egg. *J. Acad. Nat. Sci. Philadelphia* **13**.

Conlon, I. and Raff, M. (2003). Differences in the way a mammalian cell and yeast cells coordinate cell growth and cell-cycle progression. *J. Biol.* **2**, 7.

Connell, M., Cabernard, C., Ricketson, D., Doe, C. Q. and Prehoda, K. E. (2011). Asymmetric cortical extension shifts cleavage furrow position in Drosophila neuroblasts. *Mol. Biol. Cell* **22**, 4220–4226.

Consortium., C. elegans S. (1998). Genome sequence of the nematode C. elegans: A platform for investigating biology. *Science* **282**, 2012–2018.

Cook, S. J., Jarrell, T. A., Brittin, C. A., Wang, Y., Bloniarz, A. E., Yakovlev, M. A., Nguyen, K. C. Q., Tang, L. T. H., Bayer, E. A., Duerr, J. S., et al. (2019). Whole-animal connectomes of both Caenorhabditis elegans sexes. *Nature* **571**, 63–71.

Cordes, S., Frank, C. A. and Garriga, G. (2006). The C. elegans MELK ortholog PIG-1 regulates cell size asymmetry and daughter cell fate in asymmetric neuroblast divisions. *Development* **133**, 2747–56.

Cowing, D. and Kenyon, C. (1996). Correct Hox gene expression established independently of position in Caenorhabditis elegans. *Nature* **382**, 353–6.

Dejima, K., Kang, S., Mitani, S., Cosman, P. C., Chisholm, A. D., Ai, X., Do, A.-T., Lozynska, O., Kusche-Gullberg, M., Lindahl, U., et al. (2014). Syndecan defines precise spindle orientation by modulating Wnt signaling in C. elegans. *Development* **141**, 4354–65.

Denning, D. P., Hatch, V. and Robert Horvitz, H. (2012). Programmed elimination of cells by caspase-independent cell extrusion in C. elegans. *Nature* **488**, 226–230.

Deppe, U., Schierenberg, E., Cole, T., Krieg, C., Schmitt, D., Yoder, B. and von Ehrenstein, G. (1978). Cell lineages of the embryo of the nematode Caenorhabditis elegans. *Proc. Nat. Acad Sci USA* **75**, 376–380.

Desai, C., Garriga, G., McIntire, S. L. and Horvitz, H. R. (1988). A genetic pathway for the development of the Caenorhabditis elegans HSN motor neurons. *Nature* **336**, 638–646.

Dickinson, D. J., Pani, A. M., Heppert, J. K., Higgins, C. D. and Goldstein, B. (2015). Streamlined genome engineering with a self-excising drug selection cassette. *Genetics* **200**, 1035–1049.

Dineen, A. and Gaudet, J. (2014). TGF-β signaling can act from multiple tissues to regulate C. elegans body size. *BMC Dev. Biol.* **14**, 43.

Doe, C. Q. (2017). Temporal Patterning in the Drosophila CNS . *Annu. Rev. Cell Dev. Biol.* **33**, 219–240.

Doe, C. Q., Chu-LaGraff, Q., Wright, D. M. and Scott, M. P. (1991). The prospero gene specifies cell fates in the drosophila central nervous system. *Cell* **65**, 451–464.

Doitsidou, M., Flames, N., Lee, A. C., Boyanov, A. and Hobert, O. (2008). Automated screening for mutants affecting dopaminergic-neuron specification in C. elegans. *Nat. Methods* **5**, 869–872.

Doitsidou, M., Jarriault, S. and Poole, R. J. (2016). Next-Generation Sequencing-Based Approaches for Mutation Mapping and Identification in Caenorhabditis elegans. *Genetics* **204**, 451–474.

Doitsidou, M., Minevich, G., Kroll, J. R., Soete, G., Gowtham, S., Korswagen, H. C., van Zon, J. S. and Hobert, O. (2018). A Caenorhabditis elegans zinc finger transcription factor, ztf-6, required for the specification of a dopamine neuron-producing lineage. *G3 Genes, Genomes, Genet.* **8**, 17–26.

Doonan, R., Hatzold, J., Raut, S., Conradt, B. and Alfonso, A. (2008). HLH-3 is a C. elegans Achaete/Scute protein required for differentiation of the hermaphrodite-specific motor neurons. *Mech. Dev.* **125**, 883–893.

Draper, B. W., Mello, C. C., Bowerman, B., Hardin, J. and Priess, J. R. (1996). MEX-3 is a KH domain protein that regulates blastomere identity in early C-elegans embryos. *Cell* **87**, 205–216.

Edgar, R. S. and Lielausis, I. (1964). Temperature-Sensitive Mutants of Bacteriophage T4d: Their Isolation and Genetic Characterization. *Genetics* **49**, 649–662.

Edgar, L. G., Carr, S., Wang, H. and Wood, W. B. (2001). Zygotic expression of the caudal homolog pal-1 is required for posterior patterning in Caenorhabditis elegans embryogenesis. *Dev. Biol.* **229**, 71–88.

Evans, T. C., Crittenden, S. L., Kodoyianni, V. and Kimble, J. (1994). Translational control of maternal glp-1 mRNA establishes an asymmetry in the C. elegans embryo. *Cell* **77**, 183–194.

Evsen, L., Sugahara, S., Uchikawa, M., Kondoh, H. and Wu, D. K. (2013). Progression of neurogenesis in the inner ear requires inhibition of Sox2 transcription by neurogenin1 and neurod1. *J. Neurosci.* **33**, 3879–90.

Felton, T. (2019). PhD Thesis: “Cellular and molecular regulation of left-right asymmetric neurogenesis in the C. elegans C-lineage”, University College London.

Femino, A. M., Fay, F. S., Fogarty, K. and Singer, R. H. (1998). Visualization of single RNA transcripts in situ. *Science (80-.).* **280**, 585–590.

Feng, H., Reece-Hoyes, J. S., Walhout, A. J. M. and Hope, I. A. (2012). A regulatory cascade of three transcription factors in a single specific neuron, DVC, in Caenorhabditis elegans. *Gene* **494**, 73–84.

Feng, G., Yi, P., Yang, Y., Chai, Y., Tian, D., Zhu, Z., Liu, J., Zhou, F., Cheng, Z., Wang, X., et al. (2013). Developmental stage-dependent transcriptional regulatory pathways control neuroblast lineage progression. *Development* **140**, 3838–47.

Fickentscher, R. and Weiss, M. (2017). Physical determinants of asymmetric cell divisions in the early development of Caenorhabditis elegans. *Sci. Rep.* **7**, 9369.

Fielmich, L.-E., Schmidt, R., Dickinson, D. J., Goldstein, B., Akhmanova, A. and van den Heuvel, S. (2018). Optogenetic dissection of mitotic spindle positioning in vivo. *Elife* **7**, e38198.

Finney, M. and Ruvkun, G. (1990). The unc-86 gene product couples cell lineage and cell identity in C. elegans. *Cell* **63**, 895–905.

Fire, A., Xu, S., Montgomery, M. K., Kostas, S. A., Driver, S. E. and Mello, C. C. (1998). Potent and specific genetic interference by double-stranded RNA in caenorhabditis elegans. *Nature* **391**, 806–811.

Fode, C., Ma, Q., Casarosa, S., Ang, S.-L., Anderson, D. J. and Guillemot, F. (2000). A role for neural determination genes in specifying the dorsoventral identity of telencephalic neurons. *Genes Dev.* **14**, 67–80.

Frank, C. A., Baum, P. D. and Garriga, G. (2003). HLH-14 is a C. elegans achaete-scute protein that promotes neurogenesis through asymmetric cell division. *Development* **130**, 6507–6518.

Frank, C. A., Hawkins, N. C., Guenther, C., Horvitz, H. R. and Garriga, G. (2005). C. elegans HAM-1 positions the cleavage plane and regulates apoptosis in asymmetric neuroblast divisions. *Dev. Biol.* **284**, 301–310.

Friedland, A. E., Tzur, Y. B., Esvelt, K. M., Colaiácovo, M. P., Church, G. M. and Calarco, J. A. (2013). Heritable genome editing in C. elegans via a CRISPR-Cas9 system. *Nat. Methods* **10**, 741–3.

Frise, E., Knoblich, J. A., Younger-Shepherd, S., Jan, L. Y. and Jan, Y. N. (1996). The Drosophila Numb protein inhibits signaling of the Notch receptor during cell-cell interaction in sensory organ lineage. *Proc. Natl. Acad. Sci. U. S. A.* **93**, 11925–11932.

Fukushige, T. and Krause, M. (2005). The myogenic potency of HLH-1 reveals wide-spread developmental plasticity in early C. elegans embryos. *Development* **132**, 1795–1805.

Fukushige, T., Brodigan, T. M., Schriefer, L. A., Waterston, R. H. and Krause, M. (2006). Defining the transcriptional redundancy of early bodywall muscle development in C. elegans: evidence for a unified theory of animal muscle development. *Genes Dev.* **20**, 3395–406.

Fusco, D., Accornero, N., Lavoie, B., Shenoy, S. M., Blanchard, J. M., Singer, R. H. and Bertrand, E. (2003). Single mRNA molecules demonstrate probabilistic movement in living mammalian cells. *Curr. Biol.* **13**, 161–167.

Fuse, N., Hisata, K., Katzen, A. L. and Matsuzaki, F. (2003). Heterotrimeric G Proteins Regulate Daughter Cell Size Asymmetry in Drosophila Neuroblast Divisions. *Curr. Biol.* **13**, 947–954.

Galli, M., Muñoz, J., Portegijs, V., Boxem, M., Grill, S. W., Heck, A. J. R. and van den Heuvel, S. (2011). aPKC phosphorylates NuMA-related LIN-5 to position the mitotic spindle during asymmetric division. *Nat. Cell Biol.* **13**, 1132–1138.

Gendrel, M., Atlas, E. G. and Hobert, O. (2016). A cellular and regulatory map of the GABAergic nervous system of C. elegans. *Elife* **5**, e17686.

Gilleard, J. S. and McGhee, J. D. (2001). Activation of hypodermal differentiation in the Caenorhabditis elegans embryo by GATA transcription factors ELT-1 and ELT-3. *Mol. Cell. Biol.* **21**, 2533–44.

Gilleard, J. S., Shafi, Y., Barry, J. D. and McGhee, J. D. (1999). ELT-3: ACaenorhabditis elegansGATA Factor Expressed in the Embryonic Epidermis during Morphogenesis. *Dev. Biol.* **208**, 265–280.

Ginzberg, M. B., Kafri, R. and Kirschner, M. (2015). Cell biology. On being the right (cell) size. *Science* **348**, 1245075.

Ginzberg, M. B., Chang, N., D'Souza, H., Patel, N., Kafri, R. and Kirschner, M. W. (2018). Cell size sensing in animal cells coordinates anabolic growth rates and cell cycle progression to maintain cell size uniformity. *Elife* **7**, e26957.

Gissendanner, C. R. and Sluder, A. E. (2000). nhr-25, the Caenorhabditis elegans Ortholog of ftz-f1, Is Required for Epidermal and Somatic Gonad Development. *Dev. Biol.* **221**, 259–272.

Goldstein, B., Takeshita, H., Mizumoto, K. and Sawa, H. (2006). Wnt signals can function as positional cues in establishing cell polarity. *Dev. Cell* **10**, 391–6.

Gradwohl, G., Fode, C. and Guillemot, F. (1996). Restricted expression of a novel murine atonal-related bHLH protein in undifferentiated neural precursors. *Dev. Biol.* **180**, 227–241.

Graham, V., Khudyakov, J., Ellis, P. and Pevny, L. (2003). SOX2 functions to maintain neural progenitor identity. *Neuron* **39**, 749–765.

Grants, J. M., Goh, G. Y. S. and Taubert, S. (2015). The Mediator complex of Caenorhabditis elegans: Insights into the developmental and physiological roles of a conserved transcriptional coregulator. *Nucleic Acids Res.* **43**, 2442–2453.

Grants, J. M., Ying, L. T. L., Yoda, A., You, C. C., Okano, H., Sawa, H. and Taubert, S. (2016). The mediator kinase module restrains epidermal growth factor receptor signaling and represses vulval cell fate specification in Caenorhabditis elegans. *Genetics* **202**, 583–599.

Grill, S. W., Gönczy, P., Stelzer, E. H. K. and Hyman, A. A. (2001). Polarity controls forces governing asymmetric spindle positioning in the caenorhabditis elegans embryo. *Nature* **409**, 630–633.

Grove, C. A., De Masi, F., Barrasa, M. I., Newburger, D. E., Alkema, M. J., Bulyk, M. L. and Walhout, A. J. M. (2009). A Multiparameter Network Reveals Extensive Divergence between C. elegans bHLH Transcription Factors. *Cell* **138**, 314–327.

Gruner, M., Grubbs, J., McDonagh, A., Valdes, D., Winbush, A. and van der Linden, A. M. (2016). Cell-Autonomous and Non-Cell-Autonomous Regulation of a Feeding State-Dependent Chemoreceptor Gene via MEF-2 and bHLH Transcription Factors. *PLoS Genet.* **12**, e1006237.

Guenther, C. and Garriga, G. (1996). Asymmetric distribution of the C. elegans HAM-1 protein in neuroblasts enables daughter cells to adopt distinct fates. *Development* **122**, 3509–3518.

Guo, M., Jan, L. Y. and Jan, Y. N. (1996). Control of daughter cell fates during asymmetric division: Interaction of Numb and Notch. *Neuron* **17**, 27–41.

Guo, M., Pegoraro, A. F., Mao, A., Zhou, E. H., Arany, P. R., Han, Y., Burnette, D. T., Jensen, M. H., Kasza, K. E., Moore, J. R., et al. (2017). Cell volume change through water efflux impacts cell stiffness and stem cell fate. *Proc. Natl. Acad. Sci. U. S. A.* **114**, E8618–E8627.

Hall, D. and Russell, R. (1991). The posterior nervous system of the nematode Caenorhabditis elegans: serial reconstruction of identified neurons and complete pattern of synaptic interactions. *J. Neurosci.* **11**, 1–22.

Hallam, S., Singer, E., Waring, D. and Jin, Y. (2000). The C. elegans NeuroD homolog cnd-1 functions in multiple aspects of motor neuron fate specification. *Development* **127**, 4239–52.

Hartwell, L. H. (1967). Macromolecule synthesis in temperature-sensitive mutants of yeast. *J. Bacteriol.* **93**, 1662–1670.

Hashimshony, T., Wagner, F., Sher, N. and Yanai, I. (2012). CEL-Seq: Single-Cell RNA-Seq by Multiplexed Linear Amplification. *Cell Rep.* **2**, 666–673.

Hashimshony, T., Feder, M., Levin, M., Hall, B. K. and Yanai, I. (2015). Spatiotemporal transcriptomics reveals the evolutionary history of the endoderm germ layer. *Nature* **519**, 219–222.

Hatzold, J. and Conradt, B. (2008). Control of apoptosis by asymmetric cell division. *PLoS Biol.* **6**, 771–784.

Hazelrigg, T., Liu, N., Hong, Y. and Wang, S. (1998). GFP expression in drosophila tissues: Tissue requirements for formation of a fluorescent product. *Dev. Biol.* **199**, 245–249.

Heim, R., Cubitt, A. B. and Tsien, R. Y. (1995). Improved green fluorescence. *Nature* **373**, 663–664.

Heitzler, P., Bourouis, M., Ruel, L., Carteret, C. and Simpson, P. (1996). Genes of the Enhancer of split and achaete-scute complexes are required for a regulatory loop between Notch and Delta during lateral signalling in Drosophila. *Development* **122**, 161–71.

Helms, A. W., Abney, A. L., Ben-Arie, N., Zoghbi, H. Y. and Johnson, J. E. (2000). Autoregulation and multiple enhancers control Math1 expression in the developing nervous system. *Development* **127**,.

Hirata, J., Nakagoshi, H., Nabeshima, Y. and Matsuzaki, F. (1995). Asymmetric segregation of the homeodomain protein Prospero during Drosophila development. *Nature* **377**, 627–30.

Hirose, T. and Horvitz, H. R. (2013). An Sp1 transcription factor coordinates caspase-dependent and -independent apoptotic pathways. *Nature* **500**, 354–358.

Ho, V. W. S., Wong, M.-K., An, X., Guan, D., Shao, J., Ng, H. C. K., Ren, X., He, K., Liao, J., Ang, Y., et al. (2015). Systems-level quantification of division timing reveals a common genetic architecture controlling asynchrony and fate asymmetry. *Mol. Syst. Biol.* **11**, 814.

Hobert, O. (2016). A map of terminal regulators of neuronal identity in *Caenorhabditis elegans*. *Wiley Interdiscip. Rev. Dev. Biol.* **5**, 474–498.

Hobert, O., Glenwinkel, L. and White, J. (2016). Revisiting Neuronal Cell Type Classification in Caenorhabditis elegans. *Curr. Biol.* **26**, R1197–R1203.

Holguera, I. and Desplan, C. (2018). Neuronal specification in space and time. *Science* **362**, 176–180.

Horowitz, N. H. (1950). Biochemical Genetics of Neurospora. *Adv. Genet.* **3**, 33–71.

Horvitz, H. R. and Herskowitz, I. (1992). Mechanisms of asymmetric cell division: Two Bs or not two Bs, that is the question. *Cell* **68**, 237–255.

Huang, S., Shetty, P., Robertson, S. M. and Lin, R. (2007). Binary cell fate specification during C. elegans embryogenesis driven by reiterated reciprocal asymmetry of TCF POP-1 and its coactivator beta-catenin SYS-1. *Development* **134**, 2685–95.

Huang, C., Chan, J. A. and Schuurmans, C. (2014). Proneural bHLH genes in development and disease. *Curr. Top. Dev. Biol.* **110**, 75–127.

Huh, D. and Paulsson, J. (2011). Random partitioning of molecules at cell division. *Proc. Natl. Acad. Sci.* **108**, 15004–15009.

Hunter, C. P. and Kenyon, C. (1995). Specification of anteroposterior cell fates in Caenorhabditis elegans by Drosophila Hox proteins. *Nature* **377**, 229–32.

Hunter, C. P. and Kenyon, C. (1996). Spatial and temporal controls target pal-1 blastomere-specification activity to a single blastomere lineage in C. elegans embryos. *Cell* **87**, 217–226.

Ietswaart, R., Rosa, S., Wu, Z., Dean, C. and Howard, M. (2017). Cell-Size-Dependent Transcription of FLC and Its Antisense Long Non-coding RNA COOLAIR Explain Cell-to-Cell Expression Variation. *Cell Syst.* **4**, 622-635.e9.

Iizuka, R., Yamagishi-Shirasaki, M. and Funatsu, T. (2011). Kinetic study of de novo chromophore maturation of fluorescent proteins. *Anal. Biochem.* **414**, 173–178.

Ikeshima-Kataoka, H., Skeath, J. B., Nabeshima, Y., Doe, C. Q. and Matsuzaki, F. (1997). Miranda directs Prospero to a daughter cell during Drosophila asymmetric divisions. *Nature* **390**, 625–9.

Imayoshi, I., Sakamoto, M., Yamaguchi, M., Mori, K. and Kageyama, R. (2010). Essential roles of Notch signaling in maintenance of neural stem cells in developing and adult brains. *J. Neurosci.* **30**, 3489–3498.

Imayoshi, I., Isomura, A., Harima, Y., Kawaguchi, K., Kori, H., Miyachi, H., Fujiwara, T., Ishidate, F. and Kageyama, R. (2013). Oscillatory control of factors determining multipotency and fate in mouse neural progenitors. *Science* **342**, 1203–8.

Izumi, Y., Ohta, N., Itoh-Furuya, A., Fuse, N. and Matsuzaki, F. (2004). Differential functions of G protein and Baz-aPKC signaling pathways in Drosophila neuroblast asymmetric division. *J. Cell Biol.* **164**, 729–738.

Jarman, A. P., Grau, Y., Jan, L. Y. and Jan, Y. N. (1993). atonal is a proneural gene that directs chordotonal organ formation in the Drosophila peripheral nervous system. *Cell* **73**, 1307–1321.

Jarman, A. P., Grell, E. H., Ackerman, L., Jan, L. Y. and Jan, Y. N. (1994). Atonal is the proneural gene for Drosophila photoreceptors. *Nature* **369**, 398–400.

Jarrell, T. A., Wang, Y., Bloniarz, A. E., Brittin, C. A., Xu, M., Thomson, J. N., Albertson, D. G., Hall, D. H. and Emmons, S. W. (2012). The connectome of a decision-making neural network. *Science* **337**, 437–444.

Jennings, B., Preiss, A., Delidakis, C. and Bray, S. (1994). The Notch signalling pathway is required for Enhancer of split bHLH protein expression during neurogenesis in the Drosophila embryo. *Development* **120**, 3537–48.

Jiménez, F. and Campos-Ortega, J. A. (1990). Defective neuroblast commitment in mutants of the achaete-scute complex and adjacent genes of D. melanogaster. *Neuron* **5**, 81–89.

Jin, Y., Hoskins, R. and Horvitz, H. R. (1994). Control of type-D GABAergic neuron differentiation by C. elegans UNC-30 homeodomain protein. *Nature* **372**, 780–783.

Johnson, H. E. and Toettcher, J. E. (2018). Illuminating developmental biology with cellular optogenetics. *Curr. Opin. Biotechnol.* **52**, 42–48.

Johnson, J. E., Birren, S. J. and Anderson, D. J. (1990). Two rat homologues of Drosophila achaete-scute specifically expressed in neuronal precursors. *Nature* **346**, 858–861.

Johnson, S. A., Zitserman, D. and Roegiers, F. (2016). Numb regulates the balance between Notch recycling and late-endosome targeting in Drosophila neural progenitor cells. *Mol. Biol. Cell* **27**, 2857–66.

Kagoshima, H., Cassata, G., Tong, Y. G., Pujol, N., Niklaus, G. and Bürglin, T. R. (2013). The LIM homeobox gene ceh-14 is required for phasmid function and neurite outgrowth. *Dev. Biol.* **380**, 314–323.

Kaletta, T., Schnabel, H. and Schnabel, R. (1997). Binary specification of the embryonic lineage in Caenorhabditis elegans. *Nature* **390**, 294–298.

Karlsson, D., Baumgardt, M. and Thor, S. (2010). Segment-specific neuronal subtype specification by the integration of anteroposterior and temporal cues. *PLoS Biol.* **8**, e1000368.

Kellis, J. T., Nyberg, K. and Fersht, A. R. (1989). Energetics of Complementary Side-Chain Packing in a Protein Hydrophobic Core. *Biochemistry* **28**, 4914–4922.

Kemphues, K. J., Priess, J. R., Morton, D. G. and Cheng, N. (1988). Identification of genes required for cytoplasmic localization in early C. elegans embryos. *Cell* **52**, 311–320.

Kidd, A. R., Miskowski, J. A., Siegfried, K. R., Sawa, H. and Kimble, J. (2005). A beta-catenin identified by functional rather than sequence criteria and its role in Wnt/MAPK signaling. *Cell* **121**, 761–72.

Kim, K. and Li, C. (2004). Expression and regulation of an FMRFamide-related neuropeptide gene family in Caenorhabditis elegans. *J. Comp. Neurol.* **475**, 540–550.

Kimble, J. and Hirsh, D. (1979). The postembryonic cell lineages of the hermaphrodite and male gonads in Caenorhabditis elegans. *Dev. Biol.* **70**, 396–417.

Kitajima, A., Fuse, N., Isshiki, T. and Matsuzaki, F. (2010). Progenitor properties of symmetrically dividing Drosophila neuroblasts during embryonic and larval development. *Dev. Biol.* **347**, 9–23.

Knight, C. G., Patel, M. N., Azevedo, R. B. R. and Leroi, A. M. (2002). A novel mode of ecdysozoan growth in Caenorhabditis elegans. *Evol. Dev.* **4**, 16–27.

Knoblich, J. A. (2008). Mechanisms of Asymmetric Stem Cell Division. *Cell* **132**, 583–597.

Knoblich, J. A. (2010). Asymmetric cell division: Recent developments and their implications for tumour biology. *Nat. Rev. Mol. Cell Biol.* **11**, 849–860.

Kratsios, P., Stolfi, A., Levine, M. and Hobert, O. (2011). Coordinated regulation of cholinergic motor neuron traits through a conserved terminal selector gene. *Nat. Neurosci.* **15**, 205–14.

Kratsios, P., Kerk, S. Y., Catela, C., Liang, J., Vidal, B., Bayer, E. A., Feng, W., De La Cruz, E. D., Croci, L., Consalez, G. G., et al. (2017). An intersectional gene regulatory strategy defines subclass diversity of C. elegans motor neurons. *Elife* **6**, e25751.

Krause, M., Fire, A., Harrison, S. W., Priess, J. and Weintraub, H. (1990). CeMyoD accumulation defines the body wall muscle cell fate during C. elegans embryogenesis. *Cell* **63**, 907–19.

Krause, M., Park, M., Zhang, J. M., Yuan, J., Harfe, B., Xu, S. Q., Greenwald, I., Cole, M., Paterson, B. and Fire, A. (1997). A C. elegans E/Daughterless bHLH protein marks neuronal but not striated muscle development. *Development* **124**, 2179–89.

Krieg, C., Cole, T., Deppe, U., Schierenberg, E., Schmitt, D., Yoder, B. and von Ehrenstein, G. (1978). The cellular anatomy of embryos of the nematode Caenorhabditis elegans. Analysis and reconstruction of serial section electron micrographs. *Dev. Biol.* **65**, 193–215.

Krueger, L. E., Wu, J.-C., Tsou, M.-F. B. and Rose, L. S. (2010). LET-99 inhibits lateral posterior pulling forces during asymmetric spindle elongation in C. elegans embryos. *J. Cell Biol.* **189**, 481–95.

Kunisch, M., Haenlin, M. and Campos-Ortega, J. A. (1994). Lateral inhibition mediated by the Drosophila neurogenic gene delta is enhanced by proneural proteins. *Proc. Natl. Acad. Sci. U. S. A.* **91**, 10139–10143.

Labouesse, M., Sookhareea, S. and Horvitz, H. R. (1994). The Caenorhabditis elegans gene lin-26 is required to specify the fates of hypodermal cells and encodes a presumptive zinc-finger transcription factor. *Development* **120**, 2359–68.

Lanjuin, A., Claggett, J., Shibuya, M., Hunter, C. P. and Sengupta, P. (2006). Regulation of neuronal lineage decisions by the HES-related bHLH protein REF-1. *Dev. Biol.* **290**, 139–151.

Lassiter, R. N. T., Stark, M. R., Zhao, T. and Zhou, C. J. (2014). Signaling mechanisms controlling cranial placode neurogenesis and delamination. *Dev. Biol.* **389**, 39–49.

Laufer, J. S., Bazzicalupo, P. and Wood, W. B. (1980). Segregation of developmental potential in early embryos of caenorhabditis elegans. *Cell* **19**, 569–577.

Ledent, V. and Vervoort, M. (2001). The basic helix-loop-helix protein family: Comparative genomics and phylogenetic analysis. *Genome Res.* **11**, 754–770.

Lee, R. Y. N., Sawin, E. R., Chalfie, M., Horvitz, H. R. and Avery, L. (1999). EAT-4, a Homolog of a Mammalian Sodium-Dependent Inorganic Phosphate Cotransporter, Is Necessary for Glutamatergic Neurotransmission in *Caenorhabditis elegans*. *J. Neurosci.* **19**, 159–167.

Lee, J., Taylor, C. A., Barnes, K. M., Shen, A., Stewart, E. V, Chen, A., Xiang, Y. K., Bao, Z. and Shen, K. (2019a). A Myt1 family transcription factor defines neuronal fate by repressing non-neuronal genes. *Elife* **8**, e46703.

Lee, C. H., Shin, H. and Kimble, J. (2019b). Dynamics of Notch-Dependent Transcriptional Bursting in Its Native Context. *Dev. Cell* **50**, 426-435.e4.

Lei, H., Liu, J., Fukushige, T., Fire, A. and Krause, M. W. (2009). Caudal-like PAL-1 directly activates the bodywall muscle module regulator hlh-1 in C. elegans to initiate the embryonic muscle gene regulatory network. *Development* **136**, 1241–1249.

Leung, A., Hua, K., Ramachandran, P., Hingwing, K., Wu, M., Koh, P. L. and Hawkins, N. (2016). C. elegans HAM-1 functions in the nucleus to regulate asymmetric neuroblast division. *Dev. Biol.* **410**, 56–69.

Li, Y. C., Chao, T. C., Kim, H. J., Cholko, T., Chen, S. F., Li, G., Snyder, L., Nakanishi, K., Chang, C. E., Murakami, K., et al. (2021). Structure and noncanonical Cdk8 activation mechanism within an Argonaute-containing Mediator kinase module. *Sci. Adv.* **7**,.

Lin, R., Hill, R. J. and Priess, J. R. (1998). POP-1 and anterior-posterior fate decisions in C. elegans embryos. *Cell* **92**, 229–239.

Liro, M. J. and Rose, L. S. (2016). Mitotic spindle positioning in the EMS cell of Caenorhabditis elegans requires LET-99 and LIN-5/NuMA. *Genetics* **204**, 1177–1189.

Liro, M. J., Morton, D. G. and Rose, L. S. (2018). The kinases PIG-1 and PAR-1 act in redundant pathways to regulate asymmetric division in the EMS blastomere of C. elegans. *Dev. Biol.* **444**, 9–19.

Lizcano, J. M., Göransson, O., Toth, R., Deak, M., Morrice, N. A., Boudeau, J., Hawley, S. A., Udd, L., Mäkelä, T. P., Hardie, D. G., et al. (2004). LKB1 is a master kinase that activates 13 kinases of the AMPK subfamily, including MARK/PAR-1. *EMBO J.* **23**, 833–43.

Lloret-Fernández, C., Maicas, M., Mora-Martínez, C., Artacho, A., Jimeno-Martín, Á., Chirivella, L., Weinberg, P. and Flames, N. (2018). A transcription factor collective defines the HSN serotonergic neuron regulatory landscape. *Elife* **7**, e32785.

Lo, L., Dormand, E., Greenwood, A. and Anderson, D. J. (2002). Comparison of the generic neuronal differentiation and neuron subtype specification functions of mammalian achaete-scute and atonal homologs in cultured neural progenitor cells. *Development* **129**, 1553–67.

Lo, M. C., Gay, F., Odom, R., Shi, Y. and Lin, R. (2004). Phosphorylation by the β-catenin/MAPK complex promotes 14-3-3-mediated nuclear export of TCF/POP-1 in signal-responsive cells in C. elegans. *Cell* **117**, 95–106.

Lorenzo, R., Onizuka, M., Defrance, M. and Laurent, P. (2020). Combining single-cell RNA-sequencing with a molecular atlas unveils new markers for Caenorhabditis elegans neuron classes. *Nucleic Acids Res.* **48**, 7119–7134.

Lorson, M. A., Horvitz, H. R. and Van Den Heuvel, S. (2000). LIN-5 is a novel component of the spindle apparatus required for chromosome segregation and cleavage plane specification in Caenorhabditis elegans. *J. Cell Biol.* **148**, 73–86.

Lu, B., Rothenberg, M., Jan, L. Y. and Jan, Y. N. (1998). Partner of Numb colocalizes with Numb during mitosis and directs Numb asymmetric localization in Drosophila neural and muscle progenitors. *Cell* **95**, 225–35.

Luo, S. and Horvitz, H. R. (2017). The CDK8 Complex and Proneural Proteins Together Drive Neurogenesis from a Mesodermal Lineage. *Curr. Biol.* **27**, 661–672.

Ma, Q., Kintner, C. and Anderson, D. J. (1996). Identification of neurogenin, a vertebrate neuronal determination gene. *Cell* **87**, 43–52.

Maduro, M. F., Meneghini, M. D., Bowerman, B., Broitman-Maduro, G. and Rothman, J. H. (2001). Restriction of mesendoderm to a single blastomere by the combined action of SKN-1 and a GSK-3β homolog is mediated by MED-1 and -2 in C. elegans. *Mol. Cell* **7**, 475–485.

Maduro, M. F., Kasmir, J. J., Zhu, J. and Rothman, J. H. (2005). The Wnt effector POP-1 and the PAL-1/Caudal homeoprotein collaborate with SKN-1 to activate C. elegans endoderm development. *Dev. Biol.* **285**, 510–23.

Masoudi, N., Tavazoie, S., Glenwinkel, L., Ryu, L., Kim, K. and Hobert, O. (2018). Unconventional function of an Achaete-Scute homolog as a terminal selector of nociceptive neuron identity. *PLoS Biol.* **16**, e2004979.

Mathies, L. D., Henderson, S. T. and Kimble, J. (2003). The C. elegans hand gene controls embryogenesis and early gonadogenesis. *Development* **130**, 2881–2892.

Matsuzaki, F., Ohshiro, T., Ikeshima-Kataoka, H. and Izumi, H. (1998). miranda localizes staufen and prospero asymmetrically in mitotic neuroblasts and epithelial cells in early Drosophila embryogenesis. *Development* **125**, 4089–98.

Maupas, E. (1899). La mue et l'enkystement chez les nématodes. *Arch. Zool. Exp. Gen.* **7**, 563–628.

Maupas, E. (1900). Modes et formes de reproduction des nematodes. *Arch. Zool. Exp. Gen.* **8**, 463–624.

McClay, D. R., Miranda, E. and Feinberg, S. L. (2018). Neurogenesis in the sea urchin embryo is initiated uniquely in three domains. *Development* **145**, dev167742.

Mello, C. C., Kramer, J. M., Stinchcomb, D. and Ambros, V. (1991). Efficient gene transfer in C.elegans: extrachromosomal maintenance and integration of transforming sequences. *EMBO J.* **10**, 3959–70.

Mello, C. C., Draper, B. W., Krause, M., Weintraub, H. and Priess, J. R. (1992). The pie-1 and mex-1 genes and maternal control of blastomere identity in early C. elegans embryos. *Cell* **70**, 163–176.

Mello, C. C., Schubert, C., Draper, B., Zhang, W., Lobel, R. and Priess, J. R. (1996). The PIE-1 protein and germline specification in C. elegans embryos. *Nature* **382**, 710–712.

Mickey, K. M., Mello, C. C., Montgomery, M. K., Fire, A. and Priess, J. R. (1996). An inductive interaction in 4-cell stage C. elegans embryos involves APX-1 expression in the signalling cell. *Development* **122**, 1791–8.

Miettinen, T. P. and Björklund, M. (2016). Cellular Allometry of Mitochondrial Functionality Establishes the Optimal Cell Size. *Dev. Cell* **39**, 370–382.

Miettinen, T. P., Caldez, M. J., Kaldis, P. and Björklund, M. (2017). Cell size control – a mechanism for maintaining fitness and function. *BioEssays* **39**,.

Mila, D., Calderon, A., Baldwin, A. T., Moore, K. M., Watson, M., Phillips, B. T. and Putzke, A. P. (2015). Asymmetric Wnt pathway signaling facilitates stem cell-like divisions via the nonreceptor tyrosine kinase FRK-1 in caenorhabditis elegans. *Genetics* **201**, 1047–1060.

Miller, R. M. and Portman, D. S. (2011). The wnt/β-catenin asymmetry pathway patterns the atonal ortholog lin-32 to diversify cell fate in a caenorhabditis elegans sensory lineage. *J. Neurosci.* **31**, 13281–13291.

Minevich, G., Park, D. S., Blankenberg, D., Poole, R. J. and Hobert, O. (2012). CloudMap: A Cloud-Based Pipeline for Analysis of Mutant Genome Sequences. *Genetics* **192**, 1249–1269.

Mishra, N., Wei, H. and Conradt, B. (2018). Caenorhabditis elegans ced-3 caspase is required for asymmetric divisions that generate cells programmed to die. *Genetics* **210**, 983–998.

Mizumoto, K. and Sawa, H. (2007). Cortical beta-catenin and APC regulate asymmetric nuclear beta-catenin localization during asymmetric cell division in C. elegans. *Dev. Cell* **12**, 287–99.

Morise, H., Shimomura, O., Johnson, F. H. and Winant, J. (1974). Intermolecular energy transfer in the bioluminescent system of aequorea. *Biochemistry* **13**, 2656–2662.

Moskowitz, I. P. G., Gendreau, S. B. and Rothman, J. H. (1994). Combinatorial specification of blastomere identity by glp-1 dependent cellular interactions in the nematode Caenorhabditis elegans. *Development* **120**, 3325–3338.

Mueller, F., Senecal, A., Tantale, K., Marie-Nelly, H., Ly, N., Collin, O., Basyuk, E., Bertrand, E., Darzacq, X. and Zimmer, C. (2013). FISH-quant: Automatic counting of transcripts in 3D FISH images. *Nat. Methods* **10**, 277–278.

Muller, H. J. (1932). Further studies on the nature and causes of gene mutations. *Proc. Sixth Int. Cong. Genet. Ithaca, New York, USA* **1**, 213–255.

Murgan, S., Kari, W., Rothbächer, U., Iché-Torres, M., Mélénec, P., Hobert, O. and Bertrand, V. (2015). Atypical Transcriptional Activation by TCF via a Zic Transcription Factor in C. elegans Neuronal Precursors. *Dev. Cell* **33**, 737–745.

Murray, J. I., Boyle, T. J., Preston, E., Vafeados, D., Mericle, B., Weisdepp, P., Zhao, Z., Bao, Z., Boeck, M. and Waterston, R. H. (2012). Multidimensional regulation of gene expression in the C. elegans embryo. *Genome Res.* **22**, 1282–94.

Murre, C., McCaw, P. S. and Baltimore, D. (1989a). A new DNA binding and dimerization motif in immunoglobulin enhancer binding, daughterless, MyoD, and myc proteins. *Cell* **56**, 777–83.

Murre, C., McCaw, P. S., Vaessin, H., Caudy, M., Jan, L. Y., Jan, Y. N., Cabrera, C. V, Buskin, J. N., Hauschka, S. D. and Lassar, A. B. (1989b). Interactions between heterologous helix-loop-helix proteins generate complexes that bind specifically to a common DNA sequence. *Cell* **58**, 537–44.

Nagamatsu, Y. and Ohshima, Y. (2004). Mechanisms for the control of body size by a G-kinase and a downstream TGFbeta signal pathway in Caenorhabditis elegans. *Genes Cells* **9**, 39–47.

Nair, G., Walton, T., Murray, J. I. and Raj, A. (2013). Gene transcription is coordinated with, but not dependent on, cell divisions during C. elegans embryonic fate specification. *Development* **140**, 3385–94.

Nakamura, K., Kim, S., Ishidate, T., Bei, Y., Pang, K., Shirayama, M., Trzepacz, C., Brownell, D. R. and Mello, C. C. (2005). Wnt signaling drives WRM-1/beta-catenin asymmetries in early C. elegans embryos. *Genes Dev.* **19**, 1749–54.

Nakano, S., Ellis, R. E. and Horvitz, H. R. (2010). Otx - dependent expression of proneural bHLH genes establishes a neuronal bilateral asymmetry in C . elegans. *Development* **4027**, 4017–4027.

Neves, A. and Priess, J. R. (2005). The REF-1 family of bHLH transcription factors pattern C. elegans embryos through Notch-dependent and Notch-independent pathways. *Dev. Cell* **8**, 867–79.

Nguyen-Ngoc, T., Afshar, K. and Gönczy, P. (2007). Coupling of cortical dynein and Gα proteins mediates spindle positioning in Caenorhabditis elegans. *Nat. Cell Biol.* **9**, 1294–1302.

Nicosia, V., Vértes, P. E., Schafer, W. R., Latora, V. and Bullmore, E. T. (2013). Phase transition in the economically modeled growth of a cellular nervous system. *Proc. Natl. Acad. Sci. U. S. A.* **110**, 7880–7885.

Nigon, V., P, G. and H, M. (1960). L'architecture polaire de l'œuf et les mouvements des constituants cellulaires au cours des premières étapes du développement chez quelques Nématodes. *Bull. Biol. Fr. Belg.* **93**, 131–202.

Offenburger, S.-L., Bensaddek, D., Murillo, A. B., Lamond, A. I. and Gartner, A. (2017). Comparative genetic, proteomic and phosphoproteomic analysis of C. elegans embryos with a focus on ham-1/STOX and pig-1/MELK in dopaminergic neuron development. *Sci. Rep.* **7**, 4314.

Ou, G., Stuurman, N., D'Ambrosio, M. and Vale, R. D. (2010). Polarized myosin produces unequal-size daughters during asymmetric cell division. *Science* **330**, 677–680.

Packer, J. S., Zhu, Q., Huynh, C., Sivaramakrishnan, P., Preston, E., Dueck, H., Stefanik, D., Tan, K., Trapnell, C., Kim, J., et al. (2019). A lineage-resolved molecular atlas of C. elegans embryogenesis at single-cell resolution. *Science* eaax1971.

Pacquelet, A., Uhart, P., Tassan, J.-P. and Michaux, G. (2015). PAR-4 and anillin regulate myosin to coordinate spindle and furrow position during asymmetric division. *J. Cell Biol.* **210**, 1085–99.

Padovan-Merhar, O., Nair, G. P., Biaesch, A. G., Mayer, A., Scarfone, S., Foley, S. W., Wu, A. R., Churchman, L. S., Singh, A. and Raj, A. (2015). Single Mammalian Cells Compensate for Differences in Cellular Volume and DNA Copy Number through Independent Global Transcriptional Mechanisms. *Mol. Cell* **58**, 339–352.

Pagano, J. M., Farley, B. M., Essien, K. I. and Ryder, S. P. (2009). RNA recognition by the embryonic cell fate determinant and germline totipotency factor MEX-3. *Proc. Natl. Acad. Sci. U. S. A.* **106**, 20252–20257.

Page, B. D., Zhang, W., Steward, K., Blumenthal, T. and Priess, J. R. (1997). ELT-1, a GATA-like transcription factor, is required for epidermal cell fates in Caenorhabditis elegans embryos. *Genes Dev.* **11**, 1651–1661.

Pakula, A. A. and Sauer, R. T. (1989). Genetic analysis of protein stability and function. *Annu. Rev. Genet.* **23**, 289–310.

Park, D. H. and Rose, L. S. (2008). Dynamic localization of LIN-5 and GPR-1/2 to cortical force generation domains during spindle positioning. *Dev. Biol.* **315**, 42.

Park, F. D., Tenlen, J. R. and Priess, J. R. (2004). C. elegans MOM-5/Frizzled functions in MOM-2/Wnt-independent cell polarity and is localized asymmetrically prior to cell division. *Curr. Biol.* **14**, 2252–2258.

Parras, C. M., Schuurmans, C., Scardigli, R., Kim, J., Anderson, D. J. and Guillemot, F. (2002). Divergent functions of the proneural genes Mash1 and Ngn2 in the specification of neuronal subtype identity. *Genes Dev.* **16**, 324–338.

Peck Justice, S. A., Barron, M. P., Qi, G. D., Sagara Wijeratne, H. R., Victorino, J. F., Simpson, E. R., Vilseck, J. Z., Wijeratne, A. B. and Mosley, A. L. (2020). Mutant thermal proteome profiling for characterization of missense protein variants and their associated phenotypes within the proteome. *J. Biol. Chem.* **295**, 16219–16238.

Pereira, L., Kratsios, P., Serrano-Saiz, E., Sheftel, H., Mayo, A. E., Hall, D. H., White, J. G., LeBoeuf, B., Garcia, L. R., Alon, U., et al. (2015). A cellular and regulatory map of the cholinergic nervous system of C.elegans. *Elife* **4**, e12432.

Pham, T. T., Monnard, A., Helenius, J., Lund, E., Lee, N., Müller, D. J. and Cabernard, C. (2019). Spatiotemporally Controlled Myosin Relocalization and Internal Pressure Generate Sibling Cell Size Asymmetry. *iScience* **13**, 9–19.

Phillips, B. T., Kidd, A. R., King, R., Hardin, J. and Kimble, J. (2007). Reciprocal asymmetry of SYS-1/beta-catenin and POP-1/TCF controls asymmetric divisions in Caenorhabditis elegans. *Proc. Natl. Acad. Sci. U. S. A.* **104**, 3231–6.

Pichon, X., Lagha, M., Mueller, F. and Bertrand, E. (2018). Molecular Cell Technology Review A Growing Toolbox to Image Gene Expression in Single Cells: Sensitive Approaches for Demanding Challenges. *Mol. Cell* **71**, 468–480.

Pocock, R., Ahringer, J., Mitsch, M., Maxwell, S. and Woollard, A. (2004). A regulatory network of T-box genes and the even-skipped homologue vab-7 controls patterning and morphogenesis in C. elegans. *Development* **131**, 2373–2385.

Podbilewicz, B. and White, J. G. (1994). Cell fusions in the developing epithelia of C. elegans. *Dev. Biol.* **161**, 408–424.

Poole, R. J., Bashllari, E., Cochella, L., Flowers, E. B. and Hobert, O. (2011). A Genome-Wide RNAi Screen for Factors Involved in Neuronal Specification in Caenorhabditis elegans. *PLoS Genet.* **7**, e1002109.

Portegijs, V., Fielmich, L. E., Galli, M., Schmidt, R., Muñoz, J., van Mourik, T., Akhmanova, A., Heck, A. J. R., Boxem, M. and van den Heuvel, S. (2016). Multisite Phosphorylation of NuMA-Related LIN-5 Controls Mitotic Spindle Positioning in C. elegans. *PLoS Genet.* **12**, e1006291.

Portman, D. S. and Emmons, S. W. (2000). The basic helix-loop-helix transcription factors LIN-32 and HLH-2 function together in multiple steps of a C. elegans neuronal sublineage. *Development* **127**, 5415–26.

Praitis, V., Casey, E., Collar, D. and Austin, J. (2001). Creation of low-copy integrated transgenic lines in Caenorhabditis elegans. *Genetics* **157**, 1217–1226.

Price, K. L. and Rose, L. S. (2017). LET-99 functions in the astral furrowing pathway, where it is required for myosin enrichment in the contractile ring. *Mol. Biol. Cell* **28**, 2360–2373.

Priess, J. R. (2005). Notch signaling in the C. elegans embryo. *WormBook* 1–16.

Putzke, A. P. and Rothman, J. H. (2010). Repression of Wnt signaling by a Fer-type nonreceptor tyrosine kinase. *Proc. Natl. Acad. Sci. U. S. A.* **107**, 16154–16159.

Putzke, A. P., Hikita, S. T., Clegg, D. O. and Rothman, J. H. (2005). Essential kinase-independent role of a Fer-like non-receptor tyrosine kinase in Caenorhabditis elegans morphogenesis. *Development* **132**, 3185–3195.

Raj, A., van den Bogaard, P., Rifkin, S. A., van Oudenaarden, A. and Tyagi, S. (2008). Imaging individual mRNA molecules using multiple singly labeled probes. *Nat. Methods* **5**, 877–879.

Reber, S. and Goehring, N. W. (2015). Intracellular Scaling Mechanisms. *Cold Spring Harb. Perspect. Biol.* **7**, a019067.

Reece-Hoyes, J. S., Deplancke, B., Shingles, J., Grove, C. A., Hope, I. A. and Walhout, A. J. M. (2005). A compendium of Caenorhabditis elegans regulatory transcription factors: A resource for mapping transcription regulatory networks. *Genome Biol.* **6**, R110.

Rhyu, M. S., Jan, L. Y. and Jan, Y. N. (1994). Asymmetric distribution of numb protein during division of the sensory organ precursor cell confers distinct fates to daughter cells. *Cell* **76**, 477–491.

Ringstad, N. and Horvitz, H. R. (2008). FMRFamide neuropeptides and acetylcholine synergistically inhibit egg-laying by C. elegans. *Nat. Neurosci.* **11**, 1168–1176.

Rishal, I. and Fainzilber, M. (2019). Cell size sensing - A one-dimensional solution for a three-dimensional problem? *BMC Biol.* **17**, 36.

Rocheleau, C. E., Downs, W. D., Lin, R., Wittmann, C., Bei, Y., Cha, Y. H., Ali, M., Priess, J. R. and Mello, C. C. (1997). Wnt signaling and an APC-related gene specify endoderm in early C. elegans embryos. *Cell* **90**, 707–716.

Rocheleau, C. E., Yasuda, J., Tae Ho Shin, Lin, R., Sawa, H., Okano, H., Priess, J. R., Davis, R. J. and Mello, C. C. (1999). WRM-1 activates the LIT-1 protein kinase to transduce anterior/posterior polarity signals in C. elegans. *Cell* **97**, 717–726.

Rolls, M. M., Albertson, R., Shih, H. P., Lee, C. Y. and Doe, C. Q. (2003). Drosophila aPKC regulates cell polarity and cell proliferation in neuroblasts and epithelia. *J. Cell Biol.* **163**, 1089–1098.

Romanos, T. R., Pladevall-Morera, D., Langebeck-Jensen, K., Hansen, S., Ng, L. and Pocock, R. (2017). LIN-32/Atonal Controls Oxygen Sensing Neuron Development in Caenorhabditis elegans. *Sci. Rep.* **7**, 7294.

Rose, L. and Gönczy, P. (2014). Polarity establishment, asymmetric division and segregation of fate determinants in early C. elegans embryos. *WormBook* 1–43.

Rose, L. S. and Kemphues, K. (1998). The let-99 gene is required for proper spindle orientation during cleavage of the C. elegans embryo. *Development* **125**, 1337–46.

Roth, M., Roubinet, C., Iffländer, N., Ferrand, A. and Cabernard, C. (2015). Asymmetrically dividing Drosophila neuroblasts utilize two spatially and temporally independent cytokinesis pathways. *Nat. Commun.* **6**, 6551.

Roubinet, C., Tsankova, A., Pham, T. T., Monnard, A., Caussinus, E., Affolter, M. and Cabernard, C. (2017). Spatio-temporally separated cortical flows and spindle geometry establish physical asymmetry in fly neural stem cells. *Nat. Commun.* **8**, 1383.

Rueden, C. T., Schindelin, J., Hiner, M. C., DeZonia, B. E., Walter, A. E., Arena, E. T. and Eliceiri, K. W. (2017). ImageJ2: ImageJ for the next generation of scientific image data. *BMC Bioinformatics* **18**,.

Sagasti, A., Hisamoto, N., Hyodo, J., Tanaka-Hino, M., Matsumoto, K. and Bargmann, C. I. (2001). The CaMKII UNC-43 activates the MAPKKK NSY-1 to execute a lateral signaling decision required for asymmetric olfactory neuron fates. *Cell* **105**, 221–232.

Sahni, N., Yi, S., Taipale, M., Fuxman Bass, J. I., Coulombe-Huntington, J., Yang, F., Peng, J., Weile, J., Karras, G. I., Wang, Y., et al. (2015). Widespread macromolecular interaction perturbations in human genetic disorders. *Cell* **161**, 647–660.

Sammut, M., Cook, S. J., Nguyen, K. C. Q., Felton, T., Hall, D. H., Emmons, S. W., Poole, R. J. and Barrios, A. (2015). Glia-derived neurons are required for sex-specific learning in C. elegans. *Nature* **526**, 385–390.

Sawa, H. and Korswagen, H. C. (2013). Wnt signaling in C. elegans. *WormBook* 1–30.

Schaefer, M., Shevchenko, A., Shevchenko, A. and Knoblich, J. A. (2000). A protein complex containing Inscuteable and the Gα-binding protein Pins orients asymmetric cell divisions in Drosophila. *Curr. Biol.* **10**, 353–362.

Schierenberg, E. (1986). Developmental strategies during early embryogenesis of Caenorhabditis elegans. *J. Embryol. Exp. Morphol.* **97**, 31–44.

Schierenberg, E. (1988). Localization and segregation of lineage-specific cleavage potential in embryos of Caenorhabditis elegans. *Roux's Arch. Dev. Biol.* **197**, 282–293.

Schindelin, J., Arganda-Carreras, I., Frise, E., Kaynig, V., Longair, M., Pietzsch, T., Preibisch, S., Rueden, C., Saalfeld, S., Schmid, B., et al. (2012). Fiji: an open-source platform for biological-image analysis. *Nat. Methods* **9**, 676–682.

Schmoller, K. M. (2017). The phenomenology of cell size control. *Curr. Opin. Cell Biol.* **49**, 53–58.

Schnabel, R. (1994). Autonomy and nonautonomy in cell fate specification of muscle in the Caenorhabditis elegans embryo: A reciprocal induction. *Science* **263**, 1449–1452.

Schnabel, R. (1995). Duels without obvious sense: Counteracting inductions involved in body wall muscle development in the Caenorhabditis elegans embryo. *Development* **121**, 2219–2232.

Schnabel, R., Hutter, H., Moerman, D. and Schnabel, H. (1997). Assessing normal embryogenesis in Caenorhabditis elegans using a 4D microscope: Variability of development and regional specification. *Dev. Biol.* **184**, 234–265.

Schober, M., Schaefer, M. and Knoblich, J. A. (1999). Bazooka recruits inscuteable to orient asymmetric cell divisions in Drosophila neuroblasts. *Nature* **402**, 548–551.

Schrons, H., Knust, E. and Campos-Ortega, J. A. (1992). The Enhancer of split complex and adjacent genes in the 96F region of Drosophila melanogaster are required for segregation of neural and epidermal progenitor cells. *Genetics* **132**, 481–503.

Schulenburg, H. and Félix, M.-A. (2017). The Natural Biotic Environment of Caenorhabditis elegans. *Genetics* **206**, 55–86.

Serrano-Saiz, E., Poole, R. J., Felton, T., Zhang, F., De La Cruz, E. D. and Hobert, O. (2013). Modular control of glutamatergic neuronal identity in C. elegans by distinct homeodomain proteins. *Cell* **155**, 659–73.

Seydoux, G., Mello, C. C., Pettitt, J., Wood, W. B., Priess, J. R. and Fire, A. (1996). Repression of gene expression in the embryonic germ lineage of C. elegans. *Nature* **382**, 713–716.

Shao, J., He, K., Wang, H., Ho, W. S., Ren, X., An, X., Wong, M. K., Yan, B., Xie, D., Stamatoyannopoulos, J., et al. (2013). Collaborative regulation of development but independent control of metabolism by two epidermis-specific transcription factors in Caenorhabditis elegans. *J. Biol. Chem.* **288**, 33411–33426.

Shelton, C. A. and Bowerman, B. (1996). Time-dependent responses to glp-1-mediated inductions in early C. elegans embryos. *Development* **122**, 2043–50.

Shen, C.-P., Jan, L. Y. and Jan, Y. N. (1997). Miranda Is Required for the Asymmetric Localization of Prospero during Mitosis in Drosophila. *Cell* **90**, 449–458.

Shen, C. P., Knoblich, J. A., Chan, Y. M., Jiang, M. M., Jan, L. Y. and Jan, Y. N. (1998). Miranda as a multidomain adapter linking apically localized Inscuteable and basally localized Staufen and Prospero during asymmetric cell division in Drosophila. *Genes Dev.* **12**, 1837–46.

Shimojo, H., Ohtsuka, T. and Kageyama, R. (2008). Oscillations in notch signaling regulate maintenance of neural progenitors. *Neuron* **58**, 52–64.

Shimomura, O., Johnson, F. H. and Saiga, Y. (1962). Extraction, Purification and Properties of Aequorin, a Bioluminescent Protein from the Luminous Hydromedusan,Aequorea. *J. Cell. Comp. Physiol.* **59**, 223–239.

Simionato, E., Ledent, V., Richards, G., Thomas-Chollier, M., Kerner, P., Coornaert, D., Degnan, B. M. and Vervoort, M. (2007). Origin and diversification of the basic helix-loop-helix gene family in metazoans: Insights from comparative genomics. *BMC Evol. Biol.* **7**, 33.

Simpson, P. and Carteret, C. (1990). Proneural clusters: equivalence groups in the epithelium of Drosophila. *Development* **110**, 927–32.

Slota, L. A. and McClay, D. R. (2018). Identification of neural transcription factors required for the differentiation of three neuronal subtypes in the sea urchin embryo. *Dev. Biol.* **435**, 138–149.

Smith, C. A., Lau, K. M., Rahmani, Z., Dho, S. E., Brothers, G., She, Y. M., Berry, D. M., Bonneil, E., Thibault, P., Schweisguth, F., et al. (2007). aPKC-mediated phosphorylation regulates asymmetric membrane localization of the cell fate determinant Numb. *EMBO J.* **26**, 468–80.

Southall, T. D., Brand, A. H., Arlotta, P., Molyneaux, B., Chen, J., Inoue, J., Kominami, R., Macklis, J., Ashraf, S., Ip, Y., et al. (2009). Neural stem cell transcriptional networks highlight genes essential for nervous system development. *EMBO J.* **28**, 3799–807.

Srinivasan, D. G., Fisk, R. M., Xu, H. and van den Heuvel, S. (2003). A complex of LIN-5 and GPR proteins regulates G protein signaling and spindle function in C elegans. *Genes Dev.* **17**, 1225–39.

Stefanakis, N., Carrera, I. and Hobert, O. (2015). Regulatory Logic of Pan-Neuronal Gene Expression in C. elegans. *Neuron* **87**, 733–50.

Stiernagle, T. (2006). Maintenance of *C. elegans* (February 11, 2006), WormBook, ed. *C. elegans Res. Community, Wormb.* 1–11.

Strome, S. and Wood, W. B. (1982). Immunofluorescence visualization of germ-line-specific cytoplasmic granules in embryos, larvae, and adults of Caenorhabditis elegans. *Proc. Natl. Acad. Sci. U. S. A.* **79**, 1558–62.

Sueda, R., Imayoshi, I., Harima, Y. and Kageyama, R. (2019). High Hes1 expression and resultant Ascl1 suppression regulate quiescent vs. active neural stem cells in the adult mouse brain. *Genes Dev.* **33**, 511–523.

Sugaya, K. (2018). Let's think again about using mammalian temperature-sensitive mutants to investigate functional molecules—The perspectives from the studies on three mutants showing chromosome instability. *J. Cell. Biochem.* **119**, 7143–7150.

Sugioka, K., Fielmich, L.-E., Mizumoto, K., Bowerman, B., van den Heuvel, S., Kimura, A. and Sawa, H. (2018). Tumor suppressor APC is an attenuator of spindle-pulling forces during C. elegans asymmetric cell division. *Proc. Natl. Acad. Sci. U. S. A.* **115**, E954–E963.

Sulston, J. E. and Brenner, S. (1974). The DNA of Caenorhabditis elegans. *Genetics* **77**, 95–104.

Sulston, J. E. and Horvitz, H. R. (1977). Post-embryonic Cell Lineages of the Nematode, Caenorhabditis elegans. *Dev. Biol.* **56**, 110–156.

Sulston, J. E., Schierenberg, E., White, J. G. and Thomson, J. N. (1983). The embryonic cell lineage of the nematode Caenorhabditis elegans. *Dev. Biol.* **100**, 64–119.

Sun, V., Jan, L. Y. and Jan, Y. N. (1998). Transcriptional regulation of atonal during development of the Drosophila peripheral nervous system. *Development* **125**, 3731–3740.

Tabuse, Y., Izumi, Y., Piano, F., Kemphues, K. J., Miwa, J. and Ohno, S. (1998). Atypical protein kinase C cooperates with PAR-3 to establish embryonic polarity in Caenorhabditis elegans. *Development* **125**, 3607–14.

Takeshita, H. and Sawa, H. (2005). Asymmetric cortical and nuclear localizations of WRM-1/β-catenin during asymmetric cell division in C. elegans. *Genes Dev.* **19**, 1743–1748.

Tam, J. (2015). MRes Thesis, "The Regulation of Asymmetric Neurogenesis and Early Proneural Gene Expression: Analysis of Asymmetric Neurogenesis Defective Mutants", University College London.

Teuliere, J., Cordes, S., Singhvi, A., Talavera, K. and Garriga, G. (2014). Asymmetric neuroblast divisions producing apoptotic cells require the cytohesin GRP-1 in Caenorhabditis elegans. *Genetics* **198**, 229–247.

Teuliere, J., Kovacevic, I., Bao, Z. and Garriga, G. (2018). The Caenorhabditis elegans gene ham-1 regulates daughter cell size asymmetry primarily in divisions that produce a small anterior daughter cell. *PLoS One* **13**, e0195855.

Thorpe, C. J., Schlesinger, A., Clayton Carter, J. and Bowerman, B. (1997). Wnt signaling polarizes an early C. elegans blastomere to distinguish endoderm from mesoderm. *Cell* **90**, 695–705.

Tintori, S. C., Osborne Nishimura, E., Golden, P., Lieb, J. D. and Goldstein, B. (2016). A Transcriptional Lineage of the Early C. elegans Embryo. *Dev. Cell* **38**, 430–444.

Titlow, J. S., Yang, L., Parton, R. M., Palanca, A. and Davis, I. (2018). Super-resolution single molecule FISH at the drosophila neuromuscular junction. In *Methods in Molecular Biology*, pp. 163–175. Humana Press Inc.

Trcek, T., Lionnet, T., Shroff, H. and Lehmann, R. (2017). mRNA quantification using single-molecule FISH in Drosophila embryos. *Nat. Protoc.* **12**, 1326–1347.

Tsai, K. L., Sato, S., Tomomori-Sato, C., Conaway, R. C., Conaway, J. W. and Asturias, F. J. (2013). A conserved Mediator-CDK8 kinase module association regulates Mediator-RNA polymerase II interaction. *Nat. Struct. Mol. Biol.* **20**, 611–619.

Tsai, K. L., Tomomori-Sato, C., Sato, S., Conaway, R. C., Conaway, J. W. and Asturias, F. J. (2014). Subunit architecture and functional modular rearrangements of the transcriptional mediator complex. *Cell* **157**, 1430–1444.

Tsankova, A., Pham, T. T., Garcia, D. S., Otte, F. and Cabernard, C. (2017). Cell Polarity Regulates Biased Myosin Activity and Dynamics during Asymmetric Cell Division via Drosophila Rho Kinase and Protein Kinase N. *Dev. Cell* **42**, 143-155.e5.

Tsanov, N., Samacoits, A., Chouaib, R., Traboulsi, A. M., Gostan, T., Weber, C., Zimmer, C., Zibara, K., Walter, T., Peter, M., et al. (2016). SmiFISH and FISH-quant - A flexible single RNA detection approach with super-resolution capability. *Nucleic Acids Res.* **44**,.

Tsou, M.-F. B., Hayashi, A., DeBella, L. R., McGrath, G. and Rose, L. S. (2002). LET-99 determines spindle position and is asymmetrically enriched in response to PAR polarity cues in C. elegans embryos. *Development* **129**, 4469–81.

Tsou, M.-F. B., Hayashi, A. and Rose, L. S. (2003). LET-99 opposes Galpha/GPR signaling to generate asymmetry for spindle positioning in response to PAR and MES-1/SRC-1 signaling. *Development* **130**, 5717–30.

Tutucci, E., Vera, M. and Singer, R. H. (2018). Single-mRNA detection in living S. cerevisiae using a re-engineered MS2 system. *Nat. Protoc.* **13**, 2268–2296.

Uemura, T., Shepherd, S., Ackerman, L., Jan, L. Y. and Jan, Y. N. (1989). numb, a gene required in determination of cell fate during sensory organ formation in Drosophila embryos. *Cell* **58**, 349–360.

Urbach, R., Schnabel, R. and Technau, G. M. (2003). The pattern of neuroblast formation, mitotic domains and proneural gene expression during early brain development in Drosophila. *Development* **130**, 3589–3606.

Van Auken, K., Weaver, D. C., Edgar, L. G. and Wood, W. B. (2000). Caenorhabditis elegans embryonic axial patterning requires two recently discovered posterior-group Hox genes. *Proc. Natl. Acad. Sci. U. S. A.* **97**, 4499–503.

Van Doren, M., Powell, P. A., Pasternak, D., Singson, A. and Posakony, J. W. (1992). Spatial regulation of proneural gene activity: auto- and cross-activation of achaete is antagonized by extramacrochaetae. *Genes Dev.* **6**, 2592–605.

Varshney, L. R., Chen, B. L., Paniagua, E., Hall, D. H. and Chklovskii, D. B. (2011). Structural properties of the Caenorhabditis elegans neuronal network. *PLoS Comput. Biol.* **7**, e1001066.

Vera, M., Tutucci, E. and Singer, R. H. (2019). Imaging Single mRNA Molecules in Mammalian Cells Using an Optimized MS2-MCP System. In *Methods in Molecular Biology*, pp. 3–20. Humana Press Inc.

Vidal, B., Santella, A., Serrano-Sai, E., Bao, Z., Chuang, C. F. and Hobert, O. (2015). C. Elegans SoxB genes are dispensable for embryonic neurogenesis but required for terminal differentiation of specific neuron types. *Dev.* **142**, 2464–2477.

Villares, R. and Cabrera, C. V (1987). The achaete-scute gene complex of D. melanogaster: conserved domains in a subset of genes required for neurogenesis and their homology to myc. *Cell* **50**, 415–24.

Walston, T., Tuskey, C., Edgar, L., Hawkins, N., Ellis, G., Bowerman, B., Wood, W. and Hardin, J. (2004). Multiple Wnt signaling pathways converge to orient the mitotic spindle in early C. elegans embryos. *Dev. Cell* **7**, 831–841.

Wang, P., Hayden, S. and Masui, Y. (2000). Transition of the blastomere cell cycle from cell size-independent to size-dependent control at the midblastula stage in Xenopus laevis. *J. Exp. Zool.* **287**, 128–44.

Wang, J. C., Walker, A., Blackwell, T. K. and Yamamoto, K. R. (2004). The Caenorhabditis elegans ortholog of TRAP240, CeTRAP240/let-19, selectively modulates gene expression and is essential for embryogenesis. *J. Biol. Chem.* **279**, 29270–29277.

Waring, D. A. and Kenyon, C. (1990). Selective silencing of cell communication influences anteroposterior pattern formation in C. elegans. *Cell* **60**, 123–131.

Watanabe, N., Nagamatsu, Y., Gengyo-Ando, K., Mitani, S. and Ohshima, Y. (2005). Control of body size by SMA-5, a homolog of MAP kinase BMK1/ERK5, in C. elegans. *Development* **132**, 3175–84.

Watanabe, N., Ishihara, T. and Ohshima, Y. (2007). Mutants carrying two sma mutations are super small in the nematode C. elegans. *Genes to Cells* **12**, 603–609.

Watts, J. L., Morton, D. G., Bestman, J. and Kemphues, K. J. (2000). The C. elegans par-4 gene encodes a putative serine-threonine kinase required for establishing embryonic asymmetry. *Development* **127**, 1467–75.

Wei, H., Yan, B., Gagneur, J. and Conradt, B. (2017). Caenorhabditis elegans CES-1 Snail Represses pig-1 MELK Expression To Control Asymmetric Cell Division. *Genetics* **206**, 2069–2084.

Wei, H., Lambie, E. J., Osório, D. S., Carvalho, A. X. and Conradt, B. (2020). PIG-1 MELK-dependent phosphorylation of nonmuscle myosin II promotes apoptosis through CES-1 Snail partitioning. *PLoS Genet.* **16**,.

White, J. G., Southgate, E., Thomson, J. N. and Brenner, S. (1976). The structure of the ventral nerve cord of Caenorhabditis elegans. *Philos. Trans. R. Soc. Lond. B. Biol. Sci.* **275**, 327–348.

White, J. G., Southgate, E., Thomson, J. N. and Brenner, S. (1986). The Structure of the Nervous System of the Nematode Caenorhabditis elegans. *Philos. Trans. R. Soc. B Biol. Sci.* **314**, 1–340.

Whitman, C. O. (1878). Memoirs: The Embryology of Clepsine. *Q. J. Microsc. Sci.* **s2**-**18**, 215–315.

Wittmann, C., Bosslnger, O., Goldstein, B., Fleischmann, M., Kohler, R., Brunschwig, K., Tobler, H. and Müller, F. (1997). The expression of the C. elegans labial-like Hox gene ceh-13 during early embryogenesis relies on cell fate and on anteroposterior cell polarity. *Development* **124**, 4193–4200.

Wrischnik, L. A. and Kenyon, C. J. (1997). The role of lin-22, a hairy/enhancer of split homolog, in patterning the peripheral nervous system of C. elegans. *Development* **124**, 2875–88.

Wu, J.-C. and Rose, L. S. (2007). PAR-3 and PAR-1 inhibit LET-99 localization to generate a cortical band important for spindle positioning in Caenorhabditis elegans embryos. *Mol. Biol. Cell* **18**, 4470–82.

Wu, J.-C., Espiritu, E. B. and Rose, L. S. (2016). The 14-3-3 protein PAR-5 regulates the asymmetric localization of the LET-99 spindle positioning protein. *Dev. Biol.* **412**, 288–297.

Xu, C. and Su, Z. (2014). Identification of genes driving lineage divergence from single-cell gene expression data in C. elegans. *Dev. Biol.* **393**, 236–244.

Yanai, I., Baugh, L. R., Smith, J. J., Roehrig, C., Shen-Orr, S. S., Claggett, J. M., Hill, A. A., Slonim, D. K. and Hunter, C. P. (2008). Pairing of competitive and topologically distinct regulatory modules enhances patterned gene expression. *Mol. Syst. Biol.* **4**, 163.

Yang, X. D., Karhadkar, T. R., Medina, J., Robertson, S. M. and Lin, R. (2015). β-Cateninrelated protein WRM-1 is a multifunctional regulatory subunit of the LIT-1 MAPK complex. *Proc. Natl. Acad. Sci. U. S. A.* **112**, E137–E146.

Yeung, J. T. (2016). MSci Thesis: “Defining the Critical Period of let-19/mdt-13 in Left-Right Asymmetric Neurogenesis”, University College London.

Yoda, A., Kouike, H., Okano, H. and Sawa, H. (2005). Components of the transcriptional mediator complex are required for asymmetric cell division in C. elegans. *Development* **132**, 1885–1893.

Yu, F., Morin, X., Cai, Y., Yang, X. and Chia, W. (2000). Analysis of partner of inscuteable, a Novel Player of Drosophila Asymmetric Divisions, Reveals Two Distinct Steps in Inscuteable Apical Localization. *Cell* **100**, 399–409.

Zacharias, A. L., Walton, T., Preston, E. and Murray, J. I. (2015). Quantitative Differences in Nuclear β-catenin and TCF Pattern Embryonic Cells in C. elegans. *PLoS Genet.* **11**, e1005585.

Zhang, L., Ward, J. D., Cheng, Z. and Dernburg, A. F. (2015). The auxin-inducible degradation (AID) system enables versatile conditional protein depletion in C. elegans. *Dev.* **142**, 4374–4384.

Zhao, C. and Emmons, S. W. (1995). A transcription factor controlling development of peripheral sense organs in C. elegans. *Nature* **373**, 74–8.

Zheng, C., Diaz-Cuadros, M. and Chalfie, M. (2015). Hox Genes Promote Neuronal Subtype Diversification through Posterior Induction in Caenorhabditis elegans. *Neuron* **88**, 514–27.

Zhu, Z., Liu, J., Yi, P., Tian, D., Chai, Y., Li, W. and Ou, G. (2014). A proneural gene controls *C. elegans* neuroblast asymmetric division and migration. *FEBS Lett.* **588**, 1136–1143.